SAPIENZA
UNIVERSITÀ DI ROMA

The University Of Sheffield.

INSIGNEO Institute for *in silico* Medicine

# KINEMATIC MODELLING OF THE FOOT-ANKLE COMPLEX FOR GAIT ANALYSIS

**PhD Thesis in:**

**Industrial Production Engineering – XXVIII cycle**

**&**

**Mechanical Engineering**


**Supervisors:**

**Dr Eduardo Palermo**
**Prof Paolo Cappa**
Dept. of Mechanical and Aerospace Engineering
Sapienza University of Rome

**Dr Claudia Mazzà**
**Prof Marco Viceconti (DDP advisor)**
Dept. of Mechanical Engineering
INSIGNEO Institute for *in silico* medicine
The University of Sheffield

**PhD Candidate:**

**Roberto Di Marco**


**15th December 2016**

*To work without one thought of gain or fame,*
*To realise that journey to the moon!*
*Never to pen a line that has not sprung*
*Straight from the heart within. Embracing then*
*Modesty, say to oneself, "Good my friend,*
*Be thou content with flowers, - fruit, - nay, leaves,*
*But pluck them from no garden but thine own!"*
*And then, if glory come by chance your way,*
*To pay no tribute unto Caesar, none,*
*But keep the merit all your own! In short,*
*Disdaining tendrils of the parasite,*
*To be content, if neither oak nor elm-*
*Not to mount high, perchance, but mount alone!*

*("Cyrano de Bergerac", E. Rostand)*

# Table of content

# List of Figures

# List of Tables

# Abstract

The functional role of the foot-ankle complex is critical in terms of providing support and mobility to the whole human body. Besides those associated with common lesions or damages of its structures (e.g. sprains, bone fractures), impairments in the foot may also cause secondary chronic pathologies. Thus, a quantitative assessment of the mechanical behaviour of the joints within the foot-ankle complex is certainly of clinical value.

Gait analysis is used to assess lower limb joint kinematics during walking, and is usually performed using stereophotogrammetric systems. Conventionally, the foot is considered as a rigid segment. This oversimplification has been overcome with the use of multi-segment models to describe foot kinematics. However, these models have been only partially validated, limiting their widespread adoption. This Thesis aims at filling the gap of a repeatability and reproducibility analysis of the outcomes of the available foot modelling techniques, providing guidelines and reference values to be used in future applications, and establishing a standard for the kinematic assessment of the foot-ankle complex in gait analysis.

As a first step, different indices to quantify repeatability and reproducibility of model outcomes have been critically compared and investigated, including Linear Fit Method coefficients (LFM), Coefficient of Multiple Correlation (CMC), Mean Absolute Variability (MAV), and Root Mean Square Error (RMSE). A sensitivity analysis was performed to this purpose using artificially created curves, which were varied by imposing a set of realistic alterations in their shapes, joints' range of motion, sample by sample amplitude variability, offset, and time shift. The CMC values were found to be sensible to different curve shapes, and, as well as the LFM coefficients, were independent from the range of motion. Complex values of the CMCs were observed when large offset and time shift occurred. The LFM coefficients worsened with the time shift, invalidating the assumption of linear relationship among curves. Nonetheless, these coefficients, when used with measurement of absolute differences (e.g., MAV or RMSE), were found to be the most suitable to be used for gait curve comparisons.

The instrumental error associated with different procedures that can be adopted to calibrate a stereophotogrammetric system has then been assessed for two different systems. The results of this part of the Thesis showed that the errors are independent on the adopted calibration. In fact, the between-calibration CMC of joint kinematics were never lower than 0.93. The average differences between measured and known values of distances between pair of markers were lower than 1.7 mm. Instead, the average differences between measured and known values of angles between markers 0.7°. These findings suggest that relevant procedures do not affect the metrological performance of the systems under test and the associated errors can be neglected.

As a following step, the experimental error associated to the marker placement was quantified for the four most adopted multi-segment models of the foot. The repeatability and reproducibility of the relative measurements were assessed by comparing joint sagittal kinematics obtained when: a) the same operator placed the markers on thirteen young healthy adults in two different sessions; b) three operators placed the markers for three times on three randomly selected participants, respectively. The two most repeatable and reproducible models, according to the validated similarity and correlation indices (i.e., the LFM coefficient), displayed averaged correlation higher than 0.72, with the lowest values obtained for the between-subject comparison of the midfoot kinematics (0.69 and 0.55). Results showed that foot kinematics have low overall repeatability when evaluated with the existing models, and normative bands should be adopted with caution when used for comparison with patient data, especially when dealing with joints that interacts with the mid-foot and display range of motions smaller than 10°.

Finally, to overcome the limitations highlighted by the assessment of the existing models, a novel kinematic model of the foot-ankle complex has been designed, and the repeatability and reproducibility of the relevant sagittal kinematics have also been quantified. Results showed an improvement, especially for the joint enclosed between the mid-foot and the hindfoot, with correlation higher than 0.82.

In conclusion, the new model paves the way to a more reliable modelling of the foot and, represents an improvement with respect to the existing techniques.

# Declaration

A substantial part of the material presented in this Thesis is published or already submitted to a scientific journal:

- Part of the material presented in Paragraph §2.3.1.3 has been published in:

  Di Marco R, Rossi S, Patanè F, Cappa P. *Technical quality assessment of an optoelectronic system for movement analysis* (2015) Journal of Physics: Conference Series, **588**(1): 012030. DOI: 10.1088/1742-6596/588/1/012030;

- Part of the material presented in Chapter 3 has been submitted as:

  Di Marco R & Scalona E, Pacilli A, Cappa P, Mazzà C, Rossi S. *How to choose and interpret similarity indices to quantify the variability in gait joint kinematics*. Submitted to: Journal of Biomechanics (December 2016);

- Part of the material presented in Chapter 4 has been published in

  Di Marco R, Rossi S, Castelli E, Patanè F, Mazzà C, Cappa P. *Effect of the calibration procedure on the metrological performances of stereophotogrammetric systems for human movement analysis* (2016) Measurement, in press: 1-8. DOI: 10.1016/j.measurement.2016.01.008;

- Part of the material presented in Chapter 5 has been published in:

  Di Marco R, Rossi S, Racic V, Cappa P, Mazzà C. *Concurrent repeatability and reproducibility analyses of four marker placement protocols for the foot-ankle complex* (2016) Journal of Biomechanics, **49**(14): 3168-3176. DOI: 10.1016/j.jbiomech.2016.07.041.

The papers have been published under a Creative Common license, which means portions or extracts from the articles can be legally reused or reproduced after the other authors have given their consent. All the co-authors have been formally contacted by e-mail, and confirmed their agreement in reproducing text and figures from the mentioned papers within the present Thesis.

The materials presented in Appendix A are extracts from the International Vocabulary of Metrology – Basic and General Concepts and Associated Terms (VIM), 3rd edition, JCGM 200:2012 (www.bipm.org/en/publications/guides/vim.html) are published with permission of the Director of the International Bureau of Weights and Measures (BIPM), in his functions as Chairman of the JCGM.

# Chapter 1

# Introduction

## 1.1 Background

The foot is a structure made of 26 bones, 33 joints and more than 100 muscles, tendons and ligaments. Its inherent mechanical complexity provides resilience[1] and strength needed to guarantee support, balance and mobility to the whole human body [1]. Structural flaws and impairments in the foot may cause instability with consequent increasing of the risk of falls, as well as the development of secondary injuries elsewhere up the chain [2]. Traumatic ankle injuries, causing both mechanical and functional instabilities, represent a significant healthcare issue [3], which accounts for 20% of the US population treated in emergency facilities. Ankle sprains represent an estimated 3.5% of the visits, and it is of particular interest for both young athletes (80% recurrence rate) and general population (approximately the 8%), who report persistent symptoms following an initial sprain. As an example, four out of five cases of ankle joint osteoarthritis are the result of previous musculoskeletal trauma [4]. Given that the primary sprain occurs at early age, the ankle joint trauma affects the individuals across the lifespan. Statistics studies reported that a subject aged between ten and nineteen years-old is associated with the highest rate of ankle sprain; males aged between fifteen and twenty-four years old have higher rates of ankle sprain than their female counterparts, whereas females over thirty years old have higher rates than their male counterparts. It is worth highlighting that only half of the ankle sprains occur during athletic activity, whereas others occur in daily-life activities [5]. Considering injuries

[1] The attitude of a material to absorbing the mechanical energy without being deformed.

different from sprains, Achilles tendon injuries account for 30% to 50% of all injuries that are related to sports among athletes and the general population [6]. These tendinopathies are due to degenerative changes common in subjects older than 35 years and these changes are eventually associated with spontaneous fractures in 7 over 100,000 cases [7].

As additional examples of ankle impairment, chronic ankle instability caused by multiple trauma can outburst into stress fractures along the whole body, which are due to repetitive mechanical loading resulting in accumulated strain. Pathologies such as osteoarthritis, diabetes, obesity and juvenile idiopathic arthritis are of major importance for the ankle joint. It has been recently shown that loads and other mechanical factors could increase the foot and ankle damages and influence the diseases progression [8,9].

The observation of the foot-ankle complex is hence of clinical interest for all these and other pathologies. In fact, clinicians might choose the proper therapy benefitting of objective measurements of the foot-ankle complex kinematics.

Human joint kinematics is generally estimated solving mathematical models of the human body considered as a mechanical chain. Thus, an exhaustive modelling of the joints within the foot-ankle complex is relevant both to quantitatively assess its status, and to improve rehabilitation therapies [10,11].

Human movement analysis is the technique used to gather information about the mechanics (both kinematics and dynamics[2]) of the musculoskeletal system during the execution of a motor task [12], starting from the modelling of the human chain to the estimation of the model solution. More specifically, gait analysis aims to estimate the human joint kinematics and dynamics during walking, and the relevant outcomes are normally studied to discriminate between healthy patterns and the presence of any pathological alteration.

Gait analysis is typically performed measuring the instantaneous position of markers placed on the skin of the subjects by using stereophotogrammetric systems [12], and ground reactions using force plates implanted in the floor. Other applications,

[2] Often addressed as Kinetics variables in the human movement analysis. However, in the present Thesis the classical definition of mechanics was considered: the mechanics is the study of motion (kinematics) and its causes (dynamics).

such as real-life or out-door monitoring of patients call for different measurement techniques normally based on measuring accelerations and angular velocities via systems of inertial sensors [13–16], or, more recently, using markerless approaches [17–19]. In the present Thesis, only the marker-based gait analysis will be investigated, as it represents the gold standard as of today.

High repeatability and reproducibility[3] of the models (see §2.3.2 for details on how to define a model for gait analysis) potentially allow for distinguishing between physiological and pathological walking patterns, and more specifically, for observing differences in subsequent follow-up of patients. It is also worth noticing that joint dynamics is estimated starting from the inertial properties of the segments and the joint kinematics [20], and small errors in the kinematic patterns would therefore lead to higher errors in the dynamics. It is then desirable and required to define validated models to reconstruct the joint kinematics. Generally, a model is validated when its relevant outputs are precise and accurate [21,22]. An estimate is accurate when the obtained values are close to the true value of the measurand, and it is precise if values obtained by replicated measurements show acceptable variability under specific conditions for the specific aim of the measure. In gait analysis, the accuracy cannot be evaluated without using invasive techniques as the instantaneous true values of the joint kinematics need to be evaluated using fluoroscopy or fixing pins directly on the bony segments adjacent to the joint under analysis. Indeed, the markers mounted on the subjects' skin suffer from a number of intrinsic inaccuracies, which nowadays are impossible to eliminate. For this reason, talking about validation of the models used in gait analysis it is inappropriate. Reliability studies, which aim to evaluate the repeatability and the reproducibility of the model outcomes[4], are hence more often preferred and accepted by the scientific community. Thus, a model is reliable, and only incompletely validated, when the relevant joint kinematics and dynamics, gathered from healthy subjects, are repeatable and reproducible for the specific application. In particular, a good within- and between-subject repeatability of the model outcomes

[3] In the present Thesis, the terms repeatability and reproducibility are intended as defined in [22], and summarised in the Appendix A.
[4] See Appendix A for more details on the nomenclature.

potentially allows for quantifying the development of the pathological status of a patient under analysis. When this does not occur, the model results could represent wrong information for the clinicians and, possibly lead to inappropriate treatment selection. This Thesis mainly focuses on studying the human joint kinematics, without considering force measurements.

Errors in the kinematic patterns are mainly linked to:

- the instrumental errors, introduced by the instruments used to track the markers, and quantifiable comparing the output with known distances and angles [23];
- the soft-tissue artefacts (STA), i.e. relative movement between markers attached on the skin and underlying bones. Its content in the frequency domain is similar to the actual movement and it is, hence, difficult to eliminate with filtering [24];
- the marker misplacement errors, linked to the inaccurate landmark palpation, lead to misinterpretation of the joint rotation axes, and eventually to imprecise estimates of the model outcomes. This error can be estimated via between-operators analysis [25].

Each source of error, when possible, should be properly evaluated before performing any data collection, and relevant results should be used to drive the choice of the most appropriate model to be used for the specific situation that the clinicians are facing.

Many models have been proposed to quantify the movements of the foot-ankle complex [11,26–28], but some of them were not clearly described to be replicated by others [29]. Attempts of validating the existing models, both in terms of repeatability and reproducibility, have been carried out [19,30,31], but often limiting the analysis to values of the kinematics at specific instant of the gait cycle. Moreover, these analyses have never been concurrently performed, leading to an unclear understanding of the results.

## 1.2 Aim and objectives

This Thesis aims to establish a standard for the modelling of the foot-ankle complex in gait analysis. To this purpose the following progressive steps were needed, with the relevant intermediate objectives:

- The most suitable indices to assess repeatability and reproducibility of gait variables were chosen via a detailed analysis of their mathematical formulation, and their behaviour when applied on kinematic patterns with known imposed variabilities;
- The instrumental error affecting measurements of passive markers using stereophotogrammetry were quantified. Considering that good practice of using stereophotogrammetric systems calls for their regular calibrations, a methodology to quantify the effect of this procedure may have on the estimates of the joint kinematics was proposed;
- The existing models of the foot-ankle complex for gait analysis were critically studied and, having selected the most used among those proposed in literature, were concurrently compared to evaluate the repeatability and reproducibility of their results;
- Eventually, a new kinematic model of the foot-ankle complex for gait analysis was developed and analysed, and the relevant outcomes will be compared to those obtained for the existing models.

Unfortunately, within the present Thesis, the effect of the soft tissue artefact on the foot-ankle kinematics was not modelled or corrected anyhow, as literature is lacking of information on the magnitude of this error on the considered landmarks.

## 1.3 Outline of the thesis

Chapter 2 introduces techniques and tools that were used to reach the aim of this project. After giving an anatomical and historical background about the foot-ankle complex and the human movement analysis, it presents an analysis of the sources of errors linked to the use of stereophotogrammetry, and, finally, the description of some of the models currently available for gait analysis of the foot-ankle complex.

Chapter 3 describes the study aimed at determining the most suitable indices to evaluate repeatability and reproducibility of joint kinematics data.

Chapter 4 contains the analysis of the metrological quality of the measurements conducted with stereophotogrammetric systems performed on fixed distances and angles, and how relevant uncertainties affect the estimates of human joint kinematics.

Chapter 5 presents a concurrent analysis of the performances of the four most adopted models of the foot-ankle complex for gait analysis, in terms both of repeatability and reproducibility.

In Chapter 6, an innovative model of the foot-ankle complex is described and analysed. The outcomes are then compared to those obtained in Chapter 5 for the other models.

Finally, Chapter 7 presents the summary conclusions of the project, and suggests possible future developments aimed at improving the techniques used to assess the kinematics of the foot-ankle complex, and the human body chain in general.

Chapter 2

# Literature review

## 2.1 Introduction

This Chapter will present the background information needed to understand the various steps of the project. It starts presenting the anatomical definitions relative to bones, segments and joints that compose the foot-ankle complex. Getting closer to the application of movement analysis to study this anatomical district, the measurement techniques and the tools that will be used for this project will then be analysed and discussed, in terms of the sources of errors linked to both the measurement principles and the modelling techniques. The existing models of the foot-ankle complex will then be reviewed. The Chapter ends with a critical revision of the variability and similarity indices typically used to compare different joint kinematics.

## 2.2 Foot-ankle complex

The anatomical descriptions of the bones given in §2.2.1 were retrieved from [1], whereas the descriptions of the joints and the relevant rotation axes (§2.2.2) were retrieved from [32], except for the tarsometatarsal and metatarsophalangeal joints [1]. Coherently with the anatomy, within this project, only the major joints of the foot will be described and considered for modelling.

### 2.2.1 Bones and segments

In the books of Anatomy, the skeleton of the foot-ankle complex is generally described as composed by four segments: the shank, the tarsus, the metatarsus and phalanges (Figure 2.1).

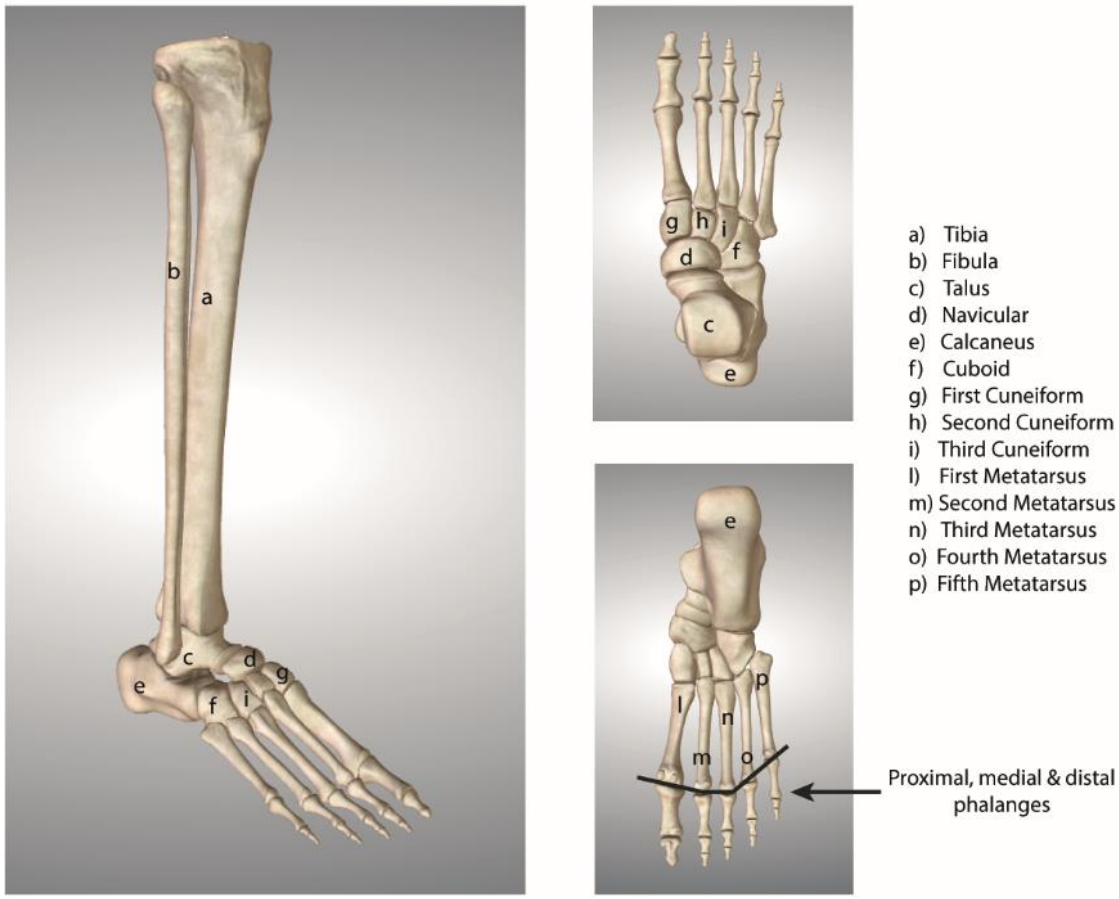


**Figure 2.1** – Skeleton of the right foot-ankle complex. This Figures has been retrieved from the Biodigital Human website (www.biodigital.com) and adapted.

### *2.2.1.1 Tibia and fibula*

The shank consists of the tibia and the fibula. The tibia is located in the middle of the leg, and is the longest bone of the skeleton after the femur. Where the tibia enters into the knee-joint, it presents an expanded above prismoid shape. The upper extremity is expanded into two protuberances, the medial and lateral condyles. The lower extremity is much smaller than the upper, and presents five surfaces, which permit the contact with the bones of the foot. The tibia is also prolonged medially and downward in the medial malleolus.

The fibula is placed laterally to the tibia, with which it is connected above and below. The fibula is smaller than the tibia, and it is the slenderest of all the long bones. Its upper extremity is small, placed backward to the head of the tibia, and downward to the knee joint, which it is excluded from. It projects below the tibia and forms the lateral part of the ankle joint. The upper extremity of the fibula has an irregular quadrate shape and presents a flattened surface directed upward, forward and medially for the

articulation with the lateral condyle of the tibia. Its lower extremity, or lateral malleolus, has a pyramidal shape and it goes down to a lower level than the medial malleolus.

#### *2.2.1.2 Tarsus*

The tarsus consists of seven bones: calcaneus, talus, cuboid, navicular, first, second and third cuneiforms. The calcaneus, the largest of the tarsal bones, is located in the lower/back side of the foot and, it allows the transmission of the body weight to the ground. It has an irregular cuboidal shape with the long axis directed forward and laterally. The talus is the second largest of the tarsal bones. It is situated in the middle and upper part of the tarsus, between the tibia and calcaneus. The cuboid is located ahead of the calcaneus and after the fourth and fifth metatarsal bones. It presents a pyramidal shape, which its tip directed medially. The navicular is placed at the medial side of the tarsus, between the talus and the cuneiform bones. Within the three cuneiform bones, the first one is the largest and the second one is the smallest. The three cuneiforms are situated in the medial side of the foot and, more precisely, the first is the outermost and the third is the innermost.

#### *2.2.1.3 Metatarsus*

The metatarsus is made of five bones which are numbered in ascending order from the medial side (first metatarsus) to the lateral side (fifth metatarsus). The hind extremity is wedge-shaped, and it is articulated with the tarsal bones in the proximal side, and its dorsal and plantar surfaces are rough permitting the ligament attachments. The former extremity is characterised by a convex articular surface. Its sides are flattened, and on each is a dip for the attachment of the ligaments. The metatarsus plantar surface permitted for the passage of the Flexor tendons.

#### *2.2.1.4 Phalanges*

The phalanges of the foot are fourteen: two in the big toe, and three in each of the other toes. They differ from the phalanges of the hand in their size since their bodies are much reduced in length, and laterally compressed. As regards the first row of phalanges, the body of each is compressed from side to side, convex above and concave below. The head shows a trochlear surface for the articulation with the second phalanx. The phalanges of the second row are small and short, but larger than the bones of the first row. The ungual phalanges are smaller and are flattened from above downward;

each presents a large base for the articulation with the reciprocal bone of the second row, and each shows a distal expanded extremity supporting the nail and the end of the toe.

## 2.2.2 Joints

### *2.2.2.1 Tibio-talar joint*

Almost without exceptions, books of Anatomy generally define the tibio-talar joint (most commonly named ankle joint) as a hinge, which implies a single rotation axis. From a literature analysis, the location of this axis appeared to be unclearly defined and many definitions of its location and inclination have been given. The most recurring definition is that the transverse axis passes through the most distal tip of the medial malleolus, runs through the talus, and passes through the outermost prominence of the lateral malleolus. Other definitions identify different points on the surfaces of the malleoli (lateral and medial) for the axis to pass through, defining not perfectly horizontal axes whose obliquity depends hence on the considered points. However, all the definitions agree that this axis is horizontal when projected onto the frontal plane. The trochlea of the talus shows differences of its typical wedge-shape from individual to individual. The wedge-shaped trochlea is hence considered as a major obstacle for the definition of a unique horizontal rotation axis together with the instable shape of its housing: i.e. the space between the malleoli, which even lie on horizontal planes at different height from the floor. The lateral malleolus is also part of the tibia, whereas the medial malleolus is part of the fibula. Altogether, this factors lead to a relative movement of bones and changes in the configurations of the ankle joint, which impede a unique definition for its rotation axis. Indeed, during dorsiflexion, a slight displacement of the lateral malleoli can be perceived as lateral displacement or bending, from 0 to 2 mm. Since the rotation axis is hardly defined, the range of motion of the tibio-talar joint was not assessed as it strongly depends on the axis itself.

### *2.2.2.2 Subtalar joint*

The talus plays a unique role in the functional anatomy of the lower extremity. The ankle joint constitutes its proximal connection to the leg and the subtalar joints (or talocalcaneal joint) is its distal connection to the foot. Differently from tibio-talar joint, the joint between talus and calcaneus is defined by a single helical oblique axis, due also

to the presence of the navicular and the cuboid. Its inclination widely varies between individuals, can be reasonably approximated to an average of 42°, but ranging from 22° to 68°. In general, the axis extends from the neck of the talus downward and laterally through the sinus tarsi and emerges on the lateral side of the calcaneus.

It is appreciated that the movement of the talus produces important and definitive effects upon the foot through its distal articulation with the navicular. In fact, being the subtalar joint the connection between leg and foot, the oblique configuration of its rotation axis imposes longitudinal rotation of the foot (pronation and supination) when the leg longitudinally rotates. Moreover, the subtalar joint has been described as a "skrewlike" joint in many Anatomy books, indicating that together with the rotation along the oblique helical axis, some subjects might display a displacement between the subtalar bones. Studies conducted on cadaver specimens and living subjects assessed with conventional goniometers have shown the range of motion of the subtalar joint to vary markedly within the population (from 10° to 60°).

#### *2.2.2.3 Tarsometatarsal joint*

This joint consists of the first, second, and third cuneiforms, and the cuboid, articulating with the bases of the five metatarsal bones. The first cuneiform articulates with the first metatarsal bone. The first and third cuneiform create the housing for the second cuneiform, which then articulates with the base of the second metatarsal bone. The third cuneiform articulates with the base of the third metatarsal. A portion of the third cuneiform and the cuboid articulate with the base of the fourth metatarsal bone. The most lateral and frontal portion of the cuboid articulates with the base of the fifth metatarsal. Between tarsal and metatarsal bones only limited sliding movements are permitted.

#### *2.2.2.4 Metatarsophalangeal joint*

The metatarsophalangeal articulations can be thought of as hinge joints, which are given by the interaction of the distal rounded head of the metatarsals and the proximal cavities of the first phalanges' base. The metatarsophalangeal joints allow plantar/dorsiflexion and ab/adduction movements.

## 2.3 Gait analysis

Interest in observing the human movements has born when arts were the only expression of such an observation [33]. The medical doctor Giovanni Alfonso Borelli (1608-1679), instructed by Galileo Galilei, was the first to apply the scientific method to the analysis of the human movement, attempting to "quantify" the movement with all the limitations linked to the knowledge of the XVII century (*De motu animalium*, 384-322 b.C.). In the XIX century the human body was started to be thought of as if it was a machine to be used to work (*Machine Animale*, Etienne Jules Marey 1873), or fight (*Moteur Humain*, Jules Amar 1904). The technological development of this century helped improving theories and techniques to assess the human movement. For example, it is worth mentioning the sensitive photographic material developed by Muybridge (1878) to observe horses' movement, or the analytical sterophotogrammetry used by Braune and Fisher [34]. Only in the first half of the XX century, the human movement has started to be studied focusing on the hidden structure of the human body (i.e. the skeleton). The *locomotor apparatus* was represented as a series of linked sticks (the *stick* diagram, 1914) in order to attempt observing the actual movement of the kinematic chain, but without the actuators (the muscles) and the envelop (the skin).

With the growing of the technologies, the ability to objectively quantify the movement increased, and it has been integrated with force measurements to characterise not only the kinematics, but also the dynamics involved in the movement (i.e. joint moments, and powers[5]). The analysis of the human walking is most commonly called gait analysis, and is the instrument used to quantify the performances of subjects, who are asked to walk under certain conditions, either affected or not by pathologies. Figure 2.2 shows a typical human movement analysis laboratory.

[5] Often addressed as Kinetics variables in the human movement analysis. However, in the present Thesis the classical definition of kinetics was considered: the kinetics is the study of motion (kinematics) and its causes (dynamics).


**Figure 2.2** – The movement analysis laboratory at The University of Sheffield (UK).

Alternative techniques to measure the joint movements have emerged, such as the Magneto-Inertial Measurement systems [13–16] or markerless based video systems [17,35–37], but nowadays the most consolidated movement analysis technique is still based on tracking the 3D position of markers attached to the skin of the subjects. This approach, known as marker-based stereophotogrammetry, will be detailed in the following paragraphs, starting from the measurement system and its inherent sources of errors (§2.3.1). Subsequently, the typical modelling techniques of the human body used in gait analysis (§2.3.2), and needed to transform marker coordinates in joint estimates will be described. The limitations proper of a marker-based approach for human movement analysis will be eventually discussed (§2.3.2.5).

## 2.3.1 Stereophotogrammetric systems

Stereophotogrammetry is a technique used to reconstruct three-dimensional coordinates of points from two-dimensional photographs, radiographs and video images via specific algorithms. Video-based stereophotogrammetry reduces potential image distortions, it is a non-invasive methodology, and it is less time consuming compared to the above mentioned techniques [23]. Two or more point of view are needed for the reconstruction of three-dimensional coordinates of a point. Thus, two or more cameras looking at the same point, with their associated solid 3D reference coordinate system (3D-CCS), are needed to reconstruct the spatial coordinates of that point. These coordinates measured in the 3D-CCS are projected in the 2D image planes of each camera, which another reference coordinate system is associated with (2D-ICS). An

algorithm then reconstructs the 3D position of the points starting from their coordinate in the 2D-ICSs, and solving a system of equations, function of the internal (or inner, or intrinsic) and the external (or extrinsic) parameters [38]. The internal parameters define the distortions imposed to the images by imperfections linked to lenses materials or assembly. For example, the radial distortion is due to impurities in the lens material, or misalignment between lens and optical axes of the camera. The relative pose between the cameras, and the pose of each camera relative to a global reference system (GCS) are instead considered as external parameters. In order to accurately reconstruct the 3D position of a set of points using stereophotogrammetry, the systematic errors need to be reduced. This means that both the internal and external parameters need to be accurately and precisely estimated via the so-called *Calibration procedure*.

#### *2.3.1.1 The Calibration procedure*

The calibration of a generic measurement instrument is defined as the "operation that, under specified conditions, in a first step, establishes a relation between the quantity values with measurement uncertainties provided by measurement standards and corresponding indications with associated measurement uncertainties and, in a second step, uses this information to establish a relation for obtaining a measurement result from an indication" in [22]. The principle is exactly the same in stereophotogrammetry, where known inputs are given to the stereophotogrammetric system to allow the calibration algorithm estimating both internal and external parameters, and defining a GCS. Subsequently, the same parameters are used to reconstruct unknown 3D coordinates of a set of points relatively to that GCS [23]. Historically, many calibration techniques have been proposed for stereophotogrammetric systems and they can be stratified as follows [39]:

- *Direct non-linear minimisation*: an iterative algorithm estimates the parameters minimising the objective functional built on the residual errors of target points placed in known positions. This method being iterative, the final solution strongly depends on the initial condition, and when considering image distortions, the algorithm could lead to instability of the solution.
- *Linear systems with closed-form solution*: parameters are directly estimated from a system of equations, which however do not consider the image distortions. An example of algorithm that used this approach was the Direct

Linear Transformation (DLT) proposed in [38], which was based on the linear modelling of the used cameras, and it has been also corrected accounting for some image distortions.

- *Two-steps method*: fusing the first two kind of algorithm, some parameters are directly estimated from a system of equations solved in a closed-form, and some others via an iterative algorithm. Examples of these algorithm are those proposed in [40,41].

Many calibration methods classified in this last category have been proposed in the past [39,42], but the pioneers of the algorithms at the basis of today's algorithms are Dapena *et al.* whose algorithm allowed calibrating the stereophotogrammetric systems by inspecting the calibration volume moving a rigid rod equipped with markers [43]. Similarly, nowadays, most of the commercial systems require the operator to perform the calibration by moving a calibration device equipped with markers, placed at known distances between each other, within the calibration volume.

#### *2.3.1.2 Sources of uncertainties and their assessment*

The stereophotogrammetry, as partially said, leads to measurements affected by different sources of uncertainties. In particular, it has been found to be dependent on: the number and position of the cameras [44], their lens distortion [39], the dimension of the capture volume [45,46] and, last but not least, the algorithms used for the reconstruction of the 3D-position of the markers [38], §2.3.1.1.

In the past years, many solutions have been proposed to quantify the measurement errors associated with measuring coordinates, distances, and angles between points or set of points with a camera-based approach. All of them had in common the comparison of the measurements obtained via stereophotogrammetry and via a conventional instrument considered as golden standard. For example, the measurement error on estimating fixed angles between markers has been quantified by placing retroreflective markers on a goniometer that is then placed in different zones of the capture volume [45,47]. The measurement error was given by the difference of the measured angles via stereophotogrammetry and the goniometer, considered as golden standard. More recently, a T-pendulum has been designed for a similar purpose, and it has been shown that increased angular velocities of the pendulum led to decrement of the accuracy of measuring angles [48]. Shifting the problem closer to the human

movement analysis, the 'walking test' [49,50] aimed at evaluating the error of measuring distances between points on a rigid aluminium bar held by a subject, who was asked to walk at a self-selected speed within the capture volume. Eight stereophotogrammetric systems were tested with this procedure, and the system that produced the least noisy measurements exhibited the best performances. Subsequently, the Movement Analysis Laboratory (MAL) test has been proposed [51], which is based on recording the position of a rod carrying a two-marker cluster, manually rotated around its tip either following a pseudo circle or two orthogonal arches. This test allowed quantifying both precision and accuracy associated with measurements conducted via stereophotogrammetric systems.

Besides all these methods are useful to quantify the uncertainties associated with static and dynamic measurements of the coordinates of points, they can be applied to measurement systems ready-to-be-used and, thus, do not consider the possible effect that the calibration procedure might have induced in the metrological performances. Indeed, as described in the previous section (§2.3.1.1), the reconstruction of the 3D position of a set of points strongly depends on the calibration procedure, which depends on how the operator performs the phases of the calibration (i.e. how he waves the calibration object within the volume, the velocity imposed to the calibration object, etc.). To this purpose, in [44] a *xy*-robot has been developed to perform repeatable dynamic calibration procedures, and also impose trajectory to a cluster of markers and perform an accuracy and precision analysis. The robot consists of:

- A servo-motor-driven sliding carriage configuration;
- Three orthogonally arranged axes with *built-in* linear encoders;
- A cluster of four passive markers arranged in a *L*-shape;
- A cardanic joint that allowed free oscillation of the cluster.

A $180 \times 180 \times 150$ mm$^3$ volume was analysed. After having calibrated the stereophotogrammetric system using the *L*-shape cluster as calibration object, the robot placed the marker in a grid of points uniformly distributed within the considered volume. The same protocol was repeated several times testing different calibrations and different configurations for the three considered cameras. Accuracy and precision associated with the marker tracking were calculated for each coordinate direction. Despite the interesting approach of testing different calibration procedures performed by the robot, the results cannot be extended to the human movement analysis field. In

fact, the dimension of the tested volume was not comparable with those normally considered for human movement analysis, and three cameras are not sufficient for a clinical scenario, where patients are asked to walk in a comfortable manner, without altering how they are walking to be perfectly visible by the system. Thus, the effect that different calibrations might have on the metrological performances of the stereophotogrammetric systems in a human movement analysis scenario is still unclear.

#### *2.3.1.3 A preliminary study on metrological performances of stereophotogrammetric systems*

This paragraph presents a preliminary study conducted before developing the methodology proposed in Chapter 4. Part of the contents of this paragraph have been published as part of a scientific paper [52], published under a Creative Common license. Written permission to reuse this material has been obtained from the authors.

##### *2.3.1.3.1 Methods*

The performances of a stereophotogrammetric system (Vicon system MX-series, 8 cameras, Vicon Motion Systems, Oxford – UK), installed at the Movement Analysis and Robotics Laboratory of the Children Hospital 'Bambino Gesù' (Palidoro, Rome IT), were tested. The capture volume (2.4 x 3.6 x 1.6 $m^3$) was initially divided into twelve sub-volumes (1.2 x 1.2 x 0.8 $m^3$), six at the floor level and six immediately above (high level), see Figure 2.3. The calibration procedure was performed waving the 5-markers calibration object within each sub-volume and the whole volume. Thus, a total of 13 calibration files have been saved.

A 1 m length rod equipped with a reflective marker was manually moved up and down within the overall volume by an operator. The 3D trajectory of the marker was reconstructed using the software provided by the system manufacturer (Vicon Nexus 1.8.5, Vicon Motion Systems, Oxford – UK), but considering each of the 13 calibration files. In order to evaluate the effect of camera redundancy, the calibration files were modified to consider five different camera configurations: the first using all the eight cameras (all-camera test) and the other four using only three cameras at a time (3-camera test), since three is the minimum number of cameras to be used recommended by the manufacturer.

The error induced by the different calibrations was evaluated with two indices. The first quantifies the effect of camera redundancy and configuration, and is the root

mean square of the difference between the trajectory reconstructed using the calibration file obtained with the *i*-th '3-camera' configurations and the 'all-camera' configuration assumed as reference ($RMSE_C$). The second index quantifies the effect of varying the calibration volume, and is the root mean square of the difference between the trajectory reconstructed using the calibration file obtained with the *j*-th sub-volume and the whole volume assumed as reference ($RMSE_V$).

Significant differences in the indices' values were evaluated via a two-way ANOVA (13 x 5, i.e. volumes x camera configurations) ($p$ = 0.05). Tukey tests were considered as *post-hoc* test with the same significance.

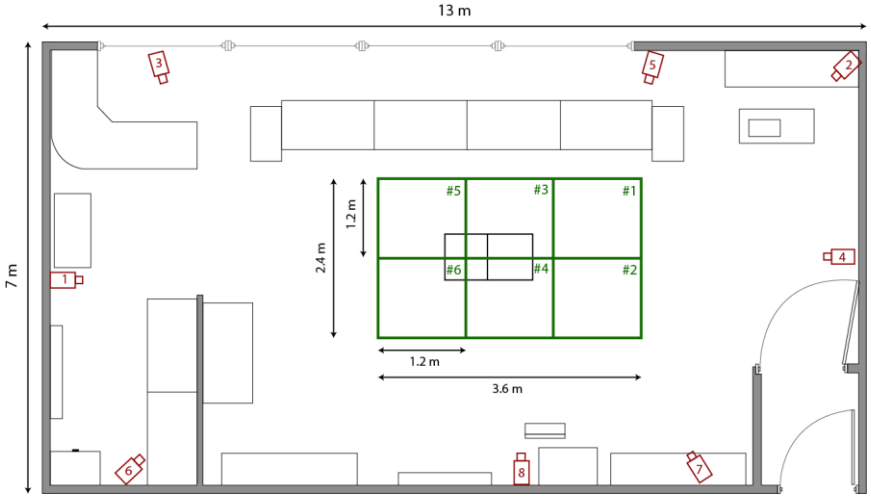


**Figure 2.3** – Plant of the Movement Analysis and Robotics Laboratory of the Children Hospital 'Bambino Gesù' in Palidoro. The green numbers marked the label for the volume at the for level, whereas the red numbers are the label for the Vicon cameras. This Figure is reproduced as published in [52] with permission of co-authors.

### *2.3.1.3.2 Results and Discussion*

Figure 2.4 shows the marker trajectory reconstructed using one of the calibration files obtained for a '3-camera' configuration and four different calibration sub-volumes, which are highlighted by a cube in the figure. Figure 2.5 shows instead the trajectory reconstructed using one of the calibration files associated with a sub-volume calibration and four different '3-camera' configurations. In both cases the line width is sample by sample equal to the RMS between the trajectory reconstructed with the selected calibration file and the relevant reference. Changing the camera configuration or the calibration volume, portions of the reconstructed trajectory could be unavailable. This is most likely due to the algorithm used to reconstruct the 3D trajectory, which probably did not find a unique position for the marker (§2.3.1.1). In fact, the calibration parameters depend on the calibration, and the trajectory reconstruction might depend

on the volume. Differently from what expected, the trajectory reconstruction is not more accurate in the sub-volume which the calibration was performed in, suggesting

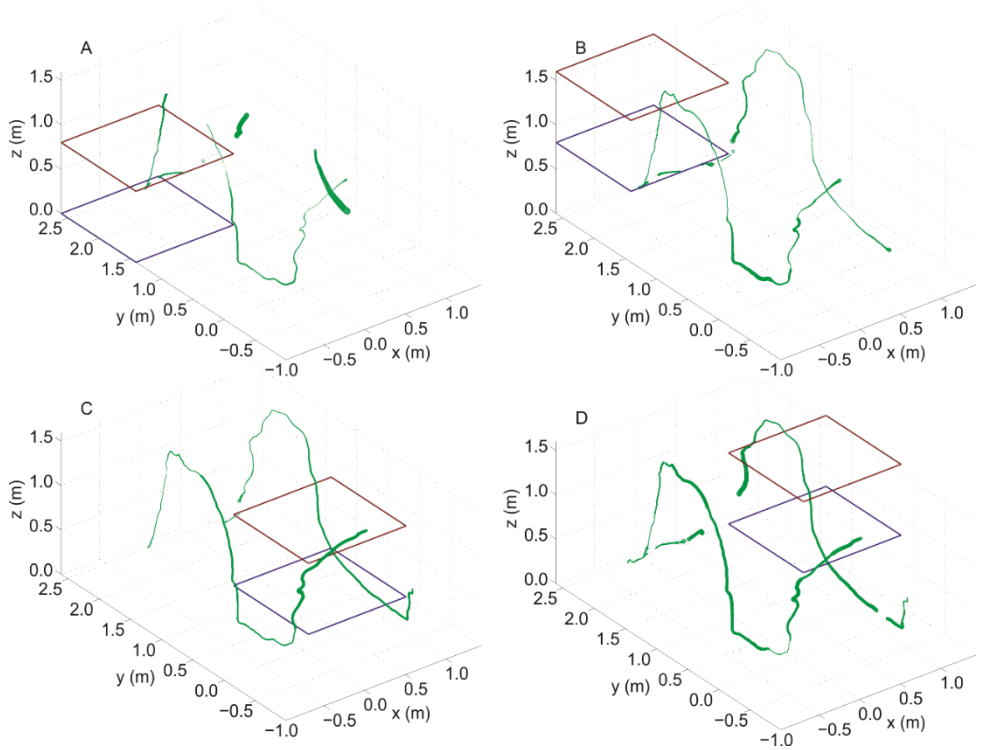


**Figure 2.4** – Marker trajectory reconstructed using different calibration files: same set of cameras, the blue and red planes in each subfigure highlight the considered calibration volume (A) 1 at floor level, (B) 1 high level, (C) 4 floor level, and (D) 4 high level. This Figure is reproduced as published in [52] with permission of co-authors.

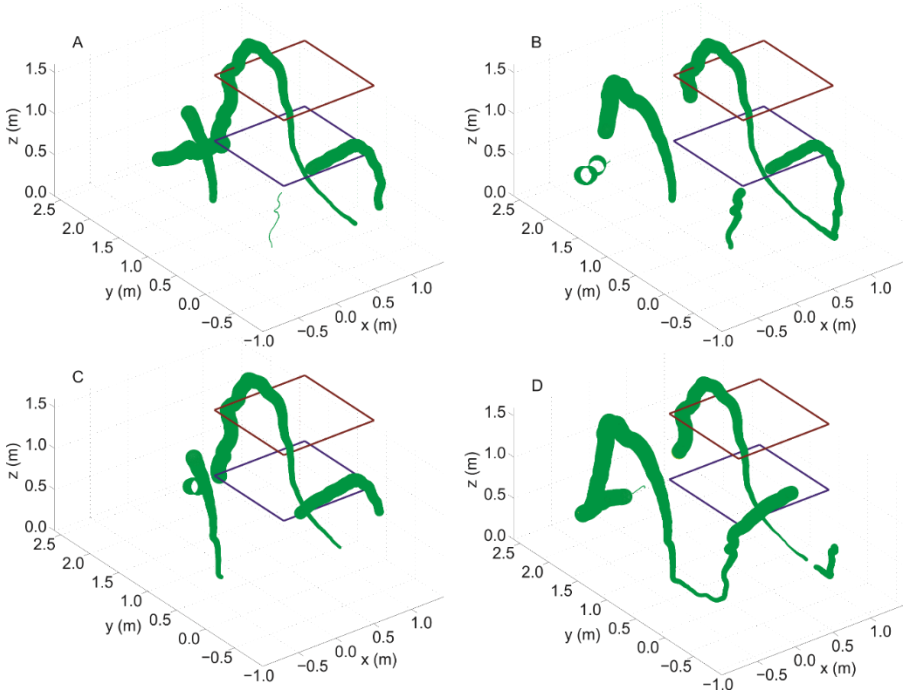


**Figure 2.5** – Marker trajectory reconstructed using different calibration files: same calibration volume highlighted by the blue and red planes in each subfigure (number 4 at high level) and (A) cameras number 1-3-5, (B) cameras number 2-4-5, (C) cameras number 3-4-6, and (D) cameras number 1-2-7. This Figure is reproduced as published in [52] with permission of co-authors.

that the calibration is not linked to the marker reconstruction accuracy. This is in contrast with the literature [44], and further investigation are worth implementing.

Considering the whole calibration volume, the averaged $RMSE_C$ was equal to 3 mm (max value 9 mm). Considering the 'all-camera' configuration and different calibration volumes, the averaged $RMSE_V$ was equal to 17 mm (max value 43 mm). The obtained results showed that the higher the number of used cameras, the lower the measurement error is. Moreover, considering the 'all-camera' configuration, $RMSE_V$ decrease from a maximum of 30 mm for the boundary sub-volumes to a minimum value of 6 mm for the whole calibration volume.

Both for $RMSE_C$ and $RMSE_V$, the two main effects gave significant differences ($p < 0.01$). The post-hoc test revealed significant differences between the trajectories reconstructed with calibration files obtained from: the sub-volume calibration and the whole volume ($p < 0.01$); and the '3-camera' and 'all cameras' configuration ($p < 0.01$). However, whether these errors are negligible or not when using stereophotogrammetric systems for human movement analysis is still not clear and further investigations are needed.

### 2.3.2 Modelling the human kinematic chain

In the anatomical literature, a movement can be completely described using terms that define position of segments (i.e. proximal or distal segments), or their rotation around joint axes relatively to other segments. In human movement analysis, the joint movements are described similarly but starting from their absolute position in space, which can be measured or estimated. Since the actual movement of a joint occurs at the skeleton level, the segments that need to be tracked are the bones, without considering muscles, tendons, blood vessels, nerves, and skin. Thus, to actually measure the movement (either absolute or relative) of the bones, techniques such as fluoroscopy, or radiograph-based stereophotogrammetry, or marker-based stereophotogrammetry, with the markers placed directly on the bones by using pins, have to be applied. Alternatively, indirect and non-invasive methods allow estimating the bone movements measuring quantities needed to solve a mathematical model that links those quantities to the bones kinematics. The most consolidated techniques used for this purpose consist of measuring trajectories of points (skin marker-based stereophotogrammetry) [12], or acceleration and angular velocities [13]. Once the quantities have been measured, and

the biomechanical model has been defined, the bones and joint kinematics are obtained solving the *inverse kinematics problem*: i.e. the solution of the model having imposed the measured quantities.

On the other hand, in the past twenty years different and more advanced techniques have been developed to model the musculoskeletal system as composed by bones and joints, which muscles and tendons are attached to and work as actuators of the kinematic chain [53,54]. Bones, joints, muscles and tendons' geometries that compose the musculoskeletal models can be either generic geometries (gathered by averaged shapes obtained studying standard populations), or obtained from imaging exams (e.g., magnetic resonance imaging or axial computer tomography) from the subject to be modelled. When the model is built, the kinematic chain is normally driven using motion data, whose time-laws together with inertia properties of the segments are the input for the solver algorithm of the inverse kinematics and dynamics problems.

#### *2.3.2.1 Marker-based gait analysis*

The analysis of the human movements during gait based on stereophotogrammetry calls for the use of markers, either active (LED-light emitting) or passive (known as retroreflective markers), placed on the skin of the subjects under analysis. Passive markers are usually plastic spheres or hemispheres covered with a retroreflective tape for IR lights, which is emitted by the array of LEDs placed around the camera objectives. Markers are usually placed on the protuberances of the bones (*anatomical landmarks*), which are recognised by palpation performed by an expert technician. With the simplifications inherent of a modelling approach, the markers are considered solid with the bones to be tracked, and the bony segments are considered non-deformable (rigid bodies), which the principles of the Classical Mechanics can be applied to. When the position of at least three markers is measured by a stereophotogrammetric system, it is possible to define the local embedded coordinate system (ECS) of the bony segment relatively to the global coordinate system (GCS), which the markers are measured in [12,55] (Figure 2.6). The opportune places on the bones for the markers are regulated by the chosen biomechanical model. Considering the gait analysis, a lot of different models are available in literature, such as the Davis' model [56], or its modified version proposed by Vicon (Oxford, UK), or the CAST and others listed in [57]. It is worth highlighting that, according to all these models, the lower

limbs are composed of the pelvis, the two thighs, the two shanks, and the two feet, considered as rigid segments. This last simplification is deeply examined in the section §2.5. The International Society of Biomechanics has proposed a standard for the definition of the landmarks to be palpated for hip, ankle ,spine, shoulder, elbow, wrist and hand, as well as the definition of the relevant coordinate axes of the local ECSs [58,59].

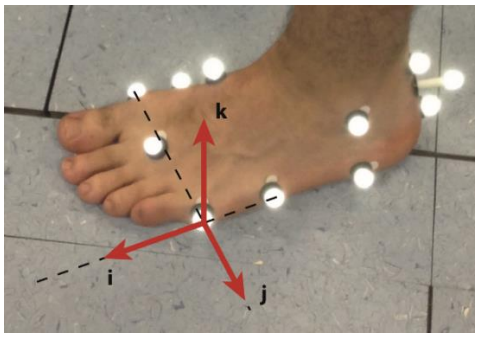


**Figure 2.6** – Example of local embedded coordinate system (ECS) build from skin markers.

The ECSs can be classified as technical or anatomical. The former is an auxiliary system, which is tracked using *technical markers* (i.e. placed on the bony segments, but not necessarily on specific landmarks). The anatomical ECS can be coincident with the technical one, and in this case the technical markers coincide with the *anatomical markers*. Anatomical ECSs mainly differ from technical ECSs for the requirement of being defined with their planes approximating frontal, transverse and sagittal anatomical planes (Appendix B), which the joint kinematics are normally defined on [12]. In case the use of both technical and anatomical ECSs is required, a procedure called *anatomical calibration* allows registering the anatomical landmarks relatively to their technical ECSs. Subsequently, the anatomical landmarks are projected onto the GCS via the technical ECSs. Finally, the local anatomical ECSs can be referenced to the GCS. When only anatomical markers are palpated, the local ECSs are already defined with the coordinate axes and planes approximating joint rotation axes and anatomical planes, and no further calibration is required.

Defining an ECS with respect to a generic coordinate system, in this case the GCS, mathematically means to write the relevant 4 x 4 homogenous transformation (or pose) matrix built as follows:

$$ {}^{0}\mathbf{H}_{1} = \begin{bmatrix} {}^{0}\mathbf{i}_{1} & {}^{0}\mathbf{j}_{1} & {}^{0}\mathbf{k}_{1} & {}^{0}\mathbf{o}_{0,1} \\ \mathbf{0} & & & 1 \end{bmatrix} = \begin{bmatrix} {}^{0}\mathbf{R}_{1} & {}^{0}\mathbf{o}_{0,1} \\ \mathbf{0} & 1 \end{bmatrix} \qquad \text{(Eq. 2.1)} $$

Where, considering only the first three rows, the first three columns represent the rotation matrix between the coordinate system **ECS**$_1$ defined in the **GCS** (indicated with the superscript zero)[6], whereas the last column is the translation vector from the origin of the **GCS** to the origin of the **ECS**$_1$ defined in the **GCS**. The rotation matrix ${}^0\mathbf{R}_1$ is composed, per columns, by the unity vectors of **ECS**$_1$ defined in the **GCS**. Using the properties of the pose matrices, relative pose and thus rotations between two adjacent coordinate systems can be calculated. The outcomes of these variables are the estimate of the joint angles between the two relevant body segments. Figure 2.7 provides an example of a typical representation of kinematic variables in gait analysis: each variable is given in degrees, and is normalised over the percentage of the gait cycle, which is defined as the time between two subsequent heel strikes[7] of the same foot (Figure 2.8).

As said, the minimum number of markers needed to build a pose matrix is three, but no constraints are theoretically imposed as upper limit for the number of the points to be tracked to define a pose matrix of a bony segment. However, the mathematical approach to define the ${}^0\mathbf{H}_1$ changes based exactly on this information. The following paragraphs present the non-optimal approach, i.e. some of the information are discarded, and the least-square fitting approach, which uses all the measured information minimising an objective functional based on error residuals of each point.

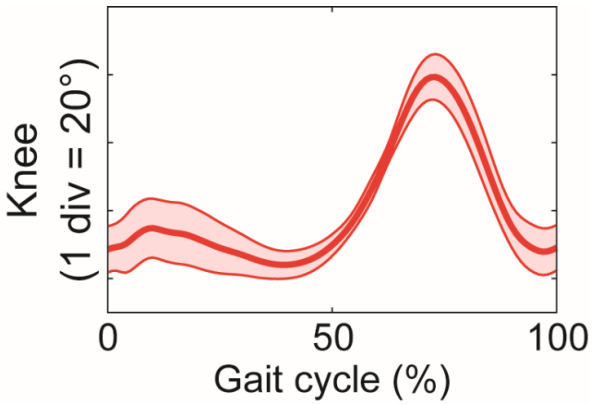


**Figure 2.7** – Example of knee joint kinematics estimated normalised over the percentage of the gait cycle.

[6] Bold font has been used for GCS and ECS to address the matrix notation, differently from per above, where no matrices but the concepts of global and embedded coordinate systems were expressed.
[7] Instant in which the heel starts being in contact with the floor during walking.

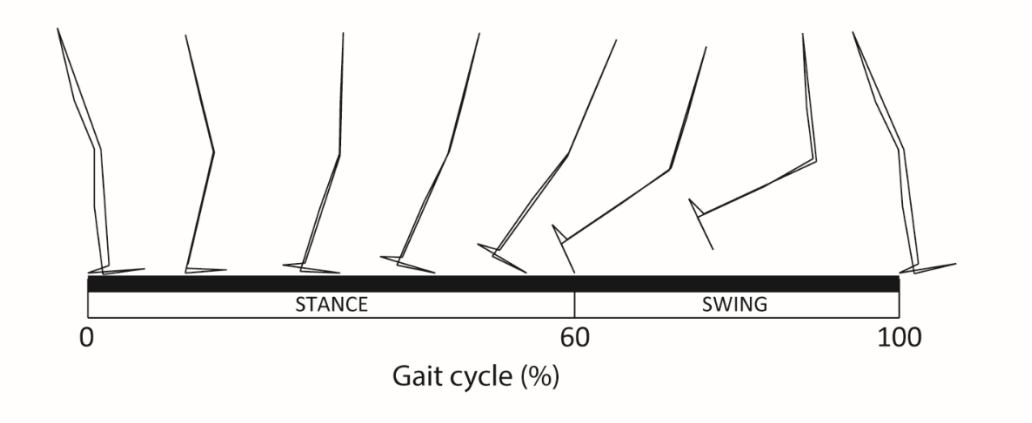


**Figure 2.8** – Gait cycle phases [60].

### *2.3.2.2 Procedures and algorithms*

Both presented approaches are based on the hypothesis of rigid body, which means that points measured on a segment are time-invariant relatively to the local **ECS**. This means:

$$\begin{bmatrix} {}^{0}\mathbf{P}_i(t) \\ 1 \end{bmatrix} = {}^{0}\mathbf{H}_1(t) \begin{bmatrix} {}^{1}\mathbf{P}_i \\ 1 \end{bmatrix} \qquad \text{(Eq. 2.2)}$$

Where $\mathbf{P}_i$ are the points defined in the $\mathbf{ECS}_1$ (left superscript 1) and **GCS** (left superscript 0). The left hand side of the equation and the pose matrix are time dependent, whereas the points defined in the local $\mathbf{ECS}_1$ do not change with time. Both procedures are reported as described in [12,61,62]. This condition is clearly a simplification of the reality, where random experimental errors add noise to the measurements, and the bones are not rigid, but are prone to compression even though with high stiffness.

#### *2.3.2.2.1 Non-optimal approach*

When the subject has been instrumented with the markers accordingly to the chosen model, this approach is the easiest to use, both from a theoretical and computational point of view. Indeed, having measured the coordinates of three points, the **ECS** is defined when the following entities are defined: a coordinate axis, a coordinate plane that contains that axis and another point, and the origin that coincides with either a point, or the center of gravity of sub-set of the measured points. For example, having measured three points ${}^{0}\mathbf{A}$, ${}^{0}\mathbf{B}$, and ${}^{0}\mathbf{O}_1$ with respect to the **GCS** (Figure 2.9), the $\mathbf{ECS}_1$ is defined as follows:

- the unity vector ${}^{0}\mathbf{i}_1$ is defined by the line joining ${}^{0}\mathbf{O}_1$ to ${}^{0}\mathbf{A}$;

- the plane ${}^0\mathbf{i}_1\mathbf{j}_1$ contains ${}^0\mathbf{i}_1$ and the point ${}^0\mathbf{B}$;
- the origin coincides with the point ${}^0\mathbf{O}_1$.

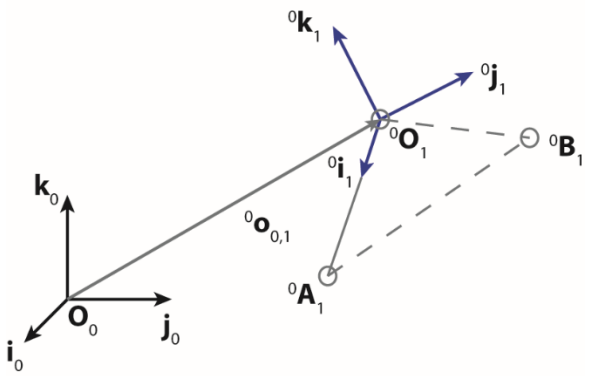


**Figure 2.9** – Example of rigid embedded coordinate system (**ECS**) associated with a segment, and defined by three markers, which position are measured with respect to the global coordinate system (**GCS**).

Following the given definitions, the unity vectors and the position vector (${}^0\mathbf{o}_{0,1}$) that univocally define the **ECS**$_1$ with respect to the **GCS**, and to be placed in the (Eq. 2.1) are:

$$\begin{cases} {}^0\mathbf{o}_{0,1} = {}^0\mathbf{O}_1 - \begin{bmatrix} 0 & 0 & 0 \end{bmatrix}^T \\ {}^0\mathbf{i}_1 = \dfrac{{}^0\mathbf{A} - {}^0\mathbf{O}_1}{\left\| {}^0\mathbf{A} - {}^0\mathbf{O}_1 \right\|} \\ {}^0\mathbf{k}_1 = \dfrac{{}^0\mathbf{i}_1 \times \left( {}^0\mathbf{B} - {}^0\mathbf{O}_1 \right)}{\left\| {}^0\mathbf{i}_1 \times \left( {}^0\mathbf{B} - {}^0\mathbf{O}_1 \right) \right\|} \\ {}^0\mathbf{j}_1 = {}^0\mathbf{k}_1 \times {}^0\mathbf{i}_1 \end{cases} \quad \text{(Eq. 2.3)}$$

The accurate estimation of the pose of a rigid bony segment from the measured position of three markers attached to the skin (or a number of markers reduced to three points within the 3D space via geometrical rules) is limited mostly by the relative motion between the markers and the bone (see §2.3.2.5) [63]. Despite being affected by not negligible inaccuracies, this approach is accepted by the biomechanical scientific society and is used in models such as the Davis, or the Plug-in-Gait (commercial version proposed by Vicon, Vicon Motion Systems – Oxford Metrics, Oxford, UK) [56], and those proposed in [64–69].

### *2.3.2.2.2 Least-square fitting approach*

This approach uses the redundancy of information to minimise the effect of random errors on the definition of the ECSs. Thus, differently from the first approach that can be applied both in static and in walking conditions, this methodology calls for two steps of data collection. Firstly, the subject is instrumented with the markers and asked to stay still for a few seconds. The non-optimal approach is then applied to register the local ECSs. Using the relevant pose matrix, points can be expressed in the local ECSs:

$$\begin{bmatrix} {}^{1}\mathbf{P}_i(t) \\ 1 \end{bmatrix} = {}^{1}\mathbf{H}_0(t) \begin{bmatrix} {}^{0}\mathbf{P}_i(t) \\ 1 \end{bmatrix} \quad \text{(Eq. 2.4)}$$

The hypothesis of time-invariance for the measured marker coordinates defined in the local frames, and the instrumental error modelled as additive white noise allow writing the (Eq. 2.4) as follows:

$$\begin{bmatrix} {}^{0}\mathbf{P}_i(t) \\ 1 \end{bmatrix} = {}^{0}\mathbf{H}_1(t) \begin{bmatrix} {}^{1}\mathbf{P}_i \\ 1 \end{bmatrix} + \begin{bmatrix} {}^{0}\mathbf{e}_i(t) \\ 1 \end{bmatrix} \quad \text{(Eq. 2.5)}$$

If an adequate high number of measurement is registered, the average of the instrumental error is zero, the points defined in **GCS** are an estimate of a free-of-error measurement, and the points defined in **ECS**$_1$ are "time-invariant":

$$\begin{bmatrix} {}^{0}\hat{\mathbf{P}}_i(t) \\ 1 \end{bmatrix} = {}^{0}\mathbf{H}_1(t) \begin{bmatrix} {}^{1}\mathbf{P}_i \\ 1 \end{bmatrix} \quad \text{(Eq. 2.6)}$$

Those "time-invariant" points estimated in their local ECSs, together with the marker coordinates collected during a dynamic trial (the subject is asked to move) are the inputs for the least-square algorithm that solves the local ECS definition.

Both during static and dynamic conditions, points should verify the hypothesis of being time-invariant with respect to the local systems. Thus, considering two configurations of the same body with the same cluster of measured markers (Figure 2.10), the rotation matrix between these two configurations can be found minimising the position residuals defined starting from the measured marker coordinates defined in the **GCS** in dynamic configuration, and its estimated true value in the local **ECS**$_1$ that is ${}^{1}\mathbf{P}_i$ in (Eq. 2.6).

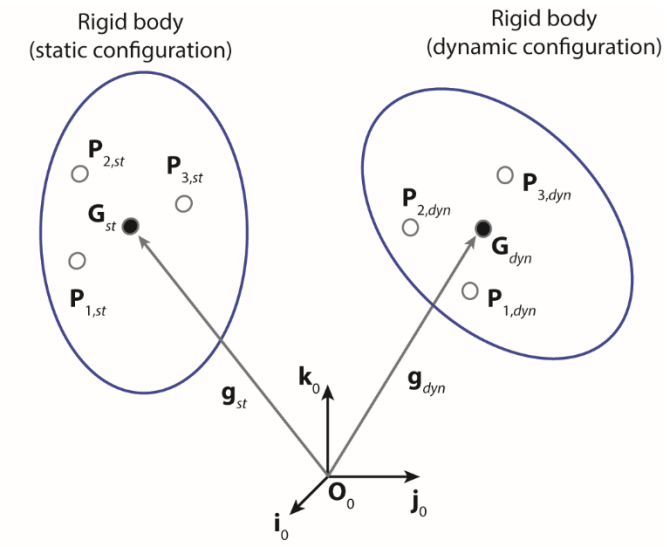


**Figure 2.10** – Example of measurement of the same cluster of markers ($\mathbf{P}_i$) placed on a generic rigid body, both in static and dynamic configurations. The centre of gravity is indicated with $\mathbf{G}$, and its position vector with $\mathbf{g}$.

The objective functional to be minimised is the sum of the squared modulus of each position residual:

$$f(\mathbf{R}) = \sum_{i=1}^{n} \mathbf{e}_i^{\mathrm{T}} \mathbf{e}_i = \sum_{i=1}^{n} \left|\mathbf{e}_i\right|^2; \;\; \mathbf{e}_i = \mathbf{P}_i - \hat{\mathbf{P}}_i \qquad \text{(Eq. 2.7)}$$

The position residuals can be expressed considering the center of gravity (**G**) of the cluster of points, and the position vector of each point relative to **G** in static and dynamic condition:

$$\begin{aligned} &\mathbf{e}_i = \mathbf{P}_{di} - \hat{\mathbf{P}}_{di} = \\ &= \left(\mathbf{p}_{di} + \mathbf{G}_d\right) - \left(\hat{\mathbf{p}}_{di} + \mathbf{G}_d\right) = \\ &= \left(\mathbf{p}_{di} + \mathbf{G}_d\right) - \left({}^{d}\mathbf{R}_s \cdot \mathbf{p}_{si} + \mathbf{G}_d\right) \end{aligned} \qquad \text{(Eq. 2.8)}$$

Which is:

$$\mathbf{e}_i = \mathbf{p}_{di} - {}^{d}\mathbf{R}_s \cdot \mathbf{p}_{si} \qquad \text{(Eq. 2.9)}$$

The objective functional is then:

$$f(\mathbf{R}) = \sum_{i=1}^{n} \left(\mathbf{p}_{di}^{\mathrm{T}} - \mathbf{p}_{si}^{\mathrm{T}} {}^{d}\mathbf{R}_s^{\mathrm{T}}\right)\left(\mathbf{p}_{di} - {}^{d}\mathbf{R}_s \mathbf{p}_{si}\right) \qquad \text{(Eq. 2.10)}$$

Considering the general term of the (Eq. 2.10), and that ${}^{d}\mathbf{R}_s$ is an orthonormal matrix and its transpose coincides with its inverse matrix, the parenthesis product gives:

$$\begin{aligned}&\mathbf{p}_{si}^{\mathrm{T}\,d}\mathbf{R}_s^{\mathrm{T}\,d}\mathbf{R}_s\mathbf{p}_{si}-\mathbf{p}_{si}^{\mathrm{T}\,d}\mathbf{R}_s^{\mathrm{T}}\mathbf{p}_{di}-\mathbf{p}_{di}^{\mathrm{T}\,d}\mathbf{R}_s\mathbf{p}_{si}+\mathbf{p}_{di}^{\mathrm{T}}\mathbf{p}_{di}=\\&=\mathbf{p}_{si}^{\mathrm{T}}\mathbf{p}_{si}-2\mathbf{p}_{di}^{\mathrm{T}\,d}\mathbf{R}_s\mathbf{p}_{si}+\mathbf{p}_{di}^{\mathrm{T}}\mathbf{p}_{di}\end{aligned} \qquad \text{(Eq. 2.11)}$$

The first and third addends are known quantities, and do not concur to the minimisation. The new functional to be maximised is then:

$$f_1(\mathbf{R})=\sum_{i=1}^{n}\mathbf{p}_{di}^{\mathrm{T}\,d}\mathbf{R}_s\mathbf{p}_{si} \qquad \text{(Eq. 2.12)}$$

It can be demonstrated that finding the maximum for (Eq. 2.12) coincides with finding the maximum of the following functional:

$$g\left(\mathbf{R}\right)=\mathrm{tr}\left({}^{d}\mathbf{R}_s\mathbf{C}\right) \qquad \text{(Eq. 2.13)}$$

Where **C** is the 3 x 3 cross-correlation matrix defined as:

$$\mathbf{C}=\frac{1}{n}\sum_{i=1}^{n}\mathbf{p}_{di}\mathbf{p}_{si}^{\mathrm{T}}=\tilde{\mathbf{P}}_d\tilde{\mathbf{P}}_s^{\mathrm{T}} \qquad \text{(Eq. 2.14)}$$

$$\begin{aligned}\tilde{\mathbf{P}}_s&=\left[\ldots\quad\mathbf{p}_{si}\quad\ldots\right]\\\tilde{\mathbf{P}}_d&=\left[\ldots\quad\mathbf{p}_{di}\quad\ldots\right]\end{aligned} \qquad \text{(Eq. 2.15)}$$

Where $\mathbf{p}_{si}$ and $\mathbf{p}_{di}$ are the position vectors of each point relative to the cluster centre of gravity, and defined in static and dynamic conditions respectively. The problem aims hence at finding the ${}^{d}\mathbf{R}_s$ as that matrix that minimises the differences when superimposing the static cluster of points to the dynamic one. The solution to this problem can be calculated in a *closed-form* via the singular value decomposition of the cross-correlation matrix:

$$\mathbf{C}=\mathbf{U}\cdot\mathbf{W}\cdot\mathbf{V}^{\mathrm{T}} \qquad \text{(Eq. 2.16)}$$

**U** and **V** are 3 x 3 orthonormal matrices, containing, per columns and respectively, the right and left eigen-vectors of the vector space defined by **C**. The eigen-vectors of **U** and **V** provides the directions of minimum deformation for the cluster. **W** is a 3 x 3 diagonal matrix containing the singular values of **C**, which are the positive squared roots of its eigen-values in ascending order.

Substituting the (Eq. 2.16) in the (Eq. 2.13), and using the properties of a matrix trace, the following equivalences are true:

$$\begin{aligned}&\mathrm{tr}\left({}^{d}\mathbf{R}_{s}\mathbf{C}\right)=\mathrm{tr}\left({}^{d}\mathbf{R}_{s}^{\mathrm{T}}\mathbf{C}\right)=\mathrm{tr}\left({}^{d}\mathbf{R}_{s}^{\mathrm{T}}\left(\mathbf{U}\mathbf{W}\mathbf{V}^{\mathrm{T}}\right)\right)=\\&=\mathrm{tr}\left(\left({}^{d}\mathbf{R}_{s}^{\mathrm{T}}\mathbf{U}\right)\left(\mathbf{W}\mathbf{V}^{\mathrm{T}}\right)\right)=\mathrm{tr}\left(\left(\mathbf{W}\mathbf{V}^{\mathrm{T}}\right)\left({}^{d}\mathbf{R}_{s}^{\mathrm{T}}\mathbf{U}\right)\right)=\\&=\mathrm{tr}\left(\mathbf{W}\left(\mathbf{V}^{\mathrm{T}}\,{}^{d}\mathbf{R}_{s}^{\mathrm{T}}\mathbf{U}\right)\right)\end{aligned}\qquad\text{(Eq. 2.17)}$$

Considering that **W** is a diagonal matrix, the last product in (Eq. 2.17) gives a diagonal matrix. Moreover, **U**, **V**, and ${}^{d}\mathbf{R}_{s}$ are orthonormal by definition (their determinant is equal to 1), which means that the elements of all these three matrices have modulus always ≤ 1. The maximum for the trace is then obtained when:

$$\mathbf{V}^{\mathrm{T}}{}^{d}\mathbf{R}_{s}{}^{\mathrm{T}}\mathbf{U}=\mathbf{I}_{(3)}\qquad\text{(Eq. 2.18)}$$

Then, being orthonormal, the transpose of **U**, **V**, and ${}^{d}\mathbf{R}_{s}$ coincide with their inverse matrices and the rotation matrix results being:

$${}^{d}\mathbf{R}_{s}=\mathbf{U}\mathbf{V}^{\mathrm{T}}\qquad\text{(Eq. 2.19)}$$

This procedure might lead to a misinterpretation of the result, as it could provide a reflection matrix rather than a rotation, which is easy to check. Indeed, if $\det\left({}^{d}\mathbf{R}_{s}\right)=-1$ the formula can be corrected as follows:

$${}^{d}\mathbf{R}_{s}=\mathbf{U}\begin{bmatrix}1&0&0\\0&1&0\\0&0&\det\left(\mathbf{U}\mathbf{V}^{\mathrm{T}}\right)\end{bmatrix}\mathbf{V}^{\mathrm{T}}\qquad\text{(Eq. 2.20)}$$

As said, the points in static and dynamic configurations of the body are defined in the **ECS**$_1$ and **GCS**, respectively. Thus, the rotation ${}^{d}\mathbf{R}_{s}$ is actually the ${}^{0}\mathbf{R}_{1}$. To conclude estimating the body pose, the position vector of the origin of the local **ECS** should be found. As per the other points, the origin can be defined via its position vector relative to the centre of gravity. Having found the rotation matrix that better fits the cluster of markers between static and dynamic conditions, the distance between the centre of gravity and the origin can be considered invariant. Thus:

$$\begin{aligned}&{}^{0}\mathbf{G}_{1}-{}^{0}\mathbf{O}_{1}={}^{0}\mathbf{R}_{1}\left({}^{1}\mathbf{G}_{1}-{}^{1}\mathbf{O}_{1}\right)\\&{}^{0}\mathbf{O}_{1}={}^{0}\mathbf{G}_{1}-{}^{0}\mathbf{R}_{1}{}^{1}\mathbf{g}_{1}\\&{}^{0}\mathbf{o}_{0,1}={}^{0}\mathbf{G}_{1}-{}^{0}\mathbf{O}_{1}\end{aligned}\qquad\text{(Eq. 2.21)}$$

The (Eq. 2.20) and (Eq. 2.21) can be substituted in the (Eq. 2.1) and the local **ECS** is univocally defined. From a mechanical point of view, looking for the directions of minimum deformations between the same cluster of points, measured in static and dynamic conditions, means to look for the configuration that would minimise the elastic energy of a system of springs connected between the static and the dynamic points. The main issue associated with this approach is that a marker affected by high inaccuracy (see following paragraph §2.3.2.5) would pull the system toward a more inaccurate estimate of segment pose. Some alternatives have been recently proposed to compensate for this undesired effect (§2.3.2.5), but this is still a relevant issue associated with marker-based gait analysis.

### *2.3.2.3 From the matrices to the estimate of joint kinematics*

The above described approaches allow defining the pose of a coordinate system with reference to a global one. The geometrical properties of rotation and pose matrices allow concatenating two or more of them, according to the following formula valid for both rotations and poses:

$$ {}^{0}\mathbf{H}_{n} = {}^{0}\mathbf{H}_{1}\,{}^{1}\mathbf{H}_{2}\cdots{}^{n-2}\mathbf{H}_{n-1}\,{}^{n-1}\mathbf{H}_{n} \qquad \text{(Eq. 2.22)} $$

This relation is useful when two rotation matrices associated with two adjacent bony segments are defined. The two concatenated matrices, having inverted one of the two, give the relative rotation between the adjacent segments:

$$ {}^{1}\mathbf{R}_{2} = {}^{0}\mathbf{R}_{1}^{\mathrm{T}}\,{}^{0}\mathbf{R}_{2} = {}^{1}\mathbf{R}_{0}\,{}^{0}\mathbf{R}_{2} \qquad \text{(Eq. 2.23)} $$

Each matrix models the attitude of each segment with respect to the **GCS**. Thus, the concatenated matrix represents the attitude of each segment with respect to the adjacent segment, and hence models the configuration of the joint between them for what concerns the angles. The use of rotation matrices simplifies the formalism of joint modelling, but the understanding of the nine elements that compose a rotation matrix is limited. However, a rotation matrix can be decomposed in elementary rotations around the three axes of an auxiliary coordinate system (minimal representation). The elementary rotations are represented as:

$$ \mathbf{R}_{x}(\varphi) = \begin{bmatrix} 1 & 0 & 0 \\ 0 & \cos\varphi & -\sin\varphi \\ 0 & \sin\varphi & \cos\varphi \end{bmatrix} \qquad \text{(Eq. 2.24)} $$

$$\mathbf{R}_y(\theta) = \begin{bmatrix} \cos\theta & 0 & \sin\theta \\ 0 & 1 & 0 \\ -\sin\theta & 0 & \cos\theta \end{bmatrix} \quad \text{(Eq. 2.25)}$$

$$\mathbf{R}_z(\psi) = \begin{bmatrix} \cos\psi & -\sin\psi & 0 \\ \sin\psi & \cos\psi & 0 \\ 0 & 0 & 1 \end{bmatrix} \quad \text{(Eq. 2.26)}$$

A minimal representation is then defined when the three rotation angles are known. The solution to this mathematical problem is however not trivial. Classical Mechanics helps solving the problem using the approach of the Euler or Cardan angles obtained combining subsequent elementary rotations around moving axes. The International Society of Biomechanics recommends defining the anatomical ECSs aligning their coordinate axes to the joint rotation axes [58,59,70]. Consequently, the rotations calculated with the mechanistic approach can be interpreted as estimate of the anatomical joint configuration. The process of solving the minimal representation as estimate of human joint kinematics starting from a rotation matrix is called *inverse kinematics problem*.

For the sake of clarity of the next steps within the present Thesis, it is worth mentioning the definitions used in Biomechanics for defining the auxiliary systems used to model the joints. In particular, this system is more commonly called Joint Coordinate Systems (**JCS**), as established by the International Society of Biomechanics, and originally proposed for the knee joint in [71], and it is defined by three not necessarily orthonormal unity vectors ($\mathbf{e}_1$, $\mathbf{e}_2$, and $\mathbf{e}_3$): two of them are body fixed, and the other one is a ‘‘floating’’ axis [58,59,70]. Since rotations obtained using this approach would be different for each chosen sequence of rotations, the International Society of Biomechanics has established a standard for the order the rotations should be defined. Generally, the axis $\mathbf{e}_1$ is chosen as the axis around which the major rotation occurs (usually the rotation defined on the sagittal plane), and it is solid with one of the coordinate axes of the **ECS** of proximal segment. The axis $\mathbf{e}_3$ is solid with one of the coordinate axes of the **ECS** of the distal segment, and $\mathbf{e}_2$ is the floating axis that completes the right-handed coordinate system.

### *2.3.2.4 The static posture*

After having placed all the markers needed for the implementation of the chosen model, the data collection procedure usually consists of two phases: a static, during which the subjects are asked to stand (or stay sit) as still as possible within the capture volume; and a dynamic phase, during which the subjects are asked to perform a specific task (e.g. to walk at their self-selected speed within the capture volume). The collection of the standing posture is needed to preliminary register the local **ECS** and, when relevant, the position of some virtual anatomical landmarks, by using the marked landmarks and some statistical regressions starting from anthropometric measurements (i.e. points that is not possible to directly track with markers, such as the femoral head) [20]. Some models call for the collection of the static posture as preliminary step to apply the least square fitting approach during the dynamic trials (see §2.3.2.2.2) [28,55,61]. Indeed, after having registered the local **ECS** and defined the virtual anatomical landmarks, the pose matrices are used to transform the global coordinates of both physical (anatomical and technical) and virtual markers into local coordinates. Considering the hypothesis of rigid body for the bony segments, these points are then averaged over the collected time-samples, and the relevant coordinates are assumed as the true values of the local landmark positions. Such local coordinates are the time-invariant ${}^{1}\mathbf{P}_i$ in the (Eq. 2.6), needed as input for the pose estimator and, hence, for the definition of the joint kinematics during the dynamic trial.

Moreover, with the definition of the local **ECS**, and the approach described in §2.3.2.3, it is possible to calculate the relative rotations between two adjacent bony segments from the data collected during the static trial. These kinematic variables provide information on: the neutral configuration of the body that can be different when collecting data on different subjects; and possible deformities that might be relevant for clinical applications. It is worth considering that a marker misplacement would lead to unreliable information of the neutral configuration, and false deformities or abnormalities might be highlighted. According to some models adopted in gait analysis, angles calculated starting from the static posture have to be subtracted to the kinematic variables calculated from data collected with the subject performing dynamic tasks [28,67]. However, this subtraction implicitly assumes that differences in static joint kinematics between two or more subjects should be ascribed to marker misplacement

only, rather than to physiological or pathological differences. Static posture should than be considered as informative as well as dynamic joint kinematics.

#### *2.3.2.5 Limitations*

The limitations of performing gait analysis with a marker-based approach, without considering the instrumental errors, are mainly linked to the made hypotheses and simplifications. In fact, what is actually tracked placing the markers on the subjects' skin is the body segment pose rather than the bone pose [12,24]. The interposition of soft tissues between the markers and the bone leads to a sliding between the markers and the underlying bones, causing the so-called soft tissue artefacts (STA) [24,72]. The only way to avoid the STA error would be to make the markers rigid with the bones using pins or screws, or fuse the gait analysis with real-time fluoroscopy imaging in order to be able to see the movement of the bones [73]. An example of the effect of the STA on joint kinematics is given in [74]. The authors performed a gait analysis on a subject who had a 1-DOF prosthesis implant to the knee: the permitted movement was the flexion/extension. The result of a gait cycle analysis on this subject showed relevant angles different from zero on the frontal and transverse planes of the knee, i.e. for ab/adduction and internal/external rotations. This phenomenon has been ascribed to the effect that STA had on the estimate of the joint kinematics, which can generate cross-talk among the components of the joint kinematics on the three anatomical planes. The STA magnitude, hence, could alter the kinematics from 0° to 10°. Furthermore, STA effect on the joint kinematics is impossible to predict: i.e., it is not possible to predict the signal to noise ratio associated with the joint kinematics estimates. A review published in 2010 summarised the literature that attempted to quantify the STA magnitude, but also highlighted the intrinsic limitations of the used methodologies, such as the use of intra-cortical pins or fluoroscopy [72]. The use of intra-cortical pins, indeed, leads to antalgic gait that is most likely different from what expected in daily life, or in in-door gait analysis, and it also constrains the movement of the soft tissues, potentially limiting the measured artefact range [24]. The use of fluoroscopy, instead, limits the evaluation of the STA to a specific portion of the gait cycle, or calls for the use of a treadmill, which has been found to lead both to different walking patterns [75,76], and different effects of the STA on the human joint kinematics [77]. Different attempts of managing the effect of the STA on the joint kinematics have

been proposed during the years. In [74,78] authors proposed discrete models, which consisted of STA value as function of the relevant joint angles. In [79], instead, authors proposed a STA analytical model, whose parameters were estimated by solving the optimisation problem to estimate the kinematics linked to the performed movement. Although a new approach has been recently proposed to model the STA and compensate for its effect on joint kinematics estimates [63,80–84], this is still a relevant issue associated with gait analysis performed via a marker-based approach.

Another source of error in tracking bone poses is the marker misplacement, which can be thought of as an apparent systematic movement to be added to the actual pose of the segments [25]. This is mainly linked to the ability of the operators who performed the marker placement, and it is hence estimated via within- and between-operator reproducibility[8] studies. Although it cannot be properly defined as a source of error, when dealing with kinematic variables gathered from human movements, the physiological between-test variability should be also accounted for [60,85]. Indeed, the human body is not able to perform identical movements when performing same tasks (e.g. walking, climbing stairs, etc). Moreover, this variability might be increased for some pathological status and could hence be interesting to be quantified. The instrumental errors, extensively described in the previous section (§2.3.1.2), are also to be accounted and result in apparent relative movements between the markers and the bones [23].

If possible, the sources of errors associated with estimating the human joint kinematics performed with a marker-based approach need to be properly evaluated before adopting any biomechanical model, and, thus, any marker placement protocol. Models are then validated via repeatability and reproducibility studies on the relevant model outcomes [64,86–88]. These studies also validate any subsequent comparison of biomechanical parameters at baseline and follow-up in clinical studies [89].

[8] As defined in the International Vocabulary of Metrology, and as summaries in the Appendix A.

## 2.4 Studying the repeatability and the reproducibility of gait analysis outcomes

In order to appreciate the clinical utility of a model for gait analysis it is worth evaluating its repeatability and reproducibility [29]. Indeed, clinical decision-making can benefit from objective quantities that provide information on the human movement. However, these quantities should be ideally not affected by errors, but in a more realistic scenario, they are required to be repeatable and reproducible. Repeatability and reproducibility are often assessed via variability or similarity indices or mathematical methodologies. A large number of indices and methodologies have been proposed and used to assess repeatability and reproducibility, but their interpretation can be limited since it is linked to many challenging aspects of the human movement analysis.

The main challenges when dealing with gait analysis data are linked to the high-dimensionality of the data set, the inherent temporal dependence of the gait time series, the high variability of the data (due to either physiological or pathological within- and between-subject variations), instrumental errors, and the correlation between curves gathered from same or similar series of data (i.e. from the same subject or the same population) [90]. The high dimensionality of gait data sets often calls for data reduction techniques to be used to enhance readability and understanding of gait analysis results. Often peak amplitude, mean or maximum values, value at the occurrence of a gait event can be extracted and analysed as summary metrics, to which further analysis can be applied. Unfortunately, as summarised in §2.3.2.5, gait data variability is nearly impossible to control, and statistical conclusions on gait data can be weak. Moreover, the parametrisation of gait variable curves into summary metrics provide limited additional understanding of the results apart from those achievable with visual inspection of simple plots [90,91]. Researchers have sought new ways to manipulate and interpret gait data, drawing from different engineering fields as, for example, computer science. These advanced techniques are summarised and deeply analysed in [90,92], which describe pros and relevant limitations of each methodology. Among those reviewed in [90,92], it is worth mentioning those methods that use the principal components [93–97], multiple correspondence analyses [98–101], or the wavelet transform [102–105]. Despite being promising, these methodologies are very unfamiliar to clinicians, who need to clearly understand whether a patient is showing

remission, stability, or development of a pathology, and eventually choose the proper treatment for the patients (§1.1).

Other methodologies, easiest to interpret for clinical users, and thus intrinsically more useful for the purpose at hand, have been proposed since gait analysis has started to be used for assessing patients. These methodologies often produce indices, either evaluated on summary metrics or on the whole curves, that provide a concise information of the variabilities within the analysed dataset allowing, for example, a comparison with normative results. In this scenario, an interesting contribution has been given by Schwartz *et al.*, who proposed a z-score method for incorporating the knowledge of point-by-point within-subject, and within- and between-operator errors into the clinical interpretation process, computing the standard errors at each point in the gait cycle [106]. However, the literature has recently given evidence that point-by-point correlations between angle values at subsequent instants of a joint kinematic curve need to be properly accounted for [107], differently from what proposed in the z-score method. Another approach is, hence, to calculate indices that provide information on the repeatability and reproducibility of the models' outcomes over the whole gait cycle. These indices, as proposed in literature, are summarised in Table 2.1. The variety of the proposed indices could lead to confusion when comparing results from studies that validate models' repeatability and reproducibility. Indeed, an index or a methodology considered as the golden standard to be used for these studies or to compare results from a subject with normative results are still lacking.

**Table 2.1** – Summary of the published indices used to assess repeatability and reproducibility of joint kinematics. The following abbreviations were used in the following table: whole gait cycle (WGC), summary metrics (SM). When papers only proposed the method without performing any analysis on gait data, or the method was originally proposed for non-gait studies, the column *Analysis* presents a 'na' (i.e. not available).

| Author | Method | Calculated on | Analysis | Studies | Used until |
|---|---|---|---|---|---|
| Statistics principles | SD | SM | na | [28,64,65,69,108–123] | 2012 |
| Statistics principles | CV | SM | na | [124–126] | 2006 |
| Statistics principles | RMSE | WGC | na | [127–129] | 2014 |
| Shrout *et al.* (1979) [130] | ICC | SM | na | [108–110,114,122,129,131–137] | 2016 |
| Kadaba *et al.* (1989) [125] | CMC | WGC | within-day between-day | [31,69,86,88,115–118,121,124,133,138–146] | 2014 |
| Stratford *et al.* (1997) | SEM | WGC | na | [89,109,115,116,137,147] | 2012 |

| Author | Method | Calculated on | Analysis | Studies | Used until |
|---|---|---|---|---|---|
| Ferrari *et al.* (2008) [57] | MAV | WGC | between-model | [137,140] | 2014 |
| Curtis *et al.* (2009) [114] | TEM | SM | between-lab | [114,127] | 2013 |
| Klejman *et al.* (2010) [109] | MDC | WGC | between-session | [89,137] | 2012 |
| Benedetti *et al.* (2013) [87] | MAD | SM | between-lab | none | 2013 |
| Benedetti *et al.* (2013) [87] | MD | SM | between-lab | none | 2013 |
| Iosa *et al.* (2014) [129] | LFM | WGC | within-subject | [148,149] | 2016 |

## 2.5 Movements of the foot-ankle complex

The movements of the foot, as well as the movements of all the human segments, can be defined with respect to the anatomical planes (Appendix B). In this case, the movements are [58] (Figure 2.11):

- *Plantarflexion*: rotation of the foot on the sagittal plane upwards, toward the tibia;
- *Dorsiflexion*: rotation of the foot on the sagittal plane downwards, away from the tibia;
- *Inversion*: rotation of the foot on the frontal plane inward and upward, showing the plantar surface of the foot medially (towards the sagittal plane) – this movement is sometimes addressed as varus rotation;
- *Eversion*: rotation of the foot on the frontal plane outward and upward, showing the plantar surface of the foot laterally (away from the sagittal plane) – this movement is sometimes addressed as valgus rotation;
- *Abduction* or *External rotation*: lateral rotation of the foot on the transverse plane;
- *Adduction* or *Internal rotation*: medial rotation of the foot on the transverse plane.

Beside these definitions, it is worth considering the joint axes defined for the tibio-talar and subtalar joints in §2.2.2. As said, the foot movements are strongly correlated along these two axes due to their configuration. Thus, it is appropriate to define the following mixed movements:

- *Pronation*: composed rotation of the foot on the sagittal, frontal and transverse planes, i.e. dorsiflexion-eversion-abduction;

- *Supination*: composed rotation of the foot on the sagittal, frontal and transverse planes, i.e. plantarflexion-inversion-adduction.

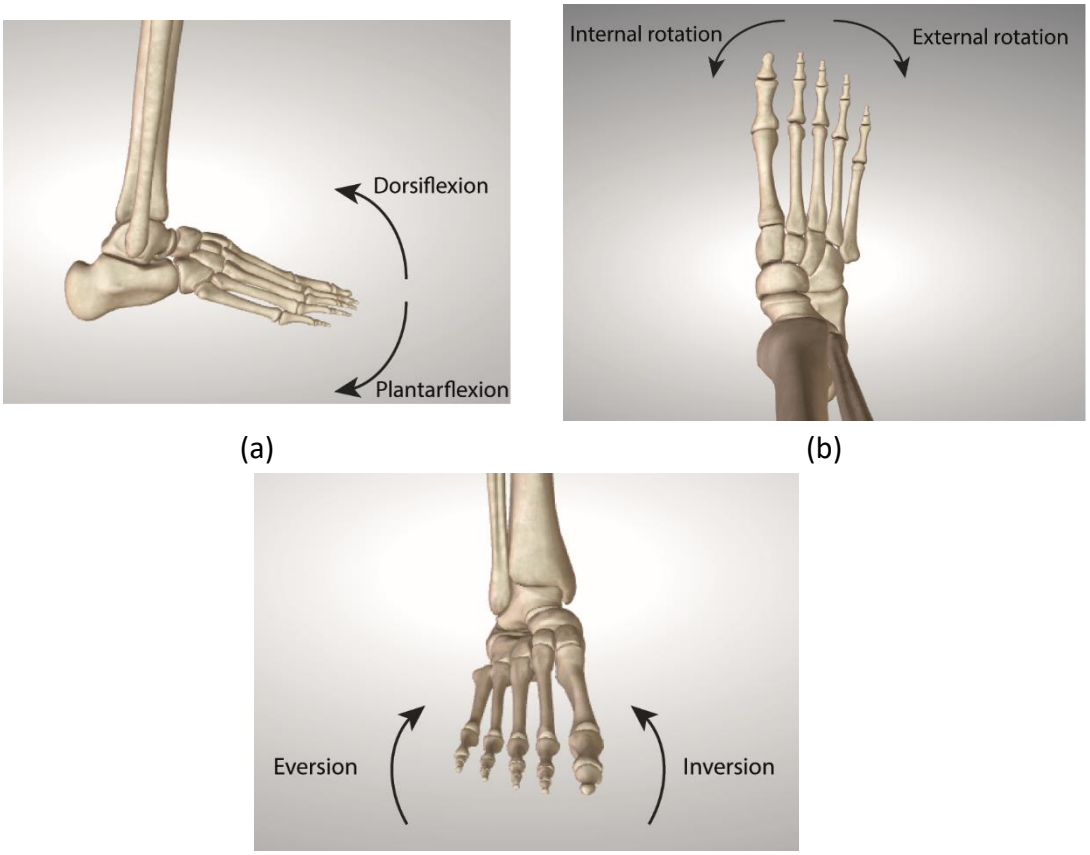


**Figure 2.11** – The movements of the foot on the three anatomical planes: (a) Plantar/dorsiflexion, (b) Internal/External rotation, and (c) Inversion/Eversion. This Figures has been retrieved from the Biodigital Human website (www.biodigital.com) and adapted.

Movements of the foot and the joints within have been descried as essential elements to accomplish the objective of the locomotor system to move the body forward during the gait [150]. The gait can be described as subsequent situations of loss of balance, in which the body weight vector is transferred from a lower limb to the other, creating forward fall positions. Thus, advancement of the body depends on redirecting some of the propulsive force exchanged between the floor and the foot, which is initially directed toward, in a manner that allows for progression and stability. Throughout this process, and mainly during the stance phase (i.e. foot in contact with the ground), heel, ankle and forefoot serve as rockers [150]. The initial contact of the foot with the ground is made by the rounded surface of the calcaneal tuberosities. The calcaneal segment works as an unstable lever between the contact point and the ankle joint, and rolls to bring the body weight toward the forefoot. Once the forefoot strikes the floor, the ankle

starts being a new fulcrum to maintain the progression movement. Indeed, the foot remain stationary on the floor and the tibia moves forward while the ankle passively dorsiflexes. When the point of application of the body weight reaches the metatarsal heads, the heel rises and the metatarsal heads works as new rockers. During this phase, the body progression is accelerated as the body falls forward, and beyond the area of foot support. The unbalanced body mass works, hence, as passive propelling force applied at the end of a long lever hinged to the floor (i.e. the leg). This unbalanced situation is not constrained until the contralateral foot strikes the ground, and its heel, ankle and forefoot start working as rockers themselves [150].

### 2.5.1 Models review

Since gait analysis has started to be accepted as a technique to evaluate human joint kinematics during walking, the model proposed by Davis *et al.* [56] has been largely adopted and almost unanimously agreed upon. Different versions of this model were then presented, but the basic principles of the modelling were very similar. An example is the commercial version of the Davis protocol proposed by Vicon (Vicon Motion System Ltd – Oxford, UK), which is shown in Figure 2.12. This model has been and is largely adopted to perform gait analysis, and it has been developed when technological advancement of both hardware and software was limited, and called hence for a simplistic approach. However, the modelling of hip and knee joints as proposed in [56] is reasonably valid, whereas considering the foot as a rigid body jointed to the tibia can be considered as an oversimplification of the problem when looking at the actual anatomy of this anatomical district (§2.2). Indeed, as an applicative example, when dealing with subjects whose feet show significant impairments at a midfoot level (tarsal bones), the forefoot (metatarsal bones) may dorsiflex with respect to the tibia during the stance phase of the gait cycle (Figure 2.8), while the hindfoot remains plantarflexed [151]. The typical visual observation of such cases, or other pathological status that affect foot motion, might benefit from an objective measurement of the joint kinematics. Modelling the ankle joint and those within the foot is, though, a difficult task, mainly due to their non-univocally defined joint rotation axes (§2.2.2), the speed with which changes in joint configuration occur, small size and closeness of the anatomical landmarks to be palpated, and the small range of motions of the joints [112,151].

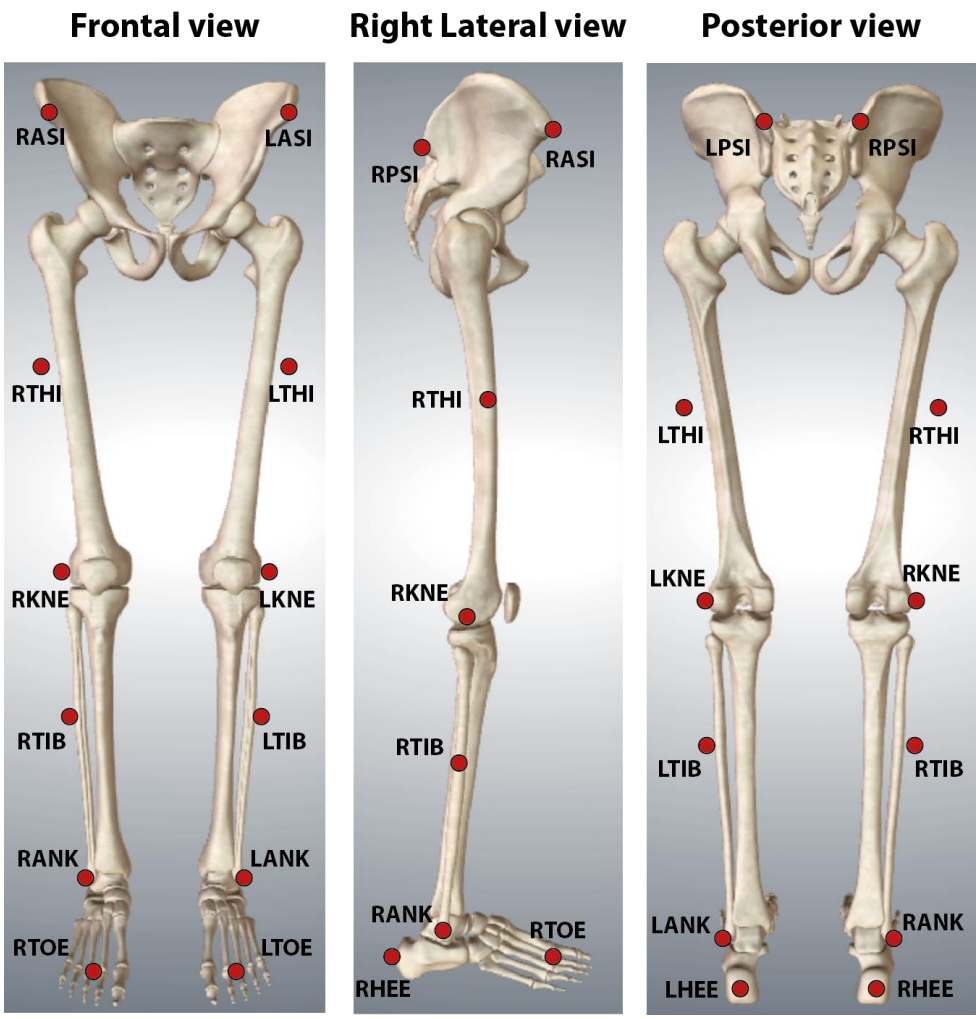


**Figure 2.12** – The markers placed according to the Plug-in-Gait protocol [56]. The images have been retrieved from the Biodigital Human website (www.biodigital.com) and adapted.

In the nineties, multisegment models of the foot started to be proposed in order to attempt overcoming the modelling simplifications and limitations presented so far. The proposed models mainly differ for the number of considered segments, and the modelling approach, either following the ISB recommendations, or considering helical rotation axes. Table 2.14 presents an overview of the proposed multisegment models for the foot-ankle complex. For the sake of readability, the Table 2.14 is presented at the end of this Chapter.

For the reasons expressed in §1.1 and §2.3.2.5, the validation of the models presented in Table 2.14 is limited [86,112,114,142] and, thus, their clinical feasibility and utility has been questioned, also considering that the first models were lacking detailed descriptions to be replicated by others [29], and STA effect on joint kinematics was not accounted for. Moreover, their performances in terms of repeatability and reproducibility of the relevant outcomes (Appendix A) are still unclear [26].

In the following sections, only the models that consider the JCS modelling approach for the joints, do not require any radiograph information, and can be integrated with the whole body conventional models for gait analysis, will be considered. Models not currently in use, either for research or clinical practice, and models that define rotations around helical axes will not be considered for the present project, as a comparison among models would be unfeasible and unattractive. Models that fit these criteria are based on the assumption of rigid bodies, and decompose the joint rotations onto the three anatomical planes (sagittal, frontal and transverse planes) [28,65,67,68]. Therefore, complex joints and relevant rotation axes within the foot are not always defined as described in §2.2.2, but they are rather modelled and decomposed on the three major anatomical planes. Where available, details follow in the next sub-paragraphs model by model. The labels associated with anatomical landmarks in the following sections have been modified with respect to those chosen in the papers that proposed the models. This choice should enhance readability of the tables and highlight coincident anatomical landmarks among models.

### 2.5.2 The modified Oxford Foot model

The Oxford Foot Model (OFM) was originally proposed by Carson *et al.* [64], modelling the foot as composed by three segments. This model was tested on two subjects by two operators, performing the marker placement for four times. The joint kinematics were presented for the stance phase only, and tested assessing the inherent repeatability and reproducibility of the outcomes due to marker repositioning, also performed by different operators, and the physiological within-subject variability.

The need of observing the kinematics for the entire gait cycle and assessing paediatric populations, together with the need of enhancing the repeatability performances of the OFM, called for an adaptation of the model proposed in [64]. Thus, Stebbins *et al.* proposed the modified Oxford Foot model and tested the repeatability of the relevant joint kinematics on fifteen healthy children in three sessions of data collection [65]. Table 2.2 and Figure 2.13 show and describe the complete marker-set of the modified Oxford Foot Model, and the considered body segments. This model mainly differs from the model proposed in [64] for the possibility of being integrated in a conventional lower body model, as for example the model described in [56]. Moreover, the hindfoot was defined considering only its pertinent markers, and the marker on the

base of the first metatarsal bone was moved medially on the forefoot. The marker cluster on the hallux was finally replaced with a single marker. The Hallux is then considered as a vector for this model.

In this Thesis, the 'Option 5' of the model will be described since it has been reported to be the most repeatable. Table 2.3 shows the definitions for the axes of the local **ECS** of each segment as reported in [65]. The approach used to define the **ECS** in the walking trials is the *non-optimal* (§2.3.2.2.1).

**Table 2.2** – Considered segments and relevant anatomical landmarks (AL) to be palpated according to [65]. Markers used in static trials only are highlighted in italic.

| Segment | AL | Description |
|---|---|---|
| Tibia | TUB | Most anterior prominence of the tibial tuberosity |
| | HFB | Most lateral aspect of the head of the fibula |
| | SHN | Anywhere along the anterior crest of the tibia |
| | ANK | Distal apex of the medial malleolus |
| | *MMA* | *Distal apex of the medial malleolus* |
| Hindfoot | CA1 | Distal end of the calcaneus midline on the sagittal plane |
| | CA2 | Proximal end of the calcaneus midline on the sagittal plane (i.e. Achilles tendon attachment) |
| | CPG[9] | Wand marker, which base is placed mid-way between CA1 and CA2 |
| | STL | At the same vertical level as the palpated landmark (maximising inter-marker distance and avoiding local muscle attachments)[10] |
| | LCA | At same distance from the most posterior point as STL (on lateral aspect of the calcaneus)[8] |
| Forefoot | P5M | Base of the 5$^{th}$ metatarsal: dorso-medial aspect |
| | D5M | Head of the 5$^{th}$ metatarsal: laterally on the foot |
| | TOE | Mid-point of heads of the 2$^{nd}$ and 3$^{rd}$ metatarsals |
| | *D1M* | *Head of 1$^{st}$ metatarsal: medially on the foot* |
| | P1M | Dorso medial aspect of the 1$^{st}$ metatarso-cuneiform joint (avoiding the flexor tendon) |
| Hallux | HLX | Proximal phalanx of the hallux (on the medial side, mid-way between superior and inferior surface) |

[9] Reported for completeness, but not used either for technical nor for anatomical ECS definition.
[10] From personal communication between Dr Joe A.I. Prinold and the corresponding author of [65]: Dr Julie Stebbins.

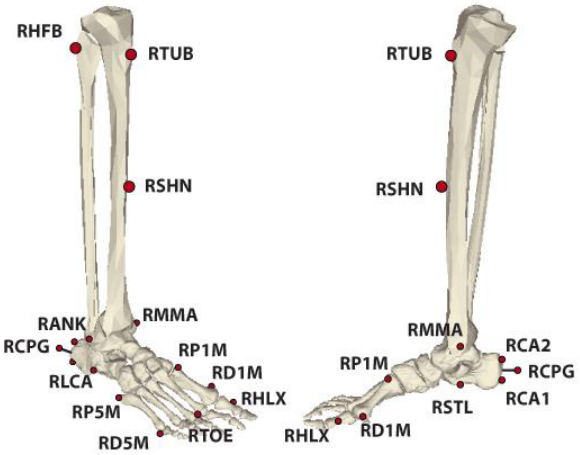


**Figure 2.13** – The anatomical landmarks to be palpated on right tibia and right foot segments according to the model proposed in [65].

**Table 2.3** – Definition of the local embedded coordinate systems (ECS) for each segment for the right lower limb [65].

| Segment | ECS | | Definition |
|---|---|---|---|
| Tibia | Technical | $\mathbf{i}$ | From HFB to ANK |
| | | $\mathbf{j}$ | Perpendicular to $\mathbf{i}$ and the vector joining SHN and the mid-point between ANK and HFB |
| | | $\mathbf{k}$ | $\mathbf{i}\times\mathbf{j}$ |
| | Anatomical | $\mathbf{j}$ | From mid-point between MMA and ANK to the KJC calculated as described in [56] |
| | | $\mathbf{i}$ | Orthonormal to the plane defined by $\mathbf{j}$ and the vector from MMA to ANK |
| | | $\mathbf{k}$ | $\mathbf{i}\times\mathbf{j}$ |
| Hindfoot | Technical | $\mathbf{i}$ | From CA1 to the mid-point between STL and LCA |
| | | $\mathbf{j}$ | Perpendicular to $\mathbf{i}$ and the vector from CA1 to LCA |
| | | $\mathbf{k}$ | $\mathbf{i}\times\mathbf{j}$ |
| | Anatomical | $\mathbf{i}$ | Parallel to the floor and on the plane defined by CA1, CA2, and mid-point between STL and LCA |
| | | $\mathbf{k}$ | Perpendicular to the plane defined by CA1, CA2, and mid-point between STL and LCA |
| | | $\mathbf{j}$ | $\mathbf{k}\times\mathbf{i}$ |
| Forefoot | Technical | $\mathbf{i}$ | From P1M to D5M |
| | | $\mathbf{j}$ | Perpendicular to $\mathbf{i}$ and the vector joining TOE to P5M |
| | | $\mathbf{k}$ | $\mathbf{i}\times\mathbf{j}$ |
| | Anatomical | $\mathbf{j}$ | Perpendicular to the plane defined by D1M, D5M and P5M |
| | | $\mathbf{i}$ | Projection onto the above defined plane of the vector joining the mid-point between P1M and P5M to TOE |
| | | $\mathbf{k}$ | $\mathbf{i}\times\mathbf{j}$ |
| Hallux | Anatomical | $\mathbf{k}$ | Aligned with $\mathbf{k}$ of the forefoot |
| | | $\mathbf{i}$ | From D1M (at height of HLX) to HLX |
| | | $\mathbf{j}$ | $\mathbf{k}\times\mathbf{i}$ |

The Hindfoot/Tibia joint models the combination of the tibio-talar and subtalar joints' motion. The tarsometatarsal joint is tracked as the relative rotations between the forefoot (composed by the five metatarsal bones as a rigid body), and the hindfoot (rather than the midfoot bones as per anatomical definition). The metatarsophalangeal joint is not modelled a part from the articulation between the hallux phalanx and the first metatarsal bone. The virtual joint between forefoot and tibia is declared to be defined to allow a comparison of this joint's motion with those obtained with conventional models. However, it is worth considering that segments and joints of different models are generally differently defined, and the solution of the inverse kinematic problem leads to non-comparable results as we might have defined angles about different rotation axes, and projected them onto different planes. The comparison described in [65], hence, should be intended as only qualitative.

The joint kinematics are estimated according to the ISB recommendations [58], and Table 2.4 reports the definitions of the **JCS** axes for each joint. This model did not call for a reference of the kinematics to the static posture, which allows observing possible foot deformities due to any pathology that may have induced alteration in the standing posture. Results were presented for the whole gait cycle, and kinematics were reported to be repeatable. Frontal and transverse kinematics resulted to be less repeatable than sagittal kinematics.

**Table 2.4** – Definition of the joint coordinate systems (JCS) for each considered joint [65].

| Joint | JCS | Definition |
|---|---|---|
| Hindfoot/Tibia | $\mathbf{e}_1$ | Plantar/dorsiflexion axis, parallel to $\mathbf{k}$ of tibia |
| | $\mathbf{e}_2$ | Internal/external rotation axis |
| | $\mathbf{e}_3$ | Inversion/eversion axis, parallel to $\mathbf{i}$ of the hindfoot |
| Forefoot/Hindfoot | $\mathbf{e}_1$ | Plantar/dorsiflexion axis, parallel to $\mathbf{k}$ of hindfoot |
| | $\mathbf{e}_2$ | Internal/external rotation axis |
| | $\mathbf{e}_3$ | Inversion/eversion[11] axis, parallel to $\mathbf{i}$ of the forefoot |
| Hallux/Forefoot | $\mathbf{e}_1$ | Plantar/dorsiflexion axis, parallel to $\mathbf{k}$ of tibia |
| | $\mathbf{e}_2$ | Internal/external rotation axis |
| | $\mathbf{e}_3$ | Inversion/eversion axis, parallel to $\mathbf{i}$ of the hindfoot |
| Forefoot/Tibia | $\mathbf{e}_1$ | Plantar/dorsiflexion axis, parallel to $\mathbf{k}$ of tibia |
| | $\mathbf{e}_2$ | Internal/external rotation axis |
| | $\mathbf{e}_3$ | Inversion/eversion axis, parallel to $\mathbf{i}$ of the hindfoot |

[11] The inversion/eversion movement is addressed as pronation/supination in the paper that proposed the model. In this Thesis terms recommended by the ISB will be used.

### 2.5.3 The "Istituti Ortopedici Rizzoli" model

The "Istituti Ortopedici Rizzoli" model, often abbreviated as IOR model, was originally developed using marker clusters that were then judged to be bulky and uncomfortable [31]. Moreover, the data collection procedure called for a time consuming calibration of the anatomical landmarks with respect to the clusters, suing a pointer. Thus, to overcome these limitations, the same authors presented a new version of the IOR model which adopted the skin mounted markers [67]. Table 2.5 and Figure 2.14 show and describe the complete marker-set of the IOR model, and the considered body segments.

Table 2.6 shows the definitions for the axes of the local **ECS** of each segment as reported in [67]. The approach used to define the **ECS** in the walking trials is the *non-optimal* (§2.3.2.2.1). It is worth mentioning that this model also allows evaluating some planar angles, which are the orientations of segment lines with respect to the ground surface or to a midline. These segment lines model the orientation of the first, the second, and the fifth metatarsal bones, as well as the proximal phalanx of the hallux. As said (§0), these angles will be not defined in the following, and will not be investigated within this project.

**Table 2.5** – Considered segments and relevant anatomical landmarks (AL) to be palpated according to [67]. Markers used in static trials only are highlighted in italic.

| Segment | AL | Description |
|---|---|---|
| Shank | TUB | Most anterior prominence of the tibial tuberosity |
| | HFB | Most lateral aspect of the head of the fibula |
| | ANK | Distal apex of the medial malleolus |
| | MMA | Distal apex of the medial malleolus |
| Calcaneus | CA2 | Proximal end of the calcaneus midline on the sagittal plane (i.e. Achilles tendon attachment) |
| | PT | Peroneal tubercle: the first bone prominence below the lateral malleolus |
| | ST | Sustentaculum tali: 2 cm below the distal border of the medial malleolus |
| Midfoot | TN | Navicular: 2nd prominence on the line between proximal epiphysis of the 1st metatarsal and the lower ridge of the calcaneus (on the interior side of the extensor longus of the hallux) |
| Metatarsus | P5M | Base of the 5th metatarsal: dorso-medial aspect |
| | VMH | Dorso-medial aspect of the 5th metatarso-phalangeal joint (avoiding the flexor tendon and the joint) |
| | SMH | Dorso-medial aspect of the 2nd metatarso-phalangeal joint |
| | SMB | Dorso-medial aspect of the 2nd metatarso-cuneiform joint |
| | FMH | Dorso-medial aspect of the 1st metatarso-phalangeal joint (avoiding the flexor tendon) |
| | P1M | Dorso medial aspect of fthe 1st metatarso-cuneiform joint (avoiding the flexor tendon) |

The joint kinematics are estimated according to the ISB recommendations [58], and Table 2.7 reports the definitions of the **JCS** axes for each joint. No explicit parallelism of the defined joints with the anatomical ones is reported in [67]. However, it is worth highlighting that this model defines the joint between midfoot and calcaneus as a 3DOF hinge; whereas, this joint is reported in literature to permit at most only translation of a few millimetres [32]. Moreover, coherently to the conventional practice of the foot modelling, the joint between the foot as a whole rigid segment and the tibia is defined. Kinematics are referenced to the static posture, assumed as neutral configuration, and possible deformities of the foot are then not highlighted in the kinematic patterns. However, some information about the deformities could be potentially retrieved from the data collected during the upright static test collected at the beginning of the data collection session.

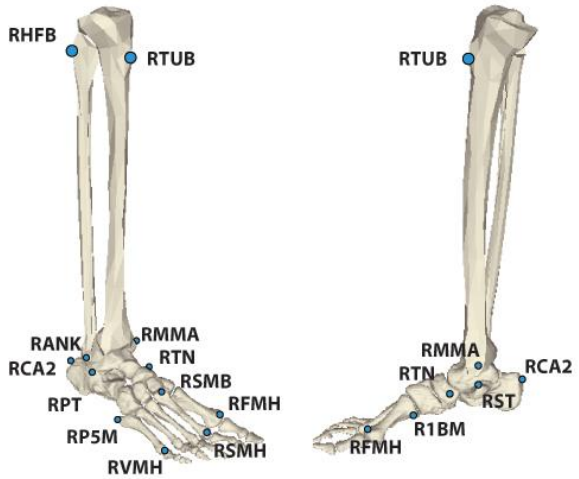


**Figure 2.14** – The anatomical landmarks to be palpated on right tibia and right foot segments according to the model proposed in [67].

**Table 2.6** – Definition of the local embedded coordinate systems (ECS) for each segment for the right lower limb [67].

| Segment | ECS | Definition |
|---|---|---|
| Shank | $\mathbf{O}$ | Mid-point between MMA and ANK |
| | $\mathbf{j}$ | Projection of the line joining $\mathbf{O}$ and TUB on the frontal plane, which is defined by ANK, HFB and $\mathbf{O}$ |
| | $\mathbf{k}$ | Lies on the frontal plane and it is orthogonal to $\mathbf{j}$ |
| | $\mathbf{i}$ | $\mathbf{i} \times \mathbf{j}$ |
| Calcaneus | $\mathbf{O}$ | Coincides with CA2 |
| | $\mathbf{i}$ | From $\mathbf{O}$ to the mid-point between ST and PT |
| | $\mathbf{k}$ | Lies in the transverse plane, defined by $\mathbf{i}$ and ST |
| | $\mathbf{j}$ | $\mathbf{k} \times \mathbf{i}$ |
| Midfoot | $\mathbf{O}$ | Coincides with the mid-point between TN and P5M |
| | $\mathbf{i}$ | From $\mathbf{O}$ to SMB |

| Segment | ECS | Definition |
|---|---|---|
| | $\mathbf{k}$ | Lies in the transverse plane defined by $\mathbf{i}$ and TN |
| | $\mathbf{j}$ | $\mathbf{k} \times \mathbf{i}$ |
| Metatarsus | $\mathbf{O}$ | Coincides with SMB |
| | $\mathbf{i}$ | Projection of the line joining SMB and SMH on the transverse plane, which passes through the $\mathbf{O}$ and FMH and VMH |
| | $\mathbf{k}$ | Lies in the transverse plane and it is orthogonal to $\mathbf{i}$ |
| | $\mathbf{j}$ | $\mathbf{k} \times \mathbf{i}$ |
| Foot | $\mathbf{O}$ | Coincides with CA2 |
| | $\mathbf{i}$ | Projection of the line joining $\mathbf{O}$ and SMH on the transverse plane, which is defined by FMH, VMH and $\mathbf{O}$ |
| | $\mathbf{k}$ | Lies in the transverse plane and it is orthogonal to $\mathbf{i}$ |
| | $\mathbf{j}$ | $\mathbf{k} \times \mathbf{i}$ |

After having described the model, the authors have studied its performances asking an operator to place the markers on ten healthy adults. Results were presented for the stance phase only, and no repeatability or reproducibility analyses were performed to validate the results [67]. A subsequent study attempt validating the IOR model testing the repeatability and reproducibility of the kinematics. The authors used an approach based on statistical methods gathered from two subjects by four operators (two with and two without experience in foot model protocols) in three testing session per operator [106,112]. The between-trial repeatability resulted to be higher than between-session repeatability and between-operator reproducibility, especially when considering the data collected by the two unexperienced operators. The major difficulty in implementing the model was placing the markers on very close and small anatomical landmarks. However, if the marker placement is performed by well-trained operators, the repeatability of foot kinematics obtained with the IOR model was comparable to those values obtained for the kinematics of other joints up to lower limb.

**Table 2.7** – Definition of the joint coordinate systems (JCS) for each considered joint [67].

| Joint | JCS | Definition |
|---|---|---|
| Calcaneus/Shank | $\mathbf{e}_1$ | Plantar/dorsiflexion axis, parallel to $\mathbf{k}$ of shank |
| | $\mathbf{e}_2$ | Inversion/eversion axis |
| | $\mathbf{e}_3$ | Internal/external[12] rotation axis, parallel to $\mathbf{j}$ of the calcaneus |
| Midfoot/Calcaneus | $\mathbf{e}_1$ | Plantar/dorsiflexion axis, parallel to $\mathbf{k}$ of calcaneus |

[12] In this Thesis the terms internal/external rotation are used rather than the abduction/adduction rotation, as in the paper that proposed the model, in order to have homogenous terminology among models.

| Joint | JCS | Definition |
|---|---|---|
| | $\mathbf{e}_2$ | Inversion/eversion axis |
| | $\mathbf{e}_3$ | Internal/external rotation axis, parallel to $\mathbf{j}$ of the midfoot |
| Metatarsus/Midfoot | $\mathbf{e}_1$ | Plantar/dorsiflexion axis, parallel to $\mathbf{k}$ of midfoot |
| | $\mathbf{e}_2$ | Inversion/eversion axis |
| | $\mathbf{e}_3$ | Internal/external rotation axis, parallel to $\mathbf{j}$ of the metatarsus |
| Metatarsus/Calcaneus | $\mathbf{e}_1$ | Plantar/dorsiflexion axis, parallel to $\mathbf{k}$ of calcaneus |
| | $\mathbf{e}_2$ | Inversion/eversion axis |
| | $\mathbf{e}_3$ | Internal/external rotation axis, parallel to $\mathbf{j}$ of the metatarsus |
| Foot/Shank | $\mathbf{e}_1$ | Plantar/dorsiflexion axis, parallel to $\mathbf{k}$ of shank |
| | $\mathbf{e}_2$ | Inversion/eversion axis |
| | $\mathbf{e}_3$ | Internal/external rotation axis, parallel to $\mathbf{j}$ of the foot |

### 2.5.4 The model proposed by Sawacha et al. (2009)

This model has been developed to be applied on patients affected by diabetes, since those available were judged not suitable to this purpose. Table 2.8 and Figure 2.15 show the considered segments and the relevant anatomical landmarks to be palpated, as described in [28]. Since ulcerations of the foot due to diabetes mainly occur on the metatarsal bones, the markers on the forefoot were placed only on the first and fifth metatarsal bones, plus one marker on the second proximal phalanx.

**Table 2.8** – Considered segments and relevant anatomical landmarks (AL) to be palpated according to [28]. Markers used in static trials only are highlighted in italic.

| Segment | AL | Description |
|---|---|---|
| Tibia | TUB | Most anterior prominence of the tibial tuberosity |
| | HFB | Most lateral aspect of the head of the fibula |
| | ANK | Distal apex of the medial malleolus |
| | MMA | Distal apex of the medial malleolus |
| Hindfoot | CA2 | Proximal end of the calcaneus midline on the sagittal plane (i.e. Achilles tendon attachment) |
| | PT | Peroneal tubercle: the first bone prominence below the lateral malleolus |
| | ST | Sustentaculum tali: 2 cm below the distal border of the medial malleolus |
| Midfoot | C | Cuboid: first recognisable bone prominence on the cuboid, from the 5$^{th}$ metatarsal bone following the direction of the axis of the tibia |
| | TN | Navicular: 2$^{nd}$ prominence on the line between proximal epiphysis of the 1$^{st}$ metatarsal and the lower ridge of the calcaneus (on the interior side of the extensor longus of the hallux) |
| Forefoot | P5M | Base of the 5$^{th}$ metatarsal: dorso-medial aspect |
| | VMH | Dorso-medial aspect of the 5$^{th}$ metatarso-phalangeal joint (avoiding the flexor tendon and the joint) |
| | IIT | Proximal epiphysis of second toe phalanx (1 cm distal from the joint interstice of the 2$^{nd}$ ray) |
| | FMH | Dorso-medial aspect of the 1$^{st}$ metatarso-phalangeal joint (avoiding the flexor tendon) |

The model was tested on ten healthy subjects and ten patients affected by diabetes. Table 2.9 shows the definitions for the axes of the local **ECS** of each segment as reported in [28]. The approach used to define the **ECS** in the walking trials is the least square fitting approach (§0), as it was presumed to minimise possible marker occlusions.

The joint kinematics are estimated according to the ISB recommendations [58], and Table 2.10 reports the definitions of the **JCS** axes for each joint. No explicit parallelism of the defined joints with the anatomical ones is reported in [28]. As per the previous model, coherently to the conventional practice of the foot modelling, the joint between the foot as a whole rigid segment and the tibia is defined. Kinematics are referenced to the static posture, assumed as neutral configuration, but it is possible to recognise the alterations correlated to the disease. The authors evaluated the between-stride and the between-day repeatability, and the between-operator reproducibility by calculating ranges of motion, mean values and standard deviations among subjects of the relevant joint kinematics, and the same statistical scores used to test the IOR model [106].

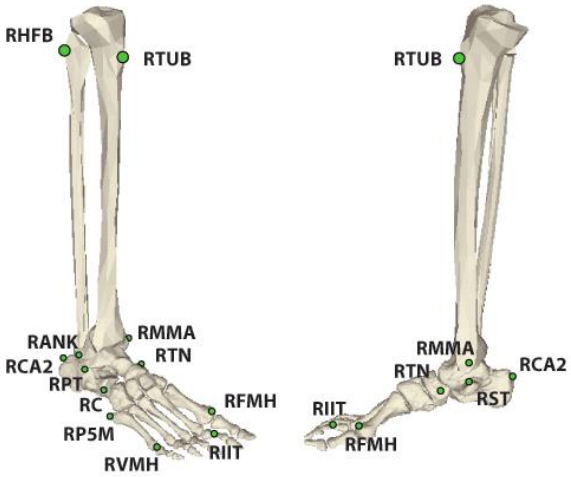


**Figure 2.15** – The anatomical landmarks to be palpated on right tibia and right foot segments according to the model proposed in [28].

**Table 2.9** – Definition of the local embedded coordinate systems (ECS) for each segment for the right lower limb [28].

| Segment | ECS | Definition |
|---|---|---|
| Tibia | $\mathbf{O}$ | Mid-point between MMA and ANK |
| | $\mathbf{j}$ | Parallel to the line that joins the mid-point between ANK and MMA to the projection of TUB onto the plane defined by ANK, MMA and HFB |
| | $\mathbf{i}$ | Pointing forward, and orthonormal to the plane defined by $\mathbf{j}$ and line that connects ANK and MMA |
| | $\mathbf{k}$ | $\mathbf{i} \times \mathbf{j}$ |
| Hindfoot | $\mathbf{O}$ | Coincides with CA2 |

| Segment | ECS | Definition |
|---|---|---|
| | $\mathbf{k}$ | From ST to PT |
| | $\mathbf{j}$ | Pointing upward and orthogonal the plane defined by $\mathbf{k}$ and the line connecting CA2 and ST |
| | $\mathbf{i}$ | $\mathbf{j}\times\mathbf{k}$ |
| Midfoot | $\mathbf{O}$ | Coincides with the mid-point between TN and C |
| | $\mathbf{k}$ | From TN to C |
| | $\mathbf{i}$ [13] | Pointing forward and orthonormal to the plane defined by $\mathbf{k}$ and the line connecting TN and P5M |
| | $\mathbf{j}$ | $\mathbf{k}\times\mathbf{i}$ |
| Forefoot | $\mathbf{O}$ | Coincides with the mid-point between FMH and VMH |
| | $\mathbf{k}$ | From FMH to VMH |
| | $\mathbf{j}$ | Pointing upward and orthogonal to the plane defined by $\mathbf{k}$ and the line connecting VMH and IIT |
| | $\mathbf{i}$ | $\mathbf{j}\times\mathbf{k}$ |
| Foot | $\mathbf{O}$ | Coincides with CA2 |
| | $\mathbf{k}$ | From FMH to VMH |
| | $\mathbf{i}$ [13] | Pointing forward and parallel to the intersection line between the plane defined by CA2, FMH and VMH, and the plane where the line from IIT to CA2 lies on |
| | $\mathbf{j}$ | $\mathbf{k}\times\mathbf{i}$ |

**Table 2.10** – Definition of the joint coordinate systems (JCS) for each considered joint [28].

| Joint | JCS | Definition |
|---|---|---|
| Hindfoot/Tibia | $\mathbf{e}_1$ | Plantar/dorsiflexion axis, parallel to $\mathbf{k}$ of tibia |
| | $\mathbf{e}_2$ | Internal/External rotation axis |
| | $\mathbf{e}_3$ | Inversion/eversion axis, parallel to $\mathbf{i}$ of the hindfoot |
| Midfoot/ Hindfoot | $\mathbf{e}_1$ | Plantar/dorsiflexion axis, parallel to $\mathbf{k}$ of hindfoot |
| | $\mathbf{e}_2$ | Internal/External rotation axis |
| | $\mathbf{e}_3$ | Inversion/eversion axis, parallel to $\mathbf{i}$ of the midfoot |
| Forefoot/Midfoot | $\mathbf{e}_1$ | Plantar/dorsiflexion axis, parallel to $\mathbf{k}$ of midfoot |
| | $\mathbf{e}_2$ | Internal/External rotation axis |
| | $\mathbf{e}_3$ | Inversion/eversion axis, parallel to $\mathbf{i}$ of the forefoot |
| Foot/Tibia | $\mathbf{e}_1$ | Plantar/dorsiflexion axis, parallel to $\mathbf{k}$ of tibia |
| | $\mathbf{e}_2$ | Internal/External rotation axis |
| | $\mathbf{e}_3$ | Inversion/eversion axis, parallel to $\mathbf{i}$ of the foot |

## 2.5.5 The modified Shriners Hospitals for Children Greenville

The model proposed in [68] represents an attempt of producing a higher repeatable model of the foot-ankle complex for gait analysis, starting from those proposed in [152,153]. Table 2.11 and Figure 2.16 show the considered segments and

[13] In the paper that originally proposed the model, this axis has been addressed as $\mathbf{j}$ by mistake (personal communication with Dr Zimi Sawacha, author and corresponding author of [28]).

the relevant anatomical landmarks to be palpated, as described in [68]. Toe markers are arranged on a triad cluster, approximately placed on the vertices of a triangle.

**Table 2.11** – Considered segments and relevant anatomical landmarks (AL) to be palpated according to [68]. Markers used in static trials only are highlighted in italic.

| Segment | AL | Description |
|---|---|---|
| Tibia | TUB | Most anterior prominence of the tibial tuberosity |
| | TIB | Wand marker, distal lateral tibia |
| | SHN | Anywhere along the anterior crest of the tibia |
| | ANK | Distal apex of the lateral malleolus |
| | *MMA* | *Distal apex of the medial malleolus* |
| Hindfoot | CA1 | Distal end of the midline in the sagittal plane |
| | STL | At the same vertical level as the palpated landmark (avoiding the heel pad), and symmetrical with LCA |
| | *PT* | *First bone prominence below the lateral malleolus* |
| | LCA | At same distance from the most posterior point as STL, on lateral calcaneus (avoiding the heel pad) |
| Forefoot | VMH | Dorso-medial aspect of the 5th metatarso-phalangeal joint (avoiding the flexor tendon and the joint) |
| | *TOE* | *Mid-point of heads of the 2nd and 3rd metatarsal* |
| | *T23* | *Mid-point of bases of the 2nd and 3rd metatarsal* |
| | FMH | Dorso-medial aspect of the 1st metatarso-phalangeal joint (avoiding the flexor tendon) |
| | *D1M* | *Head of 1st metatarsal: medially on the foot* |
| | P1M | Dorso medial aspect of the 1st metatarso-cuneiform joint (avoiding the flexor tendon) |
| | *1BM* | *Base of 1st metatarsal: medial aspect* |
| Hallux | TRX-Y-Z | Toe triad placed on the nail hallux |

Table 2.12 shows the definitions for the axes of the local **ECS** of each segment as reported in [68]. The approach used to define the **ECS** in the walking trials is the *non-optimal* (§2.3.2.2.1). The paper presented three options to define the hindfoot and the forefoot ECSs, but no radiographs have been used for the present Thesis project, and the 'Option 3' will be adopted and described for both segments. The model was tested by two operators, who performed the marker placement and registered the relevant anthropometric measurements on fifteen children.

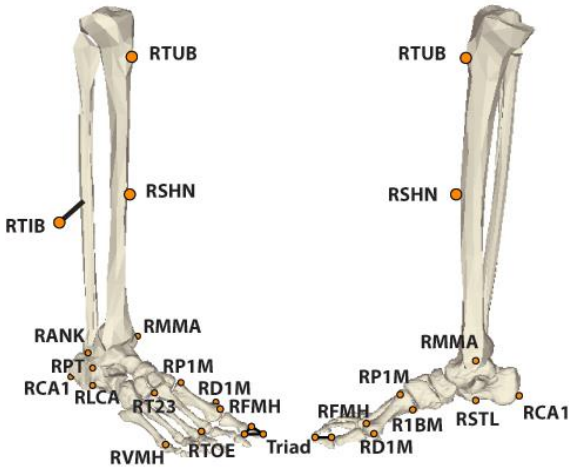


**Figure 2.16** – The anatomical landmarks to be palpated on right tibia and right foot segments according to the model proposed in [68].

Having defined the hindfoot **ECS** as described in Table 2.12, 'Option 3' prescribes to correct its inclination based on marker configuration. The PT marker is projected onto the sagittal plane, and CA1 is projected onto the transverse plane of the hindfoot. Then, the angle ($\alpha$) between the line joining these two projected points and the $\mathbf{i}$ axis of the hindfoot is calculated, and the calcaneal pitch angle (*ACP*) is estimated as:

$$ACP = 0.968 \cdot \alpha - 18.5^{\circ} \qquad \text{(Eq. 2.27)}$$

Eventually, the *ACP* angle is used to correct the hindfoot attitude by rotating the **ECS** firstly around its $\mathbf{k}$ axis, and then by rotating around the $\mathbf{i}$ of an angle measured before starting the data collection. Such and angle is measured manually by the operator using a goniometer, and it is defined as the inclination of the calcaneus midline with respect to the plantar surface. The forefoot **ECS**, similarly to the hindfoot, is corrected applying the 'Option 3' as described in [68]. In particular, the vector from 1BM to D1M is projected onto the sagittal plane of the forefoot. The angle between this vector and the $\mathbf{i}$ axis of the forefoot represents a marker-based estimate of the forefoot inclination.

**Table 2.12** – Definition of the local embedded coordinate systems (ECS) for each segment [68].

| Segment | ECS | ECS | Definition |
|---|---|---|---|
| Tibia | Anatomical | $\mathbf{j}$ | From KJC to AJC, as defined in [56] |
| | | $\mathbf{i}$ | Perpendicular to the plane defined by $\mathbf{j}$ and the vector connecting ANK and MMA |
| | | $\mathbf{k}$ | $\mathbf{i} \times \mathbf{j}$ |

| Segment | ECS | ECS | Definition |
|---|---|---|---|
| Hindfoot | Technical | $\mathbf{i}$ | Projection of the vector from CA1 to the mid-point between MMA and ANK on the plane of the plantar surface[14] |
| | | $\mathbf{j}$ | Modelled as the vertical axis of the global coordinate system (**GCS**) |
| | | $\mathbf{k}$ | $\mathbf{i}\times\mathbf{j}$ |
| Forefoot | Technical | $\mathbf{i}$ | Projection on the plantar surface of the vector from T23 to TOE |
| | | $\mathbf{k}$ | Orthonormal to the sagittal plane, which is defined by $\mathbf{i}$ and the vertical axis of the global coordinate system (**GCS**) |
| | | $\mathbf{j}$ | $\mathbf{k}\times\mathbf{i}$ |
| Hallux | Anatomical | $\mathbf{j}$ | Perpendicular to the triad plane |
| | | $\mathbf{i}$ | Parallel to the markers of the triad aligned with the big toe |
| | | $\mathbf{k}$ | $\mathbf{i}\times\mathbf{j}$ |

The forefoot **ECS** can then be corrected with this inclination via a rotation around its $\mathbf{k}$ axis. The joint kinematics are then estimated according to the ISB recommendations [58], and Table 2.13 reports the definitions of the **JCS** axes for each joint. No explicit parallelism of the defined joints with the anatomical ones is reported in [68]. However, it is reasonable to hold to be true that, as per the model in §2.5.2, §2.5.3 and §2.5.4, the virtual joint between forefoot and tibia is defined to allow comparison of the results to those obtained with conventional models, in which the foot is considered as a whole rigid segment. Between-stride and within-operator repeatability, and between-operator reproducibility were tested evaluating sample by sample standard deviations of the kinematics over the gait cycle gathered from the considered population, and subsequently averaged over the gait cycle [68]. Authors advised not considering as significant any changes lower or equal to 4° in the kinematics, since averaged standard deviation associated with the between-operator variability has been evaluated equal to 4°. The standard deviations obtained with this model were compared to those obtained with already published models. However, such a comparison was performed on different populations and tested by different operators, and it could be appropriate to implement further investigations.

[14] The plantar surface is approximated as the surface of the floor when dealing with healthy subjects (personal communication with Dr Bruce A. MacWilliams).

## 2.6 Open questions

This Chapter presented a detailed background of the measurement and modelling techniques used in gait analysis to assess the joint movements of the foot-ankle complex. Performing robust repeatability and reproducibility studies of the foot models in order to fully appreciate their clinical utility emerged as essential [29]. Thus, the sources of errors typical of a marker-based approach in gait analysis needs to be evaluated. The literature, though, is lacking of a methodology to evaluate the effect that different calibration procedures of stereophotogrammetric systems might induce on the joint kinematics estimated using a marker-based approach. This kind of analysis would call for the use of indices to evaluate the similarities among curves obtained from data processed with different calibration parameters. However, a wide number of indices has been proposed and used to assess gait data variability, but their interpretation is somehow limited since a comparative analysis of their sensitivity to the different sources of gait data variability is not available. Regarding the foot-ankle modelling, the literature analysis has highlighted that many models of the foot-ankle complex have been proposed in the past two decades, but their validation is often limited due to small size of the testing population, or to the use of different metrics among models to validate the outcomes. Moreover, the models have never been concurrently assessed and results of published comparisons are hence weak.

**Table 2.13** – Definition of the joint coordinate systems (JCS) for each considered joint [68].

| Joint | JCS | Definition |
|---|---|---|
| Hindfoot/Tibia | $\mathbf{e}_1$ | Plantar/dorsiflexion axis, parallel to $\mathbf{k}$ of tibia |
| | $\mathbf{e}_2$ | Internal/External rotation axis |
| | $\mathbf{e}_3$ | Inversion/eversion axis, parallel to $\mathbf{i}$ of the hindfoot |
| Midfoot/ Hindfoot | $\mathbf{e}_1$ | Plantar/dorsiflexion axis, parallel to $\mathbf{k}$ of hindfoot |
| | $\mathbf{e}_2$ | Internal/External rotation axis |
| | $\mathbf{e}_3$ | Inversion/eversion axis, parallel to $\mathbf{i}$ of the midfoot |
| Forefoot/Midfoot | $\mathbf{e}_1$ | Plantar/dorsiflexion axis, parallel to $\mathbf{k}$ of midfoot |
| | $\mathbf{e}_2$ | Internal/External rotation axis |
| | $\mathbf{e}_3$ | Inversion/eversion axis, parallel to $\mathbf{i}$ of the forefoot |
| Foot/Tibia | $\mathbf{e}_1$ | Plantar/dorsiflexion axis, parallel to $\mathbf{k}$ of tibia |
| | $\mathbf{e}_2$ | Internal/External rotation axis |
| | $\mathbf{e}_3$ | Inversion/eversion axis, parallel to $\mathbf{i}$ of the foot |

This Thesis aims to answer these questions step by step, starting from the choice of the most suitable indices to evaluate gait data variability. Subsequently, the metrological performances of the stereophotogrammetric systems used in a gait

analysis scenario will be evaluated, with particular focus on the calibration procedure. Then, the four most adopted models of the foot-ankle complex for gait analysis will be concurrently assessed to evaluate their repeatability and reproducibility. Eventually, a new model of the foot-ankle complex will be proposed to attempt improving the performances already obtained with the analysed models.

**Table 2.14** – Summary of the models proposed in literature. Where available, the table shows: (i) model updates, technical or clinical studies are cited as 'Other studies'; (ii) the number of modelled segments and the number of subjects the models have been tested on; (iii) if clinical studies have been performed using the pertinent model; (iv) whether the joint kinematics were shown for the whole gait cycle (WGC) or a portion of it within either the original papers or subsequent updates; (v) whether the joints are modelled with a JCS approach; and (vi) if the model is currently being used. A question mark highlights information that was not possible to retrieve either from the original papers or subsequent studies. Models that required the use of radiographs are highlighted in grey.

| Model name | First study | Other studies | Foot segments | Subjects | Clinical tests? | Stance/Gait Cycle | JCS? | Used today? |
|---|---|---|---|---|---|---|---|---|
| | Kepple *et al.* (1990) [154] | | 1 | 5 | | Stance | ? | |
| | Scott *et al*. (1991) [155] | | 1 | 3 | | Stance | ? | |
| | D'Andrea *et al*. (1993) [156] | | 3 | 1 | | Stance | ? | |
| | Siegel *et al*. (1995) [157] | | 1 | 1 | ✓ | Stance | ? | |
| Milwaukee Foot model | Kidder *et al*. (1996) [158] | [126,143,159–165] | 3 | 1 | ✓ | WGC | ✓ | ✓ |
| | Moseley *et al*. (1996) [166] | | 1 | 14 | | Stance | | |
| | Liu *et al.* (1997) [167] | | 1 | 10 | | Stance | | |
| | Rattanaprasert *et al*. (1998) [144] | | 3 | 10 | ✓ | Stance | ✓ | |
| | Cornwall *et al.* (1999) [115,116] | | 3 | 153 | | Stance | ✓ | |
| IOR model – vers 1 | Leardini *et al.* (1999) [31] | [168] | 4 | 9 | | Stance | ✓ | |
| | Wu *et al.* (2000) [169] | | 3 | 10 | ✓ | WGC | | |
| | Hunt *et al*. (2001) [170] | | 2 | 18 | | Stance | | |
| Oxford Foot Model | Carson *et al*. (2001) [64] | [65,114,117–119,171,172] | 3 | 2 | ✓ | WGC | ✓ | ✓ |
| | Arampatzis *et al*. (2002) [120] | | 6 | 6 | ✓ | Terminal swing | ✓ | |
| | MacWilliams *et al*. (2003) [69] | | 8 | 18 | | Stance | ✓ | |
| Heidelberg model | Simon *et al*. (2006) [121] | [147] | 6 | 10 | ✓ | WGC | | |
| | Tome *et al.* (2006) [122] | [173] | 5 | 24 | ✓ | Stance | ✓ | |
| Shriners Hospitals for Children Greenville | Davis *et al.* (2006) [152] | [68,153,174] | 3 | ? | | WGC | ✓ | ✓ |
| IOR model – vers 2 | Leardini *et al*. (2007) [67] | [112,142,175–177] | 4 | 10 | | WGC | ✓ | ✓ |
| | Jenkyn *et al.* (2007) [145] | | 3 | 12 | | WGC | ✓ | |
| | Rao *et al.* (2007) [123] | [178] | 3 | 15 | ✓ | Stance | ✓ | |
| | Houk *et al.* (2008) [179] | [180] | 3 | 12 | | Stance | ✓ | |
| | Sawacha *et al.* (2009) [28] | [181,182] | 3 | 20 | ✓ | WGC | ✓ | ✓ |
| | Cobb *et al.* (2009) [146] | [183] | 3 | 11 | ✓ | Stance | ✓ | ✓ |

Chapter 3

# Choice of the indices to evaluate gait data variability

## 3.1 Introduction

The assessment of human joint kinematics and dynamics via 3D gait analysis has been reported to be suitable for clinical decision-making, thanks also to repeatability and reproducibility studies that contributed to validate relevant measurements and modelling techniques [64,86–88]. These type of studies are also critical when comparing biomechanical parameters at baseline and follow-up in clinical studies [89].

In both the mentioned contexts, a number of different indices have been proposed and used as summarised in the reviews [90,92], and described in §2.4. Some of the above cited indices, including standard deviation (SD) [125], coefficient of variation (CV) [125], Intraclass Correlation Coefficient (ICC) [130], Technical Error of Measurement (TEM) [114], and Minimum Detectable Changes (MDC) [109], are meant to quantify the data dispersion around the reference value at specific instants of the gait cycle, and as such are not descriptive, for example, of the whole within-stride variability. Other indices, instead, including the Root Mean Square Deviation (RMSD) [16], Mean Absolute Variability (MAV) [140], Coefficient of Multiple Correlation (CMC) [125], and the Linear Fit Method (LFM) coefficients, which has been recently proposed [129], provide the similarity of the curve patterns along the whole gait cycle. This method has been tested and briefly validated on both synthetic and experimental data gathered from healthy adults during level walking, but tests were limited to the sagittal knee kinematics. A few methods have been recently proposed to evaluate repeatability and reproducibility of kinematic and dynamic variables based on a more complex mathematical analysis (e.g. Principal Component Analysis and Fractal method [90,92]), but their wider adoption is

possibly limited by the fact that their output might be complex to understand and unfamiliar to clinical users.

Repeatability and reproducibility indices (RI) might be influenced by some confusing-factors, leading to complicated interpretation of the relevant results. These factors are:

a) the range of motion of the considered joint [184];
b) the sample-by-sample amplitude variability, as different joints might show different distortions from the averaged pattern [60];
c) the offset among curves, mostly depending on marker repositioning [31];
d) the time shift due to physiological and pathological gait phases variability [185];
e) the different curve shapes among joints and planes [184].

Due to their concise nature, RI do not separately account for these four contributions and their interpretability is hence limited. The coefficient of multiple correlation has already been tested and questioned in [124,184,186], but it remained the most used. One of the objectives of this Thesis is to assess the repeatability and reproducibility of models used to estimate foot and ankle joint kinematics. Thus, this Chapter aims to fill the gap of the literature of a comparative analysis of RI behaviour linked to the aforementioned confusing-factors via two simulations on both synthetic and experimental data, providing a guide on how to choose the most suitable similarity index to quantify joint kinematics variability.

## 3.2 Methods

To test the mathematical formulation of the indices, accounting also for particularly challenging conditions for the confusing-factors, tests were initially conducted on a generic and easy-to-manipulate *sine-curve* [184], parametrised according to the four aforementioned confusing-factors. This allows to easily impose changes to one factor at a time, while leaving the shape of the curve unvaried, and to observe the relevant variations in RI values. Then, focusing on gait analysis applications, and to test the effect of changing the shape of the curves, sagittal hip, knee and ankle kinematics gathered from experimental data were decomposed with a Fourier's analysis. Fourier's coefficients were then modified to simulate the effect of each of the

confusing-factors on the joint kinematics (*Fourier-based data*). Results provided RI values of repeatability analysis on gait variables for an ideal population of healthy adults walking barefoot on a treadmill at a self-selected and comfortable speed.

### 3.2.1 Experimental data

Thirteen healthy adults (same as described in the following Chapter at §5.2: ten males, age: 27.0 ± 1.9 years, body mass: 76.7 ± 13.8 kg, height: 1.83 ± 0.08 m, leg length: 85.3 ± 4.6 cm, foot size: 28.5 ± 1.0 cm), with no reported pathologies influencing their walking, were enrolled in this study after having signed an informed consent form. Ethical approval was granted by The University of Sheffield research ethics committee (Appendix C).

One operator performed the marker placement on the right lower limb of each participant and registered the anthropometric measurements, following the definitions given in the Plug-in-Gait protocol, which is the commercial version of the protocol proposed by Davis [56]: 4 markers on the pelvis, 2 markers on the thigh, 2 markers on the shank, 2 on the foot (Figure 2.12). Participants walked barefoot for two minutes on a treadmill (ADAL3D-F, TECMACHINE HEF Groupe – Andreziéux Bouthéon, France) at their self-selected speed (0.82 ± 0.15 m/s). Two experimental sessions were performed one month apart, and five right strides were retained for the analysis from the central time window.

Gait data were recorded with the stereophotogrammetric system addressed as SS#2 in the following Chapter §4.2.1 (ten T-160 cameras, 100 Hz, Vicon Nexus 1.8.5, Vicon Motion System Ltd – Oxford, UK). Pre-processing was conducted within Nexus as per clinical routine: the smoothing was performed using a Woltring routine, size 30 [187][15]. Sagittal joint kinematics was calculated using MATLAB (R2015b, The MathWorks, Inc. – Natick, MA, USA) and accordingly to the definitions given in [56]. Starting from the average of the collected data, expected range of variations were

[15] Using a Woltring filter routine is demonstrated to be equal to using twice an analog Butterworth filter. The Woltring routine has been specifically developed for kinematic data and it is not a filter, but rather a spline used to smooth the kinematic and dynamic curves: https://www.vicon.com/faqs/software/what-are-the-details-of-the-woltring-filter.

defined for the parameters of interest in the following analysis: joint range of motion (ROM); joint ROM fluctuations (α) accounting for within-subject variations; offset between curves (O), representative of variations due to marker repositioning; time shift (τ), accounting for physiological variability in the gait phases. The imposed values are shown in Table 3.1 and Table 3.2, and were then used for the *Sine-curve* and the *Fourier-based* data simulations.

### 3.2.2 Selected similarity indices

As reported in the Introduction (§3.1), the literature review highlighted a large number of methods and indices to quantify the similarity within a dataset. This can lead to confusion when comparing different repeatability studies on different models to select the most reliable, which is one of the aim of this Thesis. For this part of the project, only the indices calculated over the whole gait cycle were considered, and, among those, RMSE, MAV, and CMC resulted to be the most adopted in the past years. Another promising method, which was recently proposed, was considered: the Linear Fit Method [129].

The Root Mean Square Error is the most used index to quantify measurement uncertainties [22,188], and represents the square root of the variance. In gait analysis, knowing the true value of the joint kinematics is not possible unless using invasive methods, thus the RMSE is more often called Root Mean Square Deviation, and it is evaluated sample by sample, between the curves and averaged over the gait cycle, the formula implemented for its calculus is:

$$RMSD = \sqrt{\frac{\sum_{i=1}^{T}\left(y_i - \bar{y}\right)^2}{T}} \qquad \text{(Eq. 5.1)}$$

Where:

- $y_i$ is the curve for each subject collected during a session and representative of a stride;
- $T$ is the number of time points each stride is sampled in;
- $\bar{y}$ is considered as the reference curve, and changes depending on the analysis. For example, the reference for a within-subject analysis in the case of a dataset obtained as described in §3.2.1 is equal to the averaged

curve among those retrieved from the two sessions and each stride (i.e. the average among the ten curves obtained as five strides per each of the two sessions). Instead, for a between-subject analysis, each stride collected during each session per each subject is compared to a curve obtained averaging all the strides from all the sessions and all the subjects.

Similarly, the Median Absolute Variability measures the averaged sample-by-sample difference between maximum and minimum values among the compared curves [14,140], and its formula is:

$$MAV = \frac{\sum_{i=1}^{T} \left| \max\{\mathbf{a}(i)\} - \min\{\mathbf{a}(i)\} \right|}{T} \qquad \text{(Eq. 5.2)}$$

Where the matrix $\mathbf{a}(i)$ contains the curves of the joint variables to compare, and changes coherently with the selected analysis. For example:

- for a within-subject analysis $\dim\{\mathbf{a}(i)\} = (nS \cdot T) \times nR$:
  - $nS$ is the number of strides to compare;
  - $T$ as per above;
  - $nR$ is the number of repetitions, acquisition days or sessions;
- for a between-subject analysis, kinematics is averaged among possible repetitions and $\dim\{\mathbf{a}(i)\} = (nS \cdot T) \times nSbj$, with:
  - $nS$ and $T$ as per above;
  - $nSbj$ is the number of participants to the study.

The Coefficient of Multiple Correlation as proposed in [125], is the widest used index that evaluate repeatability of waveforms [57,141,189–192]. It represents the root square of the adjusted coefficient of multiple determination, and is expected to return values between 0 and 1. A stratification for the CMC values was also proposed in [141] to interpret the results of this analysis:

a. poor similarity when 0 < CMC < 0.60;
b. moderate similarity when 0.60 ≤ CMC < 0.75;
c. good similarity when 0.75 ≤ CMC < 0.85;
d. very good similarity when 0.85 ≤ CMC < 0.95; and
e. excellent when 0.95 ≤ CMC ≤ 1.

The formulation of the CMC changes depending on the application. It was originally proposed for within- and between-session analyses, but further studies have adapted these two formulations for their aims [139]. As an example, the within-subject CMC is equal to:

$$CMC = \sqrt{1 - \frac{\frac{\sum_{l=1}^{nSbj}\sum_{r=1}^{nR}\sum_{s=1}^{nS}\sum_{t=1}^{T}\left(y_{tsrl} - \bar{y}_{lt}\right)^2}{nSbj \cdot T(nR \cdot nS - 1)}}{\frac{\sum_{l=1}^{nSbj}\sum_{r=1}^{nR}\sum_{s=1}^{nS}\sum_{t=1}^{T}\left(y_{tsrl} - \bar{y}_{l}\right)^2}{nSbj(T \cdot nR \cdot nS - 1)}}} \qquad \text{(Eq. 5.3)}$$

With:

- $nSbj$, $nR$, $nS$ and $T$ as per above;
- $y_{tsrl}$ is the observed kinematic variable at each instant per each stride collected in each session and from each subject;
- $\bar{y}_l = \frac{1}{nR \cdot nS \cdot T}\sum_{r=1}^{nR}\sum_{s=1}^{nS}\sum_{t=1}^{T} y_{tsrl}$;
- $\bar{y}_{lt} = \frac{1}{nR \cdot nS}\sum_{r=1}^{nR}\sum_{j=1}^{nS} y_{tsrl}$ .

The (Eq. 3) represents the variance about the mean at the time point *t* for a specific subject over the total variability about the grand mean for that subject. For the between-subject analysis the CMC is equal to:

$$CMC = \sqrt{1 - \frac{\frac{\sum_{l=1}^{nSbj}\sum_{r=1}^{nR}\sum_{s=1}^{nS}\sum_{t=1}^{T}\left(y_{tsrl} - \bar{y}_{t}\right)^2}{T(nSbj \cdot nR \cdot nS - 1)}}{\frac{\sum_{l=1}^{nSbj}\sum_{r=1}^{nR}\sum_{s=1}^{nS}\sum_{t=1}^{T}\left(y_{tsrl} - \bar{y}\right)^2}{(T \cdot nSbj \cdot nR \cdot nS - 1)}}} \qquad \text{(Eq. 5.4)}$$

With:

- $\bar{y}_t = \frac{1}{nSbj \cdot nR \cdot nS}\sum_{l=1}^{nSbj}\sum_{k=1}^{nR}\sum_{j=1}^{nS} y_{tsrl}$;
- $\bar{y} = \frac{1}{nSbj \cdot nR \cdot nS \cdot T}\sum_{l=1}^{nSbj}\sum_{k=1}^{nR}\sum_{j=1}^{nS}\sum_{i=1}^{T} y_{tsrl}$ .

The (Eq. 4) represents the variance about the mean at the time point *t* for all the subjects over the total variability about the grand mean of all subjects.

The Linear Fit Method compares a set of curves to a reference $P_{ref}$, returning separate information about the scaling factor ($a_1$), the weighted averaged offset ($a_0$), and the trueness of the linear model between the compared curves, providing also a measure of their correlation ($R^2$).

$$a_1 = \frac{\sum_{t=1}^{T}\left(P_{ref}(t) - \overline{P}_{ref}\right)\cdot\left(y(t) - \overline{y}\right)}{\sum_{i=1}^{T}\left(P_{ref}(t) - \overline{P}_{ref}\right)^2} \quad \text{(Eq. 5.5)}$$

$$a_0 = \overline{y} - a_1\overline{P}_{ref} \quad \text{(Eq. 5.6)}$$

$$R^2 = \frac{\sum_{t=1}^{T}\left(a_0 + P_{ref}(t) - \overline{y}\right)^2}{\sum_{t=1}^{T}\left(y(t) - \overline{y}\right)^2} \quad \text{(Eq. 5.7)}$$

With:

- $y$ and $T$ as per above;
- $\overline{y} = \frac{1}{T}\sum_{t=1}^{T} y(t)$
- $\overline{P}_{ref} = \frac{1}{T}\sum_{t=1}^{T} P_{ref}(t)$

As per the RMSE, $P_{ref}$ changes depending on the analysis. When $R^2$ is higher than 0.5, the assumption of linearity can be considered as valid, and $a_1$ and $a_0$ can be interpreted as meaningful [129]. When comparing a number of curves with their average, the scaling factor and the weighted averaged offset tend to their ideal values (i.e., $a_1 = 1$ and $a_0 = 0$). Thus, to have a measure of the variations, it is worthy to report and observe the standard deviations for both $a_1$ and $a_0$ (*SD-*$a_1$ and *SD-*$a_0$).

## 3.2.3 Data analysis

### *3.2.3.1 Simulations on the sine-curve*

Following the methodology proposed in [184], groups of five curves ($k_j(t)$ with: $j \in [1,5] \subset \mathbb{N}$ and $t \in [0,100] \subset \mathbb{N}$ time samples) were generated from the following mathematical model:

$$k_j(t) = O + (1+\alpha)\frac{ROM}{1.76}\left[0.5\sin\frac{2\pi(t-\tau)}{100} + 0.5\sin\frac{4\pi(t-\tau)}{100}\right] \quad \text{(Eq. 5.8)}$$

Where *ROM*, *α*, *O* and *τ* are the previously described parameters. To obtain the desired imposed *ROM*, the amplitude of the sine-terms in the square parenthesis (Eq. 8) was normalized by dividing the (1+*α*)·*ROM* by 1.76. Groups of five curves were obtained by modifying each of the parameters per time, generating four datasets.

**Table 3.1** – Variations imposed for the simulations on the *sine-curve* for: 1) amplitude (*ROM*); 2) amplitude variability (*α*); 3) offset (*O*); and 4) time shift (*τ*).

| | | ***ROM* (°)** | ***α* (%ROM)** | ***O* (%ROM)** | ***τ* (%GaitCycle)** |
|---|---|---|---|---|---|
| **Case 1.x** | *I* | 5 | ± 2.5 | 0 | 0 |
| | *II* | 15 | ± 2.5 | 0 | 0 |
| | *III* | 30 | ± 2.5 | 0 | 0 |
| | *IV* | 40 | ± 2.5 | 0 | 0 |
| | *V* | 50 | ± 2.5 | 0 | 0 |
| | *VI* | 60 | ± 2.5 | 0 | 0 |
| **Case 2.x** | *I* | 5 | ± 2.5 | 0 | 0 |
| | *II* | 5 | ± 5.0 | 0 | 0 |
| | *III* | 5 | ± 7.5 | 0 | 0 |
| | *IV* | 5 | ±10.0 | 0 | 0 |
| | *V* | 5 | ±12.5 | 0 | 0 |
| | *VI* | 5 | ±15.0 | 0 | 0 |
| **Case 3.x** | *I* | 5 | 0 | ± 5 | 0 |
| | *II* | 5 | 0 | ± 20 | 0 |
| | *III* | 5 | 0 | ± 40 | 0 |
| | *IV* | 5 | 0 | ± 60 | 0 |
| | *V* | 5 | 0 | ± 80 | 0 |
| | *VI* | 5 | 0 | ±100 | 0 |
| **Case 4.x** | *I* | 5 | 0 | 0 | 0-5 |
| | *II* | 5 | 0 | 0 | 0-10 |
| | *III* | 5 | 0 | 0 | 0-15 |
| | *IV* | 5 | 0 | 0 | 0-20 |
| | *V* | 5 | 0 | 0 | 0-25 |
| | *VI* | 5 | 0 | 0 | 0-30 |

When varying *α*, *O* and *τ*, ROM was set equal to 5°. The relevant values imposed to the confusing-factors are shown in the Table 3.1. Then, the four selected RI were calculated for all the generated curves. For RMSD and LFM, each *j*-th curve was compared to the mean of the five curves from the same group, taken as a reference value.

### *3.2.3.2 Simulations on Fourier-based data*

A Fourier decomposition (Eq. 3.9) was performed starting from the averaged sagittal hip, knee and ankle kinematics obtained from the *experimental-data*. Non-sagittal kinematics were discarded for simulations since they are known to be less reliable [125,193]. The Fourier's decomposition of each mean curve is:

$$y(t) = \frac{A_0}{2} + \sum_{k=1}^{n} \left[ A_k \cos(kt) + B_k \sin(kt) \right], \quad t \in [0,100] \subset \mathbb{N} \qquad \text{(Eq. 5.9)}$$

The decomposition order (*n*) has been chosen as the order that gave a RMSE between the averaged pattern and the curve reconstructed via Fourier series lower than a threshold, chosen as 1/100 of the technique precision (1° [194]). The Fourier coefficients ( $A_0$ , $A_k$ and $B_k$ ) were then modified to obtain different values for *α*, *O*, and *τ*, and to perform three simulations. For this set of simulations, ROM was not considered as a parameter to be changed as in paragraph §3.2.3.1, but was imposed directly from the curve reconstructed via the Fourier's decomposition. A mixed simulation (MS), accounting for all the previous sources of variations, was then performed to verify whether it is possible to separately observe on the RI values the effects of the different sources of variability among curves. A Monte Carlo procedure was adopted for each simulation [195]. Specifically, uniform probability density functions were considered for *α*, *O*, and *τ*, whose ranges of variations were chosen based on the experimental data, accounting for both within- (*WS*) and between-subject (*BS*) variability (Table 3.2). Finally, averaged values and standard deviations of the calculated Similarity Indices were calculated for the within- and between-subject analysis. Finally, averaged values and standard deviations for CMC and MAV among the values obtained from the 1000 simulations were calculated for the *WS* and *BS* analyses. Whereas, the average and standard deviations of the LFM coefficients and RMSD were firstly calculated among the five curves of each group. Then, the average among the 1000 groups of the obtained averages and standard deviations were reported as results for the LFM coefficients and RMSD. This procedure is summarised in Figure 3.1.

**Table 3.2** – Variations imposed to amplitude variability (*α*), offset (*O*), and time shift (*τ*) for the simulations performed on *Fourier-based data*.

| | ***Within-subject* (WS)** | | | ***Between-subject* (BS)** | | |
|---|---|---|---|---|---|---|
| | *α* (%$_{ROM}$) | *O* (%$_{ROM}$) | *τ* (%$_{GaitCycle}$) | *α* (%$_{ROM}$) | *O* (%$_{ROM}$) | *τ* (%$_{GaitCycle}$) |
| **Hip** | 5 | 5 | 5 | 10 | 30 | 10 |
| **Knee** | 5 | 5 | 5 | 5 | 15 | 10 |
| **Ankle** | 5 | 5 | 5 | 10 | 20 | 10 |

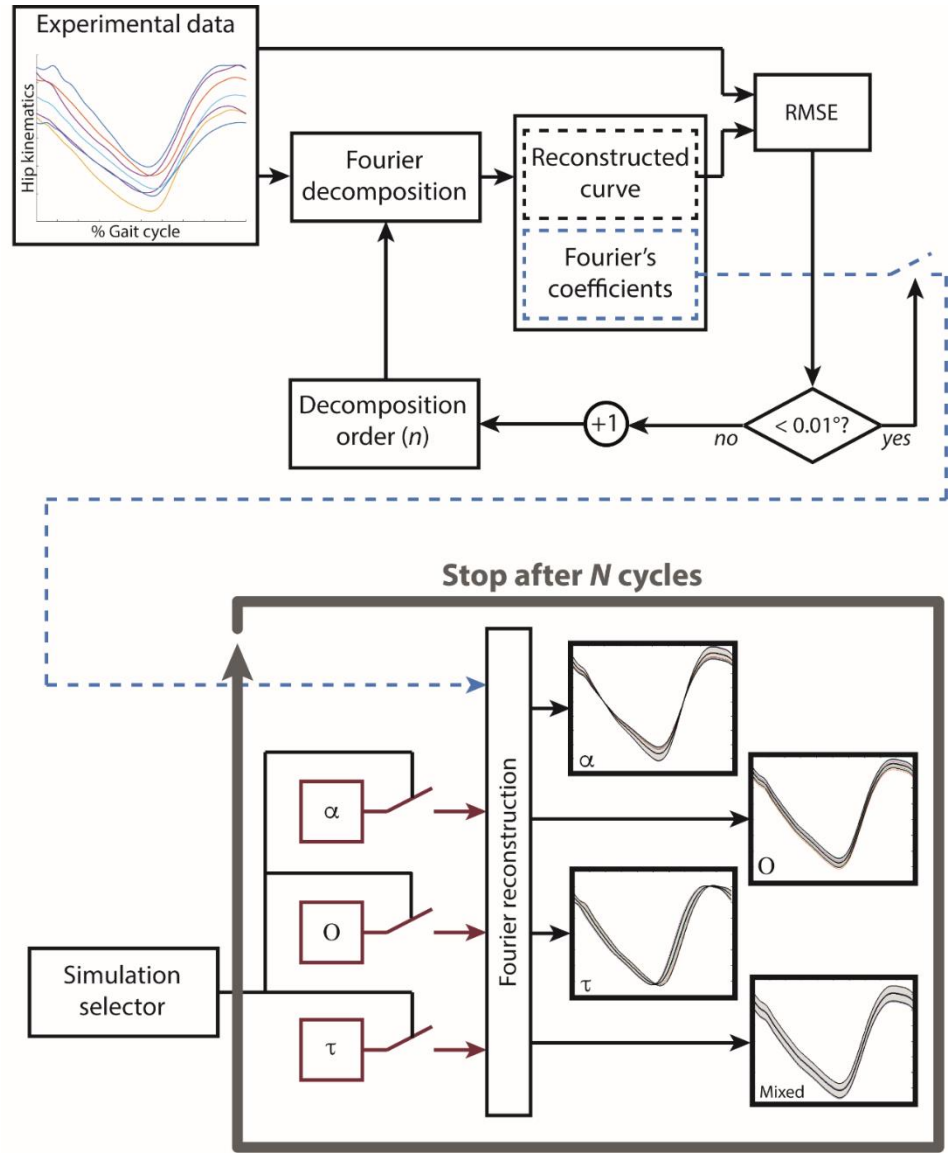


**Figure 3.1** – Procedure used to obtain the Fourier-based data and simulate the changes due to the fluctuations of the range of motion (*α*), the offset among the curves (*O*), and the physiological time-shift due to the stride-to-stride variability (*τ*).

## 3.3 Results

### 3.3.1 Sine-curve data

Table 3.3 shows the results obtained for the simulations on the *sine-curve data*. When varying *ROM* (Case 1 in Table 3.1 and Table 3.2), as the *ROM* increased, the distances between the generated curves increased and consistently did MAV and RMSD, whereas CMC and the LFM coefficients did not detected these changes. CMC, $a_0$, and $R^2$ did not significantly change when increasing of fluctuations *α* (Case 2 in Table 3.1 and Table 3.2), whereas standard deviation of $a_1$ varied proportionally with *α*; MAV and RMSD increased as the distances between the compared curves increased with *α*.

Increasing the offset between the curves (*O*, Case 3 in Table 3.1 and Table 3.2), CMC dramatically decreased from >0.99 to a complex value, indicating a complete loss of correlation among the compared curves. The standard deviation of the LFM offset coefficient ($a_0$) resulted to be the 79% of the imposed *O*, whereas $a_1$ and $R^2$ reached their ideal values (i.e., 1). As expected, MAV returned exactly the maximum imposed *O*, and the range of RMSD values was equal to 53% of MAV, and thus of *O*. Increasing the time shift (*τ*, Case 4 in Table 3.1 and Table 3.2) highlighted a worsening of both CMC and $R^2$, with consequent loss of significance for the coefficients $a_1$ and $a_0$. MAV and RMSD increased with the increasing of *τ*.

### 3.3.2 Fourier-based data

The results obtained testing the RIs on the *Fourier-based data* are shown in Table 3.4. Varying *α*, means and standard deviations of CMC displayed slightly different values among the joints. This is more evident looking at the CMC-*WS* for Hip ($0.99 \pm 0.01$), Knee ($0.99 \pm 0.01$), and Ankle ($0.98 \pm 0.03$). The *SD*-$a_1$ changed with α for each joint, whereas the $\overline{R^2}$ always reached its ideal value with null *SD*-$R^2$.

Comparing the within- and between-subjects, CMC decreased more explicitly when increasing the offset: e.g. for the hip, CMC-*WS* was higher than 0.99, whereas CMC-*BS* was equal to $0.90 \pm 0.05$. Even though less evident than in the sine-curve data, the *SD*-$a_0$ varied with the imposed *O*, whereas $\overline{a_1}$ and $\overline{R^2}$ reached their ideal values with null standard deviations.

Coherently with the results obtained in the *sine-curve* data, the increment in the imposed time shift from 5% (*WS*) to 10% (*BS*) resulted in a decreasing of the CMC values for all joints and both comparisons. Concerning the LFM coefficients, $\overline{R^2}$ decreased and *SD*-$R^2$ increased with the increase of *τ*, and the even lower values were found for the *BS* comparison of the ankle joint ( $\overline{R^2}$ = 0.87 and *SD*-$R^2$ = 0.11).

The mixed simulation (MS) from *WS* to *BS*, provided similar results of those obtained via the time shift simulation. Comparing the within- and between-subjects, MAV and RMSD increased following the increment of all the imposed variations.

**Table 3.3** – Values of Coefficient of multiple correlation (CMC), Linear Fit Method (LFM) coefficients, Mean Absolute Variability (MAV) and Root Mean Square Error (RMSD) obtained from the simulations performed on the *sine-curve*, changing its amplitude (*ROM*), amplitude variability ($\alpha$), offset ($O$), and time shift ($\tau$). (*) not a number values (**–**) has to be intended as the method has given complex values.

| | | | CMC | LFM coefficients | | | MAV (°) | RMSD (°) |
|---|---|---|---|---|---|---|---|---|
| | | | | $a_1$ | $a_0$ (°) | $R^2$ | | |
| **Case 1.x** | **ROM (°)** | *I* | > 0.99 | 1.00 ± 0.04 | 0.0 ± 0.0 | 1.00 ± 0.00 | 0.1 | 0.0 ± 0.0 |
| | | *II* | > 0.99 | 1.00 ± 0.04 | 0.0 ± 0.0 | 1.00 ± 0.00 | 0.3 | 0.1 ± 0.1 |
| | | *III* | > 0.99 | 1.00 ± 0.04 | 0.0 ± 0.0 | 1.00 ± 0.00 | 0.7 | 0.3 ± 0.2 |
| | | *IV* | > 0.99 | 1.00 ± 0.04 | 0.0 ± 0.0 | 1.00 ± 0.00 | 0.9 | 0.3 ± 0.2 |
| | | *V* | > 0.99 | 1.00 ± 0.04 | 0.0 ± 0.0 | 1.00 ± 0.00 | 1.1 | 0.4 ± 0.3 |
| | | *VI* | > 0.99 | 1.00 ± 0.04 | 0.0 ± 0.0 | 1.00 ± 0.00 | 1.3 | 0.5 ± 0.4 |
| **Case 2.x** | **$\alpha$ (%$_{ROM}$)** | *I* | > 0.99 | 1.00 ± 0.04 | 0.0 ± 0.0 | 1.00 ± 0.00 | 0.1 | 0.0 ± 0.0 |
| | | *II* | > 0.99 | 1.00 ± 0.08 | 0.0 ± 0.0 | 1.00 ± 0.00 | 0.2 | 0.1 ± 0.1 |
| | | *III* | > 0.99 | 1.00 ± 0.12 | 0.0 ± 0.0 | 1.00 ± 0.00 | 0.3 | 0.1 ± 0.1 |
| | | *IV* | > 0.99 | 1.00 ± 0.16 | 0.0 ± 0.0 | 1.00 ± 0.00 | 0.5 | 0.2 ± 0.1 |
| | | *V* | > 0.99 | 1.00 ± 0.20 | 0.0 ± 0.0 | 1.00 ± 0.00 | 0.6 | 0.2 ± 0.2 |
| | | *VI* | 0.99 | 1.00 ± 0.24 | 0.0 ± 0.0 | 1.00 ± 0.00 | 0.7 | 0.3 ± 0.2 |
| **Case 3.x** | ***O* (%$_{ROM}$)** | *I* | > 0.99 | 1.00 ± 0.00 | 0.0 ± 0.2 | 1.00 ± 0.00 | 0.5 | 0.2 ± 0.1 |
| | | *II* | 0.87 | 1.00 ± 0.00 | 0.0 ± 0.8 | 1.00 ± 0.00 | 2.0 | 0.6 ± 0.4 |
| | | *III* | 0.61 | 1.00 ± 0.00 | 0.0 ± 1.6 | 1.00 ± 0.00 | 4.0 | 1.2 ± 0.8 |
| | | *IV* | 0.37 | 1.00 ± 0.00 | 0.0 ± 2.4 | 1.00 ± 0.00 | 6.0 | 1.8 ± 1.3 |
| | | *V* | 0.04 | 1.00 ± 0.00 | 0.0 ± 3.2 | 1.00 ± 0.00 | 8.0 | 2.4 ± 1.7 |
| | | *VI* | –* | 1.00 ± 0.00 | 0.0 ± 4.0 | 1.00 ± 0.00 | 10.0 | 3.0 ± 2.1 |
| **Case 4.x** | **$\tau$ (%$_{GaitCycle}$)** | *I* | 0.98 | 1.00 ± 0.01 | 0.0 ± 0.0 | 0.97 ± 0.03 | 0.6 | 0.2 ± 0.1 |
| | | *II* | 0.92 | 1.00 ± 0.06 | 0.0 ± 0.0 | 0.89 ± 0.10 | 1.2 | 0.4 ± 0.3 |
| | | *III* | 0.84 | 1.00 ± 0.13 | 0.0 ± 0.0 | 0.77 ± 0.20 | 1.7 | 0.6 ± 0.3 |
| | | *IV* | 0.73 | 1.00 ± 0.23 | 0.0 ± 0.0 | 0.65 ± 0.28 | 2.1 | 0.8 ± 0.4 |
| | | *V* | 0.60 | 1.00 ± 0.35 | 0.0 ± 0.0 | 0.53 ± 0.33 | 2.5 | 1.0 ± 0.3 |
| | | *VI* | 0.46 | 1.00 ± 0.47 | 0.0 ± 0.0 | 0.43 ± 0.33 | 2.8 | 1.1 ± 0.3 |

## 3.4 Discussion

This part of the study presented a comparative analysis of four similarity indices widely used to assess gait data variability, aiming to differentiate the effect of the possible sources of variability. To this purpose, the sensitivity of the RI to each investigated confusing-factors (joint range of motion (*ROM*), joint ROM fluctuations ($\alpha$), offset between curves ($O$), time shift ($\tau$), and the curve shape) was highlighted using two simulated data sets. The first is based on simulations conducted on a *sine-curve* aiming to test the mathematical formulation of the indices on a generic data set. The second one is based on lower limb kinematics gathered from healthy adults and reconstructed via a Fourier's decomposition. The results of this second simulation can be considered as reference values for repeatability analysis of gait variables from similar cohorts walking self-paced barefoot on a treadmill.

The methodology here proposed could also be used to obtain the RI values specific for population of patients affected by specific pathologies, which might lead to alterations of gait patterns only in specific phases of the gait cycle [196]. These latter variations, in fact, might be simulated by running the Fourier based simulation imposing

pathology-specific time shifts. To practically choose the best index to be used for the repeatability and reproducibility studies due in the next step of this Thesis, indices will be examined one by one.

**Table 3.4** – Values of Coefficient of multiple correlation (CMC), Linear Fit Method (LFM) coefficients, Mean Absolute Variability (MAV) and Root Mean Square Error (RMSD) obtained from the simulations performed on the *Fourier-based data*, changing amplitude variability (*α*), offset (*O*), and time shift (*τ*) of the curves. *MS* stands for the simulations performed mixing the effects of *α, O,* and *τ*, respectively. *WS* and *BS* address the within- and between-subject analysis, respectively.

| | Joints | | ROM (°) | CMC | LFM coefficients | | | MAV (°) | $\overline{\text{RMSD}}$ (SD) (°) |
|---|---|---|---|---|---|---|---|---|---|
| | | | | | $\bar{a}_1$ (SD) | $\bar{a}_0$ (SD) | $\overline{R^2}$ (SD) | | |
| ***α*** **(%ROM)** | ***Hip*** | *WS* | 30 ± 2 | 0.99 ± 0.01 | 1.00 (0.09) | 0 (1) | 1.00 (0.00) | 2 ± 1 | 1 (0) |
| | | *BS* | 43 ± 6 | 0.98 ± 0.02 | 1.00 (0.10) | 0 (2) | 1.00 (0.00) | 6 ± 4 | 2 (1) |
| | ***Knee*** | *WS* | 64 ± 6 | 0.99 ± 0.01 | 1.00 (0.08) | 0 (2) | 1.00 (0.00) | 6 ± 5 | 2 (1) |
| | | *BS* | 64 ± 6 | 0.99 ± 0.01 | 1.00 (0.08) | 0 (2) | 1.00 (0.00) | -- | 2 (1) |
| | ***Ankle*** | *WS* | 14 ± 1 | 0.98 ± 0.03 | 1.00 (0.12) | 0 (0) | 1.00 (0.00) | 1 ± 1 | 0 (0) |
| | | *BS* | 19 ± 1 | 0.99 ± 0.02 | 1.00 (0.10) | 0 (0) | 1.00 (0.00) | 1 ± 1 | 0 (0) |
| ***O*** **(%ROM)** | ***Hip*** | *WS* | 31 ± 0 | > 0.99 | 1.00 (0.00) | 0 (1) | 1.00 (0.00) | 2 ± 1 | 1 (1) |
| | | *BS* | 31 ± 0 | 0.90 ± 0.05 | 1.00 (0.00) | 0 (5) | 1.00 (0.00) | 7 ± 2 | 4 (2) |
| | ***Knee*** | *WS* | 51 ± 0 | > 0.99 | 1.00 (0.00) | 0 (2) | 1.00 (0.00) | 2 ± 1 | 1 (1) |
| | | *BS* | 51 ± 0 | 0.96 ± 0.02 | 1.00 (0.00) | 0 (4) | 1.00 (0.00) | 6 ± 2 | 3 (2) |
| | ***Ankle*** | *WS* | 18 ± 0 | > 0.99 | 1.00 (0.00) | 0 (1) | 1.00 (0.00) | 1 ± 0 | 0 (0) |
| | | *BS* | 18 ± 0 | 0.91 ± 0.04 | 1.00 (0.00) | 0 (2) | 1.00 (0.00) | 3 ± 1 | 2 (1) |
| ***τ*** **(%GaitCycle)** | ***Hip*** | *WS* | 31 ± 0 | 0.99 ± 0.01 | 1.00 (0.01) | 0 (0) | 0.99 (0.01) | 3 ± 1 | 1 (1) |
| | | *BS* | 31 ± 0 | 0.97 ± 0.01 | 1.00 (0.02) | 0 (0) | 0.95 (0.04) | 5 ± 1 | 2 (1) |
| | ***Knee*** | *WS* | 51 ± 0 | 0.99 ± 0.01 | 1.00 (0.01) | 0 (0) | 0.98 (0.02) | 5 ± 1 | 2 (1) |
| | | *BS* | 51 ± 0 | 0.95 ± 0.02 | 1.00 (0.04) | 0 (0) | 0.92 (0.07) | 9 ± 2 | 4 (2) |
| | ***Ankle*** | *WS* | 18 ± 0 | 0.97 ± 0.01 | 1.00 (0.02) | 0 (0) | 0.96 (0.04) | 2 ± 1 | 1 (1) |
| | | *BS* | 18 ± 0 | 0.91 ± 0.03 | 1.00 (0.07) | 0 (0) | 0.87 (0.11) | 4 ± 1 | 2 (1) |
| **MS** | ***Hip*** | *WS* | 34 ± 1 | 0.99 ± 0.03 | 1.00 (0.01) | 0 (0) | 0.99 (0.01) | 3 ± 1 | 1 (1) |
| | | *BS* | 45 ± 5 | 0.97 ± 0.01 | 1.00 (0.02) | 0 (0) | 0.96 (0.04) | 8 ± 3 | 3 (2) |
| | ***Knee*** | *WS* | 51 ± 1 | 0.98 ± 0.01 | 1.00 (0.01) | 0 (0) | 0.97 (0.02) | 5 ± 1 | 3 (1) |
| | | *BS* | 52 ± 1 | 0.95 ± 0.02 | 1.00 (0.04) | 0 (0) | 0.92 (0.08) | 9 ± 2 | 5 (3) |
| | ***Ankle*** | *WS* | 17 ± 1 | 0.97 ± 0.01 | 1.00 (0.02) | 0 (0) | 0.96 (0.04) | 2 ± 1 | 1 (0) |
| | | *BS* | 18 ± 1 | 0.91 ± 0.03 | 1.00 (0.07) | 0 (0) | 0.87 (0.11) | 4 ± 1 | 2 (1) |

Coherently with the literature [184], the Coefficient of Multiple Correlation (CMC) appeared insensitive to the imposed range of motion of the curves. Indeed, CMCs did not change when varying the amplitude (*ROM*) of the *sine-curve* from 5° up to 60° (Table 3.3). Small variations in CMC values can be observed when varying the sample-by-sample amplitude (*α*). The same results were also obtained for the *Fourier-based* simulations. This seems to be in contrast with the literature, which reports low CMCs when dealing with curves with small range of motion [124,184,186]. Differently from the approach adopted here, where the parameters were varied one at a time, simultaneous variations of offsets, time shift and ROM fluctuations were imposed in [184], producing a data set intrinsically characterised by a small signal to noise ratio. Looking at the results from the within-subject analysis on the *Fourier-based data*, when the same ranges of variations were imposed to *α* for Hip, Knee, and Ankle, CMCs values

within the range of "excellent similarity" were obtained for both Hip and Knee, whereas lower CMCs were obtained for the Ankle, which could be classified as "very good similarity". Thus, consistently with what reported by other studies [124,186], it can be stated that the CMC is sensitive to the curve patterns, and when different joints are considered, the stratification of CMC values as proposed in [141] might lead to misinterpretation of the results and should be carefully adopted. The CMC was also affected by time shift and offset variations, with some of the latter even causing the coefficients to reach complex values (Table 3.3), as reported also by [139]. In that paper complex CMC values were reported even for smaller offsets, most likely due to a simultaneous presence of a time shift between the investigated curves. The data here presented actually showed low CMC values also when imposing a large time shift between the curves. When dealing with confusing-factors having ranges that are comparable with the variability of gait curves of healthy subjects, as done for the *Fourier-based* simulation (Table 3.4), the effect of the time shift on the CMC resulted to be predominant on the effect of the imposed offset. This trend was confirmed by the results obtained from the 'mixed simulations' (*MS*) that produced a worsening of the CMCs, highlighting the difficulty of interpreting whether low values are due to a large offset or a high time shift between the curves. The reported results recommend the CMCs to be interpreted only after a visual inspection of the curves, aiming to establish presence or absence of large offsets and time shifts.

The Linear Fit Method (LFM) yielded three coefficients, which did not vary when changing the *ROM* of the *sine-curve* (Table 3.3). The scaling factor ($a_1$) reflected the changes in the sample-by-sample amplitude variations (*α*). This emerged clearly looking at the standard deviations of $a_1$ in Table 3.3, where null $a_0$ and $R^2$ equal to 1 were found. As expected, variations of the offset reflected directly onto $a_0$, while $a_1$ and $R^2$ remained equal to their ideal value (i.e. 1). These two results were coherent with those reported in [129]. The excursion of $a_0$ was found to be the 79% of the imposed offset for the simulations on the *sine-curve*. In the case of the *Fourier-based data*, $a_0$ is exactly the offset only in the ideal case of $a_1$ equal to 1, otherwise it is not a representative measure of the offset (Table 3.4, case *α*) unless corrected accounting for $a_1$. Results in Table 3.4 (*α* = 5% of the *ROM*, *WS*) showed equal $\overline{R^2}$ and SD-$R^2$ for different joints, indicating

that the linear relation coefficient is not dependent from the curve pattern. Variations of the imposed offset reflected onto the SD-$a_0$, whereas $a_1$ and $R^2$ remained equal to their ideal values. As reported in [129], the $a_0$ represents directly the offset when comparing only two curves. However, the increasing of the number of curves under investigation led to a mismatch between the obtained $\bar{a}_0$ and SD-$a_0$, and the offset. In fact, the $\bar{a}_0$ is always equal to zero even if the offset among curves increased. The standard deviation of $a_0$ was found to be only an estimate of the offset variation, but it cannot be considered as a representative measure of it. The only confusing-factor that invalidated the assumption of a linear relationship between the compared curves was the time shift ($\tau$). Indeed, when LFM is adopted in gait studies, the decreasing of $R^2$ should be interpreted as presence of time shift between the curves, with consequent loss of significance of the other coefficients. Thus, variations of the scaling factor $a_1$ cannot be directly interpreted as variations in the *ROM* fluctuations ($\alpha$). In fact, when $R^2$ is not equal to 1, the effects of both time shift and *ROM* fluctuations might be confused. Moreover, SD-$a_1$ and SD-$a_0$ obtained for the mixed simulation were equal to those obtained for time shift simulation, despite the range of variations of amplitude variability and offset were the same of those imposed in $\alpha$ and *O* simulations. This suggests that the effect of the time-shift on the LFM coefficients predominate on the effect of the other confusing-factors. Hence, $R^2$ is a measure of the time shift between the compared curves. It can be concluded that LFM separates the effects of the confusing-factors over the three coefficients only when $R^2$ tends to its ideal value, and the $a_0$ does not measure the offset but only its standard deviation provides information on the offset variability.

By definition, Mean Absolute Variability (MAV) and Root Mean Square Deviation (RMSD) provide an absolute measure of the averaged distances among the curves over their time-histories. Consistently, their values increased with the increasing of all the sources of variability. From a crossed-comparison of the results in Table 3.3 and Table 3.4, these two indices resulted to be strongly related to the range of motion of the curve they were calculated for, and were not able to distinguish among the various confusing-factors. However, when the offset is the only imposed variation, MAV was exactly equal to the offset (Table 3.3, Case 3), whereas the range of RMSD values was equal to the

42% of the offset. When varying the time shift between curves ($\tau$), MAV and RMSD increased as they were detecting distances due to amplitude variations or offsets. This result allows concluding that MAV and RMSD are representative measures of the averaged distances between the curves only when $R^2$ tends to 1 (i.e., for null time shift). In the other cases, indices like standard deviations, median absolute deviations and maximum differences calculated on joint kinematics at specific instants of the gait cycle (e.g., at initial contact and toe-off, or maximum and minimum values) should be preferred.

## 3.5 Conclusion

As a summary, all the indices were sensitive to the sources of variability of gait data. This part of the study explained how to interpret and use the results. In particular, it was shown that the ROM of the curves does not influence the CMC or the LFM coefficients; conversely, the CMC resulted sensitive to the curve patterns, leading to possible misinterpretations of the results when comparing data from different joints. Moreover, complex values of the CMC were observed when large offset and time shift occur. Therefore, given a set of data, the LFM should be used to assess its repeatability and reproducibility. In fact, SD-$a_1$, SD-$a_0$ and $R^2$ provide information on amplitude variability, offset, and time shift respectively and a value of $R^2$ approaching to 1 leads to the conclusion that time shift might be neglected. Alternatively, MAV and RMSD might also be used as measurements of the data dispersion, but keeping in mind that they would not be able to univocally discriminate among the different confusing-factors. When time shift occurs, an assessment of data repeatability and reproducibility evaluated on summary metrics (e.g., kinematics calculated at initial contact, toe-off, maximum, and minimum values) is likely to be preferred to the here investigated indices. The methodology proposed in this paper could be also used to obtain typical values of the RI distinctive of a population affected by a pathology, which might lead to alterations of the gait patterns only in specific phases of the gait cycle.

In the next Chapters, these indices will be used to evaluate the repeatability and the reproducibility of data collected under different conditions of measurement. In Chapter 4, CMC will be used to assess the effects that different calibration procedures might induce in estimating joint kinematics using a marker-based approach. The working

hypothesis is that different calibrations do not affect the data in term of offset among the compared curves. Chapter 5 will then present a concurrent repeatability and reproducibility analysis of the four most adopted models for the foot-ankle complex for gait analysis. LFM coefficients and MAV will be used in this case, since no *a-priori* hypothesis can be formulated on the magnitude of the confusing-factors for the collected data.

Chapter 4

# Metrological performances of stereophotogrammetric systems

This Chapter presents an analysis on the metrological performances of the systems used to estimate the human bone pose and eventually the joint kinematics. Part of the contents of this Chapter have been published as part of a scientific paper [192], published under a CC-BY 4.0 license. Written permission to reuse this material has been obtained from the authors.

## 4.1 Introduction

Human movement analysis based on sterophotogrammetry is a widely used technique used to quantify movement alterations in clinical practice and, eventually, to suggest the most suitable therapy for a patient. However, data gathered via stereophotogrammetric systems (SS) suffer from the following inaccuracies: (1) the soft-tissue artefacts (STA) due to the relative movement between the markers attached on the skin and the underlying bones [24]; (2) errors in the anatomical calibration due to markers' misplacement [25], and (3) instrumental errors [23]. Although a new approach has been recently proposed to model the STA and reduce its effect on joint kinematics estimates [80–83], this is still a relevant issue associated with gait analysis performed via a marker-based approach. Errors in the anatomical calibration can be reduced with a good training of the operator performing anatomical landmarks' recognition and marker placement. It is worth highlighting that the first two errors are intrinsic in the

use of skin markers, whereas the instrumental errors are due to the use of cameras, and it has been found to depend on: number and position of cameras [44,52], their lens distortion [39], dimension of the capture volume [45,46] and, last but not least, the algorithms used for the reconstruction of the 3D position of the markers [38]. Whatever is the used SS, the algorithm that reconstruct the 3D marker trajectories is strongly linked with the calibration procedure. During the calibration procedure, the system uses the known distances imposed by using the calibration object to estimate the *calibration parameters* – extrinsic or external (camera position and orientation relative to a fixed global reference frame, i.e. the camera pose) and intrinsic or internal (linked to the characteristics of the lenses), whereas, while collecting data, the calibration parameters are used to reconstruct the 3D marker trajectories (see also §2.3.1.1, and Figure 4.1).

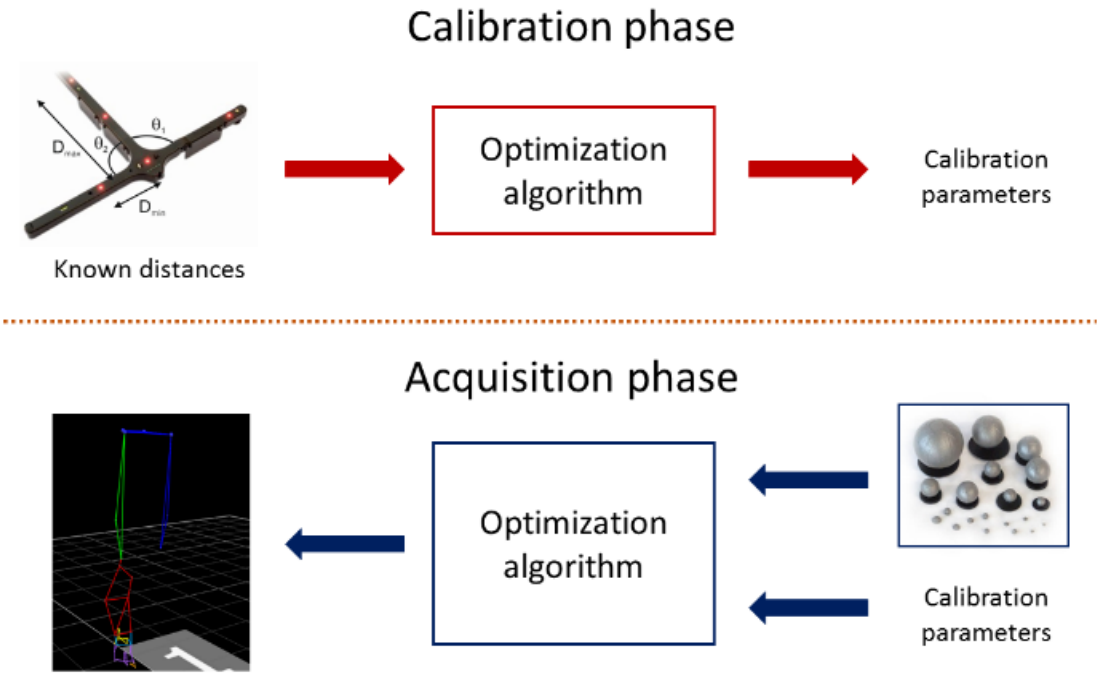


**Figure 4.1** – The two uses of the optimization algorithm used during the calibration and the acquisition phases.

Different application of SS and changes in lighting frequently call for recalibration of the systems. Indeed, SS manufacturers recommend performing a calibration before each session of data collection. The calibration is performed manually by the operator, who usually has to move an object within the capture volume, and is therefore dependent on the modality of its execution. The evaluation of possible errors associated with the calibration procedure of the SS has been the object of a few investigations. Literature reports that errors linked to the use of skin-mounted markers have amplitudes that are usually overwhelming with respect to those of photogrammetric

errors [197], but errors linked to the calibration procedure have been only partially assessed.

Two different methodologies to quantify the instrumental error linked to the calibration algorithms have been proposed [198,199], but they are by definition not useful in quantifying the variations following the need of a system recalibration. In 2008, a custom-made robot has been devised to move a L-frame equipped with retroreflective markers and able to perform the calibration [44]. The calibration performed by the robot was found to be significantly improved in terms of accuracy of the reconstructed marker trajectories. However, such a robot can be moved within a capture volume ($180 \times 180 \times 150$ mm$^3$) that is much smaller than those normally considered in human movement analysis (4 x 3 x 2.5 m$^3$). Last but not least, the robot performed the calibration imposing known trajectories to the calibration object which is far from the actuality of the daily practice. Moreover, the effects that the calibration procedure has on the metrological performances of a SS have not been fully exploited.

This Chapter proposes a methodology that can be used to evaluate the effect of different calibration procedures on the ability of the system of reconstructing accurate marker trajectories. Calibrations differ for being performed in different acquisition volumes and for different durations. Eventually, the relevance of the effects that those calibration procedures can have on the estimate of the joint kinematics will be tested. The proposed methodology will be applied to two different SSs.

## 4.2 Methods

### 4.2.1 Measurement systems

Two stereophotogrammetric systems were set up in two centres: an 8-camera Vicon system MX-series (SS#1 installed at the Movement Analysis and Robotics Laboratory 'MARLab' of the Children Hospital 'Bambino Gesù', Palidoro – Rome, Italy) and a 10-camera Vicon system T-series (SS#2 installed at The University of Sheffield, Sheffield – United Kingdom). The data collection was performed with a sampling frequency of 200 Hz at both centres and the 3D marker reconstruction was performed using the software Vicon Nexus 1.8.5 (Vicon Motion Systems, Oxford – UK). As reported in §2.3.1.2, a different number of cameras in the two system configurations does not

affect the accuracy of the calibration, since at least six cameras have been used in both cases.

## 4.2.2 Definition of the experimental protocol

### *4.2.2.1 Calibration procedure*

A 2.4 x 3.6 x 1.6 $m^3$ capture volume (Global volume, GV) was identified (Figure 4.2) in both laboratories. Two different devices were used for the calibration, both equipped with five markers, placed at the same known distance between each other (Figure 4.3). The device in SS#1 carried passive markers, whereas the device in SS#2 carried active markers.

Moving the wand only in specific sections of the laboratory produced different calibration volumes, and consequently different calibration files. The GV was partitioned into four 1.2 x 3.6 x 0.8 $m^3$ sub-volumes (SVs) defined by intersecting the half-right, half-left, half-upper and half-lower parts of the global volume, obtaining:

a) left and lower sub-volume, SV-LL;
b) left and upper sub-volume, SV-LH;
c) right and lower sub-volume, SV-RL; and
d) right and upper sub-volume, SV-RH.

This set of calibration procedures was designed to test the system performances under challenging conditions.

Following the manufacturer recommendations, each of the calibration procedures included two phases: a *dynamic phase*, in which the calibration device was waved throughout the empty capture volume, ensuring that the markers on the wand were visible to the cameras, and a *static phase* to identify the global reference frame, placing the calibration device flat on the floor.

The number of frames (Refinement Frames, RF) used by the calibration and reconstruction algorithm to compute the calibration parameters has to be set before the calibration procedure. The manufacturer of the systems used in this study recommends setting the RF to a value higher than 1,000 frames and possibly ranging between 3,000 and 5,000. With the frame rate being constant, the higher is the RF, the higher is the time length of the dynamic phase. Two sets of calibration procedures were performed:

a) the GV was calibrated varying RF from 1,000 to 5,000 in steps of 1,000;

b) each of the SVs was calibrated setting RF = 3,000 frames.

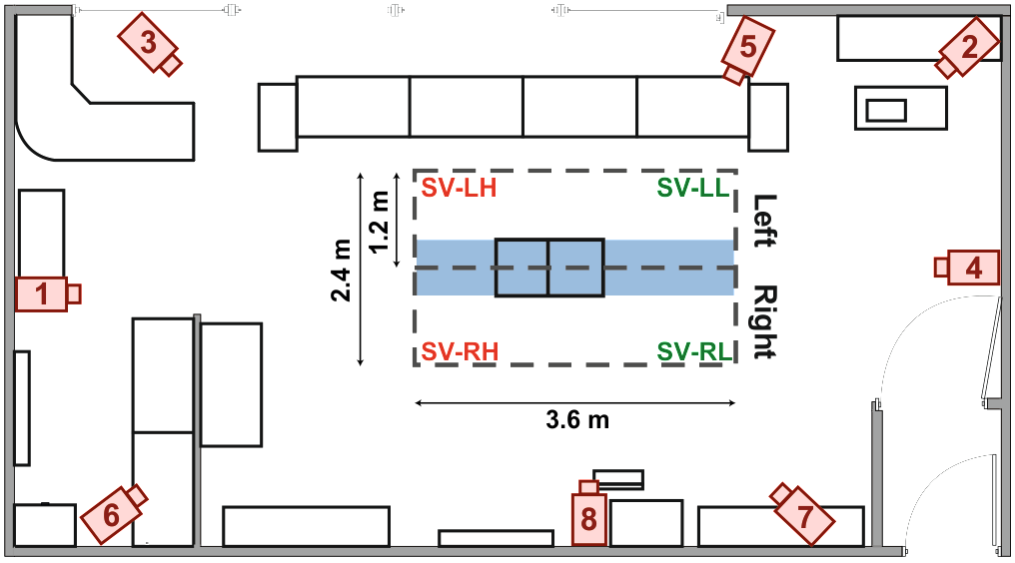


(a)

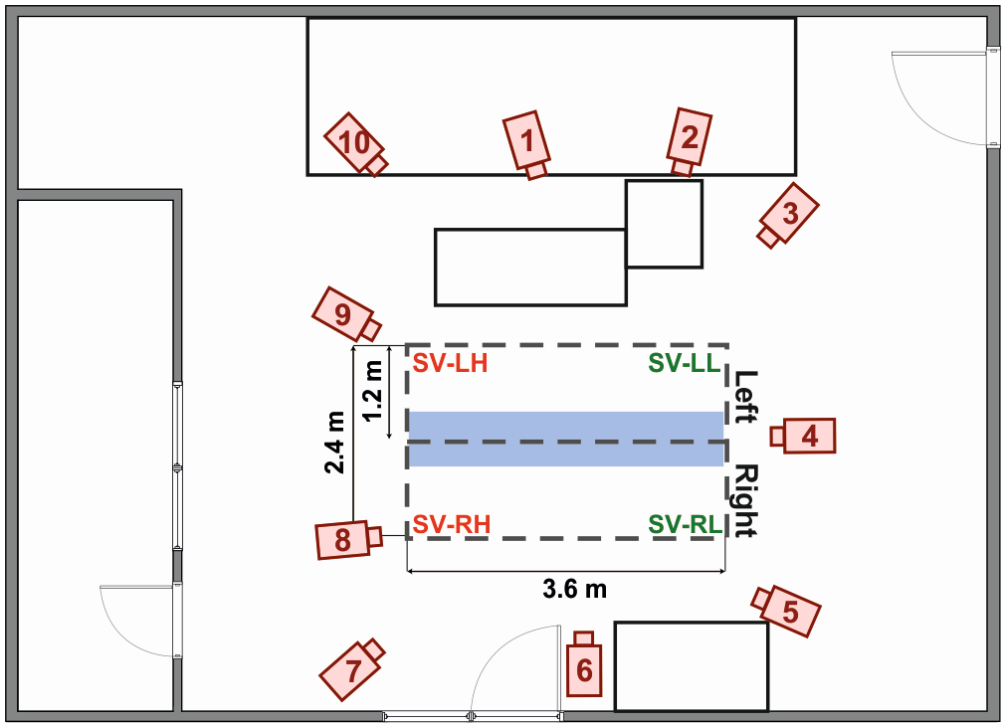


(b)

**Figure 4.2** – Maps of the considered laboratories with the highlighted volumes: (a) Movement Analysis and Robotics Laboratory 'MARLab' of the Children Hospital 'Bambino Gesù', Palidoro – Rome, Italy; (b) The University of Sheffield, Sheffield – United Kingdom. The blue area is the area where the subject was asked to walk on. The sub-volumes are bounded by a grey dashed-lines: the green tags indicate the sub-volumes on the lower part of the global volume, while the red ones indicate the higher ones. All the measures are given in meters. This Figure is reproduced as published in [192] with permission of co-authors.

In order to account for the variability related to the operator, each of the above calibration procedures was repeated three times, for a total of 27 datasets (five tests at different RF repeated three times for the GV, plus three repetitions for each of the four

SVs). The files containing the calibration parameters calculated by the calibration algorithm, were stored for the post-processing.

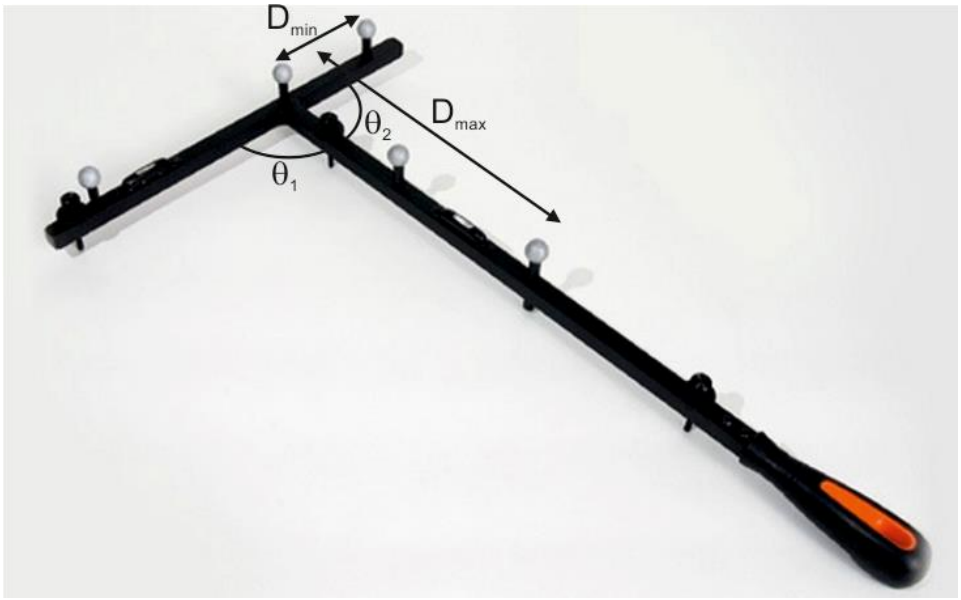


**(a)**

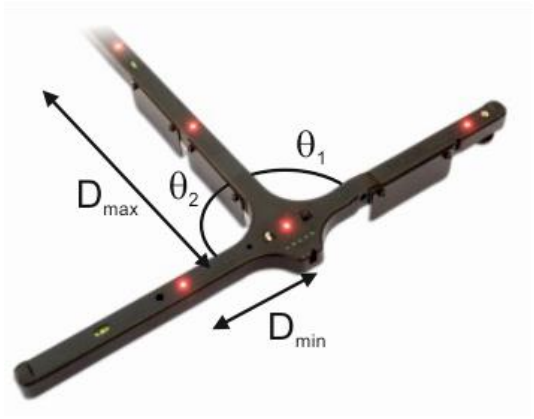


**(b)**

**Figure 4.3** – Rigid calibration device (a) equipped with retroreflective passive markers for the system SS#1; (b) and equipped with active markers for the system SS#2. This Figure is reproduced as published in [192] with permission of co-authors.

To quantify the metrological performances of the stereophotogrammetric systems, two tests were used. The first, called *low-level* test, aimed at quantifying the error[16] associated with measuring fixed distances and angles on a rigid body both in static and dynamic conditions. The second, called *high-level* test, aimed at assessing the effect that different calibration procedures might have on the estimate of the human

[16] This has to be intended as defined in the International Vocabulary of Metrology (Appendix A): measured quantity value minus a reference quantity value [22].

joint kinematics during ambulation. Post-processing was conducted via custom-made script and functions developed in MATLAB (MathWorks, Natick - USA).

#### *4.2.2.2 Low-level test*

As preliminary test to evaluate the expanded uncertainty (product of a combined standard measurement uncertainty and a factor larger than the number one)[17] associated with distance and angle measurements, the calibration device was put flat on the floor and a trial of 5 s was collected. The standard deviation of the distances between each couple of markers on the device was calculated from the static trial data, which have been reconstructed 27 times with each of the calibration files. In order to evaluate the relevant expanded uncertainties, for each of the two systems SS#1 and SS#2, the highest among the standard deviation values was multiplied by a coverage factor $k = 3$. The same procedure was carried out for quantifying the expanded uncertainties associated with measuring the angles between the arms of the device.

The calibration device was then freely moved within the capture volume by the same operator who performed the calibrations. Thus, it has been assumed that the velocity of the wand within the capture volume and during the data collection was comparable with the one used in the dynamic phase of the calibration procedure. One trial of 20 s was collected. Two pairs of markers (Figure 4.3), i.e. the two closest and the two most distant markers on the wand ($D_{\min}$ and $D_{\max}$), were considered as known input to exploit the SS ability of accurately measuring distances between points. The calculated distances between the two couple of markers were compared with those declared by the manufacturer and assumed as true values. Differently from the rational chosen for the test on the distances, and considering the possible options given by the calibration devices, the two angles defined by the markers positioned on the device arms ($\theta_1$ and $\theta_2$) were considered to verify the SS ability in accurately measuring the angles. The two measured angles were compared with the known value of 90°. For each

[17] Quantities has to be intended as defined in the International Vocabulary of Metrology, which is briefly summarised in the Appendix A [22]. The combined standard uncertainty is the standard measurement uncertainty obtained using the individual standard measurement uncertainties associated with the input quantities in a measurement model.

trial and each calibration file, the RMSE of the distances and angles, were computed as an accuracy index. Finally, the average of the RMSEs over the three calibration repetitions, were computed. When referring to RMSE values, the following notations will be used: the analysed calibration volume and RF values will be noted as superscripts and the investigated variable as subscript (e.g., the RMSE computed for the distance $D_{\max}$ considering the calibration volume GV and a number of frames with $RF = 2,000$ is $RMSE_{D\max}^{GV\,2000}$). The RF is not indicated when the RMSE was evaluated for the SVs, since it was always set to 3,000.

#### *4.2.2.3 High-level test*

One healthy adult (age 27, height 183 cm, mass 78 kg) was enrolled in this part of the study after having read and signed an informed written consent. Ethical approval was granted by the University of Sheffield (Appendix C). The subject was equipped with sixteen passive markers of 9.5 mm diameter, according to the Vicon Plug-in-Gait protocol: four markers on the pelvis, two on each thigh, two on each shank and three markers on both the feet (Figure 2.12 [56]). One gait trial was acquired asking the subject to walk barefoot at a self-selected speed in the middle of the capture volume (Figure 4.2 highlights the walkway in blue). The subject was asked to walk back and forth along a straight line and a total of five right and five left strides chosen among those recorded in the centre of the measurement volume were retained for further analysis. As in the *low-level* test, the 27 calibration files were applied to the acquired trials, and the joint kinematics were then estimated for each of them.

The Coefficient of Multiple Correlation (CMC) [125] was chosen and adjusted to calculate the between-calibration similarities over the five strides, and assess the effect that the different calibration procedures have induced on the estimated joint kinematics. The different calibrations were expected not to affect the data in terms of offset among the compared curves. Moreover, typical CMC values for a healthy adult population have been reported in Chapter 3 (Table 3.4). The CMC can hence be considered as similarity index for this study. Furthermore, in order to quantify the absolute variations induced by different calibrations on the joint kinematics, the maximum angular differences ($\Delta\theta$) among all the waveforms were determined.

#### *4.2.2.3.1 Is joint kinematics affected by the RF?*

In order to test whether joint kinematics were affected by the calibration duration (RF), a comparison among the calibration performed within GV and changing RF was performed. Assuming that a higher number of RF can improve the calibration performances, the values obtained with the calibration performed within GV at a RF of 5,000 were considered as a reference for those obtained with calibrations performed within GVs at different RFs. The relevant CMC and $\Delta\theta$ were then calculated.

In the following, RF is used as superscript for the CMC, whereas the kinematic variable for which the CMC was calculated is used as subscript: for example, $CMC^{RF}_{R-A-Abd/Add}$ stands for CMC computed among the RFs of the right (R) ankle (A) and for the Abduction/Adduction. The maximum angular differences between two calibrations were defined to have the comparison as superscript and the considered kinematic variable as subscript: i.e. $\Delta\theta^{5000/2000}_{L-H-Int/Ext}$ is the maximum difference between the left (L) hip (H) internal/external rotation computed by using the calibration GV with RF equal to 5,000 and 2,000.

#### *4.2.2.3.2 Is joint kinematics affected by the dimension and the position of the calibration volume?*

In order to test whether the joint kinematics are affected by the dimension and the position of the calibration volume, a series of comparisons between GV and each SV were performed. In this case, it was assumed that the calibration performances improve considering a GV rather than a SV. Then, CMC and $\Delta\theta$ were compared among the estimated kinematic variables when applying those calibration files.

For this setting, V (Volume) was the superscript for the CMC and the kinematic variable was again the subscript: e.g, $CMC^{V}_{R-F-Flx/Ext}$ is the CMC computed among the different volumes and for the right (R) knee (K) flexion/extension. As reported for the calibration duration (§4.2.2.3.1), the maximum angular differences were defined to have the comparison as superscript and the considered kinematic variable as subscript: i.e. $\Delta\theta^{GV/SV-RH}_{L-H-Int/Ext}$ is the maximum difference between the left (L) hip (H) internal/external rotation computed by using the calibration GV and SV-RH.

## 4.3 Results and discussion

### 4.3.1 Low-level test

Considering the static trial data collected in both the laboratories on the calibration devices, and applying the whole calibration set, the expanded uncertainties were evaluated as equal to 0.1 mm for distances between target points and 0.1° for the angles when using SS#1, and 0.3 mm and 0.3° when using SS#2, respectively. These values were considered as references to estimate the effects that the calibration procedure can have on the performances of SSs in dynamic trials. As the uncertainty is assumed as the limit to the measurement system precision, RMSE results will be presented with only the first digit for both fixed distances ( $D_{\min}$ and $D_{\max}$ ) and fixed angles ( $\theta_1$ and $\theta_2$ ).

According to the literature [48], higher inaccuracies in measuring distances and angles on rigid devices might be expected when comparing dynamic trials to statics. Results of this study confirmed this trend. Indeed, dynamic inaccuracies were found to be up to five times higher than the static ones. Table 4.1 and Figure 4.4 shows the mean values of the RMSEs computed for $D_{\min}$ , $D_{\max}$ , $\theta_1$ and $\theta_2$ , and for both systems SS#1 and SS#2. For SS#1, both $RMSE_{D\max}$ and $RMSE_{D\min}$ for each calibration condition were always less than 0.4 mm. The lowest error (0.2 mm) was obtained for $RMSE_{D\max}^{GV3000}$ and $RMSE_{D\max}^{GV4000}$. Changing among the calibration conditions, $RMSE_{\theta1}$ and $RMSE_{\theta2}$ were always equal to 0.2° and 0.5°, respectively. Considering the system SS#2, the $RMSE_{D\max}$ and $RMSE_{D\min}$ were found to be always less than 1.7 mm and 1.0 mm, respectively. The reference value obtained for the distances was 0.5 mm. With regard to the angles, the lowest value was found for $RMSE_{\theta1}^{GV5000}$ , equal to 0.2°, and the highest for $RMSE_{\theta1}^{SV-RH}$ and $RMSE_{\theta1}^{SV-RL}$ , both equal to 0.7°. For $\theta_2$ the lowest value was found for $RMSE_{\theta2}^{GV5000}$ (0.2°), while the highest was found for $RMSE_{\theta2}^{SV-RH}$ (0.6°).

It is convenient to highlight that RMSE values did not vary when comparing the effect on the measurements of distances and angles obtained with the different calibrations. Moreover, despite the fact that the cameras of the system SS#2 are technologically advanced with respect to those of the system SS#1, not only more accurate results were obtained when evaluating the data acquired from this system, but

even slightly higher values of errors were found. As mentioned in the paragraph §4.1, the accuracy of reconstructing marker time histories can depend on several aspects, even linked with the visibility of the markers [23–25,38,39,44–46,52]. While the system SS#1 was routinely used for clinical gait analysis, the cameras of the system SS#2 were set up for experiments focused particularly on assessing the kinematics of the lower limb and the dexterity of the hand, which considered smaller markers than those normally considered for gait analysis. Thus, to ensure good visibility for all the markers, cameras of SS#2 were set up with a higher value of aperture than those of the system SS#1. On the other hand, the higher is the aperture, the noisier are the measurements and this can be reasonably considered the reason of the slightly increase of the inaccuracy of tracking markers and measuring distances and angles using SS#2. It has to be highlighted, however, that this factor was certainly not relevant when comparing series of data acquired with the same system.

**Table 4.1** – RMSE values computed by considering the systems SS#1 and SS#2. This Table is reproduced as published in [192] with permission of co-authors.

| | $RMSE_{\downarrow}^{\rightarrow}$ | GV1000 | GV2000 | GV3000 | GV4000 | GV5000 | SV-LH | SV-LL | SV-RH | SV-RL |
|---|---|---|---|---|---|---|---|---|---|---|
| SS#1 | $D_{max}$ (mm) | 0.3 | 0.3 | 0.2 | 0.2 | 0.3 | 0.4 | 0.3 | 0.3 | 0.3 |
| | $D_{min}$ (mm) | 0.3 | 0.3 | 0.3 | 0.3 | 0.3 | 0.4 | 0.3 | 0.3 | 0.3 |
| | $\theta_1$ (°) | 0.2 | 0.2 | 0.2 | 0.2 | 0.2 | 0.2 | 0.2 | 0.2 | 0.2 |
| | $\theta_2$ (°) | 0.5 | 0.5 | 0.5 | 0.5 | 0.5 | 0.5 | 0.5 | 0.5 | 0.5 |
| SS#2 | $D_{max}$ (mm) | 0.7 | 0.9 | 0.9 | 0.9 | 0.5 | 0.9 | 0.9 | 1.7 | 1.1 |
| | $D_{min}$ (mm) | 0.7 | 1.0 | 0.7 | 0.7 | 0.5 | 0.7 | 0.7 | 0.9 | 0.8 |
| | $\theta_1$ (°) | 0.3 | 0.4 | 0.4 | 0.4 | <0.3 | 0.4 | 0.3 | 0.7 | 0.7 |
| | $\theta_2$ (°) | 0.3 | 0.4 | 0.5 | 0.4 | <0.3 | 0.4 | 0.4 | 0.6 | 0.5 |

## 4.3.2 High-level test

### *4.3.2.1 Is joint kinematics affected by the RF?*

Concerning the test on the articular kinematics, $CMC^{RF}$ was higher than 0.94 for both SS#1 and SS#2. This means that the waveforms were very similar to each other (Table 4.2). Considering SS#1, the worst case was found to be $CMC^{RF}_{R-A-Inv/Eve}$ (0.94), while for SS#2 it was $CMC^{RF}_{L-H-Int/Ext}$ (0.94). Instead, the higher values for the CMC (>0.99) were obtained for $CMC^{RF}_{R-H-Flx/Ext}$, considering the SS#1, and for $CMC^{RF}_{R-H-Flx/Ext}$, $CMC^{RF}_{L-H-Flx/Ext}$ and $CMC^{RF}_{R-K-Flx/Ext}$, considering the SS#2.

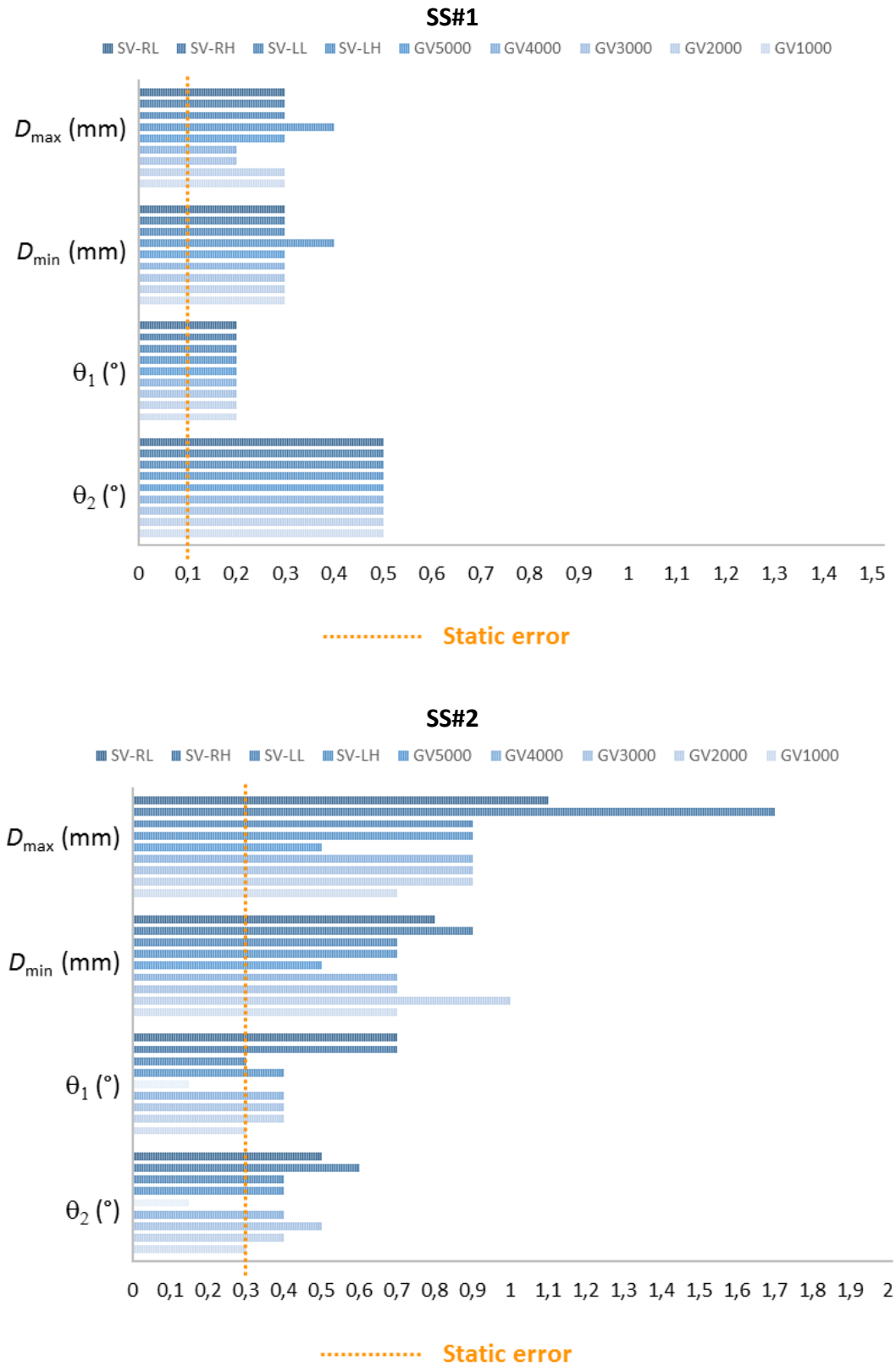


**Figure 4.4** – RMSE values computed for $D_{min}$, $D_{max}$, $\theta_1$ and $\theta_2$ by considering the systems SS#1 and SS#2. The orange dashed line highlights the static error measurement, i.e. the expanded uncertainty.

**Table 4.2** – CMC values computed on the kinematics both considering the comparison between GV5000 and other GVs ( $CMC^{RF}$ ), and between GV3000 and SVs ( $CMC^{V}$ ). This Table is reproduced as published in [192] with permission of co-authors.

| | $CMC_{\downarrow}^{\rightarrow}$ | ***RF*** | | ***V*** | |
|---|---|---|---|---|---|
| | | **SS#1** | **SS#2** | **SS#1** | **SS#2** |
| **Right Hip** | *Flx/Ext* | >0.99 | >0.99 | >0.99 | >0.99 |
| | *Abd/Add* | 0.99 | 0.98 | 0.99 | 0.98 |
| | *Int/Ext* | 0.98 | 0.98 | 0.98 | 0.97 |
| **Right Knee** | *Flx/Ext* | 0.99 | >0.99 | 0.99 | >0.99 |
| | *Abd/Add* | 0.98 | 0.98 | 0.97 | 0.98 |
| | *Int/Ext* | 0.97 | 0.97 | 0.97 | 0.97 |
| **Right Ankle** | *Plt/Drs* | 0.99 | 0.99 | 0.99 | 0.99 |
| | *Int/Ext* | 0.97 | 0.98 | 0.97 | 0.98 |
| | *Inv/Eve* | 0.94 | 0.95 | 0.93 | 0.94 |
| **Left Hip** | *Flx/Ext* | 0.99 | >0.99 | 0.99 | >0.99 |
| | *Abd/Add* | 0.98 | 0.99 | 0.98 | 0.99 |
| | *Int/Ext* | 0.98 | 0.94 | 0.98 | 0.93 |
| **Left Knee** | *Flx/Ext* | 0.99 | 0.99 | 0.99 | 0.99 |
| | *Abd/Add* | 0.97 | 0.97 | 0.97 | 0.97 |
| | *Int/Ext* | 0.97 | 0.97 | 0.97 | 0.97 |
| **Left Ankle** | *Plt/Drs* | 0.98 | 0.97 | 0.98 | 0.97 |
| | *Int/Ext* | 0.98 | 0.96 | 0.98 | 0.96 |
| | *Inv/Eve* | 0.95 | 0.95 | 0.95 | 0.94 |

The first four columns of Table 4.3 and Table 4.4 show the maximum angular differences ( $\Delta\theta$ ) between the kinematic variables when processing the static and dynamic trials with the GV calibrations. The $\Delta\theta$ were for SS#1 (Table 4.3 and Figure 4.5) never higher than 0.3° and it was found, for most of the cases, less than 0.1°. Looking at the same results for SS#2 (Table 4.4 and Figure 4.6), values lower than 0.3° were found for $\Delta\theta_{R-H-Flx/Ext}^{5000/1000}$, $\Delta\theta_{L-K-Flx/Ext}^{5000/4000}$, and for the entire set of comparison on the right and left hip abduction/adduction movement; while the higher value, equal to 2.8°, was reached only for $\Delta\theta_{R-K-Int/Ext}^{5000/3000}$. These results allow to argue that the number of Refinement Frames (RF) does not significantly affect either the waveforms or the angular values of the articular kinematic estimates during the gait cycle. Indeed, the obtained CMC values displayed a high correlation among the compared curves, and the lower values were obtained for those kinematics defined on the out-of-sagittal planes, coherently with the intrinsic higher between-stride variability that those variables usually have with respect to the sagittal joint kinematics [57]. Furthermore, the here obtained CMCs were comparable with those obtained for both within- and between-subject analyses performed on the ideal population of healthy adults generated via Fourier's decomposition in the previous Chapter (Table 3.4). Moreover, for both SS#1 and SS#2, the absolute angular differences ( $\Delta\theta$ ) were never higher than the errors that affect the outcomes of the gait analysis [197,200–203].

**Table 4.3** – Maximum angular differences between angles estimated by considering the comparison between GV5000 and other GVs ( $\Delta\theta^{5000/RF}$ ), and between GV3000 and SVs ( $\Delta\theta^{GV/SV}$ ) for the system SS#1. This Table is reproduced as published in [192] with permission of co-authors.

| | $\Delta\theta^{\rightarrow}_{\downarrow}$ | 5000/ 1000 | 5000/ 2000 | 5000/ 3000 | 5000/ 4000 | GV/ SV-LH | GV/ SV-LL | GV/ SV-RH | GV/ SV-RL |
|---|---|---|---|---|---|---|---|---|---|
| **Right Hip** | *Flx/Ext* | <0.1 | 0.1 | 0.1 | 0.1 | 0.1 | 0.1 | 0.1 | <0.1 |
| | *Abd/Add* | <0.1 | <0.1 | <0.1 | <0.1 | <0.1 | <0.1 | <0.1 | <0.1 |
| | *Int/Ext* | <0.1 | <0.1 | <0.1 | <0.1 | 0.2 | <0.1 | 0.2 | 0.1 |
| **Right Knee** | *Flx/Ext* | <0.1 | <0.1 | <0.1 | <0.1 | 0.1 | <0.1 | 0.1 | <0.1 |
| | *Abd/Add* | <0.1 | <0.1 | <0.1 | <0.1 | 0.1 | <0.1 | 0.1 | 0.1 |
| | *Int/Ext* | 0.1 | 0.1 | 0.1 | 0.1 | 0.2 | 0.1 | 0.1 | 0.1 |
| **Right Ankle** | *Plt/Drs* | 0.1 | 0.1 | 0.1 | 0.1 | 0.1 | 0.1 | 0.1 | 0.1 |
| | *Int/Ext* | 0.1 | 0.1 | 0.1 | 0.1 | 0.2 | 0.1 | 0.2 | 0.2 |
| | *Inv/Eve* | 0.2 | 0.2 | 0.2 | 0.2 | 0.7 | 0.2 | 0.6 | 0.3 |
| **Left Hip** | *Flx/Ext* | <0.1 | <0.1 | <0.1 | 0.1 | 0.1 | 0.1 | 0.1 | 0.1 |
| | *Abd/Add* | <0.1 | <0.1 | <0.1 | <0.1 | <0.1 | <0.1 | <0.1 | <0.1 |
| | *Int/Ext* | 0.1 | 0.1 | 0.1 | 0.1 | 0.1 | 0.1 | 0.2 | 0.2 |
| **Left Knee** | *Flx/Ext* | <0.1 | <0.1 | <0.1 | <0.1 | 0.1 | <0.1 | 0.1 | <0.1 |
| | *Abd/Add* | <0.1 | <0.1 | <0.1 | <0.1 | 0.1 | <0.1 | 0.1 | 0.1 |
| | *Int/Ext* | 0.1 | 0.1 | 0.1 | 0.1 | 0.2 | 0.1 | 0.1 | 0.1 |
| **Left Ankle** | *Plt/Drs* | 0.1 | 0.1 | 0.1 | 0.1 | 0.2 | 0.1 | 0.2 | 0.2 |
| | *Int/Ext* | 0.2 | 0.2 | 0.1 | 0.2 | 0.2 | 0.1 | 0.2 | 0.2 |
| | *Inv/Eve* | 0.2 | 0.3 | 0.3 | 0.3 | 0.6 | 0.2 | 1.0 | 0.4 |

#### *4.3.2.2 Is joint kinematics affected by the dimension and the position of the calibration volume?*

For the system SS#1, a CMC equal to 0.93 was obtained for the inversion/eversion rotation of the right ankle, and equal to 0.93 for the internal/external rotation of the left hip (Table 4.2). The highest values for the CMC (>0.99) were obtained for $CMC^{V}_{R-H-Flx/Ext}$ both for SS#1 and SS#2, and $CMC^{V}_{L-H-Flx/Ext}$ and $CMC^{V}_{R-K-Flx/Ext}$ for SS#2. The lowest CMC values were obtained for $CMC^{V}_{R-A-Inv/Eve}$ (0.93) for SS#1, and for $CMC^{V}_{L-H-Int/Ext}$ (0.93) for SS#2. Thus, an excellent correlation was found between the waveforms estimated using data collected with each SS and, as in the previous case, CMC values were comparable to those obtained for within- and between-subject analyses performed on healthy adults (Chapter 3, Table 3.4).

The second four columns of Table 4.3 and Table 4.4 show, instead, the maximum angular differences on kinematics when processing data from static and dynamic trials with GV and SVs calibrations. The $\Delta\theta$ for SS#1 was never higher than 0.7°, obtained for $\Delta\theta^{GV/SV-LH}_{R-A-Inv/Eve}$ (Table 4.3), and it was found to be less than 0.1° for a few cases. Examining the $\Delta\theta$ for SS#2 (Table 4.4), the higher value 3.3° was reached for $\Delta\theta^{GV/SV-LH}_{R-K-Int/Ext}$, whereas

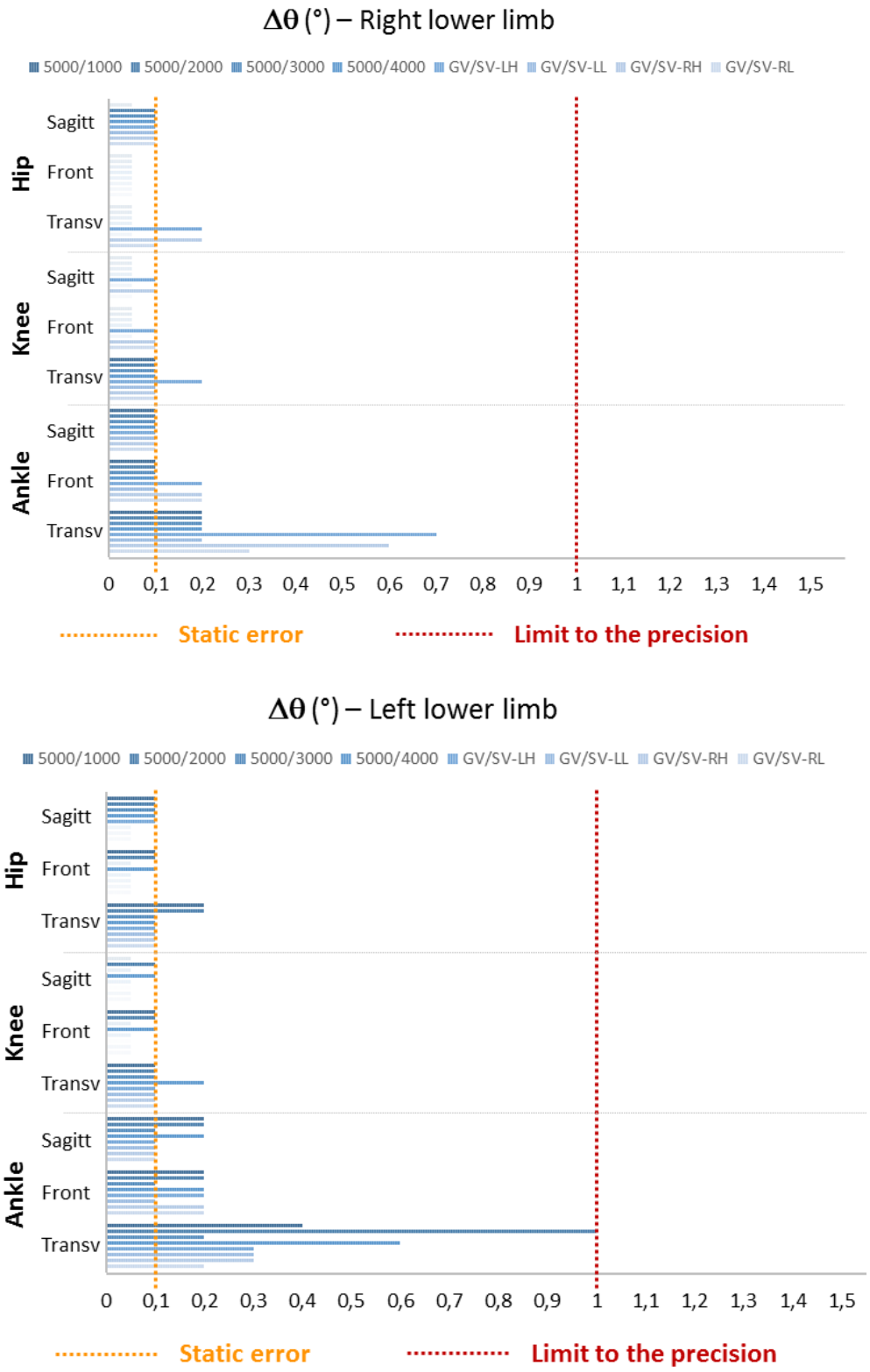


**Figure 4.5** – Maximum angular differences between angles estimated by considering the comparison between GV5000 and other GVs ( $\Delta\theta^{5000/RF}$ ), and between GV3000 and SVs ( $\Delta\theta^{GV/SV}$ ) for the system SS#1. The orange and red dashed lines highlight the static error measurement (i.e. the expanded uncertainty), and the limit to the precision of the estimate of human joint kinematics in gait analysis [194], respectively.

the lowest value was equal to 0.2° and was obtained for $\Delta\theta^{GV/SV-LH}_{L-H-Abd/Add}$, $\Delta\theta^{GV/SV-RH}_{L-H-Abd/Add}$ and $\Delta\theta^{GV/SV-RL}_{L-H-Abd/Add}$. Similarly to what was obtained for the previous analysis, results obtained

in terms of both CMCs and $\Delta\theta$ values allowed to affirm that the effect of the considered volume, in which the operator performs the calibration, is negligible on the estimate of articular kinematics during the gait cycle analysis if compared to those induced from other sources of error [200], (Chapter 3).

**Table 4.4** – Maximum angular differences between angles estimated by considering the comparison between GV5000 and other GVs ( $\Delta\theta^{5000/RF}$ ), and between GV3000 and SVs ( $\Delta\theta^{GV/SV}$ ) for the system SS#2. This Table is reproduced as published in [192] with permission of co-authors.

| | $\Delta\theta_{\downarrow}^{\rightarrow}$ | **5000/ 1000** | **5000/ 2000** | **5000/ 3000** | **5000/ 4000** | **GV/ SV-LH** | **GV/ SV-LL** | **GV/ SV-RH** | **GV/ SV-RL** |
|---|---|---|---|---|---|---|---|---|---|
| **Right Hip** | *Flx/Ext* | <0.3 | 0.3 | 0.3 | 0.4 | 0.6 | 0.7 | 0.7 | 0.4 |
| | *Abd/Add* | <0.3 | <0.3 | <0.3 | <0.3 | 0.3 | 1.0 | 0.4 | 0.4 |
| | *Int/Ext* | 1.9 | 1.9 | 1.4 | 1.2 | 2.1 | 2.3 | 2.2 | 2.2 |
| **Right Knee** | *Flx/Ext* | 0.6 | 0.8 | 0.6 | 0.3 | 0.9 | 0.9 | 0.9 | 0.8 |
| | *Abd/Add* | 1.0 | 0.9 | 0.7 | 0.7 | 1.2 | 1.3 | 1.1 | 1.2 |
| | *Int/Ext* | 0.6 | 1.2 | 2.8 | 2.1 | 3.3 | 2.7 | 2.8 | 2.8 |
| **Right Ankle** | *Plt/Drs* | 0.3 | 0.5 | 0.6 | 0.7 | 0.8 | 0.5 | 0.6 | 0.6 |
| | *Int/Ext* | 1.1 | 0.9 | 1.0 | 1.1 | 2.0 | 1.4 | 2.1 | 1.4 |
| | *Inv/Eve* | 1.2 | 1.4 | 1.4 | 1.5 | 1.9 | 1.7 | 2.4 | 2.1 |
| **Left Hip** | *Flx/Ext* | 0.3 | 0.3 | 0.3 | 0.3 | 0.5 | 0.8 | 0.6 | 0.4 |
| | *Abd/Add* | <0.3 | <0.3 | <0.3 | <0.3 | <0.3 | 1.0 | <0.3 | <0.3 |
| | *Int/Ext* | 0.5 | 0.6 | 0.7 | 0.5 | 1.3 | 1.3 | 1.3 | 1.2 |
| **Left Knee** | *Flx/Ext* | 0.4 | 0.3 | 0.4 | <0.3 | 0.5 | 0.4 | 0.7 | 0.4 |
| | *Abd/Add* | 0.3 | 0.4 | 0.6 | 0.4 | 0.9 | 0.8 | 0.7 | 0.6 |
| | *Int/Ext* | 0.8 | 0.7 | 1.2 | 0.6 | 1.7 | 1.7 | 1.3 | 1.4 |
| **Left Ankle** | *Plt/Drs* | 0.3 | 0.3 | 0.3 | 0.3 | 0.5 | 0.4 | 0.5 | 0.6 |
| | *Int/Ext* | 1.3 | 1.2 | 1.1 | 1.1 | 1.8 | 1.5 | 1.7 | 1.4 |
| | *Inv/Eve* | 0.9 | 0.8 | 0.7 | 0.7 | 1.2 | 1.2 | 1.6 | 1.4 |

## 4.4 Conclusion

In this Chapter, a methodology has been presented to evaluate the effects that a set of calibration procedures, diversified for both acquisition volumes and duration, can have on calculating distances and angles starting from trajectories measured via stereophotogrammetric systems. The methodology was applied to validate the measurements conducted with two systems, and, in general, inaccuracies associated with measured distances and angles, and estimated joint kinematics were found to be higher in dynamic than in static conditions for both systems. However, for both static and dynamic marker tracking, errors can be considered as not dependent on the performed calibration procedure and can be neglected. Indeed, getting close to the gait analysis context, the precision with which the anatomical landmarks are recognised and

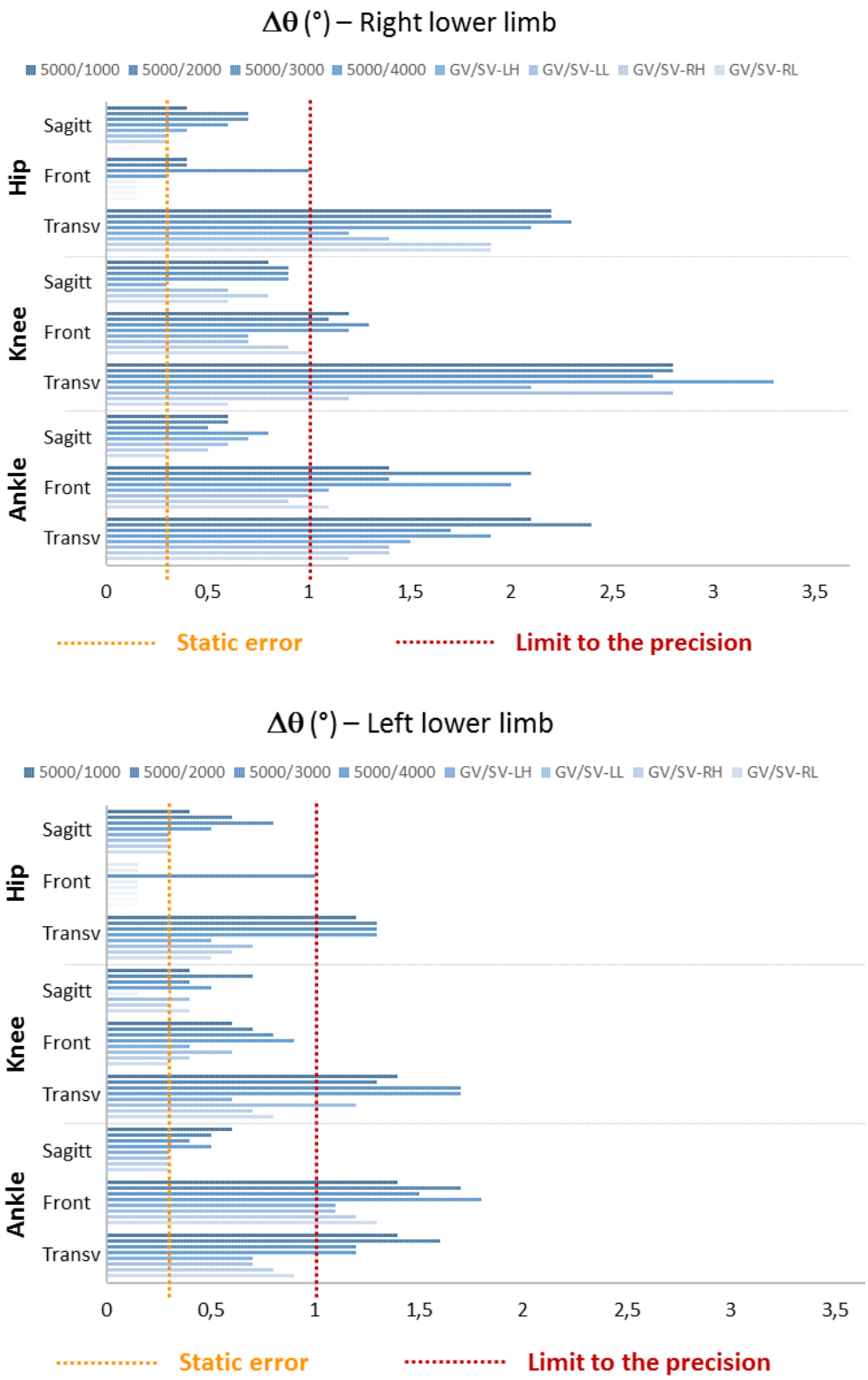


**Figure 4.6** – Maximum angular differences between angles estimated by considering the comparison between GV5000 and other GVs ( $\Delta\theta^{5000/RF}$ ), and between GV3000 and SVs ( $\Delta\theta^{GV/SV}$ ) for the system SS#2. The orange and red dashed lines highlight the static error measurement (i.e. the expanded uncertainty), and the limit to the precision of the estimate of human joint kinematics in gait analysis [194], respectively.

highlighted placing a marker was found to range between 2 and 20 mm [194]. These findings led to the conclusion that successful calibration procedures of different

durations and performed in different volumes did not affect the metrological performance of the investigated systems.

It is worth highlighting that a misplacement ranging between 2 and 30 mm in landmark recognition might induce changes in the estimate of lower limb kinematics of the 20% of the relevant nominal value, which can be equivalent also to 7-10° [200–203]. Furthermore, the similarities obtained in this research, modifying either the calibration duration or the calibration volumes, are higher than those normally obtained for intra- and inter-session repeatability studies [203], where an operator normally performs the marker placement more than once and in different testing-days, accounting also for stride variability. Coherently with the literature [57,125,203], higher variability was found on the transverse plane and for the foot joint data, whereas the sagittal plane was confirmed to be the most repeatable.

In conclusion, as long as a calibration procedure is successful, its effect on the accuracy of stereophotogrammetric systems in precisely measuring distances and angles on rigid bodies can be relevant, but it can be neglected when estimating joint kinematics in gait cycle analyses considering both waveforms similarity and absolute angular differences between curves [200].

Chapter 5

# Concurrent repeatability and reproducibility study of four foot models

This Chapter presents a concurrent analysis on the repeatability and reproducibility of foot joint kinematics estimated according to the most adopted gait analysis models. Part of the contents of this Chapter have been published as part of a scientific paper [193], published under a CC-BY 4.0 license. Written permission to reuse this material has been obtained by the authors.

## 5.1 Introduction

The observation of the foot-ankle complex is of clinical interest for various pathologies, including foot drop or deformities. Clinical decision-making might benefit from objective measurements of foot kinematics to isolate the causes of altered movements.

In gait analysis the foot is typically considered as a rigid segment linked to the tibia. This simplification, justifiable for some clinical applications, might be unsuitable for problems where the multi-segmental anatomy of the foot is needed. In the past two decades several multi-segment models of the foot-ankle complex have been proposed and reviewed [26,28,68,151]. Nowadays, the most popular models used either for research or clinical applications are those illustrated in [28,65,67,68]. The major differences are in the number and definition of the segments to be tracked, as well as in the identification of the associated anatomical landmarks. The validation of these

models is limited [86,112,114,142] and their clinical feasibility and utility has been previously questioned [29]. Moreover, their repeatability (i.e. their precision when applied on same or similar subjects by the same operator [22] – see also Appendix A) and reproducibility (i.e. their precision when applied on the same, or similar, subjects by different operators [22] – see also Appendix A) are still unclear [26].

This chapter aims to quantify the within- and between-subject repeatability, and the between-operator reproducibility of the data obtained from the four mentioned models. This analysis will leverage on the methods investigated in Chapter 3 and will be performed for overground and treadmill walking, with the objective of assessing the ability of the four protocols to highlight the changes imposed by these two walking conditions.

## 5.2 Participants

Thirteen healthy subjects were recruited (ten males, age: 27.0 ± 1.9 years, height: 1.83 ± 0.08 m, foot length: 28.5 ± 1.0 cm). Exclusion criteria were self-reported musculoskeletal pain or impairments. Ethical approval was granted by the University of Sheffield (Appendix C). Prior to the data collection, all subjects read and signed the consent form. The sample size was calculated via a power analysis with significance $\alpha$ = 0.05 and power $\beta$ = 0.80. The sagittal kinematics gathered from the first two subjects was used as inputs for the Eq. 5.1:

$$n > 2\left[\frac{\sigma\left(z_{\alpha/2} + z_{\beta}\right)}{\delta}\right]^2 \qquad \text{(Eq. 5.1)}$$

Where $n$ is the number of subjects to be enrolled in the study (sample size), with:

- $z_{\alpha/2}$ equal to 1.96 when the significance $\alpha$ is equal to 0.05;
- $z_{\beta}$ equal to 0.842 when the power $\beta$ is equal to 0.80;

Having preliminary data from the first two subjects:

- $\sigma$ is the standard deviation calculated on the joint kinematics obtained from these preliminary data;
- $\delta$, in general, is the difference between the averages of the populations that have to be statistically compared (represented by the two subjects).

## 5.3 Data collection and processing procedures

Each subject was instrumented with the marker set obtained merging those by Stebbins *et al.* [65] (M1, modified version of the model originally proposed in [189]), Leardini *et al*. [67] (M2), Sawacha *et al*. [28] (M3), Sarawat *et al*. [68] (M4) and Plug-in-Gait (commercial version of the model proposed by Davis et al. [56]). This choice allowed to avoid the effect of the between-stride variability associated with placing each marker-set once per time.

The marker placement was carefully studied for all the protocols before performing the data collection, paying close attention to the descriptions given in the relevant papers (and summarised in the sub-paragraphs of §2.5). In case something unclear emerged, clarifications were directly and privately asked to the authors of the papers who proposed the models. The merged marker-set was obtained respecting all the required critical alignments, and the descriptions of the anatomical landmark positions [28,65,67,68,204]. In addition, some prior test-sessions were performed before collecting the whole dataset to optimise the experimental set-up. The merged set of 39 markers consisted of: 4 markers on the pelvis, 2 on the thighs, 2 on the lateral femoral condyles; plus, on the right side, 6 markers on the shank, 7 on the hindfoot, 2 on the mid-foot, 12 on the forefoot, and 4 on the hallux. Table 5.1 shows the comparative analysis on the anatomical landmarks to be palpated as described in §2.5, whereas Figure 5.1 shows the fused marker-set highlighting each model with a specific colour: (a) the model M1 in red [65]; (b) the model M2 in blue [67]; (c) the model M3 in green [28]; and (d) the model M4 in orange [68]. Spherical markers (diameter: 9.5 mm) were used for pelvis, thighs and shank segments, whereas hemispherical markers (diameter: 4 mm) were used for the foot. The choice of using different marker sizes might be questioned, but a trade-off between (i) having placed markers with consistent dimensions with those proposed in the relevant papers, and (ii) being able to contemporaneously observe the same strides with the four protocols, eliminating the effect of the inter-strides variability has been chosen. Indeed, the need of placing twenty-seven markers on a foot called for using markers smaller than 9.5 mm. Different marker sizes can affect accuracy and precision of tracking marker trajectories via stereophotogrammetric systems [44]: the bigger the markers, the more camera pixels are illuminated and, thus, the estimated centroid can be differently located. However,

the authors of [44] tested tracking of markers of different sizes with a fixed configuration for the camera parameters: aperture and focus. Camera settings considered for the present project were, instead, modified to optimise visibility and tracking of markers with diameter of 4 mm, by augmenting the camera aperture and focus. As stated also in §4.4, as long as successful system calibrations have been performed, camera configuration does not significantly affect accuracy and precision in tracking marker trajectories, and estimate human joint kinematics [192].

Marker trajectories were collected with a 10-camera stereophotogrammetric system (T-160, Vicon Motion System Ltd – Oxford, UK, 100 Hz, Vicon Nexus 1.8.5). Labelling, manual cycle-events detection (from absolute vertical component of the heel marker, and 3D position of the foot), gap filling, and filtering (Woltring spline routine, size 30 [187][18]) were conducted within Nexus and C3D files were then post-processed in MATLAB (R2015b, The MathWorks, Inc. – Natick, MA, USA). The local coordinate systems for each segment were defined according to the corresponding model, selecting the pertaining markers, and used to compute joint kinematics consistently with the definitions given in each paper. As specified in §2.5.2, M1 was implemented according to its most repeatable configuration ('Option 5' in [65]), using static calibration and dynamic tracking of the hindfoot without considering the wand marker. M4 was instead implemented considering the 'Option 3' for both hindfoot and forefoot §2.5.5.

The following notations will be used to simplify the data reporting: hindfoot and calcaneus will both be indicated as HF, midfoot as MF, metatarsus and forefoot as FF, tibia and fibula as Tib, hallux as Hal, and finally, the foot modelled as a rigid segment as Foot. A left-side superscript will specify the model: e.g. the forefoot in M1 and the metatarsus in M2 will be noted as $^{M1}$FF and $^{M2}$FF, respectively. Figure 5.2 summarises the flow of data collection and processing explained in the following sections.

[18] Using a Woltring filter routine is demonstrated to be equal to using twice an analog Butterworth filter. The Woltring routine has been specifically developed for kinematic data and it is not a filter, but rather a spline used to smooth the kinematic and dynamic curves: https://www.vicon.com/faqs/software/what-are-the-details-of-the-woltring-filter.

**Table 5.1** – Anatomical Landmarks to be palpated associated with the models. All the critical alignments declared in the papers were followed, but for simplicity they are not in the table: M1 [65], M2 [67], M3 [28], and M4 [68]. This Table is reproduced as published in the Supplementary Materials of [23] with permission of co-authors. (*) indicates Marker to be used for the static trials only.

| Label | Description | M1 | M2 | M3 | M4 |
|---|---|---|---|---|---|
| L/R ASI | Anterior superior iliac spine | x | x | x | x |
| L/R PSI | Posterior superior iliac spine | x | x | x | x |
| L/R THI | Lower lateral 1/3 surface of the thigh and in the plane of hip and knee joint centres, and knee flexion/extension axis | x | x | x | x |
| L/R KNE | Most prominent aspect of the lateral femoral condyle | x | x | x | x |
| RHFB | Most lateral aspect of the head of the fibula | x | x | x | |
| RTUB | Most anterior prominence of the tibial tuberosity | x | x | x | x |
| RTIB | Wand marker, distal lateral tibia | | | | x |
| RSHN | Anywhere along the anterior crest of the tibia | x | | | x |
| RANK | Distal apex of the lateral malleolus | x | x | x | x |
| RMMA | Distal apex of the medial malleolus | x* | x | x | x* |
| RCA1 | Distal end of the midline in the sagittal plane | x | | | x |
| RCA2 | Proximal end of the midline in the sagittal plane (i.e. Achilles' tendon attachment) | x* | x | x | |
| RCPG | Wand marker, the base of which is placed mid-way between RCA1 and RCA2 | x | | | |
| RSTL | At the same vertical level as the palpated landmark (maximising inter-marker distance and avoiding local muscle attachments) | x | | | x |
| RST | 2 cm under the distal border of the medial malleolus | | x | x | |
| RPT | First bone prominence below the lateral malleolus | | x | x | x* |
| RLCA | At same distance from the most posterior point as RSTL (on lateral calcaneus) | x | | | x |
| RC | First recognisable bone prominence on the cuboid, from the 5$^{th}$ metatarsal base following the direction of the tibia axis | | | x | |
| RTN | 2$^{nd}$ prominence on the line between proximal epiphysis of the 1$^{st}$ metatarsal and the lower ridge of the calcaneus (on the interior side of the extensor longus of the hallux) | | x | x | |
| RP5M | Base of the 5$^{th}$ metatarsal: dorso-medial aspect | x | x | x | |
| RD5M | Head of 5$^{th}$ metatarsal: laterally on the foot | x | | | |
| RVMH | Dorso-medial aspect of the 5th metatarso-phalangeal joint (avoiding the flexor tendon and the joint) | | x | x | x |
| RTOE | Mid-point of heads of the 2$^{nd}$ and 3$^{rd}$ metatarsal | x | | | x* |
| RIIT | Proximal epiphysis of second toe phalanx (1 cm distal from the joint interstice of the 2nd ray) | | | x | |
| RSMH | Dorso-medial aspect of the 2$^{nd}$ metatarso-phalangeal joint | | x | | |
| RT23 | Mid-point of bases of the 2$^{nd}$ and 3$^{rd}$ metatarsal | | | | x* |
| RSMB | Dorso-medial aspect of the 2$^{nd}$ metatarso-cuneiform joint | | x | | |
| RFMH | Dorso-medial aspect of the 1$^{st}$ metatarso-phalangeal joint (avoiding the flexor tendon) | | x | x | x |
| RD1M | Head of 1$^{st}$ metatarsal: medially on the foot | x* | | | x* |
| RP1M | Dorso medial aspect of the 1$^{st}$ metatarso-cuneiform joint (avoiding the flexor tendon) | x | x | | x |
| R1BM | Base of 1$^{st}$ metatarsal: medial aspect | | | | x* |
| RHLX | Proximal phalanx of the hallux (on the medial side, mid-way between superior and inferior surface) | x | | | |
| RTRX-Y-Z | Toe triad placed on the nail hallux | | | | x |

## 5.3.1 Data collection

Figure 5.2 summarises how data have been collected. Details will be presented in the following sections.

#### *5.3.1.1 Treadmill-overground walking comparison*

A treadmill (ADAL3D-F, TECMACHINE HEF Groupe – Andreziéux Bouthéon, France) was used to collect more than one stride per trial. A comparison between treadmill and overground walking conditions allowed to check whether the models were all sensitive enough to detect expected changes in the kinematic patterns, known to differ mainly due to the inherent different walking speeds [75,76].

A trained operator placed the entire marker-set on the thirteen subjects, who were asked to walk barefoot at a self-selected speed on both the treadmill and overground. The observed walking speeds were 0.82 ± 0.15 m/s and 0.99 ± 0.11 m/s, respectively. A total of five right strides were retained from each session for the analysis.


**Figure 5.1** – The complete marker set adopted for the tibia and foot segments. Markers not pertaining to the model of interest are coloured in grey, whereas those pertaining to each model are highlighted as follows: (a) in red the model M1 [65]; (b) in blue the model M2 [67]; (c) in green the model M3 [28]; and (d) in orange the model M4 [68]. This Figure is reproduced as published in [193] with permission of co-authors.

### 5.3.1.2 Within- and between-subject repeatability analyses

Two sessions of data collection for the treadmill walking were carried out one month apart, and by the same operator. This analysis allowed to quantify the variability of the kinematics due to marker repositioning on the same subjects, and the variability of the kinematics among different subjects, also accounting for the between-stride variability.

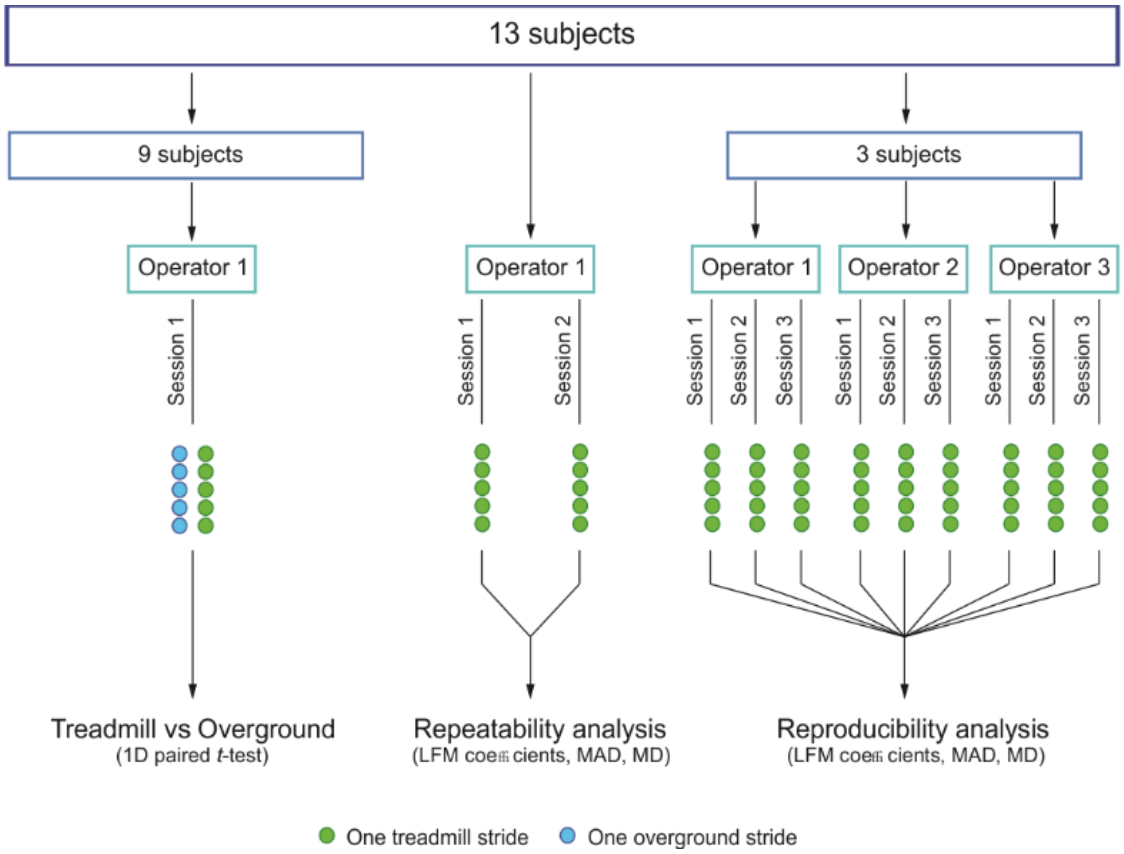


**Figure 5.2** – Flowchart of the experimental design applied in the present study. This Figure is reproduced as published in [193] with permission of co-authors.

### 5.3.1.3 Between-operator reproducibility analysis

Differently from the rationale chosen for the within- and between-subject repeatability analyses, a subset of three male subjects (age: 25.7 ± 2.3 years, height: 1.84 ± 0.08 m, foot length: 28.7 ± 0.2 cm), randomly selected among those recruited, was considered. This analysis allowed to quantify the effect that different operators performing the same measurement might induce on the results. The subject sample size for the reproducibility analysis does not need to be equal to the one considered for the repeatability analysis. Indeed, kinematic curves were averaged in order to isolate only

the effect of different operators performing the experimental protocol, and other studies performed reproducibility analysis on only one subject [87,111]. Three operators, with a background in human movement analysis, attended a session of training to recognise the anatomical landmarks required for the marker set adopted for the present study, repeated the marker placement three times, and measured the relevant anthropometric parameters. Subjects walked barefoot on the treadmill at self-selected speed (walking speed: 0.97 ± 0.24 m/s). This condition is considered the most controlled and produces least variations in the relevant joint kinematics. Five right strides were isolated for the analysis.

## 5.3.2 Data processing

### *5.3.2.1 Treadmill-overground walking comparison*

Data from four subjects among the thirteen recruited were discarded due to poor marker visibility in the overground trials, which impeded to retain the minimum of five strides per trial for the analysis. For the remaining subjects, the ability of the models to discriminate between treadmill and overground walking was tested with the 1D paired *t*-test (α = 0.05) [205]. This test is based on the Statistical Parametric Mapping (SPM) theory [206], which is used to analyse statistical differences among continuous curves, without reducing the test to summary metrics such as maximum or minimum values. The analysis was performed using the SPM1D open-source package for MATLAB (spm1d.org) and generated: map of *t*-values (SPM{t}), *t** limit, and areas where differences were found with their relevant *p*-values.

### *5.3.2.2 Within- and between-subject repeatability analyses*

Following the conclusion of Chapter 3, the within- and between-subject repeatability was assessed both for overground and treadmill walking using the Linear Fit Method (LFM) [129] and the Mean Absolute Variability (MAV) [140] that have been extensively described (§3.2.2 and §3.4). The LFM yields three coefficients comparing each curve to a reference chosen as in §3.2.2: $a_1$ is the scaling factor between the comparing curves and the similarity index (the closer to 1, the more similar the curves); $a_0$ measures the shift between the curves, quantifying the offset when $a_1$ tends to 1; $R^2$ validates the linear relationship between the curves and measures their correlation (the closer to 1, the stronger the linear model). As reported in [129] and showed in

§3.2.2, $a_1$ and $a_0$ tend to their ideal values (i.e., 1 and 0, respectively) when comparing *n* curves with their averaged pattern. Thus, to have a measure of the variations, it is relevant to report and observe the standard deviations for both $a_1$ and $a_0$. The MAV was calculated as described in §3.2.2.

The LFM coefficients and MAV were complemented considering the sagittal joint angles at initial contact (IC) and toe-off (TO) as summary metrics [137], and the Median Absolute Deviation (MAD) and the Maximum Difference (MD) were calculated [87]: the former is a variability index reported to be robust to the outliers, the latter measures the differences obtained in the worst case.

#### *5.3.2.3 Between-operator reproducibility analysis*

The agreement among the kinematic curves was tested using the LFM. For each subject, the *i*-th kinematic variable associated with each of the five strides retained from each *j*-th repetition for the *k*-th operator was compared to the same kinematic variable averaged among the five strides, the three repetitions and the three operators. Averaged distance among the kinematic curves was assessed by calculating the MAV. Median Absolute Deviations (MAD) and Maximum Differences (MD) were also calculated on the sagittal kinematics at the Initial Contact (IC) and the Toe-Off (TO).

## 5.4 Results

### 5.4.1 Treadmill-overground walking comparison

Figure 5.3 and Figure 5.4 show the joint kinematics and the relevant mapping of *t*-values (SPM{t}) obtained from the 1D paired *t*-test over the two walking conditions. Despite corresponding joints being differently defined, the Knee and FF-MF (where relevant) obtained from the four models showed differences in the same part of the gait cycle. For the other kinematics some inconsistencies among the models were highlighted: for example, HF-Tib displayed differences between the 40 and 50% of the gait cycle for M2 and M3 ($p<0.001$), whereas M1 and M4 did not. These inconsistencies are not relevant for this study, which aimed to assess the models ability highlighting the changes imposed by the two walking conditions (treadmill and overground walking).

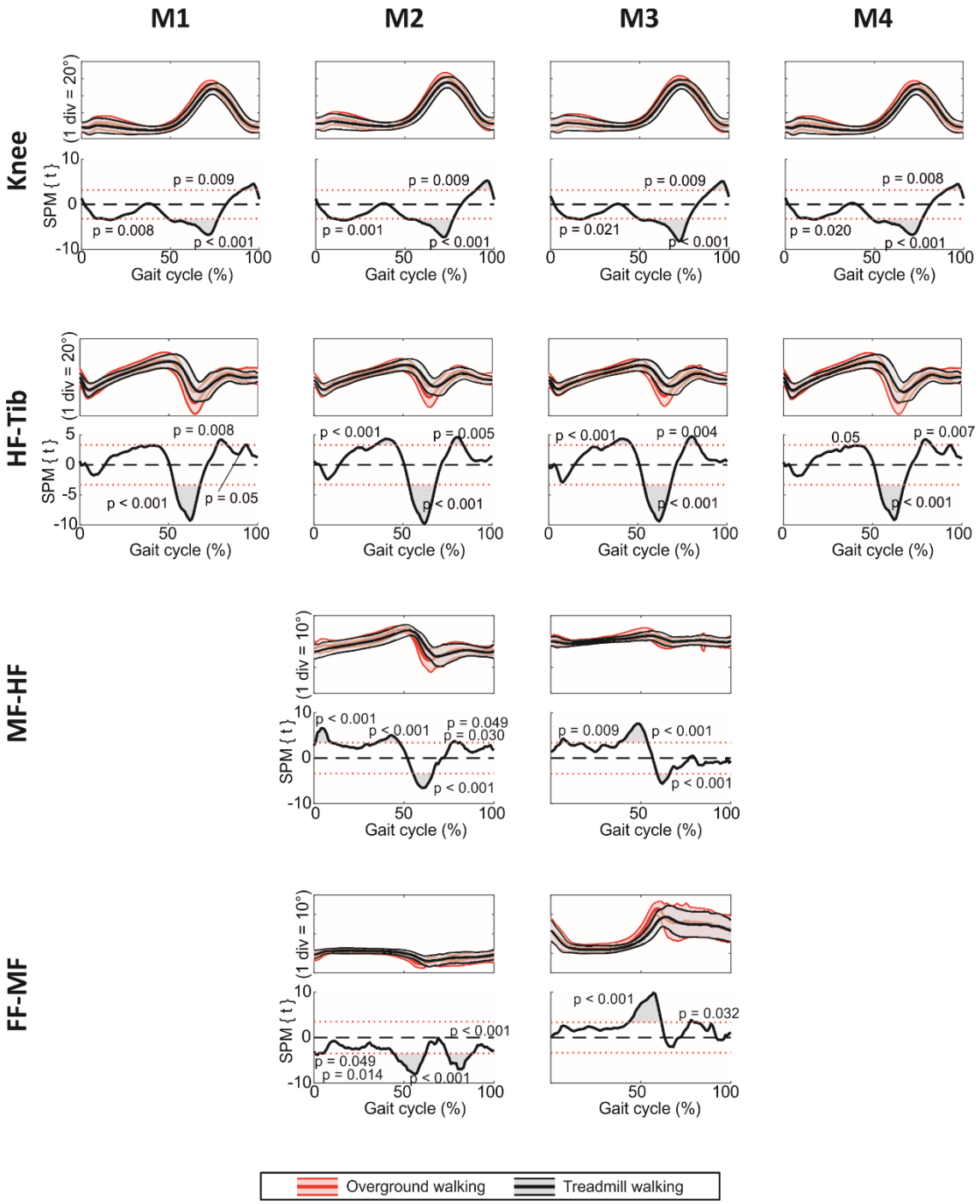


**Figure 5.3** – Comparison between treadmill and overground walking conditions. Sagittal kinematics and relative statistical parametric mapping of the t-value from the 1D paired t-test for: Knee, tibia/fibula and calcaneus/hindfoot (HF-Tib), calcaneus/hindfoot and midfoot (MF-HF), midfoot and forefoot (FF-MF). This Figure is reproduced as published in [193] with permission of co-authors.

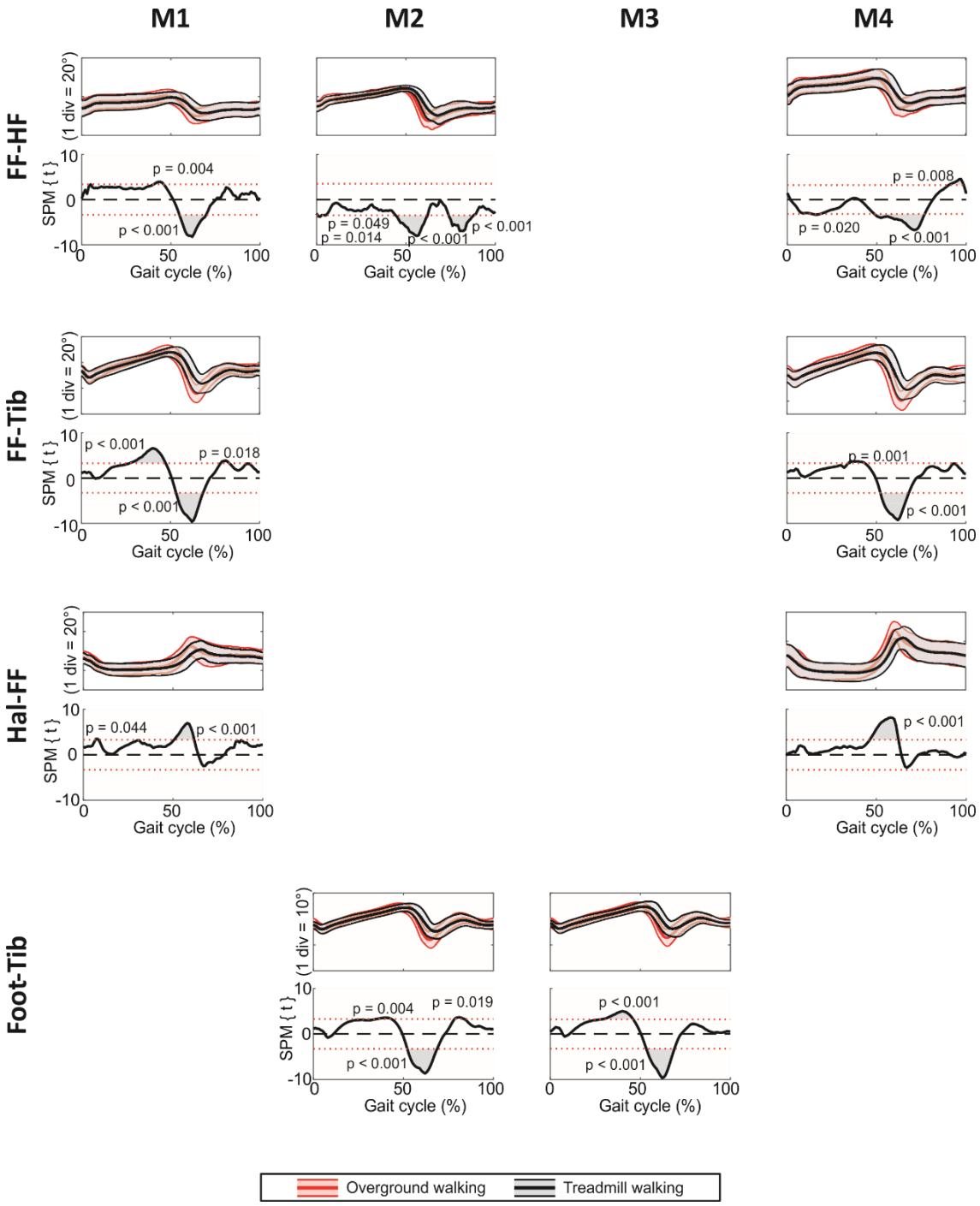


**Figure 5.4** – Comparison between treadmill and overground walking conditions. Sagittal kinematics and relative statistical parametric mapping of the t-value from the 1D paired t-test for: calcaneus/hindfoot and forefoot (FF-HF), tibia/fibula and forefoot (FF-Tib), forefoot and hallux (Hal-FF), tibia/fibula and foot as a rigid segment (Foot-Tib). This Figure is reproduced as published in [193] with permission of co-authors.

## 5.4.2 Within- and between-subject repeatability analyses

Table 5.2-Table 5.3 and Table 5.4-Table 5.5 show the results of the within- and between-subject repeatability analyses in terms of LFM coefficients, MAV, and absolute differences (MAD and MD at Initial Contact and Toe-Off), for treadmill and overground

walking, respectively. The tables also report the Range of Motion (ROM) values for the targeted joints.

For treadmill walking (Table 5.2), the within-subject analysis yielded high averaged correlations ( $R^2$ ) among the curves for all the kinematics of the four models, with values ranging between 0.90 and 0.97. The exceptions were only observed for $^{M2}$FF-MF and $^{M3}$MF-HF (0.87 and 0.77, respectively). These were also the kinematics with the smallest range of motion: 9° and 5°, respectively. Averaged $a_1$ was equal to 1 for all the kinematics and its standard deviation was always lower than 0.27: peaks for *SD*-$a_1$ occurred for $^{M2}$FF-MF (*SD*-$a_1$ = 0.22) and $^{M3}$MF-HF (*SD*-$a_1$ = 0.27). Interestingly, standard deviations of the offset $a_0$ were comparable among M1, M2 and M3 (between 0° and 3°), whereas higher values were found for M4 (between 3° and 10°). MAVs were compa rable between M2 and M3 (between 1 and 4°), whereas slightly higher values were obtained for M1 and M4 (between 2° and 6°). Although less marked, a similar trend was detected by MAD and MD at both IC and TO.

The between-subject results (Table 5.3) confirmed the trend observed from the within-subject analysis. Indeed, the averaged $a_1$ were equal to 1 for all the kinematics. The only exceptions were obtained for $^{M2-M3}$HF-Tib: averaged $a_1$ = 0.99. The maximum *SD*-$a_1$ were found for those joints whose linearity coefficients were poor: $^{M2}$FF-MF (*SD*-$a_1$ = 0.58; $R^2$ = 0.67); and $^{M3}$MF-HF (*SD*-$a_1$ = 0.59; $R^2$ = 0.51). The between-subject *SD*-$a_0$ was higher for M4 (from 3° to 14°) than M1 (from 3° to 7°), M2 and M3 (from 1° to 6°). As for the within-subject results, MAV values were comparable between M2 and M3 (from 4° to 22°), with slightly higher values for M1 (from 9° to 23°) and M4 (from 9° to 26°). Maximum values for $MAD_{IC}$ were: 4° for M1-M2-M3, and 6° for M4; for $MAD_{TO}$ were: 7° for M1-M4, 5° for M2, 4° for M3. MDs, as expected, were higher than MADs. Overall, MDs obtained for M1 are equivalent to those obtained for M4, and values obtained for M2 are equivalent to those obtained for M3.

Although only one session of data collection was performed for the overground walking, the comments given for the results showed by Table 5.2 and Table 5.3 (treadmill walking) are also valid for the results in Table 5.4 and Table 5.5 (overground walking). Interestingly, the kinematics $^{M3}$MF-HF showed the worst behaviour also in

between-subject analysis for this walking condition: $a_1$ = 1.00 ± 0.37 and $R^2$ = 0.55 ± 0.23.

**Table 5.2** – Within-subject repeatability analysis for treadmill walking: Range of Motion (ROM), Linear Fit Method (LFM) coefficients, Mean Absolute Variability (MAV), Median Absolute Deviation (MAD) and Maximum Difference (MD) at Initial Contact (IC) and Toe-Off (TO). Segment names are abbreviated as follows: tibia (Tib), calcaneus and hindfoot (HF), midfoot (MF), metatarsus and forefoot (FF), hallux (Hal), and foot as rigid segment (Foot). M1 stands for the model described in [65], M2 for [67], M3 for [28], and M4 for [68]. This Table has been partially published in [193], and reproduced in this Thesis with permission of co-authors.

| | Joints | ROM (°) | LFM coefficients | | | MAV (°) | MAD (°) | | MD (°) | |
|---|---|---|---|---|---|---|---|---|---|---|
| | | | $a_1$ | $a_0$ (°) | $R^2$ | | IC | TO | IC | TO |
| **M1** | *Knee* | 50 ± 8 | 1.00 ± 0.07 | 0 ± 3 | 0.97 ± 0.04 | 5 ± 4 | 1 ± 0 | 1 ± 0 | 9 ± 5 | 11 ± 2 |
| | *HF-Tib* | 19 ± 4 | 1.00 ± 0.11 | 0 ± 2 | 0.91 ± 0.08 | 3 ± 3 | 1 ± 0 | 1 ± 0 | 6 ± 3 | 8 ± 2 |
| | *FF-HF* | 9 ± 2 | 1.00 ± 0.18 | 0 ± 2 | 0.92 ± 0.06 | 3 ± 3 | 1 ± 0 | 0 ± 0 | 6 ± 3 | 5 ± 1 |
| | *FF-Tib* | 28 ± 5 | 1.00 ± 0.11 | 0 ± 1 | 0.93 ± 0.07 | 2 ± 1 | 1 ± 1 | 2 ± 1 | 5 ± 2 | 10 ± 2 |
| | *Hal-FF* | 28 ± 5 | 1.00 ± 0.15 | 0 ± 3 | 0.92 ± 0.08 | 6 ± 4 | 1 ± 1 | 1 ± 1 | 9 ± 4 | 12 ± 1 |
| **M2** | *Knee* | 53 ± 7 | 1.00 ± 0.06 | 0 ± 2 | 0.97 ± 0.04 | 4 ± 2 | 1 ± 0 | 1 ± 0 | 6 ± 3 | 10 ± 2 |
| | *HF-Tib* | 16 ± 3 | 1.00 ± 0.13 | 0 ± 1 | 0.90 ± 0.10 | 2 ± 1 | 1 ± 0 | 1 ± 0 | 3 ± 1 | 6 ± 2 |
| | *MF-HF* | 11 ± 3 | 1.00 ± 0.17 | 0 ± 0 | 0.92 ± 0.08 | 1 ± 1 | 0 ± 0 | 1 ± 0 | 3 ± 1 | 4 ± 1 |
| | *FF-MF* | 9 ± 2 | 1.00 ± 0.22 | 0 ± 1 | 0.87 ± 0.12 | 1 ± 1 | 0 ± 0 | 1 ± 0 | 2 ± 2 | 4 ± 1 |
| | *FF-HF* | 16 ± 4 | 1.00 ± 0.15 | 0 ± 1 | 0.93 ± 0.08 | 2 ± 1 | 0 ± 0 | 1 ± 0 | 3 ± 1 | 5 ± 1 |
| | *Foot-Tib* | 22 ± 4 | 1.00 ± 0.10 | 0 ± 1 | 0.92 ± 0.08 | 2 ± 1 | 1 ± 0 | 1 ± 0 | 3 ± 1 | 8 ± 3 |
| **M3** | *Knee* | 51 ± 7 | 1.00 ± 0.06 | 0 ± 2 | 0.97 ± 0.04 | 4 ± 3 | 1 ± 1 | 1 ± 1 | 4 ± 2 | 6 ± 2 |
| | *HF-Tib* | 14 ± 3 | 1.00 ± 0.13 | 0 ± 1 | 0.90 ± 0.09 | 2 ± 1 | 1 ± 0 | 1 ± 0 | 2 ± 1 | 4 ± 2 |
| | *MF-HF* | 5 ± 1 | 1.00 ± 0.27 | 0 ± 1 | 0.77 ± 0.20 | 1 ± 1 | 0 ± 0 | 0 ± 0 | 1 ± 1 | 1 ± 1 |
| | *FF-MF* | 20 ± 4 | 1.00 ± 0.15 | 0 ± 1 | 0.93 ± 0.08 | 2 ± 1 | 1 ± 1 | 1 ± 1 | 4 ± 2 | 5 ± 2 |
| | *Foot-Tib* | 20 ± 3 | 1.00 ± 0.11 | 0 ± 1 | 0.91 ± 0.09 | 2 ± 1 | 1 ± 1 | 1 ± 1 | 2 ± 1 | 6 ± 3 |
| **M4** | *Knee* | 50 ± 8 | 1.00 ± 0.07 | 0 ± 3 | 0.97 ± 0.04 | 6 ± 4 | 1 ± 0 | 1 ± 0 | 9 ± 5 | 11 ± 6 |
| | *HF-Tib* | 19 ± 4 | 1.00 ± 0.11 | 0 ± 2 | 0.91 ± 0.08 | 4 ± 3 | 1 ± 0 | 1 ± 1 | 6 ± 3 | 8 ± 5 |
| | *FF-HF* | 15 ± 4 | 1.00 ± 0.18 | 0 ± 5 | 0.93 ± 0.08 | 3 ± 2 | 1 ± 0 | 0 ± 0 | 6 ± 3 | 6 ± 3 |
| | *FF-Tib* | 34 ± 6 | 1.00 ± 0.10 | 0 ± 3 | 0.93 ± 0.08 | 4 ± 2 | 1 ± 0 | 1 ± 1 | 6 ± 2 | 11 ± 5 |
| | *Hal-FF* | 47 ± 8 | 1.00 ± 0.17 | 0 ± 10 | 0.94 ± 0.06 | 6 ± 5 | 1 ± 1 | 2 ± 1 | 13 ± 6 | 15 ± 7 |

### 5.4.3 Between-operator reproducibility analysis

Table 5.6 shows the between-operators reproducibility for treadmill walking. Averaged correlations ranged from 0.85 to 0.98 for M1, from 0.87 to 0.98 for M2, from 0.72 to 0.98 for M3, and from 0.90 to 0.98 for M4. As for the within- and between-subject analyses, $^{M2}$FF-MF (*SD*-$a_1$ = 0.24 and $R^2$ = 0.87) and $^{M3}$MF-HF (*SD*-$a_1$ = 0.29 and $R^2$ = 0.72) showed the highest *SD*-$a_1$ and correlations were lower than those of other joints. In addition the *SD*-$a_0$ confirmed what had been observed in the previous analysis: the highest values were obtained for M1 and M4. As per the previous analyses, averaged MAVs were comparable between M2 and M3 (from 1° to 5°), whereas slightly higher values were found for M1 (from 3° to 9°) and M4 (from 4° to 6°). Averaged MAD values at IC and TO were in the range 0-3° for M1 and M4, and 0-1° for M2 and M3. The highest

values for MDs were found for M4 (3-12°), followed by M1 (2-9°, with the highest values for Hal-FF).

**Table 5.3** – Between-subject repeatability analysis for treadmill walking: Range of Motion (ROM), Linear Fit Method (LFM) coefficients, Mean Absolute Variability (MAV), Median Absolute Deviation (MAD) and Maximum Difference (MD) at Initial Contact (IC) and Toe-Off (TO). Segment names are abbreviated as follows: tibia (Tib), calcaneus and hindfoot (HF), midfoot (MF), metatarsus and forefoot (FF), hallux (Hal), and foot as rigid segment (Foot). M1 stands for the model described in [65], M2 for [67], M3 for [28], and M4 for [68]. This Table has been partially published in [193], and reproduced in this Thesis with permission of co-authors.

| | Joints | ROM (°) | LFM coefficients | | | MAV (°) | MAD (°) | | MD (°) | |
|---|---|---|---|---|---|---|---|---|---|---|
| | | | $a_1$ | $a_0$ (°) | $R^2$ | | IC | TO | IC | TO |
| **M1** | *Knee* | 50 ± 8 | 1.00 ± 0.18 | 0 ± 6 | 0.91 ± 0.07 | 20 | 4 | 5 | 22 | 15 |
| | *HF-Tib* | 19 ± 4 | 1.00 ± 0.24 | 0 ± 3 | 0.74 ± 0.16 | 10 | 2 | 4 | 8 | 14 |
| | *FF-HF* | 9 ± 2 | 1.00 ± 0.30 | 0 ± 3 | 0.81 ± 0.13 | 9 | 2 | 3 | 12 | 12 |
| | *FF-Tib* | 28 ± 5 | 1.00 ± 0.21 | 0 ± 3 | 0.79 ± 0.15 | 15 | 2 | 5 | 15 | 24 |
| | *Hal-FF* | 28 ± 5 | 1.00 ± 0.27 | 0 ± 7 | 0.77 ± 0.16 | 23 | 5 | 7 | 20 | 33 |
| **M2** | *Knee* | 53 ± 7 | 1.00 ± 0.17 | 0 ± 6 | 0.92 ± 0.07 | 21 | 4 | 4 | 22 | 18 |
| | *HF-Tib* | 16 ± 3 | 0.99 ± 0.26 | 0 ± 2 | 0.69 ± 0.19 | 9 | 1 | 3 | 10 | 14 |
| | *MF-HF* | 11 ± 3 | 1.00 ± 0.36 | 0 ± 1 | 0.79 ± 0.15 | 7 | 1 | 1 | 6 | 12 |
| | *FF-MF* | 9 ± 2 | 1.00 ± 0.58 | 0 ± 1 | 0.67 ± 0.27 | 4 | 1 | 2 | 8 | 8 |
| | *FF-HF* | 16 ± 4 | 1.00 ± 0.35 | 0 ± 1 | 0.81 ± 0.14 | 8 | 2 | 4 | 7 | 15 |
| | *Foot-Tib* | 22 ± 4 | 1.00 ± 0.19 | 0 ± 3 | 0.74 ± 0.16 | 11 | 1 | 5 | 10 | 18 |
| **M3** | *Knee* | 51 ± 7 | 1.00 ± 0.17 | 0 ± 6 | 0.92 ± 0.07 | 22 | 4 | 3 | 24 | 19 |
| | *HF-Tib* | 14 ± 3 | 0.99 ± 0.26 | 0 ± 2 | 0.70 ± 0.18 | 8 | 1 | 2 | 10 | 13 |
| | *MF-HF* | 5 ± 1 | 1.00 ± 0.59 | 0 ± 1 | 0.51 ± 0.28 | 4 | 1 | 1 | 6 | 8 |
| | *FF-MF* | 20 ± 4 | 1.00 ± 0.34 | 0 ± 2 | 0.79 ± 0.13 | 14 | 4 | 3 | 22 | 22 |
| | *Foot-Tib* | 20 ± 3 | 1.00 ± 0.20 | 0 ± 3 | 0.74 ± 0.16 | 11 | 1 | 4 | 11 | 19 |
| **M4** | *Knee* | 50 ± 8 | 1.00 ± 0.18 | 0 ± 6 | 0.91 ± 0.07 | 20 | 4 | 5 | 22 | 16 |
| | *HF-Tib* | 19 ± 4 | 1.00 ± 0.25 | 0 ± 3 | 0.74 ± 0.16 | 11 | 2 | 4 | 8 | 14 |
| | *FF-HF* | 15 ± 4 | 1.00 ± 0.38 | 0 ± 11 | 0.81 ± 0.15 | 9 | 2 | 4 | 16 | 13 |
| | *FF-Tib* | 34 ± 6 | 1.00 ± 0.23 | 0 ± 7 | 0.80 ± 0.14 | 17 | 3 | 4 | 15 | 24 |
| | *Hal-FF* | 47 ± 8 | 1.00 ± 0.31 | 0 ± 14 | 0.82 ± 0.15 | 26 | 6 | 7 | 30 | 30 |

## 5.5 Discussion

This study evaluated the repeatability and the reproducibility of four models for the foot-ankle complex used for gait analysis. Tests were conducted on healthy adults and, thus, no comparison of the presented results can be performed with studies that include patients. Indeed, *ad-hoc* studies investigating within- and between-subject, and between-operator variability are recommended for patients with pathologies that cause foot deformities. Out-of-sagittal kinematics have not been analysed, since they have already been reported to be the least repeatable and reproducible [57,125], also for the four models here investigated [28,65,67,68,112,175]. Although this choice could be addressed as a limitation, it is safe to assume that kinematics on frontal and transverse planes would be even less repeatable and reproducible than sagittal kinematics.

**Table 5.4 –** Within-subject repeatability analysis for overground walking: Range of Motion (ROM), Linear Fit Method (LFM) coefficients, Mean Absolute Variability (MAV), Median Absolute Deviation (MAD) and Maximum Difference (MD) at initial contact (IC) and toe-off (TO). Segment names are abbreviated as follows: tibia (Tib), calcaneus and hindfoot (HF), midfoot (MF), metatarsus and forefoot (FF), hallux (Hal), and foot as rigid segment (Foot). M1 stands for the model described in [65], M2 for [67], M3 for [28], and M4 for [68]. This Table has been partially published in [193], and reproduced in this Thesis with permission of co-authors.

| | Joints | ROM (°) | LFM coefficients | | | MAV (°) | MAD (°) | | MD (°) | |
|---|---|---|---|---|---|---|---|---|---|---|
| | | | $a_1$ | $a_0$ (°) | $R^2$ | | IC | TO | IC | TO |
| **M1** | *Knee* | 57 ± 5 | 1.00 ± 0.06 | 0 ± 1 | 0.98 ± 0.02 | 7 ± 2 | 1 ± 1 | 2 ± 1 | 6 ± 4 | 8 ± 2 |
| | *HF-Tib* | 24 ± 4 | 1.00 ± 0.07 | 0 ± 1 | 0.93 ± 0.05 | 4 ± 1 | 1 ± 1 | 1 ± 1 | 5 ± 3 | 6 ± 2 |
| | *FF-HF* | 12 ± 3 | 1.00 ± 0.15 | 0 ± 1 | 0.90 ± 0.11 | 3 ± 1 | 0 ± 0 | 0 ± 0 | 3 ± 2 | 2 ± 1 |
| | *FF-Tib* | 36 ± 5 | 1.00 ± 0.07 | 0 ± 1 | 0.94 ± 0.04 | 5 ± 1 | 1 ± 1 | 1 ± 2 | 5 ± 2 | 8 ± 3 |
| | *Hal-FF* | 31 ± 5 | 1.00 ± 0.15 | 0 ± 2 | 0.90 ± 0.12 | 6 ± 2 | 1 ± 1 | 2 ± 2 | 5 ± 3 | 10 ± 7 |
| **M2** | *Knee* | 61 ± 5 | 1.00 ± 0.06 | 0 ± 2 | 0.98 ± 0.02 | 7 ± 2 | 1 ± 1 | 2 ± 1 | 6 ± 4 | 8 ± 3 |
| | *HF-Tib* | 20 ± 4 | 1.00 ± 0.08 | 0 ± 0 | 0.92 ± 0.05 | 4 ± 1 | 1 ± 1 | 1 ± 1 | 3 ± 2 | 5 ± 2 |
| | *MF-HF* | 13 ± 4 | 1.00 ± 0.09 | 0 ± 0 | 0.92 ± 0.07 | 2 ± 0 | 1 ± 1 | 0 ± 0 | 3 ± 2 | 2 ± 1 |
| | *FF-MF* | 10 ± 2 | 1.00 ± 0.12 | 0 ± 1 | 0.91 ± 0.06 | 2 ± 0 | 0 ± 0 | 0 ± 1 | 2 ± 1 | 3 ± 2 |
| | *FF-HF* | 19 ± 4 | 1.00 ± 0.06 | 0 ± 1 | 0.96 ± 0.03 | 3 ± 1 | 1 ± 0 | 0 ± 0 | 3 ± 2 | 3 ± 2 |
| | *Foot-Tib* | 28 ± 3 | 1.00 ± 0.07 | 0 ± 1 | 0.94 ± 0.04 | 4 ± 1 | 1 ± 1 | 1 ± 1 | 4 ± 3 | 6 ± 2 |
| **M3** | *Knee* | 59 ± 4 | 1.00 ± 0.06 | 0 ± 2 | 0.98 ± 0.02 | 7 ± 2 | 1 ± 1 | 2 ± 1 | 4 ± 4 | 6 ± 4 |
| | *HF-Tib* | 20 ± 4 | 1.00 ± 0.08 | 0 ± 0 | 0.92 ± 0.05 | 4 ± 1 | 1 ± 1 | 1 ± 1 | 3 ± 3 | 4 ± 3 |
| | *MF-HF* | 7 ± 1 | 1.00 ± 0.18 | 0 ± 0 | 0.85 ± 0.14 | 2 ± 0 | 0 ± 1 | 0 ± 0 | 1 ± 1 | 1 ± 1 |
| | *FF-MF* | 26 ± 4 | 1.00 ± 0.11 | 0 ± 2 | 0.92 ± 0.09 | 5 ± 2 | 1 ± 1 | 2 ± 2 | 5 ± 4 | 5 ± 5 |
| | *Foot-Tib* | 27 ± 4 | 1.00 ± 0.07 | 0 ± 1 | 0.94 ± 0.04 | 4 ± 1 | 1 ± 0 | 1 ± 1 | 3 ± 3 | 5 ± 3 |
| **M4** | *Knee* | 57 ± 5 | 1.00 ± 0.06 | 0 ± 1 | 0.98 ± 0.02 | 7 ± 2 | 1 ± 1 | 2 ± 1 | 6 ± 4 | 8 ± 2 |
| | *HF-Tib* | 25 ± 4 | 0.99 ± 0.14 | 0 ± 1 | 0.93 ± 0.05 | 4 ± 1 | 1 ± 1 | 1 ± 1 | 5 ± 3 | 6 ± 2 |
| | *FF-HF* | 18 ± 4 | 0.98 ± 0.14 | 0 ± 2 | 0.95 ± 0.03 | 3 ± 0 | 1 ± 0 | 0 ± 0 | 3 ± 2 | 2 ± 1 |
| | *FF-Tib* | 41 ± 4 | 0.98 ± 0.15 | 0 ± 2 | 0.95 ± 0.04 | 6 ± 1 | 1 ± 1 | 2 ± 1 | 6 ± 3 | 8 ± 2 |
| | *Hal-FF* | 51 ± 5 | 0.98 ± 0.15 | 0 ± 2 | 0.94 ± 0.03 | 8 ± 1 | 1 ± 1 | 3 ± 2 | 7 ± 4 | 13 ± 4 |

The obtained kinematics have been verified by comparing the Range of Motion (ROM) to those reported in the original articles for M1 [65], M2 [67], M3 [28] and M4 [68]. A good match of the kinematics was observed, even though M1 and M4 were originally proposed for a children population. In particular, the obtained *ROM* differed at the most of 6° for M1 ($^{M1}$FF-Tib), of 8° for M3 ($^{M3}$FF-MF), and of 10° for M4 ($^{M4}$FF-HF), respectively. A comparison of the kinematics over the entire gait cycle was not possible for M2, since authors reported the kinematics only of the stance phase [67]. However, Deschamps *et al*. [142] provided the ROM of the relevant joints for M2 and the largest discrepancy from the results presented here (10°) was obtained for $^{M2}$HF-Tib. These differences could be ascribed either to a non-age matched sample with the cited papers, or to the different sample sizes. Indeed, six subjects aged between 22 and 54 years-old were recruited in [142], whereas thirteen subjects were recruited for the present study: in general, the smaller the sample size, the more the average could be biased by a single value. However, subjects' details given in [142] are not sufficient to discern between these two hypotheses.

**Table 5.5** – Between-subject repeatability analysis for overground walking: Range of Motion (ROM), Linear Fit Method (LFM) coefficients, Mean Absolute Variability (MAV), Median Absolute Deviation (MAD) and Maximum Difference (MD) at initial contact (IC) and toe-off (TO). Segment names are abbreviated as follows: tibia (Tib), calcaneus and hindfoot (HF), midfoot (MF), metatarsus and forefoot (FF), hallux (Hal), and foot as rigid segment (Foot). M1 stands for the model described in [65], M2 for [67], M3 for [28], and M4 for [68]. This Table has been partially published in [193], and reproduced in this Thesis with permission of co-authors.

| | Joints | ROM (°) | LFM coefficients | | | MAV (°) | MAD (°) | | MD (°) | |
|---|---|---|---|---|---|---|---|---|---|---|
| | | | $a_1$ | $a_0$ (°) | $R^2$ | | IC | TO | IC | TO |
| **M1** | *Knee* | 57 ± 5 | 1.00 ± 0.11 | 0 ± 5 | 0.95 ± 0.04 | 18 | 5 | 3 | 15 | 13 |
| | *HF-Tib* | 24 ± 4 | 1.01 ± 0.17 | 0 ± 3 | 0.83 ± 0.08 | 10 | 1 | 1 | 16 | 9 |
| | *FF-HF* | 12 ± 3 | 1.00 ± 0.35 | 0 ± 4 | 0.82 ± 0.15 | 12 | 2 | 3 | 11 | 14 |
| | *FF-Tib* | 36 ± 5 | 1.01 ± 0.13 | 0 ± 3 | 0.87 ± 0.07 | 12 | 2 | 3 | 11 | 16 |
| | *Hal-FF* | 31 ± 5 | 1.00 ± 0.33 | 0 ± 6 | 0.73 ± 0.17 | 22 | 6 | 7 | 20 | 7 |
| **M2** | *Knee* | 61 ± 5 | 1.00 ± 0.10 | 0 ± 5 | 0.95 ± 0.03 | 16 | 2 | 1 | 18 | 10 |
| | *HF-Tib* | 20 ± 4 | 0.99 ± 0.24 | 0 ± 2 | 0.79 ± 0.10 | 9 | 1 | 2 | 12 | 7 |
| | *MF-HF* | 13 ± 4 | 1.08 ± 0.35 | 0 ± 1 | 0.84 ± 0.12 | 7 | 1 | 2 | 6 | 13 |
| | *FF-MF* | 10 ± 2 | 1.00 ± 0.39 | 0 ± 1 | 0.69 ± 0.19 | 6 | 2 | 1 | 8 | 7 |
| | *FF-HF* | 19 ± 4 | 1.02 ± 0.25 | 0 ± 1 | 0.87 ± 0.08 | 8 | 3 | 1 | 10 | 1 |
| | *Foot-Tib* | 28 ± 3 | 1.00 ± 0.14 | 0 ± 3 | 0.84 ± 0.09 | 11 | 2 | 3 | 16 | 10 |
| **M3** | *Knee* | 59 ± 4 | 0.97 ± 0.11 | -1 ± 4 | 0.95 ± 0.04 | 16 | 3 | 1 | 19 | 7 |
| | *HF-Tib* | 20 ± 4 | 0.96 ± 0.22 | 0 ± 1 | 0.81 ± 0.10 | 9 | 2 | 1 | 12 | 7 |
| | *MF-HF* | 7 ± 1 | 1.00 ± 0.37 | 0 ± 1 | 0.55 ± 0.23 | 5 | 2 | 1 | 6 | 6 |
| | *FF-MF* | 26 ± 4 | 1.07 ± 0.34 | 0 ± 2 | 0.73 ± 0.17 | 12 | 9 | 7 | 17 | 19 |
| | *Foot-Tib* | 27 ± 4 | 0.98 ± 0.15 | 0 ± 2 | 0.83 ± 0.09 | 11 | 2 | 2 | 14 | 10 |
| **M4** | *Knee* | 57 ± 5 | 0.94 ± 0.15 | 0 ± 5 | 0.95 ± 0.04 | 18 | 5 | 4 | 15 | 14 |
| | *HF-Tib* | 25 ± 4 | 0.92 ± 0.22 | 0 ± 3 | 0.82 ± 0.08 | 10 | 2 | 1 | 15 | 10 |
| | *FF-HF* | 18 ± 4 | 0.94 ± 0.29 | 0 ± 9 | 0.87 ± 0.07 | 13 | 4 | 4 | 15 | 12 |
| | *FF-Tib* | 41 ± 4 | 0.95 ± 0.20 | 0 ± 6 | 0.87 ± 0.07 | 18 | 8 | 3 | 23 | 14 |
| | *Hal-FF* | 51 ± 5 | 0.98 ± 0.28 | 0 ± 10 | 0.79 ± 0.13 | 29 | 7 | 4 | 29 | 4 |

### 5.5.1 Treadmill-overground walking comparison

This part of the study was designed to overcome some of the limitations of the most common analyses of joint angles estimated in these two conditions. Indeed, when testing statistical differences, not only time history correlations or point-by-point differences were calculated, but also the intrinsic correlation between subsequent time-samples of the same variable [26,106,205]. The 1D paired *t*-test on the kinematics showed statistically significant differences between the two walking conditions (Figure 5.3 and Figure 5.4). These differences are likely to be ascribed to the different walking speeds, coherently with the literature [75]. For the majority of the kinematics, the different definitions adopted for segments and joints did not allow a direct comparison of the differences observed in the various models. This, as highlighted in Figure 5.3 and Figure 5.4, led to some inconsistent statistical differences in the kinematics among models during the stance phase (§5.4.1). However, the reported results showed an overall ability of distinguishing between the two walking conditions. In conclusion, the four models are sensitive to the examined walking conditions.

**Table 5.6** – Between-operator reproducibility analysis for treadmill walking: Range of Motion (ROM), Linear Fit Method (LFM) coefficients, Mean Absolute Variability (MAV), Median Absolute Deviation (MAD) and Maximum Difference (MD) at Initial Contact (IC) and Toe-Off (TO). Segment names are abbreviated as follows: tibia (Tib), calcaneus and hindfoot (HF), midfoot (MF), metatarsus and forefoot (FF), hallux (Hal), foot as rigid segment (Foot). M1 stands for the model described in [65], M2 for [67], M3 for [28], and M4 for [68]. This Table has been partially published in [193], and reproduced in this Thesis with permission of co-authors.

| | Joints | ROM (°) | LFM coefficients | | | MAV (°) | MAD (°) | | MD (°) | |
|---|---|---|---|---|---|---|---|---|---|---|
| | | | $a_1$ | $a_0$ (°) | $R^2$ | | IC | TO | IC | TO |
| **M1** | *Knee* | 51 ± 4 | 1.00 ± 0.10 | 0 ± 3 | 0.98 ± 0.03 | 6 ± 2 | 1 ± 0 | 2 ± 1 | 5 ± 2 | 8 ± 2 |
| | *HF-Tib* | 21 ± 1 | 1.00 ± 0.14 | 0 ± 3 | 0.93 ± 0.07 | 5 ± 1 | 1 ± 1 | 0 ± 0 | 2 ± 2 | 4 ± 1 |
| | *FF-HF* | 10 ± 1 | 1.00 ± 0.17 | 0 ± 3 | 0.90 ± 0.07 | 3 ± 3 | 1 ± 1 | 1 ± 1 | 6 ± 2 | 5 ± 2 |
| | *FF-Tib* | 30 ± 2 | 1.00 ± 0.14 | 0 ± 3 | 0.94 ± 0.06 | 6 ± 3 | 2 ± 1 | 3 ± 3 | 7 ± 2 | 8 ± 4 |
| | *Hal-FF* | 26 ± 2 | 1.00 ± 0.23 | 0 ± 6 | 0.85 ± 0.13 | 9 ± 6 | 3 ± 1 | 1 ± 1 | 9 ± 6 | 9 ± 4 |
| **M2** | *Knee* | 56 ± 4 | 1.00 ± 0.09 | 0 ± 3 | 0.98 ± 0.03 | 5 ± 1 | 1 ± 1 | 1 ± 1 | 3 ± 2 | 5 ± 4 |
| | *HF-Tib* | 18 ± 2 | 1.00 ± 0.14 | 0 ± 1 | 0.91 ± 0.08 | 2 ± 1 | 0 ± 1 | 1 ± 2 | 1 ± 0 | 3 ± 2 |
| | *MF-HF* | 10 ± 3 | 1.00 ± 0.15 | 0 ± 1 | 0.90 ± 0.08 | 1 ± 0 | 0 ± 0 | 1 ± 1 | 1 ± 1 | 2 ± 1 |
| | *FF-MF* | 8 ± 3 | 1.00 ± 0.24 | 0 ± 1 | 0.87 ± 0.11 | 1 ± 0 | 0 ± 0 | 1 ± 0 | 1 ± 1 | 2 ± 1 |
| | *FF-HF* | 16 ± 5 | 1.00 ± 0.14 | 0 ± 1 | 0.93 ± 0.05 | 2 ± 0 | 0 ± 0 | 1 ± 0 | 1 ± 1 | 2 ± 1 |
| | *Foot-Tib* | 25 ± 1 | 1.00 ± 0.12 | 0 ± 2 | 0.93 ± 0.07 | 2 ± 1 | 1 ± 0 | 1 ± 0 | 1 ± 0 | 3 ± 2 |
| **M3** | *Knee* | 55 ± 4 | 1.00 ± 0.05 | 0 ± 3 | 0.98 ± 0.03 | 5 ± 1 | 1 ± 1 | 1 ± 1 | 3 ± 2 | 4 ± 4 |
| | *HF-Tib* | 17 ± 2 | 1.00 ± 0.07 | 0 ± 3 | 0.98 ± 0.03 | 2 ± 1 | 1 ± 1 | 1 ± 1 | 1 ± 0 | 3 ± 2 |
| | *MF-HF* | 5 ± 1 | 1.00 ± 0.29 | 0 ± 1 | 0.72 ± 0.15 | 1 ± 0 | 0 ± 0 | 0 ± 0 | 1 ± 0 | 1 ± 0 |
| | *FF-MF* | 24 ± 4 | 1.00 ± 0.15 | 0 ± 1 | 0.92 ± 0.06 | 2 ± 1 | 0 ± 1 | 0 ± 1 | 3 ± 2 | 3 ± 2 |
| | *Foot-Tib* | 23 ± 1 | 1.00 ± 0.12 | 0 ± 2 | 0.93 ± 0.07 | 2 ± 1 | 0 ± 0 | 1 ± 1 | 1 ± 0 | 3 ± 2 |
| **M4** | *Knee* | 51 ± 4 | 0.99 ± 0.11 | 0 ± 3 | 0.98 ± 0.03 | 6 ± 1 | 1 ± 0 | 2 ± 1 | 5 ± 2 | 8 ± 1 |
| | *HF-Tib* | 21 ± 1 | 0.96 ± 0.13 | 0 ± 3 | 0.93 ± 0.07 | 5 ± 1 | 1 ± 1 | 0 ± 0 | 3 ± 3 | 4 ± 3 |
| | *FF-HF* | 16 ± 5 | 0.97 ± 0.18 | 0 ± 6 | 0.90 ± 0.09 | 4 ± 2 | 2 ± 1 | 1 ± 1 | 5 ± 3 | 4 ± 2 |
| | *FF-Tib* | 35 ± 7 | 0.97 ± 0.12 | 0 ± 4 | 0.94 ± 0.06 | 5 ± 1 | 1 ± 1 | 1 ± 1 | 7 ± 3 | 7 ± 5 |
| | *Hal-FF* | 47 ± 13 | 0.98 ± 0.14 | 0 ± 5 | 0.90 ± 0.06 | 6 ± 2 | 3 ± 2 | 2 ± 2 | 11 ± 2 | 12 ± 4 |

## 5.5.2 Within- and between-subject repeatability analyses

The within-subject repeatability analysis performed on the treadmill data (Table 5.2) provided information on the effects of the marker repositioning. Considering the standard deviation of $a_0$, MAVs, MADs and MDs for each of the four models, it was evident that the kinematics obtained from M4 were the most affected by the marker repositioning. This is most likely due to the lack of a neutral configuration definition for the joints, i.e. the alignment with the static posture. Although M1 does not require any reference posture to define the joint angles, the relevant kinematics did not display the same large variability, but still larger than those obtained for the kinematics estimated according to M2 and M3. It is worth highlighting that referencing the kinematics to the static posture, as required for M2 and M3, would lead to a loss of information on possible anatomical deformities. The within-subject results obtained for the overground walking (Table 5.4) were similar to those obtained for the treadmill walking. However, the overground results, obtained from a single session of data collection, showed a smaller *SD*-$a_0$, MADs and MDs strengthening the conclusion that marker repositioning

affects mainly the outputs of M4 and M1. This is most likely due to the subtraction of the static posture required only for M2 and M3. Being obtained from a single session of data collection, within-subject results in Table 5.4 are, hence, an assessment of the between-stride variability. This trend is not confirmed by MAV values, which were slightly lower for treadmill walking rather than for overground walking. Although this aspect might be read as an inconsistency with other results, MAV gives information on the absolute variability among curves over the whole gait cycle, and the higher variability of the curve patterns obtained for the overground walking, confirmed by the higher *SD*-$a_1$ (and some $a_1$ values) observed for this walking condition, could have led to higher MAV values.

$^{M2}$FF-MF and $^{M3}$MF-HF were the angles that led to the worst similarity and correlation indices. These two variables showed a small range of motion, and a large magnitude for the soft tissue artefact could have concealed the actual information, reducing both $a_1$ and $R^2$. Moreover, the midfoot segment (MF) is tracked by markers placed on very close landmarks in both the models, and this could increase the variability on the midfoot-based kinematics.

The presented results seem to contrast those reported in [112], which showed $^{M2}$Foot-Tib to be the most repeatable among the foot joints, which would call for higher values of $a_1$ and $R^2$. This is most likely due to the two different methods used to quantify the repeatability: averaged standard deviation in [112] and LFM coefficients, MAV, MAD and MD, in the present study.

The between-subject repeatability analysis, performed both for overground and treadmill walking, highlighted some critical issues concerning the clinical meaningfulness of normative bands (Table 5.3 and Table 5.5). As in case of the overground walking, particular care should be paid when handling: $^{M1}$HF-Tib, $^{M1}$Hal-FF, $^{M2}$HF-Tib, $^{M2}$FF-MF, $^{M2}$MF-HF, $^{M3}$MF-HF, $^{M3}$HF-Tib, $^{M3}$Foot-Tib, as well as at $^{M4}$HF-Tib values, due to their large between-subject variability. These findings are in line with those reported in [112] for M2. Among all the kinematics, $^{M2}$FF-MF and $^{M3}$MF-HF appear to be the least reliable, in terms of both similarity and correlation. Incidentally, $^{M2}$FF-MF was already found to be the least reliable among the M2 kinematics [142], according to a *z*-score analysis for this purpose [106].

Although in [142] it is reported that for M2 the use of absolute angles did not have a critical impact on the variability of 3D rotations, the results presented on this Thesis indicate that a static posture subtraction might be crucial for foot kinematics repeatability. Indeed, M4 yielded larger normative bands than the other protocols, as shown in Figure 5.3 and Figure 5.4, and confirmed by the between-subject MAVs for both treadmill and overground walking. M1 did not call for a posture subtraction either, but appeared to be more robust to the marker repositioning. Generally, MADs and MDs were always higher than those obtained for M2 and M3, but lower than the values obtained for M4. It is worth considering that, even though kinematic variability might be reduced by subtracting the static posture, this is equivalent to the assumption that any static offset should be ascribed only to marker misplacement, and not to possible foot deformities, which might occur in patient populations.

The models M2 and M3 were comparable in terms within-subject repeatability, and similar values for the chosen indices were observed, whereas the variability linked to M1 and M4 led to slightly worst values of the same indices. This was true both for treadmill and overground walking, with the latter condition leading, as expected, to the highest values for MADs and MDs. The same trend was confirmed by the between-subject analysis. It is worth considering that among the analysed models, only M3 was defined considering a least square fitting approach for the joint kinematics calculation during walking (procedure described in §2.3.2.2.2 and §2.3.2.4). Some prior tests were performed by applying the same approach also to the other models. Relevant results were not included in this Thesis in order to not make confusion with those obtained coherently with what published within the original papers. However, different values for the repeatability indices were obtained, with some of them showing higher and some others lower repeatability than what presented in §5.4 and without considering the least square approach for M1, M2, and M4. The lack of a defined trend for the increasing or the decreasing of the kinematics repeatability does not allow to conclude that using the least square approach should be preferred to the *non-optimal* approach described in (§2.3.2.2.1) when dealing with foot kinematics. This is probably due to the still little knowledge of the effect of STA on the anatomical landmarks of the foot, and the resulting effect on using the least square "*spring-like*" pose estimator (see §2.3.2.2.2).

### 5.5.3 Between-operator reproducibility analysis

Reported LFM-$a_0$ (Table 5.6) and MAVs showed that the effect of the marker repositioning on the same subject (repeatability) produces similar effects of the repositioning performed by different trained operators (reproducibility). MAVs were actually slightly higher for the within-subject repeatability analysis, but this is likely to be ascribed to the different considered sample size. This was also confirmed by MAD and MD values. Although a bias might be introduced to the results by the different sample sizes considered for the repeatability and reproducibility analyses, the equivalence of the two effects suggests that the variability of the foot motion is higher than any other source of variability. The presented results seem to contrast those previously reported for M2 [142], where between-operator reproducibility was assessed with the CMC, and was lower than the within- and the between-day repeatability for a sample of six subjects. As well as for the within-subject analysis, this is likely due to the different methodologies used to assess the curve similarities. Indeed, CMC sensibly decreases when large offset occurs between the compared curves, whereas $R^2$ does not (§3.4).

Both between-operator similarity and correlation indices confirmed what discussed for the within- and between-subject analyses: $^{M2}$MF-HF should be interpreted with attention, and $^{M2}$FF-MF and $^{M3}$MF-HF were the least reliable, having the lowest similarities and correlations. M1 and M4 were confirmed to be the models leading to the highest differences in terms of MAVs, MADs and MDs with consequent larger normative bands. As reported in [112], subject's foot size might play a role in assessing foot kinematic since the anatomical landmarks to be palpated are particularly small, and often close to each other.

It is worth considering that the design of the study in terms of amount of markers to be placed on a single foot, and closeness of some of the anatomical landmarks to be palpated led to the choice of performing the study only on an adult population, rather than adolescence or paediatric populations. Thus, it is an intrinsic limit of this study not to be able to account for subject's foot size when assessing the kinematics of the foot-ankle joints.

## 5.6 Conclusion

The four most adopted models for gait analysis to assess the foot-ankle complex kinematics have been concurrently assessed in terms of both repeatability and reproducibility, together with an assessment of their ability to highlight changes imposed by treadmill and overground walking. All the models were able to distinguish between the two walking conditions, and the models M2 [67] and M3 [28] proved to be the most repeatable and reproducible. Nevertheless, this part of the project clearly showed that it is questionable to assume the foot kinematics to be repeatable and, subsequently, to rely on normative bands for the clinical assessment of patients. Particularly, kinematics characterised by a small range of motion, as for $^{M2}$FF-MF and $^{M3}$MF-HF, should be considered as meaningless, especially when comparing results among different subjects. The development of a new model that overcomes the highlighted limitations seems to be a reasonable attempt to go through, and will be presented in the next Chapter.

Chapter 6

# A new model of the foot-ankle complex for gait analysis

## 6.1 Introduction

The previous Chapter presented a comparative analysis of the four most adopted models for gait analysis of the foot-ankle complex in terms of repeatability and reproducibility of their outcomes. The results led to the conclusion that assuming the foot kinematics to be repeatable is questionable. In particular, normative bands for the clinical assessment of patients should be adopted with care, and kinematics characterised by a small range of motion should be considered as meaningless.

This Chapter presents a novel model of the foot-ankle complex for gait analysis, which attempts to overcome the highlighted limitations, and to improve the repeatability and reproducibility of the relevant outcomes. The description of the model will start from the chosen anatomical landmarks. Then the definitions adopted for the local embedded coordinate systems (**ECS**) of each segment, and the joint coordinate systems (**JCS**) of each joint will be illustrated. The repeatability and reproducibility of the joint kinematics will finally be assessed and compared to those obtained for the models analysed in Chapter 5. Moreover, similarly to what presented in §5.3.2.1, the kinematics obtained for both treadmill and overground walking will be tested to check whether the new model was sensitive enough to detect the expected changes in the kinematic patterns due to the inherent different walking speeds [75,76].

## 6.2 Model description

The anatomical landmarks chosen for the new model were selected among those already defined in Stebbins *et al.* (M1) [65], Leardini *et al.* (M2) [67], Sawacha *et al.* (M3) [28], and Saraswat *et al.* (M4) [68], since the fused marker-set described in Chapter 5 (§5.3) already included all the anatomical landmarks that can be easily palpated on the foot. This choice allowed for a comparison of the outcomes of the new model (M5) with those of the models M1, M2, M3, and M4. Moreover, the chosen marker-set allowed a perfect integration with the whole body models conventionally used in gait analysis, such as the Davis' model [56], or the Plug-in-Gait (Vicon Motion System Ltd – Oxford).

### 6.2.1 Anatomical landmarks

Figure 6.1 and Table 6.1 show the modelled segments, the bones, and the relevant anatomical landmarks to be palpated to define all the needed coordinate systems. Table 6.2 highlights the differences in the anatomical landmarks between M5 and the previous models.

**Table 6.1** – Segments, and relevant bones and anatomical landmarks (AL) to be palpated. Static only markers are written in italic.

| Segment | Bones | AL | Description |
|---|---|---|---|
| Tibia | Tibia, Fibula | ANK | Distal apex of the lateral malleolus |
| | | HFB | Most lateral aspect of the head of fibula |
| | | TUB | Most anterior prominence of the tibial tuberosity |
| | | *MMA* | *Distal apex of the medial malleolus* |
| Hindfoot | Calcaneus, Talus | CA2 | Proximal end of the calcaneus midline on the sagittal plane (i.e. Achilles tendon attachment) |
| | | PT | Peroneal tubercle: the first bone prominence below the lateral malleolus |
| | | LCA | Laterally on the calcaneus, avoiding the heel bulge pad, with no critical alignments required |
| | | ST | Sustentaculum tali: 2 cm below the distal border of the medial malleolus |
| Midfoot | Navicular, Cuboid, Cuneiforms | TN | Navicular: 2$^{nd}$ prominence on the line between proximal epiphysis of the 1$^{st}$ metatarsal and the lower ridge of the calcaneus (on the interior side of the extensor longus of the hallux) |
| | | C | Cuboid: first recognisable bone prominence on the cuboid, from the 5$^{th}$ metatarsal bone following the direction of the axis of the tibia |
| | | P5M | Base of the 5$^{th}$ metatarsal: dorso-medial aspect |
| | | SMB | Dorso-medial aspect of the 2$^{nd}$ metatarso-cuneiform joint |
| Forefoot | Metatarsals | P1M | Dorso medial aspect of fthe 1$^{st}$ metatarso-cuneiform joint (avoiding the flexor tendon) |
| | | FMH | Dorso-medial aspect of the 1$^{st}$ metatarso-phalangeal joint (avoiding the flexor tendon) |
| | | SMH | Dorso-medial aspect of the 2$^{nd}$ metatarso-phalangeal joint |
| | | *VMH* | Dorso-medial aspect of the 5$^{th}$ metatarso-phalangeal joint (avoiding the flexor tendon and the joint) |

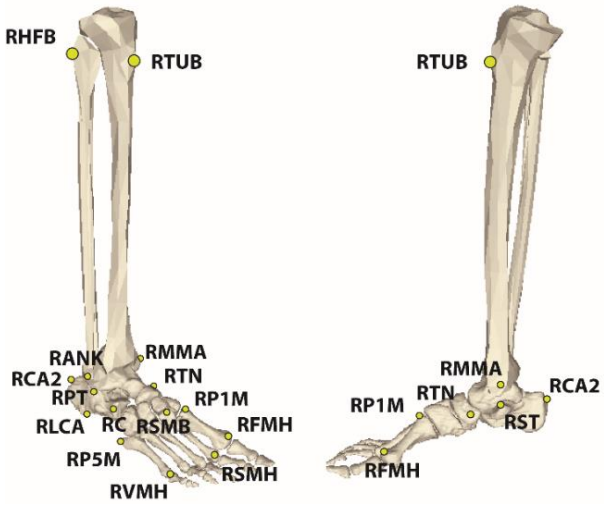


**Figure 6.1** – The anatomical landmarks to be palpated on right tibia and right foot segments.

## 6.2.2 Acquisition procedure and data processing

The following paragraphs explain the data processing flow, from the acquisition of the standing posture data to the estimate of the joint kinematics.

### *6.2.2.1 Embedded coordinate systems*

The proposed model has been designed with the goal of being easy to integrate with those routinely used for whole body gait analysis. Thigh segment, and consequently knee joint, are hence defined consistently with the adopted lower limb model. In the present Thesis, thigh segment was modelled following the description given by Vicon for the Plug-in-Gait model. Table 6.3 shows the definitions for the axes of the local **ECS** for all the other segments.

Technical **ECS** were defined considering possible deformations of the segment during walking. For example, the forefoot consists of five metatarsal bones that change their configuration like the elements of a hand-fan. Thus, the transverse axis of the anatomical **ECS** has been defined considering the bases of the first and second metatarsals as they were visually judged to be those less affected by the squeezing effect of the forefoot.

Anatomical **ECS** were defined with respect to the technical **ECS** using data from a static standing posture acquisition. The markers placed on anatomical landmarks were used so that the anatomical **ECS** axes would be aligned to the actual joint rotation axes.

The anatomical calibration matrices were then defined using the approach explained in §2.3.2.2.1 ($^{tech}\mathbf{H}_{anat}$). The technical **ECS** in the walking trials ($^{0}\mathbf{H}_{tech}(t)$) were calculated with a *least square fitting approach* (§0) accounting for redundant

**Table 6.2**– Anatomical Landmarks to be palpated associated with the models: M1 [65], M2 [67], M3 [28], and M4 [68] are highlighted in grey, whereas those pertinent to M5 model are not.

| Label | Description | M1 | M2 | M3 | M4 | M5 |
|---|---|---|---|---|---|---|
| L/R ASI | Anterior superior iliac spine | x | x | x | x | x |
| L/R PSI | Posterior superior iliac spine | x | x | x | x | x |
| RTHI | Lower lateral 1/3 surface of the thigh and in the plane of hip and knee joint centres, and knee flexion/extension axis | x | x | x | x | x |
| RKNE | Most prominent aspect of the lateral femoral condyle | x | x | x | x | x |
| RHFB | Most lateral aspect of the head of fibula | x | x | x | | x |
| RTUB | Most anterior prominence of the tibial tuberosity | x | x | x | x | x |
| RTIB | Wand marker, distal lateral tibia | | | | x | |
| RSHN | Anywhere along the anterior crest of the tibia | x | | | x | |
| RANK | Distal apex of the lateral malleolus | x | x | x | x | x |
| RMMA | Distal apex of the medial malleolus | x[19] | x[20] | x | x[20] | x[20] |
| RCA1 | Distal end of the midline in the sagittal plane | x | | | x | |
| RCA2 | Proximal end of the midline in the sagittal plane (i.e. Achilles' tendon attachment) | x[20] | x | x | | x |
| RCPG | Wand marker, the base of which is placed mid-way between RCA1 and RCA2 | x | | | | |
| RSTL | At the same vertical level as the palpated landmark (maximising inter-marker distance and avoiding local muscle attachments) | x | | | x | |
| RST | 2 cm under the distal border of the medial malleolus | | x | x | | x |
| RPT | First bone prominence below the lateral malleolus | | x | x | x[20] | x |
| RLCA | At same distance from the most posterior point as RSTL (on lateral calcaneus) | x | | | x | x |
| RC | First recognisable bone prominence on the cuboid, from the 5th metatarsal base following the direction of the tibia axis | | | x | | x |
| RTN | 2nd prominence on the line between proximal epiphysis of the 1st metatarsal and the lower ridge of the calcaneus (on the interior side of the extensor longus of the hallux) | | x | x | | x |
| RP5M | Base of the 5th metatarsal: dorso-medial aspect | x | x | x | | x |
| RD5M | Head of 5th metatarsal: laterally on the foot | x | | | | |
| RVMH | Dorso-medial aspect of the 5th metatarso-phalangeal joint (avoiding the flexor tendon and the joint) | | x | x | x | x[20] |
| RTOE | Mid-point of heads of the 2nd and 3rd metatarsal | x | | | x[20] | |
| RIIT | Proximal epiphysis of second toe phalanx (1 cm distal from the joint interstice of the 2nd ray) | | | x | | |
| RSMH | Dorso-medial aspect of the 2nd metatarso-phalangeal joint | | x | | | x |
| RT23 | Mid-point of bases of the 2nd and 3rd metatarsal | | | | x[20] | |
| RSMB | Dorso-medial aspect of the 2nd metatarso-cuneiform joint | | x | | | x |
| RFMH | Dorso-medial aspect of the 1st metatarso-phalangeal joint (avoiding the flexor tendon) | | x | x | x | x |
| RD1M | Head of 1st metatarsal: medially on the foot | x[20] | | | x[20] | |
| RP1M | Dorso medial aspect of the 1st metatarso-cuneiform joint (avoiding the flexor tendon) | x | x | | x | x |
| R1BM | Base of 1st metatarsal: medial aspect | | | | x[20] | |
| RHLX | Proximal phalanx of the hallux (on the medial side, mid-way between superior and inferior surface) | x | | | | |
| RTR X-Y-Z | Toe triad placed on the nail hallux | | | | x | |
| | ***Total number of markers*** | ***24*** | ***20*** | ***19*** | ***25*** | ***22*** |
| | *Of whom are static-markers* | *3* | *1* | *0* | *6* | *2* |

[19] Marker to be used for the static trials only.

measurements where available (e.g., LCA for the hindfoot, and P5M for the mid-foot). Eventually, the anatomical calibration matrix ( ${}^{tech}\mathbf{H}_{anat}$ ) allowed defining the pose of the anatomical **ECS** with respect to the **GCS** as in (Eq. 6.1). Figure 6.2 summarises the entire procedure. When technical and anatomical **ECS** are coincident, the ${}^{tech}\mathbf{H}_{anat}$ is the identity matrix.

$$ {}^{0}\mathbf{H}_{anat}(t) = {}^{0}\mathbf{H}_{tech}(t)\,{}^{tech}\mathbf{H}_{anat} \qquad \text{(Eq. 6.1)} $$

**Table 6.3** – Definition of the local embedded coordinate systems (ECS) for each segment for the right lower limb.

| Segment | ECS | | Definition |
|---|---|---|---|
| Tibia | Technical | $\mathbf{O}$ | Coincides with HFB |
| | | $\mathbf{i}$ | Parallel to the line from HFB to ANK |
| | | $\mathbf{j}$ | Orthonormal to the plane defined by $\mathbf{i}$ and TUB |
| | | $\mathbf{k}$ | $\mathbf{i}\times\mathbf{j}$ |
| | Anatomical | $\mathbf{O}$ | Mid-point between MMA and ANK |
| | | $\mathbf{k}$ | Pointing from left to right and connecting MMA and ANK |
| | | $\mathbf{i}$ | Pointing forward and orthonormal to the plane defined by $\mathbf{k}$ and HFB |
| | | $\mathbf{j}$ | $\mathbf{k}\times\mathbf{i}$ |
| Hindfoot | Anatomical | $\mathbf{O}$ | Coincides with CA2 |
| | | $\mathbf{k}$ | Pointing from left to right and connecting PT and ST |
| | | $\mathbf{j}$ | Pointing upward, orthonormal to the plane defined by $\mathbf{k}$ and $\mathbf{O}$ |
| | | $\mathbf{i}$ | $\mathbf{j}\times\mathbf{k}$ |
| Mid-foot | Anatomical | $\mathbf{O}$ | Mid-point between TN and C |
| | | $\mathbf{k}$ | Pointing from left to right and connecting TN and C |
| | | $\mathbf{j}$ | Pointing upward, orthonormal to the plane defined by $\mathbf{k}$ and SMB |
| | | $\mathbf{i}$ | $\mathbf{j}\times\mathbf{k}$ |
| Forefoot | Technical | $\mathbf{O}$ | Coincides with FMH |
| | | $\mathbf{k}$ | Pointing from left to right, connecting FMH and VMH |
| | | $\mathbf{i}$ | Pointing forward, orthogonal to the plane defined by $\mathbf{k}$ and P5M |
| | | $\mathbf{j}$ | $\mathbf{k}\times\mathbf{i}$ |
| | Anatomical | $\mathbf{O}$ | Coincides with P1M |
| | | $\mathbf{k}$ | Pointing from left to right, connecting P1M and SMB |
| | | $\mathbf{i}$ | Pointing forward, orthogonal to the plane defined by $\mathbf{k}$ of the anatomical **ECS,** and $\mathbf{j}$ of the technical **ECS** |
| | | $\mathbf{j}$ | $\mathbf{k}\times\mathbf{i}$ |

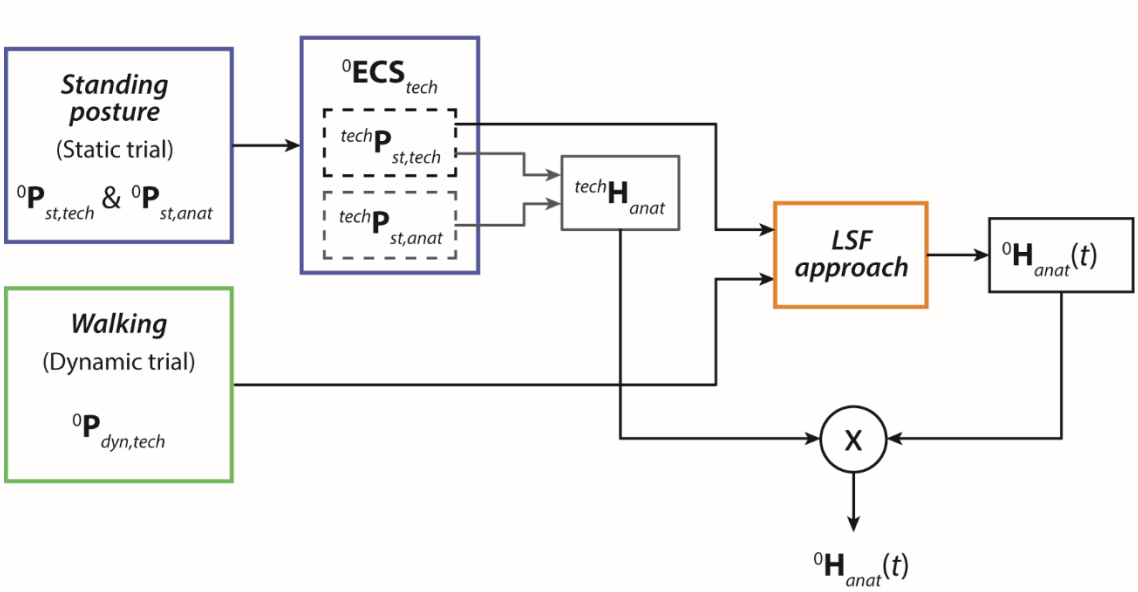


**Figure 6.2** – The flow of data collection and processing from the acquisition of the standing posture to the estimation of the joint kinematics. The **P** indicates the coordinates of the points: a left superscript indicates whether they are measured in the **GCS** (0), or defined on the technical **ECS** (*tech*); the right subscripts indicate whether they are collected in static (*st*) and dynamic (*dyn*) conditions, and are associated with the technical or anatomical **ECS** (*anat*).

### *6.2.2.2 Joint coordinate systems*

Joint kinematics were estimated according to the International Society of Biomechanics (ISB) recommendations [58]. The implemented model allows for estimating the kinematics of: the knee joint, the hindfoot-tibia (HF-Tib) joint, the midfoot-hindfoot (MF-HF) joint, and the forefoot-hindfoot (FF-HF). The combination of the movements of HF-Tib and MF-HF joints model the foot rotations allowed by the tibio-talar and the subtalar joints. FF-HF, instead, attempted to model a virtual joint between these two non-consecutive segments that, however, relatively rotate during walking. Differently from what proposed for M2 [67] and M3 [28], the FF-MF joint was not modelled also considering that the tarsometatarsal joint actually permit only limited sliding between tarsal and metatarsal bones (§2.2.2.4). Thus, any result for this kinematic should most likely be considered as noise. Finally, the metatarsophalangeal joint was not modelled as the five groups of phalanges clearly could not be considered as a unique segment to be tracked using a cluster of markers. The modelling of the hallux as representative of the movement of all the phalanges could have been attempted. However, considering the results presented in Chapter 5, in which the hallux kinematics resulted unreliable, it seemed reasonable to not consider this segment due to the lack

of room for more than one marker directly placed on the subject hallux. Table 6.4 reports the definitions of the **JCS** axes for each modelled joint.

**Table 6.4** – Definition of the joint coordinate systems (**JCS**) for each considered joint.

| Joint | JCS | Definition |
|---|---|---|
| Knee | $\mathbf{e}_1$ | Flexion/extension axis, parallel to the transverse axis of the thigh |
| | $\mathbf{e}_2$ | Abduction/adduction rotation axis |
| | $\mathbf{e}_3$ | Internal/external axis, parallel to $\mathbf{j}$ of the tibia |
| HF-Tib | $\mathbf{e}_1$ | Plantar/dorsiflexion axis, parallel to $\mathbf{k}$ of tibia |
| | $\mathbf{e}_2$ | Internal/external rotation axis |
| | $\mathbf{e}_3$ | Inversion/eversion axis, parallel to $\mathbf{i}$ of the hindfoot |
| MF-HF | $\mathbf{e}_1$ | Plantar/dorsiflexion axis, parallel to $\mathbf{k}$ of hindfoot |
| | $\mathbf{e}_2$ | Internal/external rotation axis |
| | $\mathbf{e}_3$ | Inversion/eversion axis, parallel to $\mathbf{i}$ of the midfoot |
| FF-HF | $\mathbf{e}_1$ | Plantar/dorsiflexion axis, parallel to $\mathbf{k}$ of hindfoot |
| | $\mathbf{e}_2$ | Internal/external rotation axis |
| | $\mathbf{e}_3$ | Inversion/eversion axis, parallel to $\mathbf{i}$ of the forefoot |

## 6.3 Methods

Participants and data collection procedures have already been described in the sections §5.2, §5.3, §5.3.1, and in the Figure 5.2. Relevant joint kinematics were calculated according to the definitions in §6.2.2.

Consistently with the ISB recommendations, the joint kinematics were calculated as projected onto the three anatomical planes (Appendix B) [58,207]. However, out-of-sagittal kinematics have been reported to be generally non repeatable nor reproducible [28,57,65,67,68,112,125,175]. Thus, only sagittal kinematics were considered in the further analyses.

### 6.3.1 Treadmill-overground walking comparison

As per the analysis presented in §5.3.2.1, data from four subjects among those recruited were discarded for poor marker visibility in the overground trials. For the remaining subjects, data were analysed to assess the ability of the model to discriminate between treadmill and overground walking. Sagittal joint kinematics were tested using the 1D paired *t*-test ($\alpha = 0.05$) [205], based on the Statistical Parametric Mapping (SPM) theory [206], without the need of reducing the test on summary metrics. The analysis was performed using the SPM1D open-source package for MATLAB (spm1d.org), which

generated map of *t*-values (SPM{t}), *t** limit, and areas where differences were found with the associated *p*-values.

### 6.3.2 Within- and between-subject repeatability analyses

Since no *a-priori* hypothesis could be formulated on the joint kinematics patterns, and following the conclusion inferred from the analysis on the similarity indices (Chapter 3), the within- and between-subject repeatability were assessed both for overground and treadmill walking using the LFM coefficients [129] and the MAV [140]: (Eq. 3.5), (Eq. 3.6) and (Eq. 3.7), and (Eq. 3.2), respectively. For the within-subject analysis, the *i*-th kinematic curve associated with each stride retrieved from each *j*-th repetition was compared to the same kinematic variable averaged among the ten strides collected in the two repetitions for the same subject. Instead, the between-subject comparison was performed between the *i*-th kinematic curve associated with each stride retrieved from each *j*-th repetition and each subject, and the same kinematic variable averaged among strides, repetitions and subjects.

As described in §3.2.2 and [129], when comparing *n* curves with their averaged pattern, $a_1$ and $a_0$ tend to their ideal values (i.e., 1 and 0, respectively). Coherently with the conclusion of Chapter 3, LFM coefficients and MAV were complemented with MAD and MD [87] on the sagittal joint angles at initial contact (IC) and toe-off (TO) considered as summary metrics [137]. MAD is a variability index that is robust to the outliers, whereas MD measures the maximum differences obtained among the joint kinematics.

### 6.3.3 Between-operator reproducibility analysis

Between-operator reproducibility was assessed with LFM coefficients [129] and MAV [140]. LFM coefficients were calculated comparing the *i*-th kinematic variable associated with each of the five strides retained from each *j*-th repetition for the *k*-th operator, and the same kinematic variable averaged among the five strides, the three repetitions and the three operators for each subject. MAD and MD were also calculated on the sagittal kinematics at Initial Contact (IC) and Toe-Off (TO).

### 6.3.4 Comparison with the existing models

Results obtained from the above described analyses were discussed also performing a comparison with those obtained for the same analyses of the models M1, M2, M3, and M4 described in §5.3.2.2 and §5.3.2.3.

## 6.4 Results

### 6.4.1 Model outputs

Figure 6.3 shows the normative bands of the joint kinematics obtained both for overground and treadmill walking. Typical range of motion (ROM) for the modelled joints are shown in Table 6.5 and Table 6.7 for treadmill and overground walking, respectively. Especially for the knee joint, kinematics calculated for overground walking showed the highest range of motion.

### 6.4.2 Treadmill-overground walking comparison

In addition to the normative bands of the calculated kinematics, Figure 6.3 shows the mapping of the *t*-values obtained from the 1D paired *t*-test performed over the two walking conditions. Statistical differences were obtained for all the joint kinematics. Differences were found for the knee both during stance and swing phases: from 10% to 20% of the gait cycle ($p = 0.04$), from 55% to 80% ($p < 0.001$), and from 95% to 100% ($p = 0.04$). For the HF-Tib, joint differences were obtained during the terminal stance and swing phases: from 50% to 60% ($p < 0.001$), and from 75% to 80% ($p = 0.008$). For both MF-HF and FF-HF joints, differences were found in the first 10% of the gait cycle ($p = 0.006$ and $p = 0.012$, respectively), and nearly significant differences were obtained for the portion between 80% and 90% of the gait cycle for MF-HF ($p = 0.05$).

### 6.4.3 Within- and between-subject repeatability analyses

Table 6.5 and Table 6.6 show the results of the within- and between-subject repeatability analyses for treadmill walking. The averaged coefficients $a_1$ and $a_0$ reached their ideal values, and the highest value of *SD*- $a_1$ (0.17) was obtained for MF-HF which was the kinematics with the smallest ROM (averaged ROM equal to 11°). Averaged $R^2$ were always higher than 0.91, obtained for HF-Tib. Within-subject MAV were never higher than 3°, except for the knee joint (7°) which was the joint with higher ROM. Similar trend was confirmed by MD at IC and TO, whereas MAD were comparable among the kinematics.

The between-subject analysis showed less repeatable results (Table 6.6). Indeed, the averaged $R^2$ was never higher than 0.91 (obtained for the knee), but never lower than 0.69 (obtained for HF-Tib). The averaged scaling coefficients ( $a_1$ ) tended to its ideal

value, with the *SD-* $a_1$ never higher than 0.35 (MF-HF). The highest MAV values were obtained for the knee and the FF-HF joints (27° and 12°, respectively). Same happened for MAD and MD at both IC and TO.

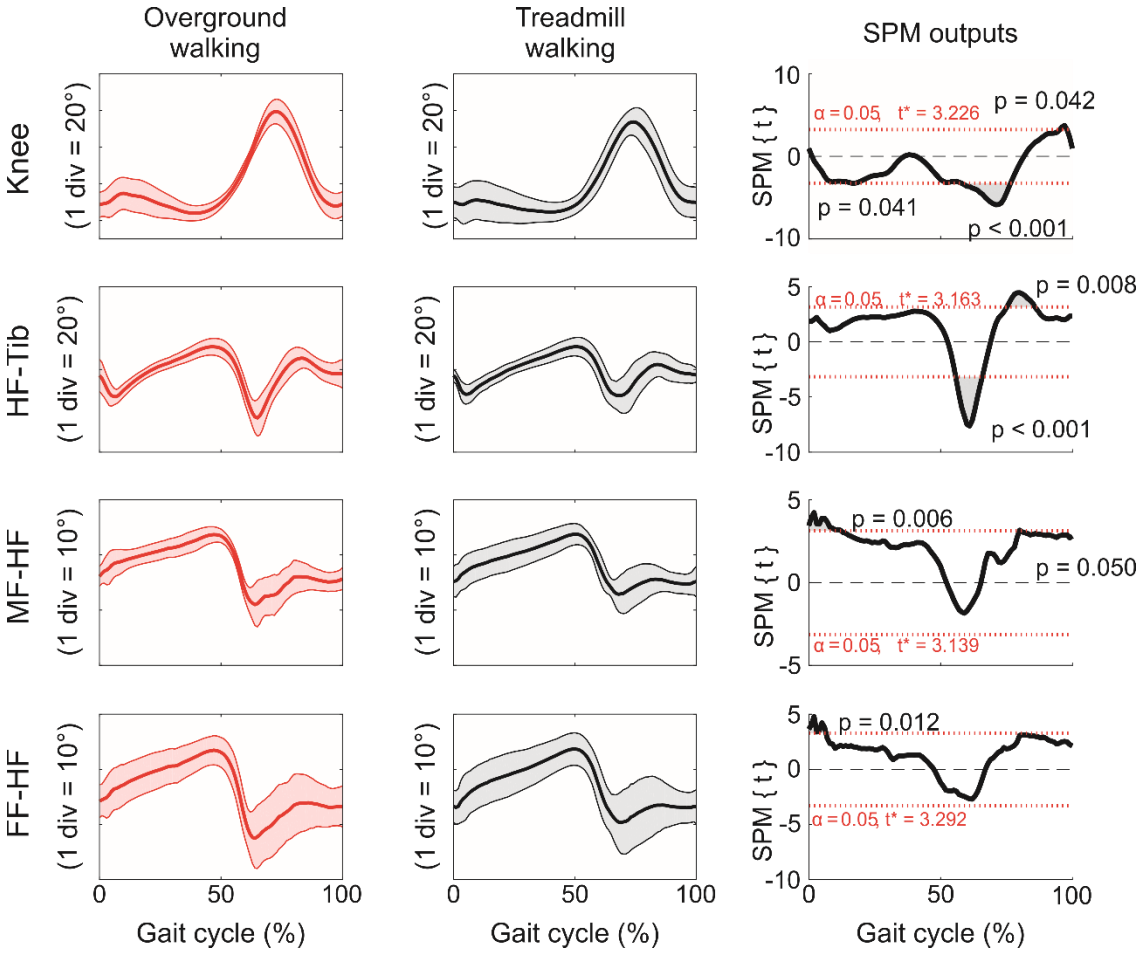


**Figure 6.3** – Sagittal kinematics obtained according to the definitions given by the new model for overground walking (left hand side), for treadmill walking (midline), and the relative statistical parametric mapping of the t-value from the 1D paired t-test for: Knee, shank and hindfoot (HF-Tib), hindfoot and midfoot (MF-HF), and metatarsus and hindfoot (FF-HF).

Table 6.7 and Table 6.8 show the results of the within- and between-subject repeatability analyses for the overground walking. The results for the within-subject analysis (Table 6.7) showed high values of $R^2$: between 0.92 ± 0.05 for the HF-Tib joint, and 0.98 ± 0.02 for the knee. The scaling factor reached its ideal value and the *SD-* $a_1$ was never higher than 0.10 (MF-HF). MAV, MAD and MD were comparable with those obtained for the treadmill walking. Table 6.8, as happened for treadmill walking, shows that comparing the kinematics among subjects yielded less repeatable results than the within-subject analysis. Averaged $R^2$ ranged from 0.82 (HF-Tib) to 0.94 (knee), the averaged scaling factor tended to 1 and its standard deviation never exceeded 0.26 (MF-HF). Values obtained for $a_1$, MAV, MAD, and MD were coherent with those obtained

for the treadmill walking, with the only exception of HF-Tib showing MD equal to 12° at IC, and 7° at TO.

**Table 6.5** – Within-subject repeatability analysis for treadmill walking: Range of Motion (ROM), Linear Fit Method (LFM) coefficients, Mean Absolute Variability (MAV), Median Absolute Deviation (MAD) and Maximum Difference (MD) at Initial Contact (IC) and Toe-Off (TO). Segment names are abbreviated as follows: tibia (Tib), hindfoot (HF), midfoot (MF), metatarsus and forefoot (FF).

| Joints | ROM (°) | LFM coefficients | | | MAV (°) | MAD (°) | | MD (°) | |
|---|---|---|---|---|---|---|---|---|---|
| | | $a_1$ | $a_0$ (°) | $R^2$ | | IC | TO | IC | TO |
| *Knee* | 49 ± 13 | 1.00 ± 0.08 | 0 ± 2 | 0.97 ± 0.04 | 7 ± 5 | 1 ± 0 | 1 ± 0 | 7 ± 4 | 10 ± 4 |
| *HF-Tib* | 15 ± 5 | 1.00 ± 0.11 | 0 ± 1 | 0.91 ± 0.09 | 3 ± 1 | 1 ± 0 | 1 ± 0 | 3 ± 1 | 6 ± 3 |
| *MF-HF* | 11 ± 4 | 1.00 ± 0.17 | 0 ± 0 | 0.93 ± 0.07 | 2 ± 1 | 0 ± 0 | 0 ± 0 | 2 ± 1 | 4 ± 1 |
| *FF-HF* | 15 ± 5 | 1.00 ± 0.14 | 0 ± 1 | 0.95 ± 0.05 | 2 ± 1 | 1 ± 0 | 1 ± 0 | 4 ± 1 | 5 ± 2 |

**Table 6.6** – Between-subject repeatability analysis for treadmill walking: Range of Motion (ROM), Linear Fit Method (LFM) coefficients, Mean Absolute Variability (MAV), Median Absolute Deviation (MAD) and Maximum Difference (MD) at Initial Contact (IC) and Toe-Off (TO). Segment names are abbreviated as follows: tibia (Tib), hindfoot (HF), midfoot (MF), metatarsus and forefoot (FF).

| Joints | ROM (°) | LFM coefficients | | | MAV (°) | MAD (°) | | MD (°) | |
|---|---|---|---|---|---|---|---|---|---|
| | | $a_1$ | $a_0$ (°) | $R^2$ | | IC | TO | IC | TO |
| *Knee* | 49 ± 13 | 1.00 ± 0.20 | 0 ± 7 | 0.91 ± 0.07 | 27 | 4 | 3 | 24 | 18 |
| *HF-Tib* | 15 ± 5 | 0.99 ± 0.27 | 0 ± 1 | 0.69 ± 0.18 | 8 | 1 | 1 | 7 | 12 |
| *MF-HF* | 11 ± 4 | 1.01 ± 0.35 | 0 ± 1 | 0.82 ± 0.12 | 7 | 1 | 2 | 4 | 12 |
| *FF-HF* | 15 ± 5 | 1.02 ± 0.33 | 0 ± 3 | 0.83 ± 0.12 | 12 | 2 | 2 | 9 | 14 |

### 6.4.4 Between-operator reproducibility analysis

Table 6.9 shows the between-operators reproducibility for treadmill walking. Averaged $R^2$ values ranged from 0.91 for the HF-Tib to 0.98 for the knee. Both $a_1$ and $a_0$ reached their ideal values, and *SD*-$a_1$ never exceeded 0.15. The *SD*-$a_0$ values ranged between 0.12 and 0.15. MAVs were in the range 1°-3°. MAD at both IC and TO were similar and in the range 0°-2°. The lowest values for MD were obtained for the joint MF-HF (3°), whereas the other joints showed slightly higher values. The highest value was obtained for the knee ($MD_{TO}$ = 12° ± 5°).

## 6.5 Discussion

This study presented a novel model of the foot-ankle complex for gait analysis that attempted to overcome some of the limitations highlighted in the four models analysed in Chapter 5. Since the anatomical landmarks were easy to palpate, marker placement was conducted with no difficulty. The number of markers to be used for M5 is inferior to those needed for M1 and M4, both for static and dynamic trials, but one more marker is needed with respect to M2 and M3 (Table 6.2). All the markers were perfectly visible to the stereophotogrammetric system, both in static and walking trials, and extensive

procedures of gap filling were not needed. Same consideration is not valid for the medial markers in M2 and M3, which were difficult to track during walking. Altogether these considerations led to concluding that M5 implementation was easier than for the others, either for the number of markers to be placed or for the visibility of the entire marker set.

Averaged range of motion for the relevant joints for treadmill walking were equal to: 49° for the knee, 15° for HF-Tib, 11° for MF-HF, and 15° for FF-HF. As expected, slightly higher values were obtained for overground walking: 53° for the knee, 18° for HF-Tib, 14° for MF-HF, and 16° for FF-HF.

**Table 6.7 –** Within-subject repeatability analysis for overground walking: Range of Motion (ROM), Linear Fit Method (LFM) coefficients, Mean Absolute Variability (MAV), Median Absolute Deviation (MAD) and Maximum Difference (MD) at initial contact (IC) and toe-off (TO). Segment names are abbreviated as follows: tibia (Tib), hindfoot (HF), midfoot (MF), metatarsus and forefoot (FF).

| Joints | ROM (°) | LFM coefficients | | | MAV (°) | MAD (°) | | MD (°) | |
|---|---|---|---|---|---|---|---|---|---|
| | | $a_1$ | $a_0$ (°) | $R^2$ | | IC | TO | IC | TO |
| *Knee* | 53 ± 18 | 1.00 ± 0.06 | 0 ± 2 | 0.98 ± 0.02 | 8 ± 2 | 1 ± 1 | 2 ± 0 | 6 ± 4 | 8 ± 3 |
| *HF-Tib* | 18 ± 7 | 1.00 ± 0.07 | 0 ± 0 | 0.92 ± 0.05 | 4 ± 1 | 1 ± 1 | 1 ± 1 | 3 ± 2 | 6 ± 3 |
| *MF-HF* | 14 ± 6 | 1.00 ± 0.10 | 0 ± 1 | 0.93 ± 0.04 | 3 ± 0 | 1 ± 1 | 1 ± 0 | 3 ± 2 | 2 ± 1 |
| *FF-HF* | 16 ± 6 | 1.00 ± 0.07 | 0 ± 1 | 0.94 ± 0.04 | 3 ± 1 | 1 ± 0 | 1 ± 0 | 3 ± 1 | 3 ± 1 |

**Table 6.8** – Between-subject repeatability analysis for overground walking: Range of Motion (ROM), Linear Fit Method (LFM) coefficients, Mean Absolute Variability (MAV), Median Absolute Deviation (MAD) and Maximum Difference (MD) at initial contact (IC) and toe-off (TO). Segment names are abbreviated as follows: tibia (Tib), hindfoot (HF), midfoot (MF), metatarsus and forefoot (FF).

| Joints | ROM (°) | LFM coefficients | | | MAV (°) | MAD (°) | | MD (°) | |
|---|---|---|---|---|---|---|---|---|---|
| | | $a_1$ | $a_0$ (°) | $R^2$ | | IC | TO | IC | TO |
| *Knee* | 53 ± 18 | 1.00 ± 0.11 | 0 ± 6 | 0.94 ± 0.04 | 17 | 3 | 1 | 19 | 11 |
| *HF-Tib* | 18 ± 7 | 1.00 ± 0.23 | 0 ± 1 | 0.82 ± 0.10 | 7 | 1 | 1 | 12 | 7 |
| *MF-HF* | 14 ± 6 | 1.01 ± 0.26 | 0 ± 1 | 0.87 ± 0.07 | 6 | 2 | 2 | 5 | 11 |
| *FF-HF* | 16 ± 6 | 1.00 ± 0.23 | 0 ± 3 | 0.88 ± 0.07 | 10 | 3 | 3 | 9 | 15 |

**Table 6.9** – Between-operator reproducibility analysis for treadmill walking: Range of Motion (ROM), Linear Fit Method (LFM) coefficients, Mean Absolute Variability (MAV), Median Absolute Deviation (MAD) and Maximum Difference (MD) at Initial Contact (IC) and Toe-Off (TO). Segment names are abbreviated as follows: tibia (Tib), hindfoot (HF), midfoot (MF), metatarsus and forefoot (FF).

| Joints | ROM (°) | LFM coefficients | | | MAV (°) | MAD (°) | | MD (°) | |
|---|---|---|---|---|---|---|---|---|---|
| | | $a_1$ | $a_0$ (°) | $R^2$ | | IC | TO | IC | TO |
| *Knee* | 52 ± 7 | 1.00 ± 0.12 | 0 ± 4 | 0.98 ± 0.03 | 3 ± 1 | 1 ± 0 | 2 ± 1 | 5 ± 1 | 12 ± 5 |
| *HF-Tib* | 17 ± 3 | 1.00 ± 0.14 | 0 ± 2 | 0.91 ± 0.09 | 2 ± 0 | 1 ± 1 | 1 ± 0 | 6 ± 3 | 9 ± 3 |
| *MF-HF* | 10 ± 3 | 1.00 ± 0.15 | 0 ± 1 | 0.92 ± 0.10 | 1 ± 0 | 0 ± 0 | 0 ± 0 | 3 ± 1 | 3 ± 1 |
| *FF-HF* | 15 ± 4 | 1.00 ± 0.15 | 0 ± 3 | 0.93 ± 0.09 | 3 ± 2 | 0 ± 0 | 1 ± 0 | 6 ± 3 | 7 ± 2 |

Joint kinematics were analysed to check whether the model was able to distinguish between treadmill and overground walking, and to test their repeatability and reproducibility. Since out-of-sagittal kinematics have been reported to be generally the least reliable [28,57,65,67,68,112,125,175], only sagittal kinematics were considered and analysed in the present study. The joint kinematics were estimated using

the same data set and marker set used in Chapter 5, and thus the analyses performed on the results of the new model can be directly compared to those presented in Chapter 5.

As per the four existing models (M1, M2, M3 and M4), the treadmill-overground comparison was performed testing the joint kinematics considering not only the point-by-point differences, but their time history correlation. The 1D paired *t*-test found significant differences in all the kinematics (Figure 6.3), which is most likely to be ascribed to the two inherently different walking speeds. Differently from what happened among M1, M2, M3 and M4, the new proposed model yielded significant differences in different portion of the gait cycle, but it was still sensitive enough to discriminate between treadmill and overground conditions, which was the aim of this part of the study.

From the within- and between-subject analyses and for treadmill walking, a good repeatability emerged for the kinematics estimated according to the new model. Concerning the LFM coefficients, comparing the performances obtained among the five considered models, the knee joint kinematics showed equivalent results both for the within- and between-subject analyses. The within-subject results of M5 for HF-Tib were equivalent to those obtained for the other models, whereas with respect to M1 and M4 slightly lower values of between-subject correlation were reported. The M5's MF-HF kinematics, not defined in M1 and M4, yielded results equivalent to M2 (e.g., $R^2$ = 0.92 ± 0.08) and better than M3 (e.g., $R^2$ = 0.77 ± 0.20), with the same trend observed for the $a_1$ coefficients. This consideration is reinforced by the between-subject results. Indeed, $R^2$ was equal to 0.83 ± 0.12 for the new model, whereas it was 0.79 ± 0.15 and 0.51 ± 0.28 for M2 and M3, respectively. It is worth considering that the HF-Tib and MF-HF joints modelled the tibio-talar and subtalar joints interaction during walking. The MF-HF kinematics in M3 was found to display a ROM equal to 5°, and it was heavily affected by noise (low values of $R^2$ and high *SD*-$a_1$). Unfortunately, no stereophotogrammetry based on radiographs nor fluoroscopy were performed, and hence actual ROM could not be measured. Altogether, the above considerations allowed affirming that the proposed modelling of the MF-HF joint represents an improvement of the state of the art. The FF-HF, which was not considered in M4, modelled the virtual joint that allows rotations between metatarsals and hindfoot bones, and showed slightly better performances both for within- and between-subject

analyses: $R^2$ equal to 0.95 ± 0.05 and 0.83 ± 0.12, respectively; whereas it never exceeded 0.93 ± 0.08 for the within-, and 0.81 ± 0.13 for the between-subject analysis. The scaling factors $a_1$ were comparable among models for the within- and between-subject analyses (except for a few highlighted cases). MAVs, MADs and MDs values obtained from the all the joint kinematics estimated using M5 were overall comparable to those obtained with the other models. The only exception was found for the knee in M5 with respect to the other four models, which showed slightly higher absolute differences, and for MF-HF with respect to M3. However, it was previously highlighted that MF-HF for M3 was the least reliable kinematic, which displayed a ROM of 5°. Instead, for M5, the ROM of MF-HF was 11°, which could potentially lead to higher absolute differences among curves.

Same conclusions could be inferred for the kinematics obtained for the overground walking (Table 6.7 and Table 6.8). With the only exception for the FF-HF joint, which displayed almost equivalent values of correlation with those obtained for M1, M2 and M4, but less variations in the scaling factors. This led to concluding that less variability in the sample by sample amplitude variations than those obtained with the other models affected the FF-HF joint kinematics (§3.4), which hence resulted in more repeatable patterns.

Coherently with what obtained for M1, M2, M3 and M4, LFM coefficients obtained for the between-operator reproducibility produced similar results of those obtained for the within- and between-subject analyses. Measurement of absolute differences (MAVs, MADs and MDs) were slightly higher for the within- and between-subject analyses, but this is likely due to the different considered sample sizes. Thus, as per M1, M2, M3 and M4, the equivalence of the two effects suggests that the variability of the foot motion is higher than any other source of variability.

## 6.6 Conclusion

A new model of the foot-ankle complex was proposed, and repeatability and reproducibility of the relevant sagittal kinematics were concurrently tested with the four models analysed in Chapter 5. The implementation of this novel model resulted to be easier than those previously analysed, both for the number of markers to be placed and their visibility. However, further investigations to quantify the reproducibility of the

landmark's palpation are recommended. The ability to highlight changes imposed by treadmill and overground walking was also tested and confirmed with a 1D statistical analysis. The new proposed model improved the repeatability and reproducibility of the joint kinematics gathered from healthy subjects with respect to those obtained with the existing models. Although the presented model is promising, it is still questionable to assume foot kinematics to be repeatable among subjects. Thus, before testing the model on patients affected by specific pathologies, further improvements of the model are needed and should be pursued before testing also out-of-sagittal kinematics.

# Chapter 7

# Conclusions and future work

This Thesis aimed at establishing a standard for the modelling of the foot-ankle complex kinematics in gait analysis. An initial critical review of the literature and of the background concepts represented the basis to pursue and achieve the following objectives:

- To choose the most suitable indices to assess gait data repeatability and reproducibility;
- To evaluate the instrumental error associated with the calibration procedure of the stereophotogrammetric systems that affects the measurements of markers coordinates, and hence the estimates of the joint kinematics;
- To concurrently compare the repeatability and reproducibility of the most adopted models of the foot;
- To design and develop a novel model of the foot-ankle complex kinematics for gait analysis to overcome limitations of the ones previously proposed.

The study on the indices (Chapter 3) led to concluding that the Linear Fit Method coefficients, complemented with absolute measurements of differences among curves (Mean Absolute Variability or Root Mean Square Error), are the most suitable to assess gait data repeatability and reproducibility. However, when the LFM correlation coefficient is far from its ideal value, the absolute differences are worth to be evaluated on summary metrics such as, kinematics values at specific instant of the gait cycle. Beside having provided a clear understanding of the indices used to assess gait data repeatability and reproducibility, the results of this part of the study also represent a step forward in the state of the art since they can represent a valuable baseline of the indices for a population of healthy young adults.

The methodology proposed in Chapter 4 to evaluate the effect of the calibration of stereophotogrammetric systems on the estimate of the joint is easy to implement, and could be adopted for future preliminary tests on measuring set-up chosen for specific applications. As an example, camera configuration could be changed according to the need of specific applications. The presented methodology would allow quantifying the effect of the calibration procedure on joint kinematics, and for a specific system configuration. In general, inaccuracies associated with measured distances, angles, and estimated joint kinematics were found to be higher in dynamic than in static conditions, but negligible in both cases if compared to errors inherent to the use of a marker-based approach (e.g. the soft tissue artefacts, and between-test variability), which lead to higher imprecision in estimating joint kinematics.

The concurrent analysis of the four most adopted models to assess the foot-ankle complex kinematics has leveraged on the first two achievements. Indeed, the analysis was performed considering that instrumental error was negligible, and the repeatability and the reproducibility associated with the kinematics were assessed using and interpreting those indices previously studied. This part of the project clearly highlighted that it is questionable to assume the foot kinematics to be repeatable when assessed with tested models and, hence, to rely on normative bands for the clinical assessment of patients. In particular, kinematics presenting a range of motion lower than 10°, such as the relative rotations between the forefoot and the mid-foot for the model proposed in [67], and between mid-foot and hindfoot for the model proposed in [28], should be considered meaningless.

Finally, to overcome the limitations highlighted in the analysed models, and coherently with what observed from the previous analysis, a new model was proposed to assess the foot kinematics. Joints with range of motion smaller than 10°, or joints that should not allow any anatomically rotation, were not considered. Although still presenting some limitations, the proposed model displayed higher repeatability and reproducibility for all the joint kinematics, especially for those describing the movement between mid-foot and hindfoot, which was the least repeatable when evaluated through the existing models. As soon as the model is published, the MATLAB code to define the embedded coordinate systems, and calculating the joint kinematics will be shared via open source cloud platforms, such as *Figshare* (figshare.com).

Besides the novel model is promising, further improvements are worth pursuing to obtain more reliable results. Three possible steps could be implemented: a) the model could be re-designed considering different definitions for the embedded coordinate systems or the anatomical landmarks, attempting at defining more reliable embedded coordinate systems and, subsequently, more reliable foot kinematics; b) a new algorithm based on a *weighted* least square approach to estimate the joint kinematics from walking trials could be developed; or c) a combination of the steps a) and b). In particular, solution b) could be implemented considering an algorithm that solves the least square optimization problem, accounting for a 'correction' of the least reliable markers due to high soft tissue artefact. To address these markers as not reliable, though, invasive methods would be needed, but recent studies, aimed at quantifying the effect of the STA, provided shared results [208,209], which might be considered as inputs for preliminary tests of such an algorithm. This novel approach would be relevant not only to improve the quality of foot kinematics estimate, but could be applied to every other joint in the human kinematic chain, paving the way to more repeatable and reproducible results.

After having developed a reliable model of the foot, it is appropriate to test whether this model is suitable for the totality of the clinical applications, for a part of them, or any changes needed for applications linked to specific pathologies, for example allowing the detection of foot deformities.

This study provided the guidelines to perform solid repeatability and reproducibility studies of gait variables, and more specifically of the foot-ankle kinematics, which is critical to provide information on the possible development of foot impairments and on the severity of movement dysfunctions. Having tested the most adopted models of the foot, and having found weak repeatability and reproducibility for some of the relevant outcomes, a novel model was designed and analysed. This model paves the way to a more reliable modelling of the foot. More specifically, it allows for improving the existing techniques to estimate reliable joint kinematics gathered from a population of healthy subjects. This achievement allows not confusing imprecisions due to the modelling with the features distinctive of a specific pathology. Even though some limitations have been highlighted, new potential methods to defeat them were suggested for future developments.

# Appendix A

# Vocabulary of Metrology

The Joint Committee for Guides in Metrology (JCGM) was formed in 1997, fusing the international organizations that worked to establish standards in different scientific fields, such as: chemistry, physics and engineering. Two working groups have produced the Guide to the expression of uncertainty in measurement (GUM) and the International vocabulary of basic and general terms in metrology (VIM), respectively. The metrology is intended as the science of measuring and its application [21,22]. The JCGM is continuously updating this two fundamental documents. In this Appendix, it has been reported only the relevant definitions for the present Thesis. A close reading of GUM and VIM is recommended for an exhaustive and deepen knowledge of the principles of metrology.



**Table A.1** – Terms and definitions extracted from the International vocabulary of basic and general terms in metrology [21,22].

| Term | Article | Definition |
|---|---|---|
| Quantity | VIM 1.1 | property of a phenomenon, body, or substance, where the property has a magnitude that can be expressed as a number and a reference |
| Quantity value | VIM 1.19 | number and reference together expressing magnitude of a quantity |

| Term | Article | Definition |
|---|---|---|
| Measurand | VIM 2.3 | quantity to be measured |
| Measurement | VIM 2.1 | process of experimentally obtaining one or more quantity values that can reasonably be attributed to a quantity |
| Measurement result | VIM 2.9 | set of quantity values being attributed to a measurand together with any other available relevant information |
| Measured quantity value | VIM 2.10 | quantity value representing a measurement result |
| True quantity value | VIM 2.11 | quantity value consistent with the definition of a quantity |
| Accuracy | VIM 2.13 | closeness of agreement between a measured quantity value and a true quantity value of a measurand[20] |
| Trueness | VIM 2.14 | closeness of agreement between the average of an infinite number of replicate measured quantity values and a reference quantity value[21] |
| Indication | VIM 4.1 | quantity value provided by a measuring instrument or a measuring system |
| Precision | VIM 2.15 | closeness of agreement between indications or measured quantity values obtained by replicate measurements on the same or similar objects under specified conditions[22] |
| Measurement error | VIM 2.16 | measured quantity value minus a reference quantity value[23] |

[20] The concept 'measurement accuracy' is not a quantity and is not given a numerical quantity value. A measurement is said to be more accurate when it offers a smaller measurement error.

[21] Measurement trueness is not a quantity and thus cannot be expressed numerically, but measures for closeness of agreement are given in ISO 5725. It is inversely related to systematic measurement error, but is not related to random measurement error.

[22] Measurement precision is usually expressed numerically by measures of imprecision, such as standard deviation, variance, or coefficient of variation under the specified conditions of measurement. It should not be confused 'measurement accuracy'.

[23] The concept of 'measurement error' can be used both a) when there is a single reference quantity value to refer to, which occurs if a calibration is made by means of a measurement standard with a measured quantity value having a negligible measurement uncertainty or if a conventional quantity value is given, in which case the measurement error is known, and b) if a measurand is supposed to be represented by a unique true quantity value or a set of true quantity values of negligible range, in which case the measurement error is not known.

| Term | Article | Definition |
|---|---|---|
| Repeatability condition | VIM 2.20 | condition of measurement, out of a set of conditions that includes the same measurement procedure, same operators, same measuring system, same operating conditions and same location, and replicate measurements on the same or similar objects over a short period of time |
| Repeatability | VIM 2.21 | measurement precision under a set of repeatability conditions of measurement |
| Reproducibility condition | VIM 2.24 | condition of measurement, out of a set of conditions that includes different locations, operators, measuring systems, and replicate measurements on the same or similar objects |
| Reproducibility | VIM 2.25 | measurement precision under reproducibility conditions of measurement |
| Uncertainty | VIM 2.26 | non-negative parameter characterizing the dispersion of the quantity values being attributed to a measurand, based on the information used |
| Standard uncertainty | VIM 2.30 | measurement uncertainty expressed as a standard deviation |
| Combined standard uncertainty | VIM 2.31 | standard measurement uncertainty obtained using the individual standard measurement uncertainties associated with the input quantities in a measurement model |
| Expanded uncertainty | VIM 2.35 | product of a combined standard measurement uncertainty and a factor larger than the number one |

# Appendix B

# Anatomical definitions

The anatomical planes are theoretical geometric planes, which allow virtual sectioning of the human body useful to locate joints and segments, and describe the direction of movements. According to human anatomy, three anatomical planes are defined (Figure B.1):

1. The *sagittal plane* (or lateral, or Y-Z plane) runs perpendicularly to the ground, and divides the body into left and right sections of the human body;
2. The *coronal plane* (or frontal, or X-Z plane) runs perpendicularly to the ground, and separates the anterior from the posterior section of the body;
3. The *transverse plane* (or horizontal, or X-Z plane) runs parallel to the ground, passes through the centre of the body, and divides the body in upper and lower segments.

The body segments can be addressed as *proximal* or *distal* with respect to their location relatively to the centre of the body, assumed as placed in the thorax. In particular, having considered two segments, the proximal is the segment of the two which is located closest to the thorax, whereas the distal segment is the segment most distant from the thorax (Figure B.2).

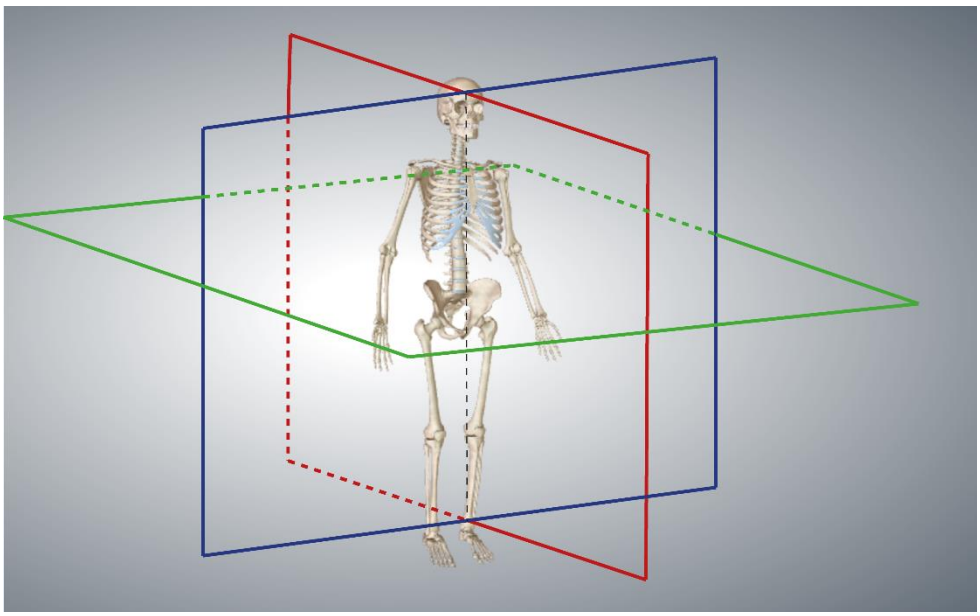

**Figure B.1** – The three anatomical planes: sagittal plane (red); frontal plane (blue); and transverse plane (green). This Figures has been retrieved from the Biodigital Human website (www.biodigital.com) and adapted.

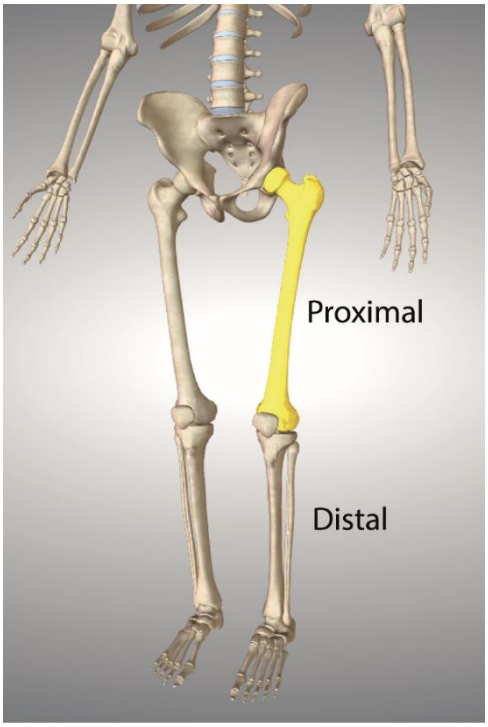


**Figure B.2** – Paradigmatic example of proximal and distal segments. This Figures has been retrieved from the Biodigital Human website (www.biodigital.com) and adapted.

Appendix C

# Ethical approvals

The ethical board of the University of Sheffield has granted the ethics approval for the studies presented in this Thesis. Each participant has read the Information Sheet and signed the Consent form prior the data collection. Both forms are appended below.

University of Sheffield

# Information sheet

You are being invited to take part in a research project. Before you decide it is important for you to understand why the research is being done and what it will involve. Please take time to read the following information carefully and discuss it with others if you wish. Ask us if there is anything that is not clear or if you would like more information. Take time to decide whether or not you wish to take part. Thank you for reading this.

**Summary**

This research will contribute to the development of innovative tools and methods for the measurement and modelling of human movement and balance.

**Aims**

The aim of the research is to analyse human movement and balance while you perform simple tasks and activities of daily living. The analysis will be performed with measuring instruments that are regularly used in biomechanical studies.

**Your involvement**

During the experiments you will be asked to perform a series of activities during which we will record your movements using a number of different instruments. Inertial sensors will be attached to you with appropriate straps or dermatological patches: one on the forehead, one on the sternum (middle of the chest), one on the pelvis, one on each arm and one on each shank (lower leg). Some reflective markers will be attached directly onto your skin with double-side adhesive tape. If necessary, we will shave the small area where we have to apply the electromyography electrodes.

The protocol consists of two phases. In the first you will be fully clothed with all the equipment and sensors attached. In the second phase you will be required to perform some or all the simple tasks and activities of daily living as described:

1. Standing trial. You will be asked to stand as still as possible for about 60 seconds.
2. Walking Trial. You will either be asked to walk on a treadmill or on a walkway at a self-selected speed. If capable you may be asked to increase your walking speed for additional trials. In some cases you may be asked to perform under both conditions i.e. on a walkway and then on a treadmill.
3. Reaching task. You will be required to retrieve something from a table or some other surface.
4. Drink/Eat. You will be required to simulate drinking a glass of water and eating food.
5. Rising from a chair. You will be asked to sit on an ordinary chair with a firm seat and backrest and to assume a relaxed posture. Starting from this position you will be required to stand up and then sit back down in the same position as you started in.
6. Ascending or descending steps: You will be asked to rise or descend either a few steps or a whole ramp of stairs.

The entire protocol will take a maximum of 2 hours to perform (1 hour in most of the cases).

To apply the reflective markers and the electromyography electrodes you have to be partially undressed. The minimum level of undress for women will be equivalent to wearing a bikini and for men equivalent to wearing swimming trunks. This part of the experiments will take place in a closed room, with screened windows. You will have access to a separate adjacent room to get changed in complete privacy. If this causes you any discomfort or embarrassment then please do not consent to take part in this study. If you do consent then we strongly encourage you to cease your participation if discomfort of embarrassment is caused or felt.

If strictly needed, the parts of your body where the electromyography electrodes have to be applied will be shaved. Those electrodes, as with the markers, will be stuck on your skin with dermatological adhesive tape, but first we will clean your skin with some pure alcohol. If you have (or may have) allergy to the adhesive tape and/or to the alcohol, please do not sign the form consenting to this study. If you start to feel any pain or irritation as a result of the alcohol or tape, please ask us to stop the protocol immediately.

At the end of the protocol we will remove all the sensors and equipment. This can cause a little pain on hairy subjects because of the adhesive tape.

**Confidentiality**

Your involvement will be kept confidential and anonymous. Data will be stored securely on the laboratory desktop and/or on the researcher's laptop. Access will be restricted to the researchers working on this project.

**Audio and video recordings**

During the experiments we might use camera or video recordings. These will be used exclusively for the purpose of this research and in the context of scientific presentations. Please do not hesitate to tell us if you feel uncomfortable with this.

**Your rights**

You are free to withdraw from the project at any point and request that your data be destroyed.

**Consent**

We would like you to state (by signing) that you understand the above, are willing to participate on a voluntary basis and give your consent for the data collected to be used in this research project and publicity about the research.

**Contact**

Should you wish to withdraw or contact us about the research project for any other reason, please contact us on the following email and/or phone number:

Dr Claudia Mazzà c.mazza@sheffield.ac.uk +44(0) 114 2226073

| Lead Researcher<br>*To be signed and dated in presence of the participant* | Date | Signature |
|---|---|---|

University of Sheffield

# Consent Form

**Title of Research Project**: Innovative methods for human movement analysis

**Name of Researcher**: Dr Claudia Mazzà

**Participant Identification Number for this project:** **Please initial box**

1. I confirm that I have read and understand the **information sheet** dated / / explaining the above research project and I have had the opportunity to ask questions about the project. ☐

2. I understand that my participation is voluntary and that I am free to withdraw at any time without giving any reason and without there being any negative consequences. In addition, should I not wish to answer any particular question or questions, I am free to decline. Finally, I understand that I can request that my data are destroyed if I withdraw ☐

   Contact details:
   Dr Claudia Mazzà, c.mazza@sheffield.ac.uk, +44(0)114 2226073.

3. I understand that my responses will be kept strictly confidential. I give permission for members of the research team to have access to my anonymised responses. I understand that my name will not be linked with the research materials, and I will not be identified or identifiable in the report or reports that result from the research. ☐

4. I understand that video and pictures taken during the experiments might be used in anonymised form in the context of scientific presentations. ☐

5. I agree for the data collected from me to be used in future research ☐

6. I agree to take part in the above research project. ☐

| | | |
|---|---|---|
| _____ | _____ | _____ |
| Name of Participant (*or legal representative*) | Date | Signature |
| _____ | _____ | _____ |
| Name of person taking consent (*if different from lead researcher*) | Date | Signature |
| _____ | _____ | _____ |
| Lead Researcher | Date | Signature |

*To be signed and dated in presence of the participant*

# Appendix D

# Publications, Grants, and Awards

## D.1 Publications

### D.1.1 Papers

1. Di Marco R & Scalona E, Pacilli A, Cappa P, Mazzà C, Rossi S. *How to choose and interpret similarity indices to quantify the variability in gait joint kinematics*. Submitted to: Gait and Posture (May 2017).
2. Di Marco R, Rossi S, Racic V, Cappa P, Mazzà C. *Concurrent repeatability and reproducibility analyses of four marker placement protocols for the foot-ankle complex* (2016) Journal of Biomechanics, **49**(14): 3168-3176. DOI: 10.1016/j.jbiomech.2016.07.041
3. Di Marco R, Rossi S, Castelli E, Patanè F, Mazzà C, Cappa P. *Effect of the calibration procedure on the metrological performances of stereophotogrammetric systems for human movement analysis* (2016) Measurement, in press: 1-8. DOI: 10.1016/j.measurement.2016.01.008
4. Prinold JAI, Mazzà C, Di Marco R, Malattia C, Magni-Manzoni S, Petrarca M, Ronchetti AB, Tanturri de Horatio L, van Dijkhuizen EHP, Wesarg S, Viceconti M, MD-PAEDIGREE Consortium. *A patient-specific foot model for the estimate of ankle joint forces in patients with Juvenile Idiopathic Arthritis* (2016) Annals of Biomedical Engineering, **44**(1): 247-257. DOI: 10.1007/s10439-015.1451-z
5. Di Marco R, Rossi S, Patanè F, Cappa P. *Technical quality assessment of an optoelectronic system for movement analysis* (2015) Journal of Physics: Conference Series, **588**(1): 012030. DOI: 10.1088/1742-6596/588/1/012030

### D.1.2 Conference Proceedings

1. Di Marco R, Rossi S, Bachetti B, Mazzà C, Cappa P. *Effect of the calibration procedure of an optoelectronic system on the joint kinematics*. 2015 IEEE International Symposium on Medical Measurement and Applications (MeMeA). DOI: 10.1109/MeMeA.2015.7145220

### D.1.3 Conference Abstracts:

1. Di Marco R, Scalona E, Palermo E, Mazzà C. *A novel kinematic model of the foot-ankle complex for gait analysis*. Submitted to: XVIII SIAMOC Congress 2017 (Italian Society of Movement Analysis in Clinics).
2. Di Marco R, Pacilli A, Scalona E, Rossi S, Mazzà C, Cappa P. *Choosing a similarity index to quantify gait data variability*. Gait & Posture **49**(Supplement 1): S7. XVII SIAMOC Congress 2016 (Italian Society of Movement Analysis in Clinics), 5-8 October 2016. DOI: 10.1016/j.gaitpost.2016.07.032
3. Di Marco R, Rossi S, Racic V, Cappa P, Mazzà C. *Concurrent reliability assessment of three foot models for gait analysis*. XVI SIAMOC Congress 2015 (Italian Society of Movement Analysis in Clinics), 30 Sept-3 Oct 2015.
4. Di Marco R, Rossi S, Racic V, Cappa P, Mazzà C. *A comparison between four foot model protocols: the effect of walking on a treadmill*. XXV Congress of the International Society of Biomechanics, 12-16 July 2015.
5. Prinold JAI, Mazzà C, Di Marco R, Malattia C, Magni-Manzoni S, Petrarca M, Ronchetti AB, Tanturri de Horatio L, van Dijkhuizen EHP, Wesarg S, Viceconti M, MD-PAEDIGREE Consortium. *A patient-specific musculoskeletal modelling pipeline applied to phalangeal loading conditions in gait.* XXV Congress of the International Society of Biomechanics, 12-16 July 2015.

## D.2 Grants

1. Sensorization of a novel X-Y robot for dynamic posturography: on-line acceleration compensation on the load-cell outputs. “Avvio alla Ricerca 2013” Projects, July 2013, €2000.
2. Analysis of the metrological quality of measurement needed to develop a musculoskeletal model of the ankle joint to study the robot-patient interaction. “Avvio alla Ricerca 2014” Projects, July 2014, €1500.

## D.3 Awards

- Second place at "Young Researchers BTS – SIAMOC2016" award presenting the research titled: *Choosing a similarity index to quantify gait data variability* (Di Marco R, Pacilli A, Scalona E, Rossi S, Mazzà C, Cappa P).

# Appendix E

# Teaching experiences

## E.1 "Cultore della Materia" (ING-IND/12-34)

Faculty of Civil and Industrial Engineering, University of Rome "La Sapienza". *Main activities*: Member of the examination boards, teacher, Master's thesis co-supervisor.

| AY | Teaching | Degree | |
|---|---|---|---|
| | | *Biomedical Eng (LM-21)* | *Mechanical Eng (LM-33)* |
| *2016-2017* | Biomechanics | ✓ | ✓ |
| | Laboratory of Measurement in Biomechanics | | ✓ |
| *2015-2016* | Biomechanics | ✓ | ✓ |
| | Laboratory of Measurement in Biomechanics | | ✓ |
| | Mechanical and Thermal Measurements | | ✓ |
| | Industrial Measurements | | ✓ |

## E.2 Teaching Tutor (ING-IND/12-34)

Faculty of Civil and Industrial Engineering, University of Rome "La Sapienza". *Main activities*: Support to teaching (seminars), exams, Master's thesis (also as co-supervisor).

| AY | Teaching | Degree | |
|---|---|---|---|
| | | *Biomedical Eng (LM-21)* | *Mechanical Eng (LM-33)* |
| *2014-2015* | Biomechanics | ✓ | ✓ |
| | Laboratory of Measurement in Biomechanics | | ✓ |
| | Industrial Measurements | | ✓ |
| *2013-2014* | Biomechanics | ✓ | ✓ |
| | Laboratory of Measurement in Biomechanics | | ✓ |
| | Industrial Measurements | | ✓ |
| *2012-2013* | Biomechanics | ✓ | ✓ |
| | Laboratory of Measurement in Biomechanics | | ✓ |
| | Industrial Measurements | | ✓ |

# Appendix F

# Courses and Seminars

## F.1 Courses

- *LabVIEW Core 1*. National Instruments. Rome, 11-13 February 2013;
- *LabVIEW Core 2*. National Instruments. Rome, 14-15 February 2013;
- *LabVIEW Core 3*. National Instruments. Rome, 11-13 March 2013;
- *Advanced Musculoskeletal Modeling Techniques (4 ECTS)*. Prof John Rasmussen – Department of Mechanical and Manufacturing Engineering, Aalborg University. Aalborg (DK), 29 April – 03 May 2013.

## F.2 Seminars

- *How to present an effective and successful proposal to the Framework Programme for Research and Innovation of UE*. APRE Agency for promotion of European research & "La Sapienza" University of Rome. Rome, 21-22 November 2013;
- *Clinical Gait Analysis.* Prof Richard Baker – professor in Biomechanics at The University of Salford. Sheffield, 03 March 2014;
- *Real Time Feedback for Human Performance Enhancement.* Frans Steenbrink, PhD – Motek Medical, Amsterdam (NL). Sheffield, 14 May 2014;
- *What is…the cytoskeleton*. Dr Cecile Perrault, Dr Corfe and Dr Hawkins – The University of Sheffield. Sheffield, 04 June 2014;
- *Producing an effective CV*. Jane Simm – The University of Sheffield. Sheffield, 09 June 2014;
- *How to write a scientific paper*. Prof Marco Viceconti – professor in Biomechanics at The University of Sheffield. Sheffield, 10 June 2014;

- *How to give a scientific presentation*. Prof Marco Viceconti – professor in Biomechanics at The University of Sheffield. Sheffield, 14 May 2015.

# Appendix G

# Extra research activities

Participation to the activities linked to the following projects:

1. **Model-Driven European Paediatric Digital Repository (MD-Paedigree)**: co-funded by the European commission (7th Framework Programme – website: http://www.md-paedigree.eu). Project number: 600932.

   *Abstract as retrieved from the Document of Work* : MD-Paedigree is a clinically-led VPH project that addresses both the first and the second actions of part B of Objective ICT-2011.5.2: 1. It enhances existing disease models stemming from former EC-funded research (Health-e-Child and Sim-e-Child) and from industry and academia, by developing robust and reusable multi-scale models for more predictive, individualised, effective and safer healthcare in several disease areas; 2. It builds on the eHealth platform already developed for Health-e-Child and Sim-e-Child to establish a worldwide advanced paediatric digital repository. Integrating the point of care through state-of-the-art and fast response interfaces, MD-Paedigree services a broad range of off-the-shelf models and simulations to support physicians and clinical researchers in their daily work. MD-Paedigree vertically integrates data, information and knowledge of incoming patients, in participating hospitals from across Europe and the USA, and provides innovative tools to define new workflows of models towards personalised predictive medicine. Conceived of as a part of the "VPH Infostructure" described in the ARGOS, MD-Paedigree encompasses a set of services for storage, sharing, similarity search, outcome analysis, risk stratification, and personalised decision support in paediatrics within its innovative model-driven data and workflow-based digital repository. As

a specific implementation of the VPH-Share project, MD-Paedigree fully interoperates with it. It has the ambition to be the dominant tool within its purview. MD-Paedigree integrates methodological approaches from the targeted specialties and consequently 167etageno biomedical data derived from a multiplicity of heterogeneous sources (from clinical, genetic and 167etagenomics analysis, to MRI and US image analytics, to haemodynamics, to real-time processing of musculoskeletal parameters and fibres biomechanical data, and others), as well as specialised biomechanical and imaging VPH simulation models.

2. **Mechanical measurements for the musculoskeletal apparatus: novel and standardizable methodologies for metrological assessment of measurement systems:** funded by MIUR – PRIN 2012. Project number: 20127XJX57. Principal Investigator: Paolo Cappa.

   *Abstract as retrieved from the Document of Work*: This project is an extension of some Work packages which will be exploited by Sapienza in a four-year project funded by the 7$^{th}$ Framework Programme entitled “MD-Paedigree” and that will start in March 2013. More the present research proposal specifically includes the skills of Roma TRE and Biomedical Campus which are not included in the European project and also extends the analysis to mechanical ventilation. More precisely, the present project proposes the further development of a quality standard for mechanical measurements conducted in movement analysis laboratories. Recent scientific literature outlines a validation issue for results from a same subject examined by different laboratories: to ensure a correct diagnosis, standard methods are required for the evaluation of the performances of measurement systems so that values and uncertainties of kinematics and dynamics quantities can be evaluated with repeatability and reproducibility. The unified group of 3 Research Units combines available instrumentations and skills with the aim of: (1) developing a method for calibration assessment and measurement uncertainty evaluation of optoelectronic system applied to movement as well as mechanical ventilation analysis; (2) developing a method for calibration assessment

and measurement uncertainty evaluation of force platforms (FPs); (3) proposing a standard procedure to establish a quality standard for mechanical measurements performed in movement analysis laboratories. The proposed procedure will be available for care centres of movement analysis and mechanical ventilation analysis as well as institutions where optoelectronics are combined with force platform equipment.

# Glossary

| | |
|---|---|
| $a_0$ **:** | shift coefficient yielded by the LFM; |
| $a_1$ **:** | scaling factor yielded by the LFM; |
| **Abd/Add:** | Abduction/Adduction; |
| **BS:** | Between-subject; |
| **CMC:** | Coefficient of Multiple Correlation; |
| **CCS:** | Camera Coordinate System; |
| **CV:** | Coefficient of Variation; |
| **DLT:** | Direct Linear Transformation; |
| **ECS:** | Embedded Coordinate System; |
| **FF:** | metatarsus and forefoot; |
| **Flx/Ext:** | Flexion/Extension; |
| **Foot:** | foot modelled as a rigid element; |
| **GV:** | Global Volume; |
| **GCS:** | Global Coordinate System; |
| **Hal:** | hallux; |
| **HF:** | hindfoot and calcaneus; |
| **IC:** | Initial Contact; |
| **ICC:** | Intraclass Correlation Coefficient; |
| **ICS:** | Image Coordinate System; |
| **Int/Ext:** | Internal/External rotation; |
| **Inv/Eve:** | Inversion/Eversion; |
| **JCS:** | Joint Coordinate System; |
| **Knee:** | Knee; |
| **LFM:** | Linear Fit Method; |
| **M1:** | model proposed by Stebbins et al., (2006) [65]; |
| **M2:** | model proposed by Leardini et al., (2007) [67]; |
| **M3:** | model proposed by Sawacha et al., (2009) [28]; |
| **M4:** | model proposed by Saraswat et al., (2012) [68]; |
| **MAD:** | Median Absolute Deviation; |
| **MAV:** | Mean Absolute Variability; |
| **MD:** | Maximum Difference; |
| **MDC:** | Minimum Detectable Changes; |

| | |
|---|---|
| **MF:** | midfoot; |
| **MS:** | Mixed simulation; |
| **Plt/Drs:** | Plantar/Dorsiflexion; |
| $R^2$**:** | coefficient of determination yielded by LFM; |
| **RF:** | Refinement Frames; |
| **RMSD:** | Root Mean Square Deviation; |
| **RMSE:** | Root Mean Square Error; |
| **ROM:** | Range Of Motion; |
| **SD:** | Standard Deviation |
| **SD-** $a_0$**:** | Standard Deviation of $a_0$; |
| **SD-** $a_1$**:** | Standard Deviation of $a_1$; |
| **SD-** $R^2$**:** | Standard Deviation of $R^2$; |
| **SEM:** | Standard Error of Measurement; |
| **SI:** | Similarity Indices; |
| **SM:** | Summary Metrics; |
| **SPM:** | Statistical Parametric Mapping; |
| **SS#1:** | Stereophotogrammetric System #1; |
| **SS#2:** | Stereophotogrammetric System #2; |
| **SS:** | Stereophotogrammetric System; |
| **STA:** | Soft Tissue Artefact; |
| **SV-LH:** | Sub-Volume Left and High; |
| **SV-LL:** | Sub-Volume Left and Low; |
| **SV-RH:** | Sub-Volume Right and High; |
| **SV-RL:** | Sub-Volume Right and Low; |
| **TEM:** | Technical Error of Measurement; |
| **Tib:** | tibia and fibula; |
| **TO:** | Toe-Off; |
| **WGC:** | Whole Gait Cycle; |
| **WS:** | Within-subject. |

# References


[1] G. Henry, Gray's Anatomy, Barnes & N, Barnes & Noble, 2010.

[2] L. Chinn, J. Hertel, Rehabilitation of ankle and foot injuries in athletes, Clin. Sports Med. 29 (2010) 157–167. doi:http://dx.doi.org/10.1016/j.csm.2009.09.006.

[3] P.A. Gribble, E. Delahunt, C.M. Bleakley, B. Caulfield, C.L. Docherty, D.T.P. Fong, F. Fourchet, J. Hertel, C.E. Hiller, T.W. Kaminski, P.O. McKeon, K.M. Refshauge, P. Van Der Wees, W. Vicenzino, E.A. Wikstrom, Selection criteria for patients with chronic ankle instability in controlled research: A position statement of the international ankle consortium, J. Athl. Train. 49 (2014) 121–127.

[4] C.L. Saltzman, M.B. Zimmerman, M. O'Rourke, T.D. Brown, J.A. Buckwalter, R. Johnston, Impact of comorbidities on the measurement of health in patients with ankle osteoarthritis., J. Bone Joint Surg. Am. 88 (2006) 2366–2372.

[5] B.R. Waterman, P.J. Belmont, K.L. Cameron, T.M. Deberardino, B.D. Owens, Epidemiology of ankle sprain at the United States Military Academy., Am. J. Sports Med. 38 (2010) 797–803.

[6] T.A.H. Järvinen, P. Kannus, N. Maffulli, K.M. Khan, Achilles tendon disorders: Etiology and epidemiology, Foot Ankle Clin. 10 (2005) 255–266.

[7] N. Maffulli, The clinical diagnosis of subcutaneous tear of the Achilles tendon. A prospective study in 174 patients, Am. J. Sport. Med. 26 (1998) 266–270.

[8] C.M. Court-Brown, B. Caesar, Epidemiology of adult fractures: A review, Injury. 37 (2006) 691–697.

[9] A.R. Long, K.A. Rouster-Stevens, The role of exercise therapy in the management of juvenile idiopathic arthritis, Curr. Opin. Rheumatol. 22 (2010) 213–217.

[10] S.J. Warden, D.B. Burr, P.D. Brukner, Stress fractures: Pathophysiology, epidemiology, and risk factors, Curr. Osteoporos. Rep. 4 (2006) 103–109.

[11] J.A.I. Prinold, C. Mazzà, R. Di Marco, I. Hannah, C. Malattia, S. Magni-Manzoni, M. Petrarca, A.B. Ronchetti, L. Tanturri de Horatio, E.H.P. van Dijkhuizen, S. Wesarg, M. Viceconti, M.-P. Consortium, A Patient-Specific Foot Model for the Estimate of Ankle Joint Forces in Patients with Juvenile Idiopathic Arthritis, Ann. Biomed. Eng. 44 (2016) 247–257. doi:10.1007/s10439-015-1451-z.

[12] A. Cappozzo, U. Della Croce, A. Leardini, L. Chiari, Human movement analysis using stereophotogrammetry. Part 1: theoretical background., Gait Posture. 21 (2005) 186–96. doi:10.1016/j.gaitpost.2004.01.010.

[13] E. Bergamini, G. Ligorio, a. Summa, G. Vannozzi, a. Cappozzo, a. M. Sabatini, Estimating Orientation Using Magnetic and Inertial Sensors and Different Sensor Fusion Approaches: Accuracy Assessment in Manual and Locomotion Tasks,

Sensors (Submitted). (2014) 18625–18649. doi:10.3390/s141018625.

[14] E. Palermo, S. Rossi, F. Marini, F. Patanè, P. Cappa, Experimental evaluation of accuracy and repeatability of a novel body-to-sensor calibration procedure for inertial sensor-based gait analysis, Measurement. 52 (2014) 145–155. doi:10.1016/j.measurement.2014.03.004.

[15] E. Palermo, S. Rossi, F. Patanè, P. Cappa, Experimental evaluation of indoor magnetic distortion effects on gait analysis performed with wearable inertial sensors., Physiol. Meas. 35 (2014) 399–415. doi:10.1088/0967-3334/35/3/399.

[16] P. Picerno, A. Cereatti, A. Cappozzo, Joint kinematics estimate using wearable inertial and magnetic sensing modules, Gait Posture. 28 (2008) 588–595. doi:10.1016/j.gaitpost.2008.04.003.

[17] B. Bonnechère, B. Jansen, P. Salvia, H. Bouzahouene, L. Omelina, F. Moiseev, V. Sholukha, J. Cornelis, M. Rooze, S. Van Sint Jan, Validity and reliability of the Kinect within functional assessment activities: Comparison with standard stereophotogrammetry, Gait Posture. 39 (2014) 593–598.

[18] M. van Diest, J. Stegenga, H.J. Wörtche, K. Postema, G.J. Verkerke, C.J.C. Lamoth, Suitability of Kinect for measuring whole body movement patterns during exergaming, J. Biomech. 47 (2014) 2925–2932. doi:10.1016/j.jbiomech.2014.07.017.

[19] A. Castelli, G. Paolini, A. Cereatti, U. Della Croce, A 2D Markerless Gait Analysis Methodology : Validation on Healthy Subjects, 2015 (2015) 186780. doi:10.1155/2015/186780.

[20] D.A. Winter, Biomechanics and motor control of human movement, Fourth Edi, John Wiley & Sons, Inc., New Jersey, 2009.

[21] JCGM, International vocabulary of metrology — Basic and general concepts and associated terms ( VIM ) Vocabulaire international de métrologie — Concepts fondamentaux et généraux et termes associés ( VIM ), (2008).

[22] JCGM, International vocabulary of metrology – Basic and general concepts and associated terms ( VIM ) 3rd edition Vocabulaire international de métrologie – Concepts fondamentaux et généraux et termes associés ( VIM ) 3 e édition, (2012).

[23] L. Chiari, U. Della Croce, A. Leardini, A. Cappozzo, Human movement analysis using stereophotogrammetry. Part 2: instrumental errors., Gait Posture. 21 (2005) 197–211. doi:10.1016/j.gaitpost.2004.04.004.

[24] A. Leardini, L. Chiari, U. Della Croce, A. Cappozzo, Human movement analysis using stereophotogrammetry. Part 3. Soft tissue artifact assessment and compensation., Gait Posture. 21 (2005) 212–25. doi:10.1016/j.gaitpost.2004.05.002.

[25] U. Della Croce, A. Leardini, L. Chiari, A. Cappozzo, Human movement analysis using stereophotogrammetry Part 4: Assessment of anatomical landmark misplacement and its effects on joint kinematics, Gait Posture. 21 (2005) 226–

237. doi:10.1016/j.gaitpost.2004.05.003.

[26] K. Deschamps, F. Staes, P. Roosen, F. Nobels, K. Desloovere, H. Bruyninckx, G.A. Matricali, Body of evidence supporting the clinical use of 3D multisegment foot models: A systematic review, Gait Posture. 33 (2011) 338–349. http://www.sciencedirect.com/science/article/pii/S0966636210004479.

[27] E. Arnold, S. Ward, R. Lieber, S. Delp, A Model of the Lower Limb for Analysis of Human Movement, Ann. Biomed. Eng. 38 (2010) 269–279. http://dx.doi.org/10.1007/s10439-009-9852-5.

[28] Z. Sawacha, G. Cristoferi, G. Guarneri, S. Corazza, G. Donà, P. Denti, A. Facchinetti, A. Avogaro, C. Cobelli, Characterizing multisegment foot kinematics during gait in diabetic foot patients., J. Neuroeng. Rehabil. 6 (2009) 37. doi:10.1186/1743-0003-6-37.

[29] R. Baker, J. Robb, Foot models for clinical gait analysis, Gait Posture. 23 (2006) 399–400. doi:10.1016/j.gaitpost.2006.03.005.

[30] S. Asfour, M. Eltoukhy, Development and Validation of a Model of the Lower Extremity, Theor. Biomech. (2011) 161–186.

[31] A. Leardini, M.G. Benedetti, F. Catani, L. Simoncini, S. Giannini, An anatomically based protocol for the description of foot segment kinematics during gait, Clin. Biomech. 14 (1999) 528–536.

[32] V.T. Inman, The joints of the ankle, The Williams & Wilkins Company, Baltimore, 1976.

[33] A. Cappozzo, Observing and Revealing the Hidden Structure of the Human Form in Motion Throughout the Centuries, in: Handb. Hum. Motion, 2017. doi:10.1007/978-3-319-30808-1.

[34] W. Braune, O. Fischer, The Human Gait, 1st ed., Springer-Verlag Berlin Heidelberg 1987, 1987. doi:10.1007/9783642703263.

[35] A. Fernández-Baena, A. Susín, X. Lligadas, Biomechanical validation of upper-body and lower-body joint movements of kinect motion capture data for rehabilitation treatments, in: Proc. 2012 4th Int. Conf. Intell. Netw. Collab. Syst. INCoS 2012, 2012: pp. 656–661.

[36] R.A. Clark, Y.H. Pua, K. Fortin, C. Ritchie, K.E. Webster, L. Denehy, A.L. Bryant, Validity of the Microsoft Kinect for assessment of postural control, Gait Posture. 36 (2012) 372–377.

[37] S. Obdrzalek, G. Kurillo, F. Ofli, R. Bajcsy, E. Seto, H. Jimison, M. Pavel, Accuracy and robustness of Kinect pose estimation in the context of coaching of elderly population, in: Proc. Annu. Int. Conf. IEEE Eng. Med. Biol. Soc. EMBS, 2012: pp. 1188–1193.

[38] Y.I. Abdel-Aziz, H.M. Karara, Direct linear transformation from comparator coordinates in close-range photogrammetry, in: ASP Symp. Close-Range Photogramm. Illinois, Urbana, 1971.

[39] J. Weng, P. Cohen, M. Herniou, Camera calibration with distortion models and accuracy evaluation, IEEE Trans. Pattern Anal. Mach. Intell. 14 (1992) 965–980.

[40] N.A. Borghese, G. Ferrigno, An algorithm for 3D automatic movement detection by means of standard TV cameras, IEEE Trans. Biomed. Eng. 37 (1990) 1221–1225.

[41] F. Gazzani, Comparative assessment of two algorithms for calibrating stereophotogrammetric systems, J. Biomech. 26 (1993) 1449–1454.

[42] H.J. Woltring, Planar control in multi-camera calibration for 3D gait studies, J. Biomech. 13 (1980) 39–48.

[43] J. Dapena, E. Harman, J.A. Miller, Three-dimensional cinematography with control object of unknown shape, J. Biomech. 15 (1982) 11–19.

[44] M. Windolf, N. Götzen, M. Morlock, Systematic accuracy and precision analysis of video motion capturing systems--exemplified on the Vicon-460 system., J. Biomech. 41 (2008) 2776–80. doi:10.1016/j.jbiomech.2008.06.024.

[45] D.W. Vander Linden, S.J. Carlson, R.L. Hubbard, Reproducibility and accuracy of angle measurements obtained under static conditions with the Motion Analysis(TM) video system, Phys. Ther. 72 (1992) 300–305.

[46] F.P. Branca, P. Cappa, An experimental study of the accuracy and precision associated to an opto-electronic system utilized for gait analysis, in: 12th Trienn. World Congr. Int. Meas. Confed., Beijin, 1991.

[47] J.P. Scholz, Reliability and validity of the WATSMART three-dimensional optoelectric motion analysis system., Phys. Ther. 69 (1989) 679–689.

[48] D.J. Wilson, B.K. Smith, J.K. Gibson, Accuracy of Reconstructed Angular Estimates Obtained With the Ariel Performance Analysis System TM, Phys. Ther. 77 (1997) 1741–1746.

[49] Y. Ehara, H. Fujimotob, S. Miyazaki, S. Tanaka, S. Yamamoto, Comparison of performance of 3D camera systems, Gait Posture. 3 (1995) 166–169.

[50] Y. Ehara, H. Fujimoto, S. Miyazaki, M. Mochimaru, S. Tanaka, S. Yamamoto, Comparison of the performance of 3D camera systems II, Gait Posture. 5 (1997) 251–255. doi:10.1016/S0966-6362(96)01093-4.

[51] U. Della Croce, A. Cappozzo, A spot check for estimating stereophotogrammetric errors, Med. Biol. Eng. Comput. 38 (2000) 260–266. doi:10.1007/BF02347045.

[52] R. Di Marco, S. Rossi, F. Patanè, P. Cappa, Technical quality assessment of an optoelectronic system for movement analysis, J. Phys. Conf. Ser. 588 (2015) 12030. doi:10.1088/1742-6596/588/1/012030.

[53] M. Damsgaard, J. Rasmussen, S.T. Christensen, E. Surma, M. de Zee, Analysis of musculoskeletal systems in the AnyBody Modeling System, Simul. Model. Pract. Theory. 14 (2006) 1100ƒ_"1111.

[54] S.L. Delp, F.C. Anderson, A.S. Arnold, P. Loan, A. Habib, C.T. John, E.

Guendelman, D.G. Thelen, OpenSim: open-source software to create and analyze dynamic simulations of movement, IEEE Trans. Biomed. Eng. 54 (2007) 1940–1950.

[55] A. Cappozzo, A. Cappello, U. Della Croce, F. Pensalfini, Surface-marker cluster design criteria for 3-D bone movement reconstruction., IEEE Trans. Biomed. Eng. 44 (1997) 1165–74. doi:10.1109/10.649988.

[56] R.B. Davis, S. Õunpuu, D. Tyburski, J.R. Gage, A gait analysis data collection and reduction technique, Hum. Mov. Sci. 10 (1991) 575–587. doi:10.1016/0167-9457(91)90046-Z.

[57] A. Ferrari, M.G. Benedetti, E. Pavan, C. Frigo, D. Bettinelli, M. Rabuffetti, P. Crenna, A. Leardini, Quantitative comparison of five current protocols in gait analysis., Gait Posture. 28 (2008) 207–16. doi:10.1016/j.gaitpost.2007.11.009.

[58] G. Wu, S. Siegler, P. Allard, C. Kirtley, A. Leardini, D. Rosenbaum, M. Whittle, D.D. Lima, L. Cristofolini, H. Witte, O. Schmid, I. Stokes, ISB recommendation on definitions of joint coordinate system of various joints for the reporting of human joint motion - part I: ankle, hip, and spine, J. Biomech. 35 (2002) 543–548. http://www.sciencedirect.com/science/article/pii/S0021929001002226.

[59] G. Wu, F.C.T. Van Der Helm, H.E.J. Veeger, M. Makhsous, P. Van Roy, C. Anglin, J. Nagels, A.R. Karduna, K. McQuade, X. Wang, F.W. Werner, B. Buchholz, ISB recommendation on definitions of joint coordinate systems of various joints for the reporting of human joint motion - Part II: Shoulder, elbow, wrist and hand, J. Biomech. 38 (2005) 981–992. doi:10.1016/j.jbiomech.2004.05.042.

[60] D. a. Winter, Kinematic and kinetic patterns in human gait: Variability and compensating effects, Hum. Mov. Sci. 3 (1984) 51–76. doi:10.1016/0167-9457(84)90005-8.

[61] I. Soderkvist, P.-A. Wedin, Determining the movement of the skeleton using well-configured markers, J. Biomech. 26 (1993) 1473–1477.

[62] K.. Arun, T.. Huang, S.. Blostein, Least-squares fitting of two 3-D point sets, in: 1987: pp. 698–700.

[63] D. Solav, M.B. Rubin, A. Cereatti, V. Camomilla, A. Wolf, Bone Pose Estimation in the Presence of Soft Tissue Artifact Using Triangular Cosserat Point Elements, Ann. Biomed. Eng. 44 (2016) 1181–1190. doi:10.1007/s10439-015-1384-6.

[64] M.C. Carson, M.E. Harrington, N. Thompson, J.J. O'connor, T.N. Theologis, Kinematic analysis of a multi-segment foot model for research and clinical applications: a repeatability analysis, J. Biomech. 34 (2001) 1299–1307.

[65] J. Stebbins, M. Harrington, N. Thompson, A. Zavatsky, T. Theologis, Repeatability of a model for measuring multi-segment foot kinematics in children, Gait Posture. 23 (2006) 401–410. http://www.sciencedirect.com/science/article/pii/S0966636205000378.

[66] A. Leardini, Z. Sawacha, G. Paolini, S. Ingrosso, R. Nativo, M.G. Benedetti, A new anatomically based protocol for gait analysis in children, Gait Posture. 26 (2007)

560–571. doi:10.1016/j.gaitpost.2006.12.018.

[67] A. Leardini, M.G. Benedetti, L. Berti, D. Bettinelli, R. Nativo, S. Giannini, Rear-foot mid-foot and fore-foot motion during the stance phase of gait, Gait Posture. 25 (2007) 453–462.

[68] P. Saraswat, B. a. MacWilliams, R.B. Davis, J.L. D'Astous, A multi-segment foot model based on anatomically registered technical coordinate systems: Method repeatability in pediatric planovalgus feet, Gait Posture. 37 (2012) 121–125. doi:10.1016/j.gaitpost.2011.11.022.

[69] B. a. MacWilliams, M. Cowley, D.E. Nicholson, Foot kinematics and kinetics during adolescent gait, Gait Posture. 17 (2003) 214–224.

[70] G. Wu, P.R. Cavanagh, ISB Recommendations in the Reporting for Standardization of Kinematic Data, J. Biomech. 28 (1995) 1257–1261.

[71] E.S. Grood, W.J. Suntay, A joint coordinate system for the clinical description of three-dimensional motions: application to the knee., J. Biomech. Eng. 105 (1983) 136–44. doi:10.1115/1.3138397.

[72] A. Peters, B. Galna, M. Sangeux, M. Morris, R. Baker, Quantification of soft tissue artifact in lower limb human motion analysis: A systematic review, Gait Posture. 31 (2010) 1–8. doi:10.1016/j.gaitpost.2009.09.004.

[73] A. Cappello, R. Stagni, S. Fantozzi, A. Leardini, Soft tissue artifact compensation in knee kinematics by double anatomical landmark calibration: performance of a novel method during selected motor tasks, IEEE Trans. Biomed. Eng. 52 (2005) 992–998.

[74] L. Lucchetti, A. Cappozzo, A. Cappello, U. Della Croce, Skin movement artefact assessment and compensation in the estimation of knee-joint kinematics, J. Biomech. 31 (1998) 977–984.

[75] F. Alton, L. Baldey, S. Caplan, M.C. Morrissey, A kinematic comparison of overground and treadmill walking, Clin. Biomech. 13 (1998) 434–440.

[76] L.H. Sloot, M.M. van der Krogt, J. Harlaar, Self-paced versus fixed speed treadmill walking, Gait Posture. 39 (2014) 478–484. doi:10.1016/j.gaitpost.2013.08.022.

[77] A. Cereatti, T. Bonci, M. Akbarshahi, K. Aminian, A. Barré, M. Begon, D.L. Benoit, C. Charbonnier, F.D. Maso, S. Fantozzi, C.-C. Lin, T.-W. Lu, M.G. Pandy, R. Stagni, A.J. van den Bogert, V. Camomilla, Standardization proposal of soft tissue artefact description for data sharing in human motion measurements, J. Biomech. (2017). doi:10.1016/j.jbiomech.2017.02.004.

[78] A. Cappello, A. Cappozzo, P.F. La Palombara, L. Lucchetti, A. Leardini, Multiple anatomical landmark calibration for optimal bone pose estimation, 1Human Mov. Sci. 16 (1997) 259–274.

[79] E.J. Alexander, T.P. Andriacchi, Correcting for deformation in skin-based marker systems, J. Biomech. 34 (2001) 355–361.

[80] T. Bonci, V. Camomilla, R. Dumas, L. Ch??ze, A. Cappozzo, A soft tissue artefact model driven by proximal and distal joint kinematics, J. Biomech. 47 (2014) 2354–2361. doi:10.1016/j.jbiomech.2014.04.029.

[81] V. Camomilla, T. Bonci, R. Dumas, L. Chèze, a. Cappozzo, A model of the soft tissue artefact rigid component, J. Biomech. 48 (2015) 1752–1759. doi:10.1016/j.jbiomech.2015.05.007.

[82] V. Camomilla, A. Cereatti, L. Chèze, A. Cappozzo, A hip joint kinematics driven model for the generation of realistic thigh soft tissue artefacts, J. Biomech. 46 (2013) 625–630. doi:10.1016/j.jbiomech.2012.09.018.

[83] T. Bonci, V. Camomilla, R. Dumas, L. Chèze, A. Cappozzo, Rigid and non-rigid geometrical transformations of a marker-cluster and their impact on bone-pose estimation, J. Biomech. (2015) 1–7. doi:10.1016/j.jbiomech.2015.10.031.

[84] D. Solav, V. Camomilla, A. Cereatti, A. Barré, K. Aminian, A. Wolf, Bone orientation and position estimation errors using Cosserat point elements and least squares methods: Application to gait, J. Biomech. (2017) 1–7. doi:10.1016/j.jbiomech.2017.01.026.

[85] D. Meldrum, C. Shouldice, R. Conroy, K. Jones, M. Forward, Test-retest reliability of three dimensional gait analysis: Including a novel approach to visualising agreement of gait cycle waveforms with Bland and Altman plots, Gait Posture. 39 (2014) 265–271. doi:10.1016/j.gaitpost.2013.07.130.

[86] J.B. Arnold, S. Mackintosh, S. Jones, D. Thewlis, Repeatability of stance phase kinematics from a multi-segment foot model in people aged 50 years and older, Gait Posture. 38 (2013) 349–351. doi:10.1016/j.gaitpost.2012.11.010.

[87] M.G. Benedetti, A. Merlo, A. Leardini, Inter-laboratory consistency of gait analysis measurements., Gait Posture. 38 (2013) 934–9. doi:10.1016/j.gaitpost.2013.04.022.

[88] R.J. Leigh, M.B. Pohl, R. Ferber, Does tester experience influence the reliability with which 3D gait kinematics are collected in healthy adults?, Phys. Ther. Sport. 15 (2014) 112–116.

[89] S. Lobet, C. Detrembleur, B. Francq, C. Hermans, Natural progression of blood-induced joint damage in patients with haemophilia: Clinical relevance and reproducibility of three-dimensional gait analysis, Haemophilia. 16 (2010) 813–821. doi:10.1111/j.1365-2516.2010.02245.x.

[90] T. Chau, A review of analytical techniques for gait data. Part 1: Fuzzy, statistical and fractal methods, Gait Posture. 13 (2001) 49–66. doi:10.1016/S0966-6362(00)00094-1.

[91] M. Benedetti, F. Catani, A. Leardini, E. Pignotti, S. Giannini, Data management in gait analysis for clinical applications, Clin. Biomech. 13 (1998) 204–215. doi:10.1016/S0268-0033(97)00041-7.

[92] T. Chau, A review of analytical techniques for gait data. Part 2: neural network and wavelet methods., Gait Posture. 13 (2001) 102–120. doi:Doi:

10.1016/s0966-6362(00)00095-3.

[93] S. Yamamoto, Y. Suto, H. Kawamura, T. Hashizume, S. Kakurai, S. Sugahara, Quantitative gait evaluation of hip diseases using principal component analysis, J. Biomech. 16 (1983) 717–726.

[94] S.J. Olney, M.P. Griffin, I.D. McBride, Multivariate examination of data from gait analysis of persons with stroke, Phys. Ther. 78 (1998) 814–828.

[95] H. Sadeghi, P. Allard, M. Dnhaime, Functional gait asymmetry in able-bodied subjects, Hum. Mov. Sci. 16 (1997) 243–258.

[96] K.J. Deluzio, U.P. Wyss, B. Zee, P.A. Costigan, C. Sorbie, Prinicipal component models of knee kinematics and kinetics: normal vs. pathological gait patterns, Hum. Mov. Sci. 16 (1997) 201–217.

[97] K.J. Deluzio, U.P. Wyss, P.A. Costigan, C. Sorbie, B. Zee, Gait assessment in unicompartmental knee arthroplasty patients: Principal component modeling of gait wavefroms and clinical status, Hum. Mov. Sci. 18 (1999).

[98] M.J. Greenacre, Theory and application of correspondence analysis, London: Academic press, London, UK, 1984.

[99] P. Loslever, Error and data coding in the multi-dimensional analysis of human movement signals, J Eng Med. 207 (1993) 103–110.

[100] P. Loslever, E. Laassel, J.C. Angue, Combined statistical study of joint angles and ground reaction forces using component and multiple correspondence-analysis, IEEE Trans. Biomed. Eng. 41 (1994) 1160–1167.

[101] P. Loslever, F.X. Lepoutre, A. Kebab, H. Sayarh, Descriptive multidimensional statistical methods for analysing signals in a multifactorial database, Med. Biol. Eng. Comput. 34 (1996) 13–20.

[102] M. Wachowiak, G. Rash, A. Desoky, P. Quesada, Wavelet transforms for smoothing kinesiological data, in: Proc. 21st Annu. Meet. Am. Soc. Biomech., South Carolina: ASB: Clemson University, 1997.

[103] A.R. Ismail, S.S. Asfour, Discrete wavelet transform: a tool in smoothing kinematic data, J. Biomech. 32 (1999) 317–321.

[104] T. Tamura, M. Sekine, M. Ogawa, T. Togawa, Y. Fukui, No TitleClassification of acceleration waveforms during walking by wavelet transform, Methods Inf. Med. 36 (1997) 356–359.

[105] D.B. Marghitu, P. Nalluri, An analysis of greyhound gait using wavelets, J. Electromyogr. Kinesiol. 7 (1997) 203–212.

[106] M.H. Schwartz, J.P. Trost, R.A. Wervey, Measurement and management of errors in quantitative gait data, Gait Posture. 20 (2004) 196–203. doi:10.1016/j.gaitpost.2003.09.011.

[107] T.C. Pataky, Generalized n-dimensional biomechanical field analysis using statistical parametric mapping, J. Biomech. 43 (2010) 1976–1982.

doi:10.1016/j.jbiomech.2010.03.008.

[108] C.J. Wright, B.L. Arnold, T.G. Coffey, P.E. Pidcoe, Repeatability of the modified Oxford foot model during gait in healthy adults, Gait Posture. 33 (2011) 108–112. doi:10.1016/j.gaitpost.2010.10.084.

[109] S. Klejman, J. Andrysek, a Dupuis, V. Wright, Test-Retest Reliability of Discrete Gait Parameters in Children With Cerebral Palsy, Arch. Phys. Med. Rehabil. 91 (2010) 781–787. doi:10.1016/j.apmr.2010.01.016.

[110] P.O. Riley, G. Paolini, U. Della Croce, K.W. Paylo, D.C. Kerrigan, A kinematic and kinetic comparison of overground and treadmill walking in healthy subjects., Gait Posture. 26 (2007) 17–24. doi:10.1016/j.gaitpost.2006.07.003.

[111] G.E. Gorton, D.A. Hebert, M.E. Gannotti, Assessment of the kinematic variability among 12 motion analysis laboratories, Gait Posture. 29 (2009) 398–402. doi:10.1016/j.gaitpost.2008.10.060.

[112] P. Caravaggi, M.G. Benedetti, L. Berti, A. Leardini, Repeatability of a multi-segment foot protocol in adult subjects, Gait Posture. 33 (2011) 133–135. doi:10.1016/j.gaitpost.2010.08.013.

[113] P. Saraswat, M.S. Andersen, B.A. MacWilliams, A musculoskeletal foot model for clinical gait analysis, J. Biomech. 43 (2010) 1645–1652.

[114] D.J. Curtis, J. Bencke, J.A. Stebbins, B. Stansfield, Intra-rater repeatability of the Oxford foot model in healthy children in different stages of the foot roll over process during gait, Gait Posture. 30 (2009) 118–121. http://www.sciencedirect.com/science/article/pii/S0966636209000666.

[115] M.W. Cornwall, T.G. McPoil, Three dimensional movement of the foot during the stance phase of walking, J Am Pod. Med Assoc. 89 (1999) 56–66.

[116] M.W. Cornwall, T.G. McPoil, Motion of the calcaneus, navicular and first metatarsal during the stance phase of walking, J Am Pod. Med Assoc. 92 (2002) 67–76.

[117] D.E. Turner, P.S. Helliwell, P. Emery, J. Woodburn, The impact of rehumatoid arthritis on foot function in the early stages of disease: a clinical case series, BMC Musculoskelet. Disord. 7 (2006) 102.

[118] D.E. Turner, J. Woodburn, Characterising the clinical and biomechanical features of severly deformed feet in rehumatoid arthritis, Gait Posture. 28 (2008) 574–580.

[119] A. Alonso-Vázquez, M.A. Villarroya, M.A. Franco, J. As'\in, B. Calvo, Kinematic assessment of paediatric forefoot varus, Gait Posture. 29 (2009) 214–219.

[120] A. Arampatzis, G. Bruggemann, G. Morey Klapsing, A three-dimensionalshank-foot model to determine the foot motion during landings, Med Sci Sport. Exerc. 34 (2002) 130–138.

[121] J. Simon, L. Doederlein, a. S. McIntosh, D. Metaxiotis, H.G. Bock, S.I. Wolf, The Heidelberg foot measurement method: Development, description and

assessment, Gait Posture. 23 (2006) 411–424. doi:10.1016/j.gaitpost.2005.07.003.

[122] J. Tome, D.A. Nawoczenski, A. Flemister, J. Houck, Comparison of foot kinematics between subjects with posterior tibialis tendon dysfunction and healthy controls, J. Orthop. Sport. Phys. Ther. 36 (2006) 635–644.

[123] S. Rao, C. Saltzman, H.J. Yack, Segmental foot mobility in individuals with and without diabetes and neuropathy, Clin. Biomech. 22 (2007) 464–471.

[124] G. Steinwender, V. Saraph, S. Scheiber, E.B. Zwick, C. Uitz, K. Hackl, Intrasubject repeatability of gait analysis data in normal and spastic children, Clin. Biomech. (Bristol, Avon). 15 (2000) 134–139.

[125] M.P. Kadaba, H.K. Ramakrishnan, M.E. Wootten, J. Gainey, G. Gorton, G. V Cochran, Repeatability of kinematic, kinetic, and electromyographic data in normal adult gait, J. Orthop. Res. 7 (1989) 849–860.

[126] M. Khazzam, J.T. Long, R.M. Marks, G.F. Harris, Pre-operative gait characterization of patients with ankle arthrosis, Gait Posture. 24 (2006) 85–93. doi:10.1016/j.gaitpost.2005.07.006.

[127] F. Stief, H. Böhm, K. Michel, A. Schwirtz, L. Döderlein, Reliability and accuracy in three-dimensional gait analysis: A comparison of two lower body protocols, J. Appl. Biomech. 29 (2013) 105–111.

[128] M.M. van der Krogt, L.H. Sloot, J. Harlaar, Overground versus self-paced treadmill walking in a virtual environment in children with cerebral palsy, Gait Posture. 40 (2014) 587–593. doi:10.1016/j.gaitpost.2014.07.003.

[129] M. Iosa, A. Cereatti, A. Merlo, I. Campanini, S. Paolucci, A. Cappozzo, Assessment of Waveform Similarity in Clinical Gait Data: The Linear Fit Method, Biomed Res. Int. 2014 (2014) 1–7. http://www.hindawi.com/journals/bmri/2014/214156/.

[130] P.E. Shrout, J.L. Fleiss, Intraclass correlations: uses in assessing rater reliability., Psychol. Bull. 86 (1979) 420–428.

[131] M. Montero-Odasso, A. Casas, K.T. Hansen, P. Bilski, I. Gutmanis, J.L. Wells, M.J. Borrie, Quantitative gait analysis under dual-task in older people with mild cognitive impairment: a reliability study, J. Neuroeng. Rehabil. 6 (2009) 35. doi:10.1186/1743-0003-6-35.

[132] D.E. Krebs, J.E. Edelstein, S. Fishman, Reliability of observational kinematic gait analysis., Phys. Ther. 65 (1985) 1027–33. doi:10.1016/0966-6362(95)99082-V.

[133] J.L. McGinley, R. Baker, R. Wolfe, M.E. Morris, The reliability of three-dimensional kinematic gait measurements: A systematic review, Gait Posture. 29 (2009) 360–369. doi:10.1016/j.gaitpost.2008.09.003.

[134] D. Laroche, A. Duval, C. Morisset, J.N. Beis, P. d'Athis, J.F. Maillefert, P. Ornetti, Test-retest reliability of 3D kinematic gait variables in hip osteoarthritis patients, Osteoarthr. Cartil. 19 (2011) 194–199. doi:10.1016/j.joca.2010.10.024.

[135] T. Jung, Y. Kim, L.E. Kelly, M.F. Abel, Biomechanical and perceived differences between overground and treadmill walking in children with cerebral palsy, Gait Posture. 45 (2016) 1–6. doi:10.1016/j.gaitpost.2015.12.004.

[136] J. Sinclair, J. Hebron, P.J. Taylor, Does tester experience affect the reliability of multisegment foot kinematics?, Int. J. Perform. Anal. Sport. 14 (2014) 208–216.

[137] J.M. Wilken, K.M. Rodriguez, M. Brawner, B.J. Darter, Reliability and minimal detectible change values for gait kinematics and kinetics in healthy adults, Gait Posture. 35 (2012) 301–307. doi:10.1016/j.gaitpost.2011.09.105.

[138] T.F. Besier, D.L. Sturnieks, J. a. Alderson, D.G. Lloyd, Repeatability of gait data using a functional hip joint centre and a mean helical knee axis, J. Biomech. 36 (2003) 1159–1168. doi:10.1016/S0021-9290(03)00087-3.

[139] A. Ferrari, A.G. Cutti, A. Cappello, A new formulation of the coefficient of multiple correlation to assess the similarity of waveforms measured synchronously by different motion analysis protocols, Gait Posture. 31 (2010) 540–542. doi:10.1016/j.gaitpost.2010.02.009.

[140] A. Ferrari, A.G. Cutti, P. Garofalo, M. Raggi, M. Heijboer, A. Cappello, A. Davalli, First in vivo assessment of “outwalk”: A novel protocol for clinical gait analysis based on inertial and magnetic sensors, Med. Biol. Eng. Comput. 48 (2010) 1–15. doi:10.1007/s11517-009-0544-y.

[141] P. Garofalo, A.G. Cutti, M.V. Filippi, S. Cavazza, A. Ferrari, A. Cappello, A. Davalli, Inter-operator reliability and prediction bands of a novel protocol to measure the coordinated movements of shoulder-girdle and humerus in clinical settings, Med. Biol. Eng. Comput. 47 (2009) 475–486. doi:10.1007/s11517-009-0454-z.

[142] K. Deschamps, F. Staes, H. Bruyninckx, E. Busschots, E. Jaspers, A. Atre, K. Desloovere, Repeatability in the assessment of multi-segment foot kinematics, Gait Posture. 35 (2012) 255–260. doi:10.1016/j.gaitpost.2011.09.016.

[143] J.T. Long, D.C. Eastwood, A.R. Graf, A.P. Smith, G.F. Harris, Repeatability and sources of variability in multi-center assessment of segmental foot kinematics in normal adults, Gait Posture. 31 (2009) 85–93.

[144] U. Rattanaprasert, R. Smith, M. Sullivan, W. Gilleard, Three-dimensional kinematics of the forefoot, rearfoot, and leg without the function of tibialis posterior in comparison with normals during stance phase of walking, Clin. Biomech. 14 (1999) 14–23. doi:10.1016/S0268-0033(98)00034-5.

[145] T.R. Jenkyn, a. C. Nicol, A multi-segment kinematic model of the foot with a novel definition of forefoot motion for use in clinical gait analysis during walking, J. Biomech. 40 (2007) 3271–3278. doi:10.1016/j.jbiomech.2007.04.008.

[146] S.C. Cobb, L.L. Tis, J.T. Johnson, Y.T. Wang, M.D. Geil, F. a. McCarty, The effect of low-mobile foot posture on multi-segment medial foot model gait kinematics, Gait Posture. 30 (2009) 334–339. doi:10.1016/j.gaitpost.2009.06.005.

[147] S. Wolf, J. Simon, D. Patikas, W. Schuster, P. Armbrust, L. Doederlein, Foot motion in children shoes - a comparison of barefoot walking with shod walking

in conventional and flexible shoes, Gait Posture. 27 (2008) 51–59.

[148] A. Castelli, G. Paolini, A. Cereatti, M. Bertoli, U. Della Croce, Application of a markerless gait analysis methodology in children with cerebral palsy: Preliminary results, Gait Posture. 42 (2015) S4–S5. doi:10.1016/j.gaitpost.2015.07.020.

[149] C. Cortés, A. de los Reyes-Guzmán, D. Scorza, Á. Bertelsen, E. Carrasco, Á. Gil-Agudo, O. Ruiz-Salguero, J. Flórez, C. Cortés, A. de los Reyes-Guzmán, D. Scorza, Álvaro Bertelsen, E. Carrasco, Ángel Gil-Agudo, O. Ruiz-Salguero, J. Flórez, de los Reyes-Guzm&#xe1, A. n, D. Scorza, &#xc1 Bertelsen, lvaro, E. Carrasco, &#xc1 Gil-Agudo, ngel, O. Ruiz-Salguero, Fl&#xf3, J. rez, n, Inverse Kinematics for Upper Limb Compound Movement Estimation in Exoskeleton-Assisted Rehabilitation, Biomed Res. Int. 2016 (2016) 1–14. doi:10.1155/2016/2581924.

[150] J. Perry, Gait Analysis. Normal and Pathological function, SLACK Incorporated, Downey, CA, 1992.

[151] T. Theologis, J. Stebbins, The Use of Gait Analysis in the Treatment of Pediatric Foot and Ankle Disorders, Foot Ankle Clin. 15 (2010) 365–382. doi:10.1016/j.fcl.2010.02.002.

[152] R.B. Davis, E.G. Jameson, J.R. Davids, L.M. Christopher, B.R. Rgozinski, J.P. Anderson, The design, development and initial evaluation of a multi-segment foot model for routine clinical gait analysis, Foot Ankle Motion Anal. Clin. Treat. Technol. (2006) 425–444.

[153] R.B. Davis, P. Saraswat, B. MacWilliams, A multicenter investigation of the repeatability o the foot anatomical landmark identification, in: Annu. Proc. Gait Clin. Motion Anal. Soc., 2008: pp. 146–147.

[154] T.M. Kepple, S.J. Stanhope, K.N. Lohmann, N.L. Roman, A video-based technique for measuring ankle-subtalar motion during stance, J. Biomed. Eng. 12 (1990) 273–280. doi:10.1016/0141-5425(90)90001-4.

[155] D. a Scott, S H; Winter, Talocrural and Talocalcaneal Joint Kinematics and Kinetics During the Stance Phase of Walking.Pdf, 24 (1991) 743–752.

[156] S. D'Andrea, C. Tylkowski, J. Losito, W. Arguedas, T. Bushman, V. Howell, Three-dimensional kinematics of the foot, in: Proc. II Int. Symp. Three-Dimensional Anal. Hum. Movement, Poiters, Fr., 1993: pp. 103–105.

[157] K.L. Siegel, T.M. Kepple, P.G. O'Connell, L.H. Gerber, S.J. Stanhope, A technique to evaluate foot function during the stance phase of gait, Foot Ankle Int. 16 (1995) 764–770.

[158] S.M. Kidder, F.S. Abuzzahab, G.F. Harris, J.E. Johnson, A system for the analysis of foot and ankle kinematics during gait, IEEE Trans. Rehabil. Eng. 4 (1996) 25–32. doi:10.1109/86.486054.

[159] K. a. Myers, M. Wang, R.M. Marks, G.F. Harris, Validation of a Multisegment Foot and Ankle Kinematic Model for Pediatric Gait, IEEE Trans. Neural Syst.

Rehabil. Eng. 12 (2004) 122–130.

[160] M. Khazzam, J.T. Long, R.M. Marks, G.F. Harris, Kinematic changes of the foot and ankle in patients with systemic rheumatoid arthritis and forefoot deformity, J. Orthop. Res. 25 (2007) 319–329.

[161] J.W. Brodsky, D.A. Charlick, S.C. Coleman, F.E. Pollo, C.T. Royer, Hindfoot motion following reconstruction for posterior tibial tendon dysfunction, Foot Ankle Int. 30 (2009) 613–618.

[162] M.E. Ness, J. Long, R. Marks, G. Harris, Foot and ankle kinematics in patients with posterior tibial tendon dysfunction, Gait Posture. 27 (2008) 331–339.

[163] R.M. Marks, J.T. Long, M.E. Ness, M. Khazzam, G.F. Harris, Surgical reconstruction of posterior tibial tendon dysfunction: prospective comparison of flexor digitorum longus substitution combined with lateral column lengthening or medial displacement calcaneal osteotomy, Gait Posture. 29 (2009) 17–22.

[164] P.A. Smith, K.N. Kuo, A.N. Graf, J. Krzak, A. Flanagan, S. Hassani, A.K. Caudill, F.R. Dietz, J. Morcuende, G.F. Harris, Long-term results of comprehensive clubfoot release versus the ponseti method: Which is better?, Clin. Orthop. Relat. Res. 472 (2014) 1281–1290. doi:10.1007/s11999-013-3386-8.

[165] N.A. Beckmann, S.I. Wolf, D. Heitzmann, A. Wallroth, S. Müller, T. Dreher, Cavovarus deformity in Charcot-Marie- Tooth disease: is there a hindfoot equinus deformity that needs treatment?, J. Foot Ankle Res. 8 (2011) 1–7. doi:10.1186/s13047-015-0121-6.

[166] L. Moseley, R. Smith, a. Hunt, R. Gant, Three-dimensional kinematics of the rearfoot during the stance phase of walking in normal young adult males, Clin. Biomech. 11 (1996) 39–45. doi:10.1016/0268-0033(95)00036-4.

[167] W. Liu, S. Siegler, H. Hillstrom, K. Whitney, Three-dimensional, six-degrees-of-freedom kinematics of the human hindfoot during the stance phase of level walking, Hum. Mov. Sci. 16 (1997) 283–298. doi:10.1016/S0167-9457(96)00057-7.

[168] C. Giacomozzi, M.G. Benedetti, A. Leardini, V. Marcellari, S. Giannini, Gait analysis with an integrated system for functional assessment to talocalcaneal coalition, J Am Pod. Med Assoc2. 26 (2006) 107–115.

[169] W.L. Wu, F.C. Su, Y.M. Cheng, P.J. Huang, Y.L. Chou, C.K. Chou, Gait analysis after ankle arthrodesis., Gait Posture. 11 (2000) 54–61. doi:http://dx.doi.org/10.1016/S0966-6362(99)00049-1.

[170] a. E. Hunt, R.M. Smith, M. Torode, a. M. Keenan, Inter-segment foot motion and ground reaction forces over the stance phase of walking, Clin. Biomech. 16 (2001) 592–600. doi:10.1016/S0268-0033(01)00040-7.

[171] T.N. Theologis, M.E. Harrington, N. Thompson, M.K.D. Benson, Dynamic foot movement in children treated for congenital talipes equinovarus, Bone Joint J. 85 (2003) 572–577.

[172] J. Woodburn, P.S. Helliwell, S. Barker, Three-dimensional kinematics at the ankle joint complex in rheumatoid arthritis patients with painful valgus deformity of the rearfoot, Rheumatology. 41 (2002) 1406–1412. doi:10.1093/rheumatology/41.12.1406.

[173] D.A. Nawoczenski, J. Ketz, J.F. Baumhauer, Dynamic kinematic and plantar pressure changes following cheilectomy for hallux rigidus: a mid-term follow up, Foot Ankle Int. 29 (2008) 265–272.

[174] P. Saraswat, B. a. MacWilliams, R.B. Davis, J.L. D'Astous, A multi-segment foot model based on anatomically registered technical coordinate systems: Method repeatability and sensitivity in pediatric planovalgus feet, Gait Posture. 37 (2013) 121–125. doi:10.1016/j.gaitpost.2012.06.023.

[175] K. Deschamps, F. Staes, H. Bruyninckx, E. Busschots, G. a. Matricali, P. Spaepen, C. Meyer, K. Desloovere, Repeatability of a 3D multi-segment foot model protocol in presence of foot deformities, Gait Posture. 36 (2012) 635–638. doi:10.1016/j.gaitpost.2012.04.007.

[176] R. Chang, R. Van Emmerik, J. Hamill, Quantifying rearfoot-forefoot coordination in human walking, J. Biomech. 41 (2008) 3101–3105. doi:10.1016/j.jbiomech.2008.07.024.

[177] D. Legault-Moore, V.L. Chester, G. de Vries, Multisegment Foot Kinematics During Walking in Younger and Older Adults, J. Clin. Med. Res. 4 (2012) 259–266. doi:10.4021/jocmr984w.

[178] S. Rao, J.F. Baumhauer, J. Tome, D.A. Nawoczenski, Comparison of in vivo segmental foot motion during walking and step descent in patients with midfoot arthritis and matched asymptomatic control subjects, J. Biomech. 42 (2009) 1054–1060.

[179] J.R. Houck, J.M. Tome, D.A. Nawoczenski, Subtalar neutral position as an offset for a kinematic model of the foot during walking, Gait Posture2. 28 (2008) 29–37.

[180] J. Houck, C.G. Neville, J.M. Tome, A. Flemister, A foot kinematics during bilateral heel rise test in participants with stage 2 posterior tibial tendon dysfunction, J Orthop Sport. Phys Ther. 39 (2009) 593–603.

[181] Z. Sawacha, G. Guarneri, G. Cristoferi, A. Guiotto, A. Avogaro, C. Cobelli, Integrated kinematics–kinetics–plantar pressure data analysis: A useful tool for characterizing diabetic foot biomechanics, Gait Posture. 36 (2012) 20–26.

[182] I. Hannah, Z. Sawacha, A. Guiotto, C. Mazzà, Relationship between sagittal plane kinematics, foot morphology and vertical forces applied to three regions of the foot, Int. Biomech. 3 (2016) 50–56. doi:10.1080/23335432.2016.1229135.

[183] A.K. Buldt, P. Levinger, G.S. Murley, H.B. Menz, C.J. Nester, K.B. Landorf, Foot posture is associated with kinematics of the foot during gait: A comparison of normal, planus and cavus feet, Gait Posture. 42 (2015) 42–48. doi:10.1016/j.gaitpost.2015.03.004.

[184] J. Røislien, Skare, a. Opheim, L. Rennie, Evaluating the properties of the coefficient of multiple correlation (CMC) for kinematic gait data, J. Biomech. 45 (2012) 2014–2018. doi:10.1016/j.jbiomech.2012.05.014.

[185] I. Mileti, J. Taborri, S. Rossi, M. Petrarca, F. Patanè, P. Cappa, Evaluation of the effects on stride-to-stride variability and gait asymmetry in children with Cerebral Palsy wearing the WAKE-up ankle module, in: 2016 IEEE Int. Symp. Med. Meas. Appl., Benevento, 2016: pp. 286–291.

[186] E. Growney, D. Meglan, M. Johnson, T. Cahalan, K.-N. An, Repeated measures of adult normal walking using a video tracking system, Gait Posture. 6 (1997) 147–162. doi:10.1016/S0966-6362(97)01114-4.

[187] H.J. Woltring, A Fortran package for generalized, cross-validatory spline smoothing and differentiation, Adv. Eng. Softw. 8 (1986) 104–113. doi:10.1016/0141-1195(86)90098-7.

[188] JCGM, Evaluation of measurement data — Guide to the expression of uncertainty in measurement, (2008).

[189] M.C. Carson, M.E. Harrington, N. Thompson, J.J. O'Connor, T.N. Theologis, Kinematic analysis of a multi-segment foot model for research, J. Biomech. 34 (2001) 1299–1307.

[190] F. Pecoraro, C. Mazzà, A. Cappozzo, E.E. Thomas, A. Macaluso, Reliability of the intrinsic and extrinsic patterns of level walking in older women, Gait Posture. 26 (2007) 386–392. doi:10.1016/j.gaitpost.2006.10.001.

[191] L.D. Duffell, N. Hope, A.H. McGregor, Comparison of kinematic and kinetic parameters calculated using a cluster-based model and Vicon's plug-in gait., Proc. Inst. Mech. Eng. H. 228 (2014) 206–10. doi:10.1177/0954411913518747.

[192] R. Di Marco, S. Rossi, E. Castelli, F. Patanè, C. Mazzà, P. Cappa, Effects of the calibration procedure on the metrological performances of stereophotogrammetric systems for human movement analysis, Measurement. (2016) 1–8. doi:10.1016/j.measurement.2016.01.008.

[193] R. Di Marco, S. Rossi, V. Racic, P. Cappa, C. Mazzà, Concurrent repeatability and reproducibility analyses of four marker placement protocols for the foot-ankle complex, J. Biomech. 49 (2016) 3168–3176. doi:10.1016/j.jbiomech.2016.07.041.

[194] U. Della Croce, A. Cappozzo, D.C. Kerrigan, Pelvis and lower limb anatomical landmark calibration precision and its propagation to bone geometry and joint angles., Med. Biol. Eng. Comput. 37 (1999) 155–161.

[195] JCGM, Evaluation of measurement data — Supplement 1 to the " Guide to the expression of uncertainty in measurement " — Propagation of distributions using a Monte Carlo method, (2008).

[196] J. Taborri, E. Scalona, E. Palermo, S. Rossi, P. Cappa, Validation of inter-subject training for hidden markov models applied to gait phase detection in children with Cerebral Palsy, Sensors (Switzerland). 15 (2015) 24514–24529.

doi:10.3390/s150924514.

[197] A. Cappozzo, F. Catani, A. Leardini, M.G. Benedetti, U. Della Croce, Position and orientation in space of bones during movement: experimental artefacts, Clin. Biomech. 11 (1996) 90.

[198] L. Chen, C.W. Armstrong, D.D. Raftopoulos, An investigation on the accuracy of three-dimensional space reconstruction using the direct linear transformation technique, J. Biomech. 27 (1994) 493–500.

[199] P.J. Klein, J.J. Dehaven, Accuracy of Three-Dimensional Linear and Angular Estimates Obtained With the Ariel Performance Analysis System, in: Am. Congr. Rehabil. Med. Am. Acad. Phys. Med. Rehabil., 1995: pp. 183–189.

[200] A. Cappozzo, Minimum measured-input models for the assessment of motor ability, J. Biomech. 35 (2002) 437–446. doi:10.1016/S0021-9290(01)00186-5.

[201] R. Stagni, A. Leardini, A. Cappozzo, M.G. Benedetti, A. Cappello, Effects of hip joint centre mislocation on gait analysis results, J. Biomech. 33 (2000) 1479–1487.

[202] A. Leardini, A. Cappozzo, F. Catani, S. Toksvig-Larsen, A. Petitto, V. Sforza, G. Cassanelli, S. Giannini, Validation of a functional method for the estimation of hip joint centre location, J. Biomech. 32 (1999) 99–103. doi:10.1016/S0021-9290(98)00148-1.

[203] O. Pinzone, M.H. Schwartz, P. Thomason, R. Baker, The comparison of normative reference data from different gait analysis services, Gait Posture. 40 (2014) 286–290. doi:10.1016/j.gaitpost.2014.03.185.

[204] S. van Sint Jan, Color atlas of skeletal landmark definitions: guidelines for reproducible manual and virtual palpations, Elsevier Health Sciences, 2007.

[205] T.C. Pataky, One-dimensional statistical parametric mapping in Python, Comput. Methods Biomech. Biomed. Engin. 15 (2012) 295–301. doi:10.1080/10255842.2010.527837.

[206] K.J. Friston, J.T. Ashburner, S.J. Kiebel, T.E. Nichols, W.D. Penny, Statistical parametric mapping: the analysis of functional brain images: the analysis of functional brain images, Elsevier/Academic Press, Amsterdam, 2007.

[207] G. Wu, F.C. van der Helm, H.E. Veeger, M. Makhsous, P. Van Roy, C. Anglin, J. Nagels, A.R. Karduna, K. McQuade, X. Wang, F.W. Werner, B. Buchholz, ISB recommendation on definitions of joint coordinate systems of various joints for the reporting of human joint motion--Part II: shoulder, elbow, wrist and hand, J Biomech. 38 (2005) 981–992. http://www.ncbi.nlm.nih.gov/entrez/query.fcgi?cmd=Retrieve&db=PubMed&dopt=Citation&list_uids=15844264.

[208] C. Nester, R.K. Jones, a. Liu, D. Howard, a. Lundberg, a. Arndt, P. Lundgren, a. Stacoff, P. Wolf, Foot kinematics during walking measured using bone and surface mounted markers, J. Biomech. 40 (2007) 3412–3423. doi:10.1016/j.jbiomech.2007.05.019.

[209] C.J. Nester, a. M. Liu, E. Ward, D. Howard, J. Cocheba, T. Derrick, P. Patterson, In vitro study of foot kinematics using a dynamic walking cadaver model, J. Biomech. 40 (2007) 1927–1937. doi:10.1016/j.jbiomech.2006.09.008.

# Acknowledgments

The presented research project has been partially funded by the MD-Paedigree Project (European Union under the Information Communication Technologies Programme: FP7-ICT-2011-9), the Italian Ministry of University and Research (PRIN 2012 – 20127XJX57), and the UK EPSRC, Great Technologies Capital Call, Robotics and Autonomous Systems (EP/J013714/1).

Apart from the funding sources that have supported my PhD in different ways, I believe there are a few people I should thank for helping me to reach this goal. My family could not be at any different place but the first. A PhD is a great experience for a young researcher; but, as all great experiences, it can be proving especially if you decide to live abroad for a while. The support of my family has been really important to go through these four years. For many different reasons. So, thank you. A lot!

Another big thanks has to go to my friends. This PhD gave me the opportunity to meet a lot of great, funny, and lovely people, who sometimes have been part of a kind of “special family”. If you are not a researcher, it can sound weird, but you actually share a big part of your life with your colleagues. And in our case, you sometimes have to “share your body” (of course, for scientific purposes). Some of them need to be named. Particularly, I have to thank Silvia for having been a great friend when I was far from home, but making me feel as if I were home. And thank you for still being a great friend, even after having understood I am completely mad person. Emilia, well… this is really difficult, because saying “thank you” sounds just not enough for your being you. That I loved working with you is not a secret, as well as it is not a secret that I will always keep working with you. I genuinely think that having met you, and having gained your friendship is the biggest gift that came from this PhD. Ok, I will stop this here.

A big thanks goes to my supervisors, Paolo and Claudia, who gave me the great opportunity of gaining a double-PhD, and for teaching me how to become a good and fair researcher. I hope you will be proud of what I am going to do during my professional life. I have thanked prof Paolo Cappa many times and in all the presentations I gave since he passed away, but I still feel it is not enough for having been a great example of kindness, courtesy and respect. Some people should have had this opportunity.

Once again, for all of you that shared this experience with me, thank you!